

# **Modelling plant variety dependent least limiting water range (LLWR)**

---

by George Themistocleous, PhD

Thesis submitted to the University of Nottingham for the degree of Doctor of  
Philosophy, March 2021

## **Declaration**

I hereby declare that this thesis has been composed by myself and that it has not been accepted in any previous applications for a degree. The work, of which it is a record, is my own, unless otherwise stated. All verbatims have been distinguished by quotation marks and sources of information specifically acknowledged by means of references.

George Themistocleous

## **Acknowledgments**

This project was funded by the STARS Centre for Doctoral Training (CDT) which is funded by NERC and BBSRC. The James Hutton Institute and the University of Nottingham provided the equipment and assistance necessary to complete this project. I would like to thank my supervisors; Dr. Tracy Valentine, Dr. Blair McKenzie and Prof. Sacha Mooney for the guidance that they have provided during my research. I obtained valuable knowledge and experience from our time together. I will also like to thank Mrs. Kirsty Binnie for all the training and assistance she has provided me in the laboratory.

Finally, I will like to thank my mother, father and brother, Christos, Ioanna and Andreas for their support. I'm certain I will never have made it this far without you in my life. This also includes my favourite canine in the world, Spike, I will always remember you.

“What you leave behind is not what is engraved in stone monuments, but what is woven into the lives of others.” ~Pericles

# Table of Contents

Declaration.....	2
Acknowledgments.....	3
Table of Contents.....	4
Abstract.....	8
List of Figures.....	9
List of Tables.....	14
List of Abbreviations and Symbols.....	16
1. Literature review.....	19
1.1 Introduction.....	19
1.2 Soil physical stressors.....	22
1.2.1 Drought.....	22
1.2.2 Soil Oxygen.....	23
1.2.3 Soil mechanical impedance.....	24
1.3 Root traits.....	25
1.3.1 Roots.....	25
1.3.2 Root system architecture (RSA).....	27
1.3.3 Root Hairs.....	29
1.3.4 Root cap.....	30
1.3.5 Root Border Cells.....	31
1.4 Root phenotyping.....	32
1.4.1 Overview.....	32
1.4.2 Field based methods.....	33
1.4.3 Greenhouse based methods.....	35
1.4.4 Laboratory based methods.....	36
1.5 Least Limiting Water Range.....	40
1.5.1 Introduction.....	40

1.5.2 Model Description.....	41
1.5.3 Limitations.....	44
1.6 Aims of this project.....	47
2. Rhizotron Development.....	49
2.1 Introduction.....	49
2.2 Design criteria.....	51
2.3 Aims.....	54
2.4 Methods.....	55
2.4.1 Assessment of initial RS criteria.....	55
2.4.2 Minirhizotron Construction.....	56
2.4.2.1 Minirhizotron design A.....	56
2.4.2.2 Minirhizotron design B.....	58
2.4.3 Growth Substrate – sample preparation.....	59
2.4.4 Growth Substrate – physical property analysis.....	60
2.4.5 Seed germination.....	61
2.4.6 Glasshouse growth conditions.....	62
2.4.7 Minirhizotron imaging.....	62
2.4.8 Root growth parameters.....	62
2.4.9 Substrate image RGB spectra.....	63
2.4.10 Image quality - Image Sharpness Index.....	64
2.4.11 Statistical Analysis.....	64
2.4.12 Rhizotron Substrate Selection.....	65
2.4.13 Rhizotron Substrate Particle Size Distribution.....	65
2.4.14 Rhizotron Scanning Surface Selection.....	67
2.4.15 Assessment of plant responses to alternative growth substrate.....	67
2.5 Results.....	68
2.6 Discussion.....	84

2.7 Conclusions.....	86
3. Root trait imaging and image analysis.....	87
3.1 Introduction.....	87
3.2 Minirhizotron System.....	89
3.2.1 Minirhizotron-based root imaging methods.....	89
3.2.2 Root hair imaging-based methods.....	91
3.2.3 Algorithm 1 – Root length and root hair analysis.....	92
3.2.4 Root length and root hair area algorithms validation.....	95
3.3 Root cap and border cell measurements.....	96
3.3.1 Root cap and border cell imaging methods.....	96
3.3.2 Root tip staining and imaging procedure.....	98
3.3.3 Algorithm 2 – Root tip geometry and border cell analysis .....	98
3.3.3.1 Root tip geometry.....	98
3.3.3.2 Dead border cell segmentations.....	101
3.3.3.3 Live border cell segmentations.....	103
3.3.4 Root border cell algorithm validation.....	105
3.3.5 Root border cell quantification.....	105
3.4 Washed root system assessment.....	105
3.4.1 Root morphology methods based on destructive sampling.....	105
3.4.2 Algorithm 3 – WRS total root length analysis.....	107
3.4.3 WRS parameter extraction algorithm validation.....	110
3.5 Results.....	111
3.6 Discussion.....	118
3.7 Conclusions.....	121
4. Constrains to the application of the LLWR.....	123
4.1 Introduction.....	123
4.2 Aims.....	125

4.3 Methods.....	125
4.3.1 Experimental Procedure.....	125
4.3.2 Root growth parameters.....	127
4.3.3 Statistical Analysis.....	127
4.3.4 LLWR for RS Substrate.....	128
4.4 Results.....	128
4.5 Discussion.....	149
4.6 Conclusions.....	152
5. Variation in root traits associated with LLWR.....	154
5.1 Introduction.....	154
5.2 Aims.....	156
5.3 Methods.....	156
5.4 Results.....	158
5.5 Discussion.....	179
5.6 Conclusions.....	182
6. General discussion and conclusions.....	184
6.1 Introduction.....	184
6.2 Genotypic variation of root traits.....	187
6.3 LLWR modification.....	193
6.4 Summary of key conclusions.....	195
6.5 Future research.....	196
References.....	199

## Abstract

Drought stress is a major limiting factor for yield on a global scale (Solh and van Ginkel, 2014), with drought effects being predicted to become more severe with increasing global temperatures (IPCC, 2014). Climate change is also expected to increase the frequency and severity of floods leading to root oxygen stress (Trenberth, 2011). At the same time, current agricultural practises are increasingly relying on heavy machinery leading to soil compaction and changes in soil structure (Chamen *et al.*, 2003), reducing the rate of cell division in the root meristem, and decreasing cell expansion (Bengough and Mullins, 1990). As such, in order to reduce yield losses it is essential to understand the complex interaction between oxygen stress, water stress and mechanical stress (Mohammadi *et al.*, 2010). The least limiting water range (LLWR) is one such model which relates the above-mentioned soil stressors in order to estimate the soil moisture range in a particular soil for which plants should be less limited in terms of growth. However, the extent to which the LLWR considers the influence of root traits in changing its boundaries is currently limited. In order to be able to assess the effects of root trait variability on the LLWR boundaries while manipulating the LLWR soil stressors a minirhizotron based system (RS) was developed. This cheap (~£10 per unit), acrylic based, A3 sized system enabled *in situ* imaging of roots and root hairs. Destructive sampling methods were also used to determine root border cell numbers and root tip geometry. To further optimise the process of data collection, Rcpp based image processing algorithms were developed to obtain automated estimates of the root traits of root length, root hair, root border cells and root tip eccentricity to further increase the efficiency of the RS phenotyping platform.

To test how contrasting root traits influence the LLWR a plant phenotyping experiment was performed comparing four spring barley (*Hordeum vulgare* L.) varieties, Optic, KWS Sassy, Derkado and Golden Promise. Root growth rates both in the vertical and horizontal directions all increased with increasing water availability and decreasing substrate density. Root hair area did not vary significantly among treatments and between varieties. Root border cell count and root tip eccentricity increased with increasing substrate density but did not vary significantly across varieties. A root micro-trait based linear interaction model was developed to describe average root growth rates and it was demonstrated that root growth rates on average follow a linear pattern for values  $\geq 8 \text{ mm day}^{-1}$ . Root micro-traits mostly failed to correlate well with root growth rates except for a negative association with root tip geometry (cor = -0.4192,  $p = 2e-05^{**}$ ).

## List of Figures

<b>Figure 1.1:</b> Schematic diagram showing the root cross sections of a monocot (A) and a dicot (B) (taken from: <a href="https://www.researchgate.net/figure/Anatomy-of-typical-a-monocot-and-b-dicot-root_fig2_278689094">https://www.researchgate.net/figure/Anatomy-of-typical-a-monocot-and-b-dicot-root_fig2_278689094</a> ).....	26
<b>Figure 1.2:</b> Example LLWR output of soil volumetric water content ( $\theta$ ) vs. bulk density (Db). The regression lines correspond to the soil volumetric content at the plant limiting conditions of 10 % soil air filled porosity ( $\theta_{AP}$ ), -0.01 MPa soil matric suction ( $\theta_{FC}$ ), 2 MPa soil penetrometer resistance ( $\theta_{PR}$ ), and -1.5 MPa soil matric ( $\theta_{PWP}$ ). The dry bulk density value represented by $Db_{crit}$ marks the transition point between the shaded LLWR zone and the non LLWR zone where plants should be least limited relative to each factor.....	43
<b>Figure 2.1:</b> Schematic diagram of the starting minirhizotron design A) Top view and B) Front view.....	57
<b>Figure 2.2:</b> Schematic diagram of new minirhizotron design B A) Top view and B) Front view (circles indicate screws).....	59
<b>Figure 2.3:</b> Spring barley root systems, growing in the four different substrates A) Bullion soil, B) Pilmore Soil, C) Black sand and D) Blue sand in rhizotron design A. Images obtained using Epson scanner at 1600 dpi, on day 14 since transfer of seedling rhizotron.....	69
<b>Figure 2.4:</b> Summary graphs of spring barley root growth in growth substrates (Black sand, Blue sand, Bullion soil and Pilmore Soil) in rhizotrons for a period of 21 days, A) ARGR vs. substrate, B) AVGR vs. substrate, C) AHGR vs. substrate, D) VRL vs. time and E) HRL vs. time.....	71
<b>Figure 2.5:</b> Summary graphs of spring barley root growth in growth substrates (1.4-0, 2.0-0, 2.8-0 and 4.0-0) in rhizotrons for a period of 21 days, A) ARGR vs. substrate, B) AVGR vs. substrate, C) AHGR vs. substrate, D) VRL vs. time and E) HRL vs. time.....	74
<b>Figure 2.6:</b> Rhizotron scanning surface experiment comparing imaging quality for A) 4 mm thick, low iron, reinforced glass, B) acrylic - 5 mm thick and C) acrylic - 2 mm thick, scanned at 1,600 dpi.....	75

<b>Figure 2.7:</b> ISI boxplot comparison for three different RS scanning surfaces. Higher Image Sharpness (ISI) score indicates a higher quality image.....	76
<b>Figure 2.8:</b> ISI boxplot comparison for four different RS substrates. Higher Image Sharpness (ISI) score indicates a higher quality image.....	77
<b>Figure 2.9:</b> Summary graphs of spring barley root growth in growth substrates (Flourite Black, Flourite and soil, Bullion soil and Pilmore soil) in rhizotrons for a period of 21 days, <b>A) ARGR vs. substrate, B) AVGR vs. substrate, C) AHGR vs. substrate, D) VRL vs. time and E) HRL vs. time</b> .....	79
<b>Figure 2.10:</b> Physical properties of “Pilmore Soil”, “Bullion Soil” and “Flourite Black” packed at 1.5 g cm <sup>-3</sup> for different PSD in terms of <b>A) Water Release Curves (van Genuchten model), B) Penetrometer Resistance (loess regression) with mean and standard deviations shown and C) effective pore diameter profile</b> .....	81
<b>Figure 2.11:</b> Histograms of RGB and greyscale spectra of tested rhizotron growth substrates with RGB mean values for <b>A) Roots, B) Blue Sand, C) Black Sand, D) Bullion Soil, E) Pilmore Soil and F) Flourite Black</b> .....	83
<b>Figure 3.1:</b> <b>A) Minirhizotron image of a 14 day old spring barley seedling, B) Pre-processing for image subset selection, C) Vessel enhancement step for enhancing roots and D) Root segmentation step for extracting roots</b> .....	94
<b>Figure 3.2:</b> Magnified image of spring barley grown in the RS and scanned at 1,600 dpi. <b>A) Raw image and B) Root hair boundary (blue) and detected root hair area (red) after thresholding the area adjacent to the root</b> .....	95
<b>Figure 3.3:</b> Root tip geometry algorithm, <b>A) Raw image, B) Greyscale conversion, C) Morphological opening, D) Binarization, E) Root Contour extraction, F) Root contour rotation and H) Conic fitting</b> .....	100
<b>Figure 3.4:</b> Non-viable RBCs algorithm, <b>A) Raw image, B) Greyscale conversion, C) Top hat filter, D) Blob enhancement and E) Binarization</b> .....	102
<b>Figure 3.5:</b> Viable RBCs algorithm, <b>A) Raw image, B) Greyscale conversion, C) Top hat filter, D) Vessel enhancement and E) Binarization</b> .....	104

<b>Figure 3.6:</b> TRL quantification image processing main steps <b>A)</b> Median filtering (Step 2), <b>B)</b> Maximum entropy thresholding (Step 3), <b>C)</b> Particle removal (Step 4), <b>D)</b> Binarization (Step 10), <b>E)</b> Skeletonization (Step 11) and <b>F)</b> Skeleton pruning (Step 12).....	109
<b>Figure 3.7:</b> Validation graph for A1 demonstrating the observed <i>vs.</i> predicted X and Y dimensional root lengths.....	111
<b>Figure 3.8:</b> Root hair area overlap of the predicted root hair area relative to the manually traced total root hair area for 20 different (300 x 300 pixels) image sections. The dashed lines represent the 0 (min), 1 <sup>st</sup> , 2 <sup>nd</sup> (Median), 3 <sup>rd</sup> and 4 <sup>th</sup> (max) quartiles.....	112
<b>Figure 3.9:</b> Probability distribution fitting diagnostic plots for <b>A)</b> live (FDA) and <b>B)</b> dead (PI) RBC populations.....	115
<b>Figure 3.10:</b> Observed <i>vs.</i> Predicted values of TRL for tested automated 2D software and the proposed algorithm. The solid black line represents the 1:1 identity line.....	118
<b>Figure 4.1:</b> Average spring barley growth rates for a period of 21 days as a function of IRE and grouped by DBD for root <b>(A)</b> Vertical length <b>(B)</b> and Horizontal length <b>(C)</b> .....	130
<b>Figure 4.2:</b> Horizontal and vertical root lengths of spring barley grown for a period of 21 days and grouped by IRE for 1.4 <b>(A, D)</b> , 1.5 <b>(B, E)</b> and 1.6 <b>(C, F)</b> DBD (g cm <sup>-3</sup> ) treatments.....	131
<b>Figure 4.3:</b> Average spring barley <b>RHtRR</b> grown for a period of 21 days as a function of IRE and grouped by DBD.....	133
<b>Figure 4.4:</b> <b>RHtRR</b> of spring barley grown for a period of 21 days and grouped by IRE for 1.4 <b>(A, D)</b> , 1.5 <b>(B, E)</b> and 1.6 <b>(C, F)</b> DBD (g cm <sup>-3</sup> ) treatments.....	134
<b>Figure 4.5:</b> <b>RBCC</b> of spring barley at the end of a 21-day growth period as a function of IRE and grouped by DBD.....	136
<b>Figure 4.6:</b> <b>RTE</b> of spring barley at the end of a 21-day growth period as a function of IRE and grouped by DBD.....	138
<b>Figure 4.7:</b> Principal Component Analysis biplots for <b>A)</b> PC2 <i>vs.</i> PC1, <b>B)</b> PC3 <i>vs.</i> PC1 and <b>C)</b> PC3 <i>vs.</i> PC2.....	141

<b>Figure 4.8:</b> Principal Component Analysis 3D plot snapshot with loadings and coloured by experimental treatment.....	142
<b>Figure 4.9:</b> Least Limiting Water Range for RS substrate (A), with sub models fitted for Buescher's PR model (B) and Silva's volumetric water content model (C).....	146
<b>Figure 4.10:</b> $\bar{x} \pm s$ of RS substrate strength curves (A) and water release curves (B) for dry bulk density values of 1.4, 1.5 and 1.6 g cm <sup>-3</sup> with connecting lines for the mean values .....	147
<b>Figure 5.1:</b> Vertical root length summary graphs for a period of 21 days grouped by IRE treatment for 1.4 (X1) and 1.6 (X2) DBD (g cm <sup>-3</sup> ) treatments. The varieties used were Optic (A), Sassy (B), Derkado (C) and Golden Promise (D).....	159
<b>Figure 5.2:</b> Horizontal root length summary graphs for a period of 21 days grouped by IRE treatment for 1.4 (X1) and 1.6 (X2) DBD (g cm <sup>-3</sup> ) treatments. The varieties used were Optic (A), Sassy (B), Derkado (C) and Golden Promise (D).....	160
<b>Figure 5.3:</b> Average horizontal (A), vertical (B) and root (C) growth rates vs. IRE treatment grouped by DBD treatments. The varieties used were Optic (X1), Sassy (X2), Derkado (X3) and Golden Promise (X4).....	163
<b>Figure 5.4:</b> RHtRR summary graphs for a period of 21 days grouped by IRE treatment for 1.4 (X1) and 1.6 (X2) DBD (g cm <sup>-3</sup> ) treatments. The varieties used were Optic (A), Sassy (B), Derkado (C) and Golden Promise (D).....	166
<b>Figure 5.5:</b> Average RHtRR of spring barley grown for 21-days as a function of IRE and grouped by DBD treatment. The varieties used were Optic (A), Sassy (B), Derkado (C) and Golden Promise (D).....	167
<b>Figure 5.6:</b> RBCC spring barley at the end of a 21-day growth period as a function of IRE and grouped by DBD treatment. The varieties used were Optic (A), Sassy (B), Derkado (C) and Golden Promise (D).....	170
<b>Figure 5.7:</b> RTE spring barley at the end of a 21-day growth period as a function of IRE and grouped by DBD treatment. The varieties used were Optic (A), Sassy (B), Derkado (C) and Golden Promise (D).....	172

**Figure 5.8:** Principal Component Analysis biplots for **A)** PC2 vs. PC1, **B)** PC3 vs. PC1 and **C)** PC3 vs. PC2.....174

**Figure 5.9:** Principal Component Analysis 3D plot snapshot with loadings and coloured by spring barley cultivar.....175

**Figure 5.10:** Predicted **ARGR** vs. Observed **ARGR** plot. The non-linear curve estimates the conditional mean value and the linear segment represent the Theil-Sen regression line.....178

**Figure 6.1:** Schematic diagram of the proposed A2 sized **RS** unit **A)** Top view and **B)** Front view.....197

## List of Tables

<b>Table 1.1:</b> A list of the advantages and disadvantages of field, greenhouse and laboratory methods (Paez-Garcia <i>et al.</i> , 2015).....	33
<b>Table 2.1:</b> Basic description of the experiments described in Chapter 2.....	55
<b>Table 2.2:</b> Physical properties of the two soils used in the experiments .....	61
<b>Table 2.3:</b> Particle size distribution treatments definition table (% of total mass).....	66
<b>Table 3.1:</b> Error matrix showing the % pixel prediction errors of 5 images for the algorithms described in Section 3.3.2.....	113
<b>Table 3.2:</b> Summary goodness of fit statistics for live (FDA) and dead (PI) RBC populations.....	116
<b>Table 3.3:</b> Summary statistics for the linear regression model of the form $y = x$ .....	118
<b>Table 4.1:</b> 3-minute irrigation event timings used in each of the three levels for the experimental factor IRE.....	126
<b>Table 4.2:</b> Root growth rankings for <b>ARGR</b> , <b>AHGR</b> and <b>AVGR</b> averages across DBD and IRE treatments.....	132
<b>Table 4.3:</b> Rankings for <b>RHtRR</b> averages across DBD and IRE treatments.....	135
<b>Table 4.4:</b> Rankings for <b>RBCC</b> averages across DBD and IRE treatments.....	137
<b>Table 4.5:</b> Rankings for <b>RTE</b> averages across DBD and IRE treatments.....	139
<b>Table 4.6:</b> Principal Components Analysis (PCA) of component importance, correlations and statistical significance.....	143
<b>Table 4.7:</b> RS sand volumetric water content ( $\theta$ ), degree of saturation ( $s$ ) and air-filled porosity ( $f_a$ ) corresponding to different matric potential ( $\Psi$ ) for cores packed at a density of $1.5 \text{ g cm}^{-3}$ .....	148
<b>Table 4.8:</b> Statistically significant effects summary for variables and PC components.....	148
<b>Table 5.1:</b> Year of introduction, pedigree and breeder information for the varieties used in this experiment.....	157

**Table 5.2:** Root growth rankings for **ARGR**, **AHGR** and **AVGR** averages across DBD and IRE treatments for the varieties Optic, KWS Sassy, Derkado and Golden Promise. Values in parenthesis are the rank order in any row.....164

**Table 5.3:** Rankings for **RHtRR** (mm mm<sup>-1</sup>) averages across DBD and IRE treatments for the varieties Optic, KWS Sassy, Derkado and Golden Promise. Values in parenthesis are the rank order in any row.....168

**Table 5.4:** Rankings for **RBCC** averages across DBD and IRE treatments for the varieties Optic, KWS Sassy, Derkado and Golden Promise. Values in parenthesis are the rank order in any row.....170

**Table 5.5:** Rankings for **RTE** averages across DBD and IRE treatments for the varieties Optic, KWS Sassy, Derkado and Golden Promise. Values in parenthesis are the rank order in any row.....173

**Table 5.6:** Principal Components Analysis (PCA) of component importance, correlations and statistical significance.....176

**Table 5.7:** Statistically significant effects summary for variables and PC components.....179

**Table 6.1:** The overall responses (grand average among varieties ± grand standard deviation) of root micro-traits to the experimental treatments.....191

## List of Abbreviations and Symbols

Aeration porosity (AP)

Air filled porosity at hypoxic conditions (AFP)

Algorithm (A)

Analysis of Variance (ANOVA)

Average horizontal growth rate (AHGR)

Average root growth rate (ARGR)

Average root growth rate (ARGR)

Average vertical growth rate (AVGR)

Computed Tomography (CT)

Confidence interval (CI)

Dry bulk density ( $D_b$  or DBD)

Field capacity (FC)

Fluorescein diacetate (FDA)

Green fluorescent protein (GFP)

Horizontal growth rate (HGR)

Horizontal root length (HRL)

Image sharpness index (ISI)

Irrigation event (IRE)

Least limiting water range (LLWR)

Magnetic resonance imaging (MRI)

Minirhizotron system (RS)

Non limiting water range (NLWR)

Nuclear Magnetic resonance microscopy (NMR)

Penetrometer Resistance (PR)

Permanent wilting point (PWP)

Positron emission tomography (PET)

Principal component (PC)

Principal component analysis (PCA)

Property (P)

Propidium iodide (PI)

Red Green Blue colour model (RGB)

Root average diameter (RAD)

Root border cell count (RBCC)

Root border cells (RBCs)

Root growth rate (RGR)

Root hair to root ratio (RHtRR)

Root length density (RLD)

Root morphology (RM)

Root system architecture (RSA)

Root tip eccentricity (RTE)

Soil matric potential ( $\Psi$ )

Soil water content ( $\theta$ )

Specific root length (SRL)

Structuring element (SE)

Synchrotron radiation computed tomography (SRCT)

ANOVA test statistic (F or psi)

Total root area (TRA)

Total root length (TRL)

Vertical growth rate (VGR)

Vertical root length (VRL)

Washed root systems (WRS)

Water retention curve (WRC)

Yellow fluorescent protein (YFP)

Sample Mean ( $\bar{x}$ )

Sample standard deviation (s)

# 1. Literature review

## 1.1 Introduction

Today, there is an unprecedented need for increasing crop productivity as it is projected that global food demand will dramatically increase by 2050 (Godfray *et al.*, 2010; Tilman *et al.*, 2011). Global food security is listed as the second of the 17 Sustainable Development Goals adopted by the United Nations as part of its 2030 Agenda for Sustainable Development (United Nations, 2015). Despite arguments/perceptions that future global food demand can be sufficiently covered with current rates and “timely distributions” (World Hunger Organisation, 2016), the current projections show that the global population will reach 9.7 billion in 2050 (United Nations Department of Economic and Social Affairs, 2015). Furthermore, climate change is expected to cause yield reductions in a range of important cereal crops due to increasing temperatures (Asseng *et al.*, 2015). Thus, in order to reduce the risk of world hunger there must be a dramatic increase in food production in the next decades with a projected overall increase in food production of about 70 % between 2005/02 and 2050 (FAO, 2009).

Maximising yield requires the root systems to be of optimum size and shape to extract the required amount of water and nutrients from the growth medium. However, soils are not always an ideal environment for plant root growth. Soil physical conditions often reduce root elongation rates and restrict the soil volume occupied by the root system thus, hindering nutrient and water uptake rates with negative consequences for plant yield (Valentine *et al.*, 2012; Whiteley and Dexter, 1982). Furthermore, current agricultural practises have a range of effects on soil structure, with heavy machinery changing the pore size distribution and connectivity of the soil pore network creating water infiltration problems and yield reductions (Keller *et al.*, 2015). In addition, most crop plants have high-water requirements and are not drought tolerant, which is reflected by the fact that agricultural irrigation is estimated to account for 70 % of the total use of available freshwater (FAO and ITPS, 2015). Furthermore, many of the resources used for food production, including irrigation water and mineral fertilisers, are becoming relatively more expensive (White *et al.*, 2013), further exacerbating existing issues such as the financial inability of many farmers to purchase mineral fertilizers (Vitousek *et al.*, 2009). This is all in addition to increasing rainfall, snow and higher temperatures due to climate change causing plant stress and reducing crop yield (Srivastava

and Misra, 2018). As a result, an appreciation of how plant growth could be limited by soil physical stressors would be beneficial in future discussions (Section 1.2).

Ultimately, to mitigate the above-mentioned issues, it is vital that crops are adapted to perform better in less than optimum environments that are limited or have an excess of water and nutrients or salts. Roots are responsible for the acquisition of both water and mineral nutrients from the soil and as such, research is increasingly aiming for the manipulation of root traits which enhance root growth (Meister *et al.*, 2014). Root properties can be viewed as the product of two basic components: root system architecture (RSA) and root morphology (RM) (Nguyen and Stangoulis, 2019). RSA refers to the spatial distribution of the root system or the geometrical character of roots. An example of its significance to root growth is demonstrated by the observation that maize genotypes with shallow root systems have a higher growth rate and P accumulation relative to deep-rooted genotypes (Zhu *et al.*, 2005). RM can be defined as the study of the features of a single root axis as an organ. This term encompasses important root traits such as root hairs which influence root growth and root-soil interactions. For example, an increase in root hair length and density in low P soil concentrations is a mechanism used by wheat to increase its absorption of P (Wang *et al.*, 2016). As such, developing an understanding of how root traits can influence the ability of the root system to cope with various soil stressors is of critical importance (Section 1.3).

Unlike above ground plant components the investment in time required to study root systems is a highly limiting factor for plant breeders (Tuberosa *et al.*, 2002). In fact, apart from specific root crops such as carrot (Stein and Nothnagel, 1995) or cassava (Nassar and Ortiz, 2007), below-ground traits are rarely of primary significance to plant breeders because of the difficulty to observe them *in situ* (Ryan *et al.*, 2016). Even so, the increasing popularity of “Plant Phenomics”, a collection of methods whose aim is to link plant genotypes to plant phenotypes (Furbank, 2009) and its importance towards the advancement of plant biotechnology and crop output (Tester and Langridge, 2010) indicates an increasing recognition of the importance of the detailed study of root systems. As a result, there is a growing body of research for image-based phenotyping of plant roots which involve the optical analysis of RSA and RM to understand how roots interact with soil. These methods may be simple and straightforward such as the traditional destructive sampling of roots grown in field soil (Smit *et al.*, 2000). Other possibilities may involve an artificial system such as minirhizotrons (Upchurch, 1987). More powerful setups such as X-ray CT

(Heeraman *et al.*, 1997), have also been used successfully in the past to study the 3D RSA in constrained (plant pots) soil systems. All such methods have their own advantages (and limitations) but an appreciation of the properties of different imaging systems is nevertheless advantageous (Section 1.4).

Ultimately, it is desirable to summarise our understanding of the interaction of the soil and root systems in the form of a model which predicts root response to different soil conditions. A range of mathematical models exist in the literature today describing the system of individual roots and gradually scaling up to the more complex system case of the entire root system (Dunbabin *et al.*, 2013). Some architectural models consider the interaction between environmental and root variables such as water and nutrient transfer to the roots from soil. However, this complexity comes at a high computational cost due to their difficulty in parameterization (Dupuy *et al.*, 2010). On the other hand, continuous root distribution models are easier to manage in terms of computational complexity but it comes at the cost of not allowing for the integration of complex plant development processes (Dupuy *et al.*, 2010). However, there are also more practical models which completely lack any consideration of root processes and simply consider the influence of the soil environmental conditions on the root system such as the least limiting water range (LLWR) model proposed by da Silva *et al.*, (1994). This concept describes the soil system in the form of three soil stressor variables: penetrometer resistance (PR), soil matric potential ( $\Psi$ ) and aeration porosity (AP). It also uses a set of assumptions concerning the limiting values at which plant growth effectively stops for each of the previously mentioned variables, namely the soil matric suction at -0.01 MPa and -1.5 MPa, soil penetration resistance at 2 MPa and soil oxygen concentration at a porosity of 10 %. The output of LLWR is a prediction of the soil moisture range for which plants should be less limited in terms of growth, in a particular soil. Unlike computationally demanding models such as architectural ones (Dupuy *et al.*, 2010), the practical definition of the LLWR makes the model computationally feasible as it only requires knowledge of the water release and soil strength curves of the soil. The LLWR decreases with increasing soil bulk density, increasing clay content, and decreasing organic matter content (da Silva and Kay, 1997) As a result, LLWR is used as an index-like variable that can help assess how different soil management practices can affect the potential productivity of the soil (Tormena *et al.*, 1999). However, the same succinctness that is responsible for its wide use also restricts its prediction accuracy because it doesn't consider the plant response beyond the simplistic assumptions concerning the limits of plant growth. The LLWR is also not an explicit RA

growth model. The concept of LLWR is the main theme of this project and as such, a more detailed assessment of the model is a pre-requisite for understanding the motivation behind the work presented in later chapters (Section 1.5).

## **1.2 Soil physical stressors**

### **1.2.1 Drought**

Drought stress is believed to be the most lethal abiotic stress affecting crops, negatively impacting plant growth, physiology, and reproduction (Barnabas *et al.*, 2008). Between 1980 to 2015 it was estimated that on a global scale drought caused a yield reduction of up to 40 % and 21 % for maize (*Zea mays* L.) and wheat (*Triticum aestivum* L.) respectively (Daryanto *et al.*, 2016). Considering that average temperature is projected to increase by at least 0.2°C per decade (IPCC, 2014) and with simulations suggesting that important cereal crops such as wheat will have a yield reduction of 6 % per 1 °C rise in temperature (Asseng *et al.*, 2015) drought stress will certainly be a challenge for future food security.

Plants begin to experience drought stress when either the water supply to the roots is sufficiently reduced or plant transpiration becomes sufficiently high that the roots cannot supply the water that is being lost (Anjum *et al.*, 2011). Water limitation restricts cell growth due to the loss of cell turgor which decreases cell volume and makes cellular contents more viscous (Taiz and Zeiger, 2006). Therefore, there is an increased frequency in protein-protein interactions causing their aggregation and denaturation with catastrophic consequences for cells (Hoekstra, 2001). In the initial stages of plant growth drought stress reduces seed germination rates and limits seedling growth (Kaya *et al.*, 2006; Teixeira *et al.*, 2020). In more mature plants the plant response of leaf stomatal closure to limit water loss also reduces the CO<sub>2</sub> availability leading to an increased risk of photo-damage and reduced photosynthesis (Lawlor and Cornic, 2002). As a result, there is an enhanced production of reactive oxygen species such as H<sub>2</sub>O<sub>2</sub> which cause lipid peroxidation leading to chlorophyll degradation (Foyer *et al.*, 1994). Reduced transpiration rates also increase heat stress further disrupting photosynthesis through disruption of photosynthetic pigments (Camejo *et al.*, 2006), inhibition of photosystem II (Camejo *et al.*, 2005) and reduced RuBP regeneration capacity (Wise *et al.*, 2004). Leaf expansion is also limited under drought conditions because of the reduction in turgor pressure and photosynthetic rates (Rucker *et al.*, 1995). In addition to the above, nutrient uptake can be dramatically reduced during drought because many nutrients are dissolved in the soil water solution and as such, their rate of diffusion is decreased

(Barber, 1995). The reduction in transpiration flow also reduces nutrient transport to the shoots (Garg, 2003). For example, reductions in N and K uptake under drought stress was demonstrated in cotton (McWilliams, 2003) and reduced P tissue concentrations in beech (Peuke *et al.*, 2002). Grossman and Takahashi, (2001), remarked how nutrient limitations under drought conditions are also related to reduction in energy availability because of the energy dependant processes required to convert nutrients in plant available forms. Drought stress also indirectly influences plant nutrition by reducing soil microbial diversity and activity which can disturb plant-microbial nutrient associated relations (Schimel *et al.*, 2007).

### **1.2.2 Soil Oxygen**

Approximately 10 % of cultivated land surface suffers from poor drainage and waterlogging (Koevoets *et al.*, 2016). This issue will likely worsen in the future as climate change is projected to increase the frequency and severity of floods (Trenberth, 2011). At 25 °C the diffusion coefficient of O<sub>2</sub> is 0.176 cm<sup>2</sup> s<sup>-1</sup> (Cussler, 1997) and as such, the surface layers of soil are usually well oxygenated, even if wet, although, the effective diffusion coefficient is less than that of air due to the tortuous nature of the soil pore network (Whitmore and Whalley, 2009). However, in water the diffusion coefficient of O<sub>2</sub> is dramatically reduced to only 2.10 x 10<sup>-5</sup> cm<sup>2</sup> s<sup>-1</sup> (Cussler, 1997). This is highly problematic for roots as limitations in oxygen supply effectively halt root growth (Gibbs *et al.*, 1998). Non-photosynthetic plant tissues such as roots normally use aerobic respiration however, under hypoxic or anoxic conditions roots switch to the (inefficient) anaerobic pathway of glycolysis to generate ATP leading to a severe reduction in energy available for maintenance, growth and ion uptake (Koevoets *et al.*, 2016). Furthermore, anaerobic respiration produces a range of by-products which are dangerous for cells because when protons accumulate in the cytoplasm and the vacuole there is sharp decrease in cell pH (Gerendás and Ratcliffe, 2002). In addition to the above, anoxic conditions induce the plant to increase the rate of the stress signalling hormone ethylene by more than 5-fold as compared to normal conditions (Mancuso and Marras, 2006) which will have negative consequences for the above ground components of the plant by inhibiting the elongation of cells in the elongation zone (Voesenek, 2013). Roots also secrete phytotoxic compounds like ethanol under low O<sub>2</sub> conditions to help prevent cell damage caused by flooding (Badri and Vivanco, 2009). In combination with the anaerobic products released by soil microbes there is an accumulation of phytotoxic compounds in waterlogged soils (Armstrong and Gaynard, 1976).

### 1.2.3 Soil mechanical impedance

From a mechanics point of view, roots are a complex material, being neither completely plastic nor completely elastic or viscous but having features of all three kinds of materials (Niklas, 1992) and as such, their response to mechanical stress is also a complex one. Mechanical impedance, a measure of motion resistance to an external force, decreases the rate of root elongation because it reduces the rate of cell division in the root meristem, and decreases cell expansion (Bengough and Mullins, 1990). As a result, mechanical impedance is almost always associated with lower shoot growth and ultimately, reduced crop yield (Whalley *et al.*, 2008). A widely used measure of the mechanical impedance that roots experience in soil is penetrometer resistance (PR) (Whalley *et al.*, 2007), with values of e.g., - 2 MPa causing a 50 % reduction in maize (Bengough *et al.*, 2011). Considering that soil PR values of 0.5-1.0 MPa and greater are commonly reported, mechanical impedance is responsible for significant reduction in root elongation rates (Bengough and Mullins, 1990; Valentine *et al.*, 2012). Furthermore, given the projected increase in average temperature (IPCC, 2014), roots will experience a higher frequency in mechanical impedance because as the water content of the soil is reduced its strength increases (Whalley *et al.*, 2005).

An increase in mechanical impedance reduces root numbers (Iijima and Kono, 1991), root axial growth and root length which results in an overall reduction in the size of the root system (Colombi *et al.*, 2017). Furthermore, it makes the root cortex thicker because it increases cell numbers (Colombi *et al.*, 2017) and causes an increase on the radial dimension of cells (Atwell, 1988). Additionally, cell numbers in the stele are also increased as its diameter increases (Bengough and Mullins, 1990). Chimungu *et al.*, (2015), analysed root anatomical phenes in maize and concluded that cortical thickness is a better predictor of root bending compared to root diameter with a similar conclusion made for stele diameter as a predictor for root tensile strength. In addition to the above, it was demonstrated that in barley roots there are significant reductions in the content of cellulose and hemicellulose and an increase in lignin concentration in root tissue in response to increase mechanical impedance (Bingham *et al.*, 2010). In contrast, reduced lignin concentrations were reported for maize roots in similar circumstances (Degenhardt and Gimmler, 2000). The influence of mechanical impedance extends beyond roots and affect the entirety of the plant (Tardieu, 1994) as plant shoots experience reduced growth rates and length (Kobaissi *et al.*, 2013), and dry weight (Donald *et al.*, 1987). Leaves also experience reduced growth rates (Iijima and Kono, 1991) and they may even induce stomata closure as a result of mechanical stress (Roberts *et al.*,

2002). Furthermore, several indirect effects can occur in the form of water and nutrient stress because changes in root morphology and architecture influence the plants ability to acquire water and nutrients (Yamauchi, 1993). For example, Chimungu *et al.*, (2014), demonstrated that a larger root cortical cell size could improve drought tolerance in maize (*Zea mays*). A reduction in net photosynthetic rate, transpiration rate and stomatal conductance was demonstrated in triticale and maize plants (Grzesiak, 2009).

It should also be noted that there is an inverse relationship between soil water concentration and mechanical impedance. This is because a drying soil experiences an increase in the total force of the capillary component which leads to reductions in soil matric potential and ultimately, an increase in soil strength (Whalley *et al.*, 2005). This nonlinear, inverse relationship results in roots experiencing greater mechanical impedance which will limit the growth of the entire root system and as such stresses can interact to produce a greater negative effect on crops (Bengough *et al.*, 2011).

## **1.3 Root traits**

### **1.3.1 Roots**

Roots are a plant organ of high significance because they are mainly responsible for the growth and survival of plants (Lynch, 1995). Although root systems demonstrate a high plasticity the roots of higher plants can be classified into roots derived from the embryo (embryonic roots) and those formed after germination from existing roots or non-root tissues (post-embryonic roots) (Atkinson *et al.*, 2014). In general terms, root systems consist of four different types of roots (Wasaya *et al.*, 2018):

1. Coarse/tap roots (first root or roots to emerge from the seed)
2. Lateral/fine roots (any root branching from another root)
3. Shoot-borne roots (roots which arise from shoot tissues)
4. Basal roots (roots which develop from the hypocotyl).

Coarse roots provide the structural basis for anchorage of the plant, the establishment of the basic root system architecture and control the rooting depth (Henry *et al.*, 2011). Fine roots are potentially less important as a structuring block, but their high permeability nature makes them highly significant for absorbing water and nutrients (Comas *et al.*, 2012), especially in herbaceous plants (Fitter, 2002). This is mainly because fine roots increase the root surface area per unit mass (Landi, 2010). In the case of cereals, the root system consists of the

following root types: the embryonic primary or seminal roots, and the post embryonic shoot borne crown roots (Hochholdinger *et al.*, 2004). The crown roots are separated from the embryonic roots by the mesocotyl, which elongates to place the shoot base close to the soil surface (Singh *et al.*, 2010).

Root structure in cereals can become highly complicated with different structural zones along the root profile formed by a series of cell elongations and differentiations with the overall root ability to survive and grow in harsh environments being dependents on physiological responses. **Figure 1.1**, contains root cross sections for monocot (A) and dicot (B) plants, demonstrating the differences between them such as a well-developed pith for monocot plants.

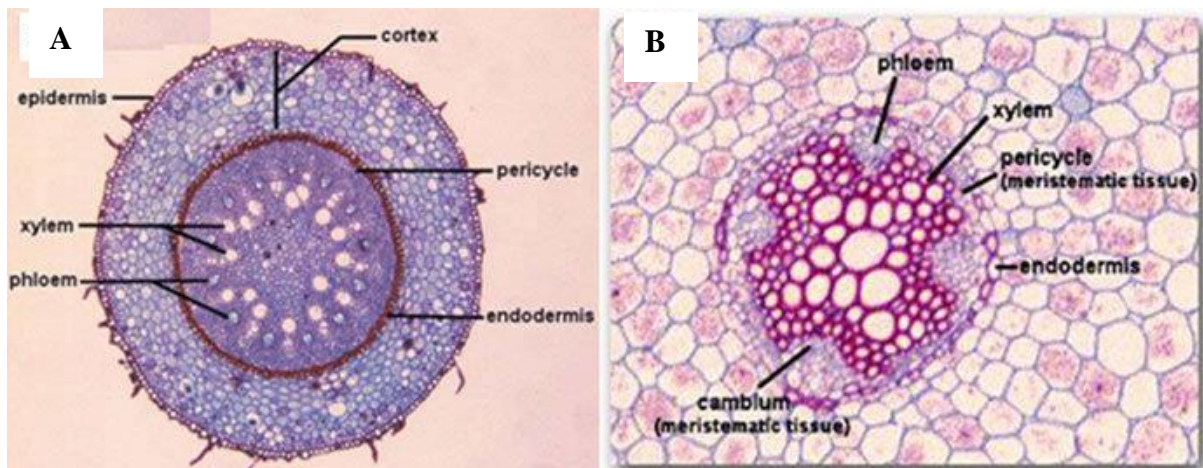


**Figure 1.1:** Schematic diagram showing the root cross sections of a monocot (A) and a dicot (B) (taken from: [https://www.researchgate.net/figure/Anatomy-of-typical-a-monocot-and-b-dicot-root\\_fig2\\_278689094](https://www.researchgate.net/figure/Anatomy-of-typical-a-monocot-and-b-dicot-root_fig2_278689094)).

Details of the cellular dynamics involved in root growth will not be discussed here, instead the reader is directed to the numerous excellent reviews in the literature (e.g., Smith and de Smet, 2012). Instead, root traits will be introduced here as they are critical for the absorption of water and nutrients (Narayanan *et al.*, 2014) and are a central theme of this study. Root traits can be defined as “any morphological, physiological or phenological feature of the root system measurable at the individual level, without reference to the environment or any other level of organization” (Violle *et al.*, 2007). However, in practise root traits are influenced by both the surrounding environment and the underlying plant genetics.

### 1.3.2 Root system architecture (RSA)

RSA expression is complex and is affected by various environmental factors such as soil strength, temperature, moisture, nutrients, soil pH (Robbins and Dinneny, 2015) and plant genotype. Despite its complexity, RSA adjustments are of immense importance for the survival and growth of the plant (Smith and De Smet, 2012). For example, Hammer *et al.*, (2009), demonstrated that RSA was strongly correlated with biomass production and could help explain the increase in yield of maize (*Zea mays* L.) observed historically in the U.S.. Selective plant breeding for increased yield has resulted in dramatically transformed the phenotype of wheat with modern varieties having an enhanced ability to absorb soil nitrogen reflected by an enhanced nitrogen nutrition index (Sadras and Richards, 2014). The same process was used in the UK to increase radiation-use efficiency, biomass, and nitrogen uptake of wheat in recent decades (Shearman *et al.*, 2005). In a similar manner, selective plant breeding and agronomic adaptations in the water and nitrogen restricted soils in Australia have increased wheat yield per unit transpiration at a steady rate of  $0.12 \text{ kg ha}^{-1} \text{ mm}^{-1} \text{ yr}^{-1}$  during the last century (Sadras and Lawson, 2013).

Since roots are primarily responsible for water absorption it is not surprising that significant efforts have been made to determine how RSA affects drought resistance. Drought reduces the soil matric potential and as a result, roots experience osmotic stress as they have to use more energy to remove the water from the soil. If the soil water potential is sufficiently reduced, then hyper-osmotic stress might occur causing water losses from root to the soil (Koevoets *et al.*, 2016). This leads to loss of turgor in plant cells and plasmolysis, i.e., the violent detachment of the living protoplast from the cell wall (Lang *et al.*, 2014). In order to avoid this catastrophic outcome, plants can induce several changes in RSA. For example, drought conditions promote the production of many lateral roots and root hairs that increase the total surface area of the root system and enhance its water absorption capacity (Agbicodo *et al.*, 2009). The diameter of roots also influences their ability to extract water (Richards *et al.*, 2001) and affects their capacity to penetrate through deeper soil layers (Bao *et al.*, 2014). A RSA with smaller root diameter and length of fine roots is believed to be better equipped to tolerate drought conditions as a higher root length density in deep soil layers (30-45 cm) was beneficial (Henry *et al.*, 2011). Roots also possess the ability to actively seek out water reserves, a phenomenon known as hydrotropism (Dietrich, 2018).

One RSA strategy to mitigate drought stress involves deep rooting as a deeper root system enables the uptake of water from deeper soil layers (Boyer, 1996). A high root density and root depth are desirable traits in low water environments (Zhao *et al.*, 2004). Researches are also actively trying to identify the genes associated with the expression of higher rooting depth. High drought tolerance was associated with the deeper rooting mutant extremely drought tolerant1 of the model plant *Arabidopsis thaliana* (Yu *et al.*, 2008). This was because the mutant had an overexpression of the HD-ZIP transcription factor HDG11 which promoted the production of proteins that stimulate root elongation thus, leading to a higher rooting depth (Xu *et al.*, 2014). In rice, the gene DEEPER ROOTING1 was demonstrated to increase rooting through alterations in the auxin distribution (Uga *et al.*, 2013). Likewise, expression of the DEHYDRATION RESPONSE ELEMENT B1A in groundnut (*Arachis hypogaea* L.), increases rooting depth (Lobet *et al.*, 2014). However, authors have cautioned that the extent to which any root trait contributes to plant drought resistance is strongly dependent on the drought scenario considered (Tardieu, 2012). More recently, Lobert *et al.*, (2014), pointed out how experiments with chickpea (*Cicer arietinum* L.) (Zaman-Allah *et al.*, 2011) and wheat (Schoppach *et al.*, 2013) suggest that drought tolerance was more related to a conservative use of water throughout the season rather than deep rooting *per se*.

RSA is also identified to be of high importance in nitrogen uptake efficiency (Comas *et al.*, 2012). An RSA composed of traits such as steeper root growth angles, reduced production of crown roots and reduced lateral root branching density are believed to enhance N uptake (Lynch, 2019). In a similar manner, RSA can enhance phosphorus absorption an essential component for numerous metabolic processes (Raghothama and Karthikeyan, 2005). An RSA response that is believed to facilitate phosphate absorption is the development of a shallower root system to explore the upper soil layers where phosphate tends to accumulate (Lynch and Brown, 2001). This will require a higher investment in lateral root production which is preferable in terms of cost because they have lower phosphate requirements in comparison to primary roots (Zhu and Lynch, 2004). A shift to a shallower rooting system was observed in experiments involving *Arabidopsis* (Péret *et al.*, 2011; Karley *et al.*, 2011).

Other RSA responses could include the ability of roots to detect and direct root growth along soil biopores which offers an advantage to the penetration of structured subsoils (McKenzie *et al.*, 2009). In a similar manner, the angle of the root when it penetrates the soil can be important for determining whether root penetration will occur, with near vertical angles giving an advantage (Dexter and Hewitt, 1978).

### 1.3.3 Root Hairs

Root hairs are a common anatomical characteristic of most vascular plants which can dramatically increase the surface area of roots (Jones and Dolan, 2012). In more precise terms, they are extensions of trichoblasts, specific root epidermal cells which develop in the maturation zone of the root tip (Taiz and Zeiger, 2006). In general, root hairs are characterized by a rapid growth rate of  $1 \mu\text{m min}^{-1}$  (Grierson and Schiefelbein, 2002) and a short life cycle, with cytoplasmic disintegration reported to occur after 2-3 days (Johnson *et al.*, 2001). Nevertheless, root hairs play a central role in the survival and growth of plants because of their numerous functions. They influence the uptake of both nutrients and water (Gilroy and Jones, 2000) with the root hair zone being the most active zone for fluid transfer in the root system due to its high permeability (Segal *et al.*, 2008). Experiments comparing the water uptake between wild-type barley and the barley mutant *brb* lacking root hairs demonstrated that wild-type barley had a much higher water uptake (Carminati *et al.*, 2017). This was attributed to the ability of root hairs to substantially reduce the rate of matric potential reduction at the root-soil interface in rapidly transpiring plants by increasing the degree of physical contact between roots and soil which influences water uptake (Carminati *et al.*, 2009).

Another function of root hairs is to enhance the ability of the roots to efficiently extract phosphorus from the soil (Keyes *et al.*, 2013). Phosphate uptake is a topic that has received considerable attention as it is a crucial component of nucleic acids and membrane phospholipids in plants. Bayuelo-Jiménez *et al.*, (2011), performed a large screening experiments with 242 accessions of maize on high and low phosphate concentration treatments and found a positive correlation between root hair density and biomass for low phosphate treatments. Experiments with *Arabidopsis* mutants lacking root hairs demonstrated a lower phosphorus uptake compared to wild type plants when grown in low-phosphorus conditions (Bates and Lynch, 2000). In a similar manner, Gahoonia *et al.*, (2001), demonstrated that barley mutants lacking root hairs could only absorb half the amount of phosphate compared to a wild type. Results reported by Gahoonia and Nielsen, (2004), suggest that root hair length is also a significant factor for phosphate uptake in low phosphate conditions. Furthermore, they are often the point of infection for the symbiotic association between legumes and rhizobia bacteria (Peterson and Farquhar 1996). In general, the density and length of root hairs are also shown to have considerable variability in response to P availability (Bates and Lynch, 1996), soil water regime and soil compression (Haling *et al.*,

2014) which is significant, because root hair density and length are thought to have significant potential in plant breeding (Brown *et al.*, 2013).

Root hairs also influence soil structure. The role of root hairs on pore structure development at the root-soil interface during the early stage of crop establishment was clearly demonstrated by Koebernick *et al.*, (2017), in an experiment with synchrotron radiation computed tomography. Moreno-Espindola *et al.*, (2007), also demonstrated how in sandy soils, root hairs helped enhance soil adhesion to roots. Furthermore, they are believed to improve soil penetration and root soil contact (Haling *et al.*, 2013), especially in compact soils (Lynch *et al.*, 2014). There is also evidence that they can offer enhanced mechanical anchorage to the plant (Bengough *et al.*, 2016; Haling *et al.*, 2014). Czarnes *et al.*, (1999), reported that maize root hairs contributed significantly to root-soil adhesion. Rebecca *et al.*, (2013), also demonstrated that barley genotypes absent of root hairs had a reduced ability to penetrate compacted soil. However, perhaps this effect is more localized as it did not scale up to the whole root system level in an experiment comparing the pullout resistance of hairless *Arabidopsis* mutants with wild types (Bailey *et al.*, 2002).

### **1.3.4 Root cap**

The root cap covers the root tip and as such, it represents the first point of contact between root and soil. It protects the meristem of the root tip from abrasion and the stresses exerted on it by the soil and determines the direction of root growth (Bengough and McKenzie, 1997). Root caps are demonstrated to have significant role over the root's ability to sense and respond to external stimuli, i.e., tropisms. This ability is crucial for reducing root abiotic stress. Experiments involving the removal of the root cap inhibit the ability of the root to sense gravitropism in plants such as *Arabidopsis*, maize and rice (Fujii *et al.*, 2018). In a similar manner, roots can sense and grow towards water, this is termed as "hydrotropism". *Arabidopsis* roots can distinguish a wet from a dry surface and induce a preferential growth response towards the wet surface (Bao *et al.*, 2014). Interestingly, there is also evidence that hydrotropism is not regulated by root tips for species such as *Arabidopsis* (Nakajima *et al.*, 2017), rice (Dietrich *et al.*, 2017) and cucumber (Fujii *et al.*, 2018) but, the mechanisms responsible are not yet known. Plants were also demonstrated to be able to redirect root growth away from higher salt concentrations, i.e., halotropism (Galvan-Ampudia *et al.*, 2013). Svistoonoff *et al.*, (2007), demonstrated that root tips of *Arabidopsis thaliana* were

able to detect the low phosphate concentration of the medium when it came into physical contact with it and subsequently, induced a halt in the growth of the primary root.

The root cap is also of great importance in influencing the root's ability to penetrate soil. For example, it was demonstrated recently that the geometry of the root tip itself influences the probability of a root to penetrate the soil (Colombi *et al.*, 2017). This is because the shape of the root tip influences cavity expansion pressure (Bengough *et al.*, 2011), a more pointed root tip enables cylindrical deformation of soil which is more efficient compared to spherical deformation of soil which is common for blunter shapes (Bengough *et al.*, 1991). Kirby and Bengough, (2002), used a finite-element method to predict the stresses around a simulated root and demonstrated that peak stress occurs in the soil adjacent to the apex of the root cap. Removal of the root cap in maize roots grown in a compacted sandy loam soil was demonstrated to halve their elongation rate as a result of the increased root PR resistance, from 0.31 MPa to 0.52 MPa (Iijima *et al.*, 2003). Vollsnes *et al.*, (2010), compared the growth of the primary roots of a mutant maize after the root cap had been removed with that of primary roots of a normal wild-type maize. Elongation rates for the roots of the mutants without a root cap was slower than that of the roots of the wild type (although the unimpeded roots elongated at the same rate), and the nature of the soil deformation around the root tip was quantifiably changed.

### **1.3.5 Root Border Cells**

Root border cells can be defined as “the cells that disperse into suspension within seconds when root tips are placed into water” (Hawes, *et al.*, 2000). These cells are originally derived from root cap meristematic cells and after a series of cell differentiations they physically separate from the root cap (Feldman, 1984). They are believed to be an important mechanism that prevents microbial and soil fauna attacks to the roots (Hawes *et al.*, 2000; Humphris *et al.*, 2005). Furthermore, their production and excretion from plant root caps can have a very strong influence on the penetration of plant roots in soil as they can potentially decrease the friction between roots and soil and thus, help them overcome soil mechanical restriction (Mckenzie *et al.*, 2013). Mckenzie *et al.*, (2013), demonstrated that the mucilage-border cell matrix around the root tips reduced the coefficient of root-soil friction to about 0.12-0.26 which was slightly larger than the 0.05-0.15 range of boundary lubricants. This is further supported by the reduced elongation rate of mutant maize with a removed root cap relative to wild-type maize in strong soil conditions which suggested a lubricating effect around the root

tip (Vollsnes *et al.*, 2010). An increase in mechanical impedance increases the rate of border cell and mucilage production to further decrease root-soil friction (Iijima *et al.*, 2000). More recently it has been demonstrated that the mucilage in seeds subjected to water stress, helps reduce their water potential during germination and reduces seed mortality (Teixeira *et al.*, 2020).

The border cell-mucilage matrix also influences soil structure in the rhizosphere. The soil of the rhizosphere normally forms a structure referred to as “rhizosheath”, a layer of strongly bound and more aggregated soil that adheres firmly to the root surface (Koebernick *et al.*, 2017). The dimensional extent and chemical composition of the rhizosheath can be rather variable between species (Brown *et al.*, 2017) and between genotypes of the same species (George *et al.*, 2014). Root exudates and microbially released compounds are known to contribute to its formation by binding soil particles together and increasing the overall stability of the rhizosphere (Hallett *et al.*, 2009). This complex interaction between root exudates, microbial activity and variations in soil water potential can induce significant changes in soil structure (Hinsinger *et al.*, 2009).

## **1.4 Root phenotyping**

### **1.4.1 Overview**

Root traits are essential for plant survival and growth. Unfortunately, unlike other easily accessible plant organs such as the stem and leaves or small embryo seeds, the imaging of undisturbed root systems is a more complicated process due to the opacity of soil. Nevertheless, as was pointed out by Walter *et al.*, (2015), the ability to link plant genotypes and root system architecture (RSA) is dependent on the detailed measurement of root phenotypes. This has motivated the development of numerous techniques able to provide information about the root system. Such methods may be indirect such as the estimation of root biomass with the use of empirical models (Hendricks *et al.*, 2006) or nutrient budgets (Kurz *et al.*, 1996). More commonly however, methods tend to involve the direct measurement of the root system. These methods can be grouped in terms of the experimental conditions under which the roots were grown (Paez-Garcia *et al.*, 2015) and include field, greenhouse/glasshouse and laboratory settings. Each of those methods has advantages and limitations (**Table 1.1**) with the choice of the method to be used being ultimately dependant on the root traits of interest, cost and time constraints. In general, there is a reduction in reproducibility, and increase in labour and time required when transitioning from a lab-based

setting to the greenhouse and the field with difficulties in the reliability of results increasing depending on the distance of the experiment from field conditions, as ultimately, the majority of modern agriculture still grows plants under field-based soil conditions.

**Table 1.1:** A list of the advantages and disadvantages of field, greenhouse and laboratory methods (Paez-Garcia *et al.*, 2015).

	<b>Advantages</b>	<b>Disadvantages</b>
Field	Accurate representation of field conditions Mature stages of plant growth	Labour intensive Time consuming Difficult to replicate Destructive sampling Highly limited imaging
Green/Glass house	Closer to field conditions when soil/sand is used Faster relative to field Good replication Imaging of roots possible	Imaging is more limited relative to laboratory methods Limited reflection of field conditions Destructive sampling
Laboratory	Low cost Time savings Non-destructive Easy to replicate Allows easy and detailed imaging of roots	Inaccurate reflection of field conditions due to the absence of soil, environmental conditions and soil biota. Restricted to early growth stages

### 1.4.2 Field based methods

One of the most traditionally used technique to assess root structure in the field is the trench profile technique, involving the careful removal of soil with fine brushes from the sides of the plant and subsequently drawing of the root system along the soil profile (Nielsen *et al.*, 1997). The obvious disadvantage of this classical method is the rather significant investment in both time and labour which prevents it being high throughput. This limitation motivated the development of methods that required less time and effort such as the soil coring method which use a tractor mounted hydraulic soil corer to push soil tubes into the soil that are then

extracted to assess root density and depth (Wasson *et al.*, 2014). More recently, this method was improved by introducing technological components such as UV illumination and fluorescence spectroscopy to automatically acquire soil core images with a superior root contrast and thus, make the process more efficient (Wasson *et al.*, 2016). Although, this method offers greater speed compared to traditional root excavation methods it is unfortunately still rather time-consuming and destructive for high-throughput root assessment. Other options such as ingrowth cores or pinboard excavation of root systems (do Rosário *et al.*, 2000) have similar limitations. Trachsel *et al.*, (2011), suggested the use of “shovelomics” as a potentially high-throughput method for root phenotyping of field grown plants. The process involves soil excavation around the plant so that it remains in the centre of the surface. The roots are subsequent washed gently, placed on a phenotyping board and scored through visual assessment. An experienced team was reported to require two minutes to visually score a rootstock. However, like other field based methods the protocol involves destructive sampling of roots which destroys the root architecture and is also labour intensive to implement (Downie *et al.*, 2015). Furthermore, the subjective assessment of roots through visual assessment rather than an objective approach could also introduce systematic errors. Although, in recognition of that limitation the method was later updated by replacing the visual scoring with manual measurements at the cost of a higher time requirement although no updated estimates were reported (Trachsel *et al.*, 2013).

As mentioned above, field-based root sampling methods have the intrinsic limitation of destroying the root system architecture. The desire to observe undisturbed root growth in field soil over time appears to date back to at least the early 1900s (McDougall, 1916). One development that was proposed as a solution to the above problem was the introduction of rhizotrons. Rhizotrons are underground enclosures with transparent windows that enabled the repeated, non-destructive, *in situ* measurement of field grown roots that lie on the soil-transparent-window interface. Rhizotron observation facilities were described in detail by authors such as Soileau *et al.*, (1974). More recently developed facilities such as rhizolysimeters (Eberbach *et al.*, 2013) are very similar in principle although, significantly more elaborate compared to early rhizotron prototypes since they enable monitoring of soil water concentration, soil solute sampling and allows for placement of minirhizotron tubes to monitor root growth. However, the development of such a facility inevitably requires significant effort and financial investment. This motivated the development of minirhizotrons which are effectively scaled down versions of rhizotrons in the form of transparent tubes

installed in the soil. According to Upchurch, (1987), minirhizotrons were originally proposed by Bates in 1937. Modern minirhizotrons systems consist of Plexiglas that contain small cameras that obtain 2D images around the transparent surface tubes and are a practically feasible option for repeated, non-destructive, *in situ* measurement of field grown roots (Johnson *et al.*, 2001). Studies as early as the 1980s which compared traditional field soil core sampling and minirhizotrons had concluded that the minirhizotron scheme was both time-efficient and non-destructive in nature for obtaining estimates of root length densities (Vincent *et al.*, 2017). However, several studies (Samson and Sinclair, 1994; Joslin and Wolfe, 1999; Taylor *et al.*, 2014) demonstrated that the installation process for minirhizotrons disturbs the soil. The installation process of minirhizotrons may also cause soil compaction, introduce light and affect soil processes (Vamerali *et al.*, 1999) and also influence root growth (Joslin and Wolfe, 1999). The alteration of root paths before and after the installation of a minirhizotron was also clearly demonstrated by Itoh, (1985). Furthermore, the time required in constructing and setting up multiple minirhizotron can be a major factor in deterring their widespread use (Eshel and Beeckman, 2012). The most intrinsic limitation of rhizotrons and minirhizotrons is that a fraction of the root system will always not be in contact with the transparent surface and as such, not all the root system can be imaged.

### **1.4.3 Greenhouse based methods**

One of the most widely used techniques for root phenotyping in greenhouse experiments is the growth of seedlings in pots filled with soil packed at a range of bulk densities (Taylor and Ratliff, 1969; Courtois *et al.*, 2000). The obvious advantage of using soil as a substrate is that it more closely resembles field soil conditions compared to horticultural sand but at the cost of reduced reproducibility, more labour and time required for root washing during destructive sampling. Alternatively, gravel mixtures are commonly used as a substrate in pot experiments (Goss, 1977). They have the advantage that they have physical properties closer to soil in comparison to laboratory-based methods while being easier to replicate compared to soil. Root washing is also significantly faster compared to soil grown roots. More recently, an improvement to the pot system was proposed in the form of clear pots which are transparent pots that allow root imaging of the root fraction in contact with the transparent surface, similar to minirhizotrons (Richard *et al.*, 2015). The disadvantage of this method is that it is restricted to the early, embryonic root system and is labour intensive to mount the pouches on the imaging station and open opaque foil covering the roots (Le Marié *et al.*, 2014)

Another approach is growing roots inside nutrient solutions, i.e., hydroponics. Hydroponics is perhaps more relevant for root phenotyping than agar systems in the sense that the method is widely used in greenhouse cultures. They were used in the past to study the effect of oxygen deficits on roots through reduced oxygen flow (Pitman, 1969). The manipulation of the concentration of an osmotic solute e.g. polyethylene glycol, can also be used to induce water stress (Whalley *et al.*, 1998). The advantages of hydroponics are that root growth occurs in 3D, enable easy imaging of the roots, replication, root harvesting and allow for the measurement of root exudates (Mathieu *et al.*, 2015). High-throughput hydroponics-based systems were developed such as the one presented by Pineros *et al.*, (2015), who used a support system inside the hydroponics to retain the 3D root architecture in rice and help determine the genes associated with root architecture. However, the environment available to roots is still absent of any physical structure and the distribution of nutrients and oxygen is by default homogenous making this method unrealistic for extrapolating to field soil. Hybrids of minirhizotron and hydroponics (rhizoponics) were also developed, being submerged minirhizotrons consisting of a nylon fabric and supported by an aluminium frame (Mathieu *et al.*, 2015). It is also possible to grow roots without any substrate, i.e., aeroponics, by spraying them regularly with nutrient solution (Zobel *et al.*, 1976) but this method has similar advantages and disadvantages to hydroponics although, roots can be more similar to field soil in terms of anatomical structure (Redjala *et al.*, 2011).

It should also be noted that both minirhizotron systems (Nagel *et al.*, 2012) and X-ray CT (Paya *et al.*, 2015) can be used in greenhouse settings in addition to its usual laboratory setting (in section below).

#### **1.4.4 Laboratory based methods**

The most widely used method for studying seedling roots is using agar or plates that contain clean gels (Clark *et al.*, 1999; French *et al.*, 2009) as a medium for 3D root growth. High-throughput completely automated systems using petri dishes have been used in the past (Subramanian, Spalding and Ferrier, 2013). Its popularity stems from its easily replicated nature, low cost, high transparency and keeping roots in place so that they don't overlap. However, its artificial nature is not a realistic depiction of root growth in soil because roots grow in a well-lit environment absent of heterogeneous physical structure and often high in both sucrose and humidity. Furthermore, space is usually limited and the process of keeping the agar free of pathogens is laborious. However, authors have proposed

improvements for the agar system, for example, the D-Root system developed by Silva-Navas *et al.*, (2015), removes non-intrinsic limitations such as light exposure by shielding roots from light. Extensions to 3D have also been made by using digital cameras and rotating an agar-filled Petri dish to obtain 3D images of seedling roots (Nagel *et al.*, 2009). Similar systems involve the placing of the seedling in a glass cylinder that contains “gellan gum” (Phytigel powder dissolved in water). This enables an automated imaging process by simply rotating the cylinder and taking images at different time intervals to reconstruct the 3D root architecture (Iyer-Pascizzi *et al.*, 2010). Nevertheless, it was demonstrated that when comparing these artificial substrate based systems with more realistic plant growth media like sand there are significant differences in root morphological traits (Clark *et al.*, 2011). This example serves to illustrate the importance of studies that are as close as possible to the desirable system, i.e., field soil. More recently, Pineros *et al.*, (2016), reported that as a result of the time required to prepare the agar, the lack of growth for some species and the risk of fungal infection the system was redesigned. This time the 3D system was hydroponics based and the seedling grows between a rotatable structure composed of Acrylonitrile butadiene styrene plastic mesh disks. Although, the root architecture did appear to be similar to “gellan gum” there were again observable differences when compared with “Turface” which is a material that has a physical structure aspect to it.

Another popular high-throughput method involving artificial media is the use of simple germination paper to grow seedlings in a pseudo-3D system that is sprayed with nutrient solution (Bonser *et al.*, 1996). Germination paper is cheap, easy to use, highly reproducible and enables very easy 2D imaging of the exposed root system, especially when coloured germination paper is used to increase root contrast (Hund *et al.*, 2009). Hybrids of minirhizotron that use coloured germination paper (rhizoslides) are also in use today (Le Marie *et al.*, 2014) However, its artificial nature raises similar concerns with the agar/gel systems.

Other 3D imaging methods like laser scanning (Fang *et al.*, 2009) are also in use today but they require simple transparent media, are expensive to use and currently demand long imaging times. It should also be mentioned that attempts to create more realistic substrates have been made and which allow 3D imaging. One such example involves the so called “transparent soils” which are particles of “Nafion”, a sulfonated tetrafluoroethylene-based fluoropolymer–copolymer, processed to mimic different physical properties similar to soil (Downie *et al.*, 2012). The material has a low refractive index matching that of water and as

such, it enables the optical imaging of the root system after saturating the growth chamber. However, the material is expensive and must always be chemically processed before it can be used for plant growth which is time-consuming. Furthermore, the aqueous solution used for imaging was reported to be a sorbitol solution with concentration between 0-13 % (w/v). This is an issue for time lapse imaging because sorbitol induces osmotic stress (Zhao and Schaller, 2004). However, solution used was later changed to one composed of sugar (trehalose) and two different colloidal suspensions (Ludox® TMA (pH 6) or Percoll®) which had a smaller effect on osmotic potential (O’Callaghan *et al.*, 2018). More recently, an alternative transparent soil based on a much cheaper “hydrogel” was developed by mixing a solution of alginate and gellan gum, with a solution of MgCl<sub>2</sub> (Ma *et al.*, 2019).

There are also a number of non invasive 3D imaging techniques that can be used to measure root traits of plants growing in soil and this list of techniques includes X-ray computed tomography (Xray-CT) (Heeraman *et al.*, 1997), nitrogen balancing (Smit *et al.*, 2000), <sup>13</sup>C labelling (Smit *et al.*, 2000), radioisotope tracing (Wen *et al.*, 2015), synchrotron radiation computed tomography (SRCT) (Koebernick *et al.*, 2017), nuclear magnetic resonance microscopy (NMR) (van der Weerd *et al.*, 2001), magnetic resonance imaging (MRI) (van Dusschoten, 2016) and Positron emission tomography (PET) (Garbout *et al.*, 2012). These methods enable the study of root-soil interactions and certain methods such as X-ray CT are used at an increasing frequency to develop models describing 3D root-soil interactions (Roose and Schnepf, 2008). According to Atkinson *et al.*, (2019), *in situ*, 3D imaging of soil grown roots currently uses three techniques: X-ray CT, MRI and PET. PET scanning uses short half-life radioactive tracers such as carbon isotopes to visualize roots grown in soil (Garbout *et al.*, 2012) although, according to Jahnke *et al.*, (2009), the resolution is currently relatively restricted to a resolution of approximately 1.4 mm. MRIs use radio-frequency waves and strong magnetic field to excite atoms such as the hydrogen component of the water molecule and they have been used successfully in the past to image roots and soil water (Leitner *et al.*, 2014; van Dusschoten *et al.*, 2016). However, the MRI signal is influenced by ferromagnetic particles as well as soil moisture which respectively poses restrictions on the soil mineral composition and the soil moisture range (Rogers and Bottomley, 1987; van Dusschoten *et al.*, 2016). It should also be noted that 2D neutron radiography, also used to image roots and soil water *in situ* (Leitner *et al.*, 2014) may be used in tomography (neutron tomography) to extend the method to 3D. More recently, the scanning time of an entire tomogram was reported to

require only 10 seconds for a soil filled column of 27 mm diameter and 100 mm height (Tötze *et al.*, 2017).

X-ray CT allows the imaging of 3D soil grown roots *in situ* by measuring the attenuation of ionizing radiation as it passes the root and subsequently, reconstructs the 3D image by combining the obtained projections. It is perhaps the most popular 3D imaging technique and it's widely used to build and test root-soil interactions models (Dunbabin *et al.*, 2013). However, like the above mentioned methods there is a trade off between sample dimensions and image resolution with pot sizes being roughly 8 cm in diameter (Metzner *et al.*, 2015) although, resolutions as high as 24  $\mu\text{m}$  for samples of 7 cm in height and 3 cm in diameter are possible today with X-ray microtomography (Tracy *et al.*, 2010). Additionally, despite being a powerful method able to penetrate the opaque nature of soil, not all roots may be detected. Lazorenic *et al.*, (2016), reported that  $\mu\text{CT}$  identified only 75 % of the roots observed during destructive harvesting. Tracy *et al.*, (2012), reported the correlation between  $\mu\text{CT}$  observed roots and those harvested destructively to be low ( $r^2 = 0.53$ ). Similarly, the review by Metzner *et al.*, (2015), reported that about 60 to 70 % of the root system can be reliably identified. Furthermore, similar to MRI, Xray-CT is significantly affected by soil moisture and the heterogeneity of soil which again places certain restrictions on the soil type and moisture content used with sieved, repacked soil providing a more homogenous background with small pores (Zappala *et al.*, 2013).

In general, these methods are not considered to be high throughput because the required equipment is expensive to obtain and maintain, is bulky and requires significant space, is difficult to operate (trained staff), has long scanning and processing steps, and depending on resolution there are limitations on the dimensions (Wen *et al.*, 2015). In addition to the above, even with automated systems the process of physically moving the sample during the scanning process can affect plants (Braam and Davis, 1990). There is also concern that repeated radiation exposure could influence roots and soil biota although results from Zappala *et al.*, (2013), suggest that in the case of Xray-CT low dosages (< 30 Gy) do not cause adverse effects for up to 24 weeks.

Minirhizotrons were also designed for monitoring root growth in closed containers. The minirhizotrons may be filled with a substrate, such as gel (Bengough *et al.*, 2004), filter paper (Gioia *et al.*, 2017), glass beads (Courtois *et al.*, 2013), grids of toothpicks (Nguyen and Stangoulis, 2019), peat (Dresbøll *et al.*, 2013) and soil (Le Marie *et al.*, 2016). Furthermore, facilities using automated conveyors for high-throughput phenotyping have already being

constructed (Jeudy *et al.*, 2016; Nagel *et al.*, 2012). Certain systems also offer excellent imaging through by using more complex optical setups (Lu *et al.*, 2019), including techniques which use luminescence-based reporters to image transgenic roots for certain species such as *Arabidopsis* (Rellan *et al.*, 2015).

## **1.5 Least Limiting Water Range**

### **1.5.1 Introduction**

The soil physical conditions that can limit crop production include oxygen stress, water stress and mechanical stress (Mohammadi, *et al.*, 2010). However, all three factors have strong associations between them. For example, it is known from soil basic principles that for a given soil porosity value the soil water content will be inversely related to soil oxygen concentration. In a similar manner, soil water content is strongly associated with soil strength. During the process of soil drying there is often a rapid increase in strength due to capillary forces making the matric potential more negative with mechanical impedance potentially reducing root growth in soil as wet as  $-100$  kPa (Whalley *et al.*, 2005). This is important because drought is identified to be a major factor limiting both the growth of crops and the distribution of natural plant communities on a global scale (Ryan *et al.*, 2016). At the same time the increasing use of heavy agricultural machinery is causing soil compaction which further exacerbates the above issues. Soil compaction modifies the soil pore size distribution and connectivity which increases the mechanical resistance of the soil and reduces its oxygen availability with negative consequences for crops (Lipiec *et al.*, 2012). Thus, understanding the relationship between those three physical factors can be a key to provide enhanced growth of crops and help with important issues such as food security.

The least limiting water range (LLWR) is an example of a mathematical model which attempts to describe the basic interaction between plants and the soil physical stressors described above within the context of plant productivity. In order to help facilitate the detailed description of the LLWR the following definitions are introduced:

Soil water content ( $\theta$ ): A measure of the amount of water (volume or mass) contained in a unit volume or mass of soil.

Soil matric potential ( $\Psi$ ): The negative gauge pressure (kPa), relative to the external gas pressure on soil water, to which a solution identical in composition with the soil solution

must be subjected in order to be in equilibrium through a porous membrane wall with the water in the soil.

Water retention curve (WRC): The relationship between  $\theta$  and  $\Psi$ . This is usually represented in a graphical form with a plot of  $\theta$  against  $\Psi$ .

Penetrometer resistance (PR): A measure of soil mechanical strength representing the force needed to push a metal cone through the soil expressed as a pressure (kPa) by dividing the force by the area of the base of the cone.

Dry bulk density ( $D_b$ ): The mass of oven dried soil divided by its volume.

### **1.5.2 Model Description**

The concept of the “least limiting water range” (LLWR) was developed by da Silva *et al.*, (1994), and it represents the first noticeable advancement of the previously established concept of the “non limiting water range” (NLWR) by Letey, (1985). A widely used definition of NLWR is “the range of water content in the soil where limitations to plant growth (such as water potential, air-filled porosity or soil strength) are minimal” (Letey, 1985). This definition theorises that the NLWR limits are determined by the water content of the soil under certain limiting conditions. However, an immediate implication of the above definition is that plant growth occurs as a step function at each limiting value rather than in a continuous way which more accurately characterises the dynamic and complex interaction between plants and soils. Furthermore, although NLWR relates soil properties and their effect on crop productivity its qualitative definition did not present a practical way of estimating the desirable range of the soil parameters for plant growth.

Based on the above limitations da Silva *et al.*, (1994), proposed the LLWR which effectively aimed at integrating the growth factors mentioned in NLWR in a single index-like variable. This mathematically quantitative model has the advantages of being computationally feasible and clearly integrating important soil variables such as dry bulk density, porosity, matric

suction and soil strength (usually measured as penetrometer resistance) to estimate a range of soil volumetric water concentration for optimum plant growth, an example of which is shown in **Figure 1.2**. In more precise terms, the first step in estimating the LLWR is the fitting of two functions to the two empirical datasets of the soil water retention and the soil penetration resistance respectively. The empirical regression model used to describe the soil water release curve is normally a simple power function used by Ross *et al.*, (1991):

$$(1) \theta = a\Psi^b.$$

However, an alternative model was proposed by da Silva *et al.*, (1994), which was derived through a stepwise multiple linear regression procedure and introduced an extra layer of complexity from equation 1 by adding  $D_b$  to the water retention curve equation:

$$(2) \theta = \exp(a + bD_b) * \Psi^c.$$

The function used for the soil penetration resistance is normally the one proposed by Busscher and Sojka, (1987):

$$(3) SR = d\theta^e D_b^f.$$

The second step is an assumption which requires the selection of four limiting values for soil stressors, with each value corresponding to a soil condition at which plant growth is severely limited. The values chosen by the authors and which appear to be used routinely to this day are as follows:

- 1) Matric Suction at field capacity ( $\Psi_{fc}$ ): -0.01 MPa
- 2) Matric Suction at wilting point ( $\Psi_{wp}$ ): -1.5 MPa
- 3) Soil resistance at impeded root elongation conditions ( $SR_{limit}$ ): 2 MPa
- 4) Air filled porosity at hypoxic conditions ( $AFP_{limit}$ ): 0.1 (or 10 %).

The estimated regression parameters a, b, c, d, e and f characterising the LLWR from the first step are then used after simple algebra manipulations to express  $\theta$  in the following equations:

$$(4) \theta_{fc} = \exp(a + bD_b) * \Psi_{fc}^c.$$

$$(5) \theta_{wp} = \exp(a + bD_b) * \Psi_{wp}^c.$$

$$(6) \theta_{sr} = [SR_{limit}/(dD_b^f)]^{(1/e)}.$$

$$(7) \theta_{afp} = [1 - (D_b/D_r)] - AFP_{limit}.$$

The LLWR is then defined to be the difference between the upper limit (UL) and the lower limit (LL) as follows:

$$(8) LLWR = UL - LL = \min(\theta_{fc}, \theta_{afp}) - \max(\theta_{sr}, \theta_{wp}).$$

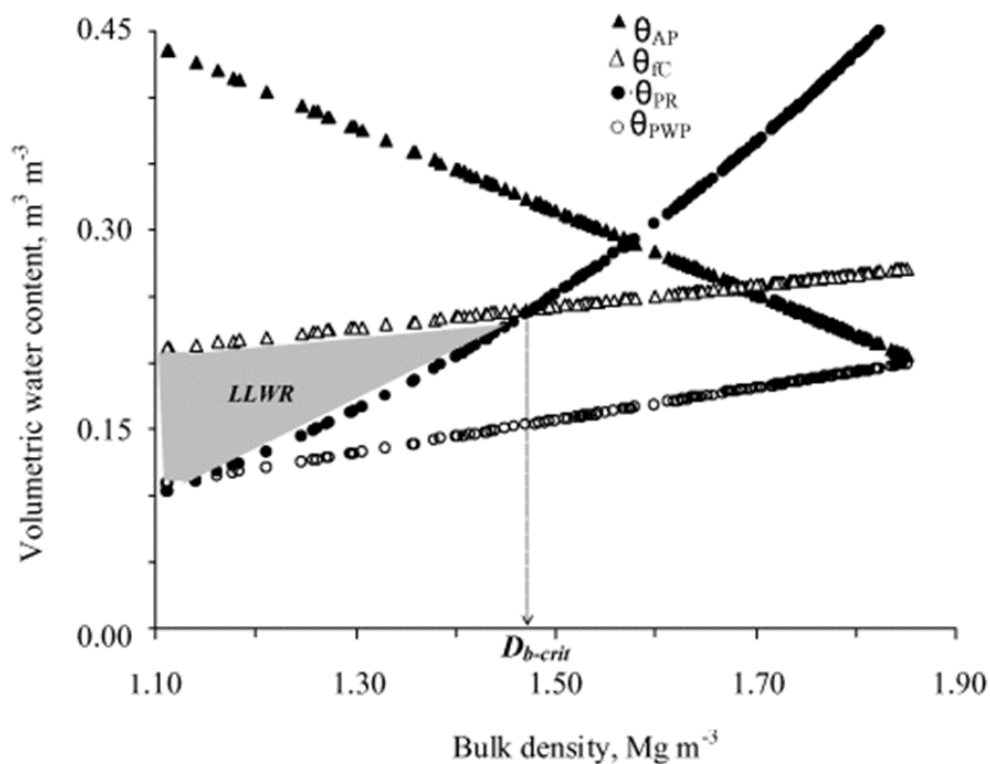


**Figure 1.2:** Example LLWR output of soil volumetric water content ( $\theta$ ) vs. bulk density ( $D_b$ ). The regression lines correspond to the soil volumetric content at the plant limiting conditions

of 10 % soil air filled porosity ( $\theta_{AP}$ ), -0.01 MPa soil matric suction ( $\theta_{FC}$ ), 2 MPa soil penetrometer resistance ( $\theta_{PR}$ ), and -1.5 MPa soil matric ( $\theta_{PWP}$ ). The dry bulk density value represented by  $D_{b-crit}$  marks the transition point between the shaded LLWR zone and the non LLWR zone where plants should be least limited relative to each factor.

### 1.5.3 Limitations

As discussed previously the basis of the LLWR is critically dependant on two assumptions:

- 1) Assumption 1: Equations 2 and 3 are accurate and precise regression models for empirically observable datasets.
- 2) Assumption 2: The LLWR limiting values are complete descriptors of the upper or lower limits for plant growth for all cases.

A potential issue with assumption 1 is that the two empirical models might not provide a good fit for the data and as such the researcher should always assess if they are appropriate descriptors of the datasets. Assumption 2 is in the authors' opinion the most problematic of the two assumptions since it effectively underscores the complexity of plant-soil interactions. For example, an immediate implication of this assumption is that all plants have identical physiological responses, something which is impossible, since several soil physical stresses are known to be influenced by a range of root traits (Bengough *et al.*, 2011).

If a crop plant was more susceptible to oxygen limitations e.g. potatoes, then the choice of the 10 % air filled porosity is completely unjustifiable from a plant physiology point of view when compared to less susceptible species such as rice. Other examples are of course not difficult to construct. For instance, Zarebanadkouki *et al.*, (2016), examined hydraulic conductivity in lupin (*Lupinus albus*) roots with neutron radiography and it was clearly demonstrated just how variable the process is between different types of roots and the roots themselves. Furthermore, da Silva *et al.*, (1994), originally indicated in their analysis that soil texture can influence the limiting value of air-filled porosity with the effect being stronger for

more heavy textures. This will effectively imply that other soil properties not included in LLWR can implicitly influence it. It can also be argued, that for soils which are rarely saturated it is highly unlikely that compaction will be a limiting growth factor for plant growth compared to soil aeration (Aust *et al.*, 1998). Siegel-Issem *et al.*, (2005), also pointed out how depending on soil properties some plants will have a higher growth rate outside the LLWR range as opposed to inside it. Other authors had also demonstrated in the past that the critical air-filled porosity will be dependent on factors such as soil temperature and the considered depth (Bartholomeus *et al.*, 2008). Similar concerns about the limiting values can be found in the literature (Mohammadi *et al.*, 2010; Bengough *et al.*, 2006), with other authors (De Jong van Lier and Gubiani, 2015) raising more severe criticisms demonstrating a range of issues arising from the simplicity of the model.

In a similar manner, it is misleading to adopt the 2 MPa threshold value for soil strength. In general, root mechanical stress decreases root elongation rates in an approximately linear way until they reach a high penetrometer pressure (Whalley *et al.*, 2006). This value originates from the work of Taylor and Ratliff, (1968), who used a blunt (30 °semi-angle) penetrometer to study how PR influences root elongation rates. However, a blunt penetrometer is related to spherical and not to cylindrical cavity expansion and may also involve the formation of soil bodies as opposed to a sharp (5 °semi-angle) penetrometer (Bengough and Mullins, 1991). It will be more accurate to say that the threshold value of 2 MPa corresponds to the soil strength where root elongation rates are reduced by half (Dexter, 1987). If that definition is adopted, then the PR threshold value could be 0.8 MPa for cotton roots and 2 MPa for maize and peanut roots in the absence of water stress according to the review of Bengough *et al.*, (2011). Gregory *et al.*, (2007), also reported that for most of the spring and summer the PR values of three contrasting soil types in the UK were higher than 2 MPa below 30 cm from the surface. Even in surface soil the LLWR can become very small under zero tillage

practices (Betz *et al.*, 1998). In contrast to a penetrometer whose movement follows a straight line, roots can exploit cracks and pores within the soil thus experiencing a much-reduced mechanical impedance (McKenzie *et al.*, 2009; Brown *et al.*, 2004; Valentine *et al.*, 2012). As a result, mean penetrometer resistance in zero tillage treatments can poorly reflect mechanical impedance because roots exploit networks of continuous channels even in a relatively strong soil matrix (Bengough *et al.*, 2006).

In regards to the drought threshold value of -1.5 MPa, root elongation may occur for a soil water potential significantly less than the -1.5 MPa threshold (Portas and Taylor, 1976) but this value is probably accurate for transpiring plants in a fully equilibrated soil (Bengough *et al.*, 2011). However, if similar to soil strength, we adopt a threshold value at which root elongation rate is halved then the threshold value will vary between species. For example, a matric potential of -0.5 MPa could be used for maize roots grown in the absence of mechanical impedance (Bengough *et al.*, 2011). For seminal roots grown in vermiculate this value could be between -0.4 MPa and -0.5 MPa for maize (Akmal and Hirasawa, 2004) and between -0.2 MPa and -0.3 MPa for wheat (Sharp *et al.*, 1988). Furthermore, hysteresis effects could change the soil water release curve during soil drying which will be definition change the LLWR.

It should also be noted that there is a certain degree of restriction as to the dimensional extent of the soil system considered in the LLWR. For example, consideration of the soil system beyond the top 20 cm and for an agricultural soil the LLWR will be affected by the nature of the agricultural practises used (Bengough *et al.*, 2006). The LLWR could then be considered for soil depths beyond the 20 cm limit. In a similar way one may assess LLWR at different time points as properties such as the soil water release curve will be influenced by soil structure which will change depending on season, agricultural practises and soil biota,

In summary, although the LLWR is a computationally feasible model that can be used as an index of soil quality it is unfortunately an example of a limited trait quantitative, mechanistic model and it does not help to increase the current knowledge of root trait-soil interactions and by implication future crop production unlike other mathematical models (Roose and Schnepf, 2008). Although, the task of modelling root architectural traits and their interaction with soil can be very challenging (Li *et al.*, 2015), the process can be invaluable in determining beneficial root traits for different plant functions such as root depth for drought resistance (Dunbabin *et al.*, 2013). Nevertheless, modification of the LLWR limits using knowledge of plant species differences (Mohammadi *et al.*, 2010) could potentially provide significantly more accurate predictions and enhance crop productivity.

## **1.6 Aims of this project**

Root micro-traits can have an enormous influence on the ability of plants to survive and grow when exposed to various soil stressors. Only, by developing methodologies which enable the accurate quantifications of those traits and evaluate those in the context of precisely defined soil stressing conditions can we develop accurate process based models that can help increase understanding of plant soil interactions. The LLWR is an easily understood, computationally feasible index of soil quality but is currently limited by assuming a singular plant response across the spectrum of plants. As such, the first aim of this thesis will be the development of a standard operating procedure (SOP) which will enable for the manipulation of the LLWR associated stressors while having the ability to quantify a list of root traits of interest. The second objective will be to assess to what extent the variability in root traits is responsible for differential root growth rates under various soil conditions. This will provide the data which can then be used as a basis for future modelling work. Finally, the third aim is the integration of root traits into the existing LLWR model by using any existing patterns or relationships among the dataset obtained in the previous step. If successful, the new model will serve as an indicator of how root traits potentially shift the boundaries of the LLWR range.

The aims of this thesis may be summarised as:

1. To develop a plant phenotyping system which enables the manipulation of the LLWR soil stressors while allowing for the imaging of seedling roots.
2. To develop methods which enable the quantification of root micro traits, e.g., root tip geometry.
3. To assess if root trait variability is responsible for differential growth rates when subjected to various soil LLWR associated conditions.
4. To modify the LLWR model through the integration of root traits and try to predict which root traits might be significant.

## 2. Rhizotron Development

### 2.1 Introduction

Modern agriculture is becoming increasingly mechanized with important crop plants such as soybean and corn being completely dependent upon machinery (Olibone *et al.*, 2010). One of the side effects of the increasing usage of heavy machinery is an increase in the compaction of the soil. Routine soil cultivation by ploughing encourages the formation of pan layers in the horizontal direction and wheel tracks form heterogeneously compacted structures in the vertical direction (Chamen *et al.*, 2003). Soil compaction has a number of negative consequences on soil functions such as an increase in its mechanical resistance, reduction in water infiltration, and increased soil saturation, all of which have negative implications for crop yield (Keller *et al.*, 2015). As such, it is essential to increase our understanding of how plant roots interact with the soil physical conditions associated with mechanical stress, water stress, and oxygen stress, to avoid losses in crop yield (Whitmore and Whalley, 2009).

The least limiting water range (LLWR) is one such concept relating the important soil stressors of penetrometer resistance (a measure of mechanical impedance), porosity and water potential to the physiological limits of plant growth (da Silva *et al.*, 1994). The output of the model is a soil moisture range indicating the limits within which plants will experience minimum restrictions in growth. The limits are effectively four threshold values indicating the points at which root growth stops for three soil physical stressors and include penetrometer resistance (2 MPa), air filled porosity at hypoxic conditions (10%), matric suction at field capacity (a measure of soil water-holding capacity) (0.01 MPa) and matric suction at the permanent wilting point (1.5 MPa). Thus, by definition, the LLWR is directly influenced by two basic components: (i) soil stressors and (ii) the root traits of the plant in question. The interaction between (i) and (ii) is what determines the limits of the LLWR. The LLWR is however limited in its scope since it does not consider the complex variability in root traits that can influence it. For example, root hairs are highly permeable structures which influence the ability of roots to extract nutrients and water (Segal *et al.*, 2008). However, in the context of LLWR the limits will be identical when comparing a plant with root hairs and a mutant variety without root hairs. Many other examples can of course be constructed but the main message is that the LLWR is determined only by soil physical properties and that the plant response is only integrated through the limiting values assumptions mentioned above defining the conditions at which root growth is halted.

In order to reformulate the LLWR a system was required which enabled the manipulation of the LLWR soil stressors and at the same time enabled the quantification of root traits. The requirement to image roots *in situ* excluded the more traditional approach which involves destructive field sampling. It also prohibited the use of soil-less systems such as clear gels (French *et al.*, 2009) or filter papers (Hetz *et al.*, 1996) as the LLWR stressor variables could not be manipulated in a manner which reflected the physical processes occurring in soil. The desirability of the system to be high throughput and to grow seedlings at least for three weeks excluded more recently developed methods such as transparent soils (Downie *et al.*, 2015). Other powerful methods which enable visualisation of roots *in situ* such as X-ray CT (Heeraman *et al.*, 1997) were also rejected due to difficulties in assessing the root micro-traits of interest. As a trade-off the proposed system that was selected was based on the design of minirhizotrons.

Rhizotrons are effectively large underground tunnels surrounded by transparent glass and enable observations of the portion of the root system that is growing against the glass. Unfortunately, its construction is rather complicated and costly which prohibits their widespread use (Klepper and Kaspar, 1994). The scaled down version of rhizotrons are referred to as minirhizotrons. Minirhizotron systems were originally described by Bates in 1937 and are similar in principle to the much larger rhizotron system but are much smaller and designed to be carried by the user. They consist of a transparent tube which is installed in the ground with a cylindrical imaging device moving into the tube to collect images. Although root growth is not identical to field soil, minirhizotron observations of root systems tend to correlate well with results from soil sampling methods (Upchurch and Ritchie, 1983; Liao *et al.*, 2010). An alternative to field rhizotron observation tubes are flat rhizotron growth chambers. These are often custom made and have been proposed by various authors over the years (Rewald and Ephrath, 2013). They normally consist of a small soil/gravel filled container made from transparent material and as such, enables the imaging of roots at the root/rhizotron interface. Minirhizotron system data has been used in the past to develop mathematical models which aim to predict root growth under different soil conditions (Dupuy *et al.*, 2010) and as such, they could provide a framework for redefining the LLWR.

## 2.2 Design criteria

Minirhizotron systems offer a relatively cheap and potentially highly detailed imaging platform that can be used to monitor seedling roots. In order to be able to measure the various root traits that can help redefine the LLWR it was essential to either adopt an existing design or create one. In order to determine if an existing minirhizotron design could be used, a list of properties that the minirhizotron system should ideally possess was compiled and then used to guide the selection process. From here on after, the term “RS” will be used to refer to an ideal/desirable minirhizotron system. The first two properties are introduced here:

Property 1 (P1): The RS structure and growth substrate must enable the manipulation of the LLWR soil stressor variables.

Property 2 (P2): The RS structure must have an imaging surface which allows the imaging and quantification of both coarse features of the roots (root detection) as well as finer root features (root hairs).

P1 is simply stating that the RS should use a growth substrate with physical structure in it. This could be soil or sand/gravel mixtures but substrates such as filter paper or agar were to be excluded. Although valuable, such growth substrates have several drawbacks, such as absence of microbial interactions, soil structure and in most cases, even absence of mechanical impedance. This was required to be able to manipulate the LLWR soil stressor variables in the RS to help redefine the model.

P2 is a requirement for high quality images obtained from the RS. If the LLWR would be redefined by considering root trait variation, then the ability to measure *in situ* not just coarse root traits but finer root traits such as root hairs known to influence root hydraulic properties, will be necessary.

Based on the above requirements the following systems were considered with the aim to encompass a range of minirhizotron designs:

Bengough *et al.*, (2004), developed a 2D gel chamber system for the rapid and sequential measurement of root growth that was used to study cereal seedlings. The chambers were constructed from two plates (one black polyvinylchloride and one transparent perspex), with dimensions of  $215 \times 300 \times 3 \text{ mm}^3$ . The root system was imaged with a flatbed scanner Epson Expression 1600XL-PRO (300 dpi/82  $\mu\text{m}$  – 1500 dpi/15  $\mu\text{m}$ ) and then manually traced to

obtain coarse root features such as root length. Sample images suggest that root hairs were visible, but they were not reported to have being measured.

Gioia *et al.*, (2017), developed a system referred to as “GrowScreen-PaGe” which consists of two-dimensional polymethyl methacrylate plates (350 x 250 mm<sup>2</sup>) covered on both sides with wetted germination paper providing water and nutrients for the developing root system. A custom-made mobile imaging box (outer dimensions: 140 x 140 x 46 cm<sup>3</sup>) was then used to image the root system at a resolution of 74 mm per pixel. Coarse root traits were measured but root hairs were not reported to have being measured.

Le Marie *et al.*, (2016), introduced a “rhizoslides” system which consists of two PVC bars (600 x 60 x 10 mm<sup>3</sup>) and a plexiglass sheet (650 x 530 x 4 mm<sup>3</sup>) fixed with two screws between the bars. A custom-made mobile imaging station (~ 168 x 164 x 110 cm<sup>3</sup>) was then used to image both the root and the shoot system after the rhizoslides were manually placed onto the imaging mount. The images themselves were taken with a 22.3 megapixel full-frame digital single-lens reflex camera (EOS 5D Mark III, Canon, Tokyo, Japan) equipped with a 50 mm lens (compact macro 50 mm f/2.5, Canon, Tokyo, Japan) giving an image resolution of ~ 0.13 mm pixel<sup>-1</sup>. Coarse root features were then traced by using the software SmartRoot but root hairs were not quantified although sample images indicate that they were visible.

Jeudy *et al.*, (2016), introduced an automated conveyor system referred to as “Rhizotubes” which are cylindrical minirhizotrons 18 cm in diameter and 50 cm high. Root growth between an inner permeable membrane (mesh size of 18 µm) and the external outer transparent polymethylmethacrylate tube, which separates the plant root from the soil. The membrane is permeable to nutrients and water but it does not allow roots to pass through which makes it a pseudo-3D system. The roots are photographed with the “Rhizocab” (automated conveyor) camera through the outer transparent tube. The final definition of the RGB image is 12,000 × 12,000 pixels with a file size of 411 MB. All root traits were manually measured from the images although it was stated that an automated image processing method was in development. These authors did not mention root hairs so it is not clear whether they might be visible for this system.

Courtois *et al.*, (2013), developed a hybrid minirhizotron design based on hydroponics referred to as “rhizoboxes”. Roots are held together by a sandwich of two transparent plexiglas plates (50 cm x 20 cm x 2 cm<sup>3</sup>) and an installed nail board that provides a degree of mechanical resistance and maintain the spatial distribution of roots during substrate removal.

The rhizoboxes are filled with glass beads of 1.5 mm diameter to provide some degree of mechanical resistance for roots compared to normal hydroponics. At the end of the experiment the rhizoboxes are removed from the hydroponics and the glass beads are removed to enable simple camera imaging of the root system that is held together by the grid of nails. Fine root traits such as root hairs were not reported to have been measured although the submerged nature of the system will almost certainly destroy fine root traits.

Nagel *et al.*, (2012), developed an automated minirhizotron system known as “GROWSCREENRhizo” which is capable of automatically imaging roots and shoots of plants grown in soil-filled rhizotrons (up to a volume of ~18 L) with an impressive throughput of 60 rhizotrons per hour. The image processing is reported to be semi-automatic with manual tracing of the portion of the root system not captured by the algorithm although no estimate of the accuracy of the algorithm was reported. There was also no mention of any root hair associated measurement, so it is not clear if they are visible or not in the images. Unfortunately, the development of this high-throughput phenotyping platform will require significant investments to develop and as such, was excluded from further consideration.

Rellan *et al.*, (2015), designed a complex minirhizotron system known as GLO-Root for *Arabidopsis* which uses luminescence-based reporters to image transgenic roots in time lapse studies. The rhizotrons are imaged on both sides and the images are merged to obtain the final image of the root system. Use of such systems however will require the genetic modification of species and specific imaging setups to detect the required wavelength of the expressed fluorescent protein. Furthermore, as was pointed out by Faget *et al.*, (2013), in many countries it is forbidden to use transformed plants in the field which will prohibit field-based validation.

In general, all the above systems were in violation of PI or P2 or were not feasible to use in this study due to costs. This led to the decision of developing an RS prototype that satisfy the criteria. Since, root hair measurement appeared to be difficult to observe or measure in the existing systems it was decided to reject the use of soil for this system as soil is a highly variable material and not of consistent quality to achieve the required image quality. This decision was also supported by the consideration that in order to test future LLWR hypotheses constant material properties for the growth substrate will be needed to remove the intrinsic variability component of soil. As a result, the following two properties were added to the list of properties:

Property 3 (P3): The RS substrate must have consistent physical properties in order to reduce the variability of results that are inherent from the variance in soil properties.

Property 4 (P4): The RS substrate must produce root growth rates that are similar to soil throughout the duration of the experiments.

P3 is simple restating the constant material properties requirement mentioned above.

P4 is an additionally requirement that was added to ensure that the RS growth substrate to be used had to be a good proxy to soil determined by similar root growth rates.

## 2.3 Aims

Based on the discussion of the previous section a list of desirable properties for the RS was established:

Property 1 (P1): The RS structure and growth substrate must enable the manipulation of the LLWR soil stressor variables.

Property 2 (P2): The RS structure must have an imaging surface which allows the imaging and quantification of both coarse features of the roots (root detection) as well as finer root features (root hairs).

Property 3 (P3): The RS substrate must have consistent physical properties in order to reduce the variability of results that are inherent from the variance in soil properties.

Property 4 (P4): The RS substrate must produce root growth rates that are similar to soil throughout the duration of the experiments.

This chapter focuses on four key experiments which were designed to develop the RS within the context of the above defined properties. The experiments described were designed to address those properties with a basic description being provided by **Table 2.1**. To convert those properties into testable experimental hypothesis the following two terms are introduced here with the understanding that their precise definitions will be provided in later sections:

**ARGR:** Average Root Growth Rate – a measure of root growth rate (Section 2.4.8).

**ISI:** Image Sharpness Index – a measure of image sharpness (Section 2.4.10).

**Table 2.1:** Basic description of the experiments described in Chapter 2.

<b>Experiment Section</b>	<b>- Property</b>	<b>Description</b>
1 - 2.5.1	P1, P3 and P4	Comparison of <b>ARGR</b> for four different RS substrates.
2 - 2.5.2	P3 and P4	Comparison of <b>ARGR</b> in RS substrate sieved to four different particle size ranges.
3 - 2.5.3	P2	Comparison of <b>ISI</b> for three different rhizotron scanning surfaces.
4 - 2.5.4	P2 and P4	Comparison of <b>ISI</b> and <b>ARGR</b> for four different RS substrates.

## 2.4 Methods

### 2.4.1 Assessment of initial RS criteria

In order to achieve the properties described above, it was necessary to first develop and test an RS design and to determine a growth substrate which will be used in future experiments. In order to satisfy P1, P3 and P4, the RS must use a substrate with a physical structure that included particles, air and water, to ensure that the basic physical mechanics of root growth in soil are mimicked to a reasonable extent. The requirement of constant physical properties (P3) would imply a material of artificial origin since naturally occurring soil can have extremely variable properties. The above conclusion was also reinforced by the requirement for high image quality (P2). As such, it was decided that artificially coloured sands would be compared with soil as they could potentially satisfy P1, P2, P3 and P4 and because horticulture sand is often used in studies as a proxy to soil (Materchera *et al.*, 1991; Bengough *et al.*, 2011).

In a similar manner, P2 will also impose certain restrictions in the design of the RS to be able to image both coarse (roots) and fine (root hairs) root traits. Conventional image sensors used in minirhizotron images have a grid size of 640 x 480 pixels and a resolution of about 60  $\mu\text{m}$  (Faget *et al.*, 2010) which eliminated most options. On the other hand, excellent image quality can be achieved with certain systems such as the one developed by Lu *et al.*, (2019), but were not appropriate here as it was reported to be as small as 1.1 x 1.1 x 1.2  $\text{cm}^3$ . Instead,

the dimensions were restricted to A3 paper size (420 x 297 mm<sup>2</sup>) because this is the largest dimension for which commercially available flatbed scanners can be obtained with high optical resolution (up to 2,400 dpi) for minirhizotron scanning. The RS was built out of acrylic plastic as opposed to glass because of its higher hardness, transparency and reduced effects on root growth (Cai, 2006), is commercially available and of low cost (£10 per unit). Reduced costs can be very important for building a high-throughput system, which is a requirement for plant root phenotyping platforms linking genotype to phenotype (Walker, 2009). In fact, classical mapping of quantitative trait loci or association mapping studies require a minimum of 100-500 individuals (Rafalski, 2010).

It should also be noted that because the RS is restricted to A3 sized dimensions root growth will be restricted to a mature seedling stage depending on the species and treatment. Seedling root phenotype can sometimes be a good predictor of later root morphology such as maize grown in hydroponics (Tuberosa *et al.*, 2002) but that is not always the case (McPhee *et al.*, 2005). However, in general, most techniques developed for high-throughput root phenotyping are restricted to young seedlings (Jeudy *et al.*, 2016). Furthermore, the imaging setups used in high-throughput systems are normally restricted to scanners or cameras which have fast image acquisition speeds and enable hundreds of plants to be phenotyped daily (Downie *et al.*, 2015). The proposed RS does seem to have potential as a high-throughput plant phenotyping platform.

## **2.4.2 Minirhizotron Construction**

### **2.4.2.1 Minirhizotron design A**

The minirhizotrons were developed in two stages. Initially they were composed of two pieces of rectangular (420 x 297 mm) acrylic (PlasticSheets.com) with smaller spacers being placed at the edges of them to seal them and to allow a 5 mm gap between the acrylic surfaces (**Figure 2.1**).

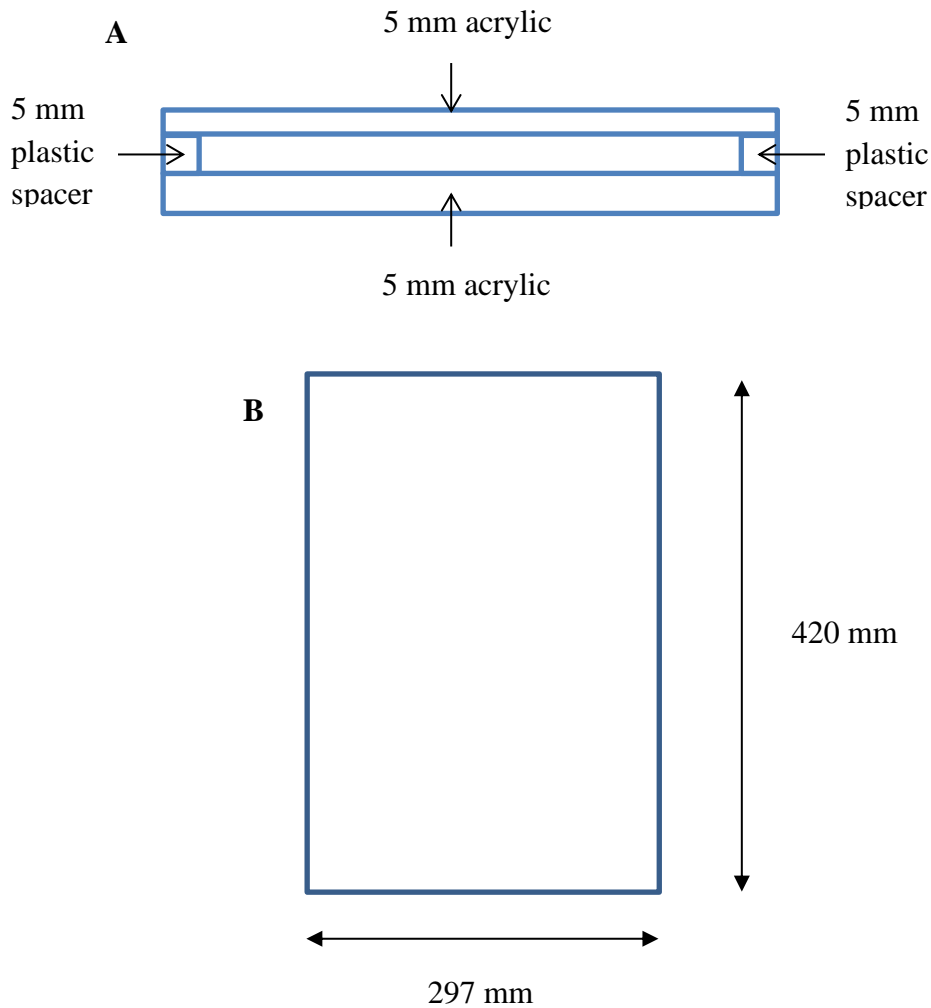


**Figure 2.1:** Schematic diagram of the starting minirhizotron design **A)** Top view and **B)** Front view.

Each minirhizotron was filled with growth substrate (Section 2.4.3) at an approximate dry bulk density (DBD) of  $1.5 \text{ g cm}^{-3}$  and subsequently watered. This relatively high density was the minimum DBD at which all substrates could be packed inside the minirhizotrons without slumping however, it is not unusual to observe it in agricultural fields where the use of heavy machinery can easily increase the surface soil density (Keller *et al.*, 2015). The apparatus was then placed at a  $30^\circ$  angle from the vertical to achieve root growth against the imaging surface and subsequent good quality images from scanning. All minirhizotrons were covered with a light, waterproof, black fabric (Do4U), so exclude light from the root growth surface. After field capacity was reached 2 pre-germinated spring barley (*var.* Optic) seedlings (Section 2.3.5) with a root length between 1-2 cm were randomly chosen and subsequently

sown at the top of minirhizotrons. The second barley seedling was removed after 48 hours so that only one actively growing seedling remained after the initial establishment phase.

#### **2.4.2.2 Minirhizotron design B**

Minirhizotron design B included a 2 mm acrylic imaging surface to allow high imaging quality. This required drilling and adding screws to maintain rhizotron integrity due to the weight of the filling substrate. An irrigation system was also added to allow consistency of irrigation over the entire experimental period, and across replicates. The internal compartment of the RS was enlarged to fit the irrigation pipes and the surplus volume was filled with a 4 mm thick acrylic. **Figure 2.2**, is a schematic diagram that demonstrates the minirhizotron design B that allowed automated irrigation while controlling the minirhizotron volume. Irrigation cables were fitted to the minirhizotron leaky pipes to slowly saturate the minirhizotron over a series of irrigation events rather than forcing a large amount of water in turn connected to an irrigation pump (Boyu FP-1500 Adjustable Pump) in a black light-absorbing water container. The irrigation pump could then be controlled through a custom-made fitted timer to operate when required. This makes the system more automated and eliminates the need for manual watering. After filling with dry growth matrix these minirhizotrons were watered for 2 days, 3 times a day each for 3 minutes at slow pressure through the leaky pipes allowing the water to equilibrate throughout the substrate. Seedlings were sown after this period as described for the minirhizotron design B above.

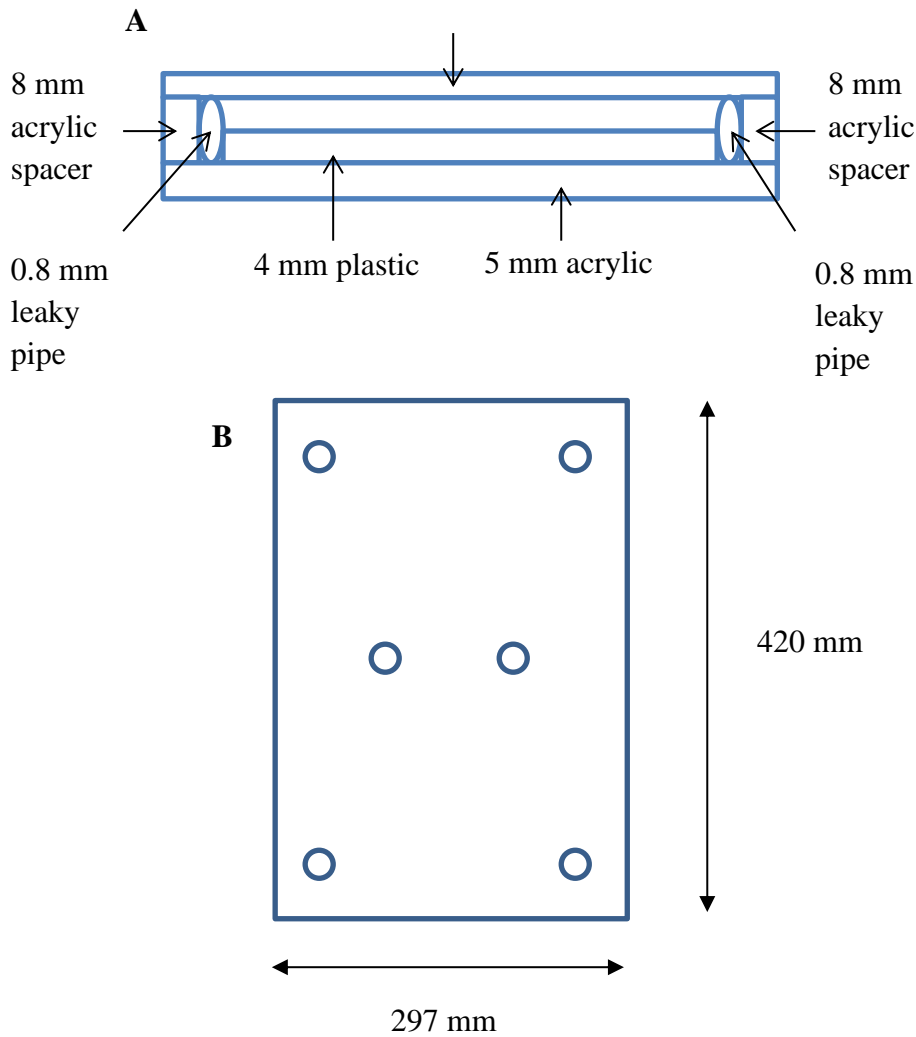


**Figure 2.2:** Schematic diagram of new minirhizotron design B **A)** Top view and **B)** Front view (circles indicate screws).

### 2.4.3 Growth Substrate – sample preparation

Five different substrates were tested as potential growth substrate materials for the rhizotrons. Two soils were collected from two fields “Mid Pilmore” (sandy texture) and “Bullion” (clay texture) at the James Hutton Institute, Invergowrie, Dundee DD2 5DA. The soil was oven dried at 105°C for 48 hours and then sieved to a range of aggregate sizes (8, 4 and 2 mm) mm. The “Blue Sand” (Stoney River) was gently washed with potassium chloride to make it more hydrophilic. Afterwards, it was washed again thoroughly with tap water to remove the residue acids and finally oven dried at 105°C for 24 hours. The “Black Sand” (Natural Color) came in two different size fractions both gravel (8 - 2 mm) and sand (2 - 0 mm). The gravel was first sieved to 4 mm and then mixed 50/50 % (gravimetric) with the sand. Afterwards, the sand was washed as recommended by the manufacturer and subsequently oven dried at

105 °C. The “Flourite Black Sand” came in two different size fractions both gravel (8 – 4 mm) and sand (4 – 0 mm). The gravel and the sand were first mixed together 50/50 % (gravimetric) and the entire mixture was subsequently sieved at 4.0, 2.8, 2.0 and 1.4 mm to create mixtures of 4.0 - 2.8, 2.8 - 2.0, 2.0 - 1.4 and 1.4 - 0 mm respectively. Each mixture was then washed with tap water for three times and subsequently oven dried at 105 °C. Oven dried materials were always used as they are not cohesive and thus, much easier to pour inside the rhizotrons. This also provided a more accurate estimate of rhizotron dry bulk density.

#### **2.4.4 Growth Substrate – physical property analysis**

Pilmore and Bullion soils were first collected, air dried for a period of 5 days, and then subsequently sieved at 8, 4 and 2 mm to create the particle ranges of 8-0, 4-0 and 2-0 mm respectively. The 2 soil types × 3 aggregate size treatments were then used to create a series of cylindrically shaped (4.5 mm diameter x 5.0 mm height) repacked soil cores of different aggregate sizes at different dry bulk densities (0.9, 1.0, 1.1, 1.25, 1.3, 1.45 and 1.6 g cm<sup>-3</sup>) in a 2 by 3 by 7 factorial design (n = 4). The gravimetric moisture content of each soil core was first adjusted to 20 % to give it consistency. Cores were saturated with degassed water, then subjected to a sequence of different matric suctions (5, 10, 20 and 50 kPa) *via* the use of sand and tension tables. A needle penetrometer (1 mm diameter, 30° cone angle, 4 mm min<sup>-1</sup> penetration rate, readings; averaged at 1-mm intervals from 5–15 mm depth range) fitted to a mechanical test frame (Instron model 5544; Instron, MA, USA), with a 50-N load cell accurate to 2 mN at maximum load, was used to measure penetration force at each matric suction and calculate penetrometer resistance (force divided by cone cross-sectional area) (Bengough and Mullins, 1990; Valentine *et al.*, 2012). The measurements of mass and penetrometer resistance enabled the estimation of the soil water release and strength curves respectively. This enabled an assessment of the differences between samples with contrasting physical properties and how that may affect their strength and water holding capacity.

The exact procedure was also used for the Flourite sand treatments used in this experiment but only for a dry bulk density of 1.6 g cm<sup>-3</sup> in a 2 by 3 by 1 factorial design due to time limitations. The soil strength curve was obtained with loess regression by using the “geom\_smooth” function from the “ggplot2” package in R. The water release curve was obtained by fitting a Van Genuchten model (Van Genuchten, 1980) by using the “fitsoilwater” function from the “soilphysics” package in R. The obtained Van Genuchten

model was then used to estimate the effective pore diameter for each substrate by using the relation:  $d = (300/\psi)$ , where  $\psi$  is the matric potential (Marshall and Holmes, 1988).

In addition to the above, laser diffraction (Mastersizer 2000 - Malvern Instruments) was used to determine the particle size distribution of the Pilmore and Bullion soils (**Table 2.2**) analysed at the James Hutton institute located in Craigiebuckler, Aberdeen AB15 8QH, Scotland.

**Table 2.2:** Physical properties of the two soils used in the experiments.

		<b>Pilmore Soil</b>	<b>Bullion Soil</b>
	200-20 $\mu\text{m}$	64.05	55.86
Percentage between (%)	20-2 $\mu\text{m}$	28.49	37.34
	2-0.02 $\mu\text{m}$	7.46	6.80
Specific Surface Area ( $\text{m}^2 \text{g}^{-1}$ )		0.84	0.856
Uniformity (n/a)		2.09	3.64
Particle density ( $\text{g cm}^{-3}$ )		2.53	2.54
Texture		Sandy	Clay

### 2.4.5 Seed germination

All the seeds used in the experiments described in this chapter were spring barley (*Hordeum vulgare var. Optic*).

The steps involved in the process of seed germination used in all experiments are as follows:

1. Seeds were placed in a beaker containing deionized water and mixed slightly to disperse air.
2. The seeds were left in the beaker overnight.
3. The seeds were sterilized by immersing them in a solution of 2% Sodium Hypochlorite for about 15 minutes.
4. The seeds were rinsed three times with sterile distilled water to remove the Sodium Hypochlorite.
5. Two layers of filter paper were placed in a Petri-dish and subsequently moistened with sterile distilled water.

6. The seeds were placed on top of the wet filter papers with the embryos facing downwards.
7. Filter paper was placed on top of seeds and moistened with sterile distilled water.
8. The plates were covered with aluminium foil and incubated at 15°C for a period of 2-3 days.

## 2.4.6 Glasshouse growth conditions

All the experiments described below took place in a temperature-controlled glasshouse located at the James Hutton Institute, Invergowrie, Dundee DD2 5DA, Scotland. The temperature was set to 18°C during the day and 14°C during the night. The threshold value at which the artificial lighting was activated was 150 W m<sup>-2</sup>. The lamp fittings installed were GAVITA GAN 400AL Ecomax fitted with 400W SON-T sodium bulbs.

## 2.4.7 Minirhizotron imaging

At intervals of 7 days the minirhizotrons were removed from the black coverings and scanned. Minirhizotrons were scanned with a flatbed scanner (EPSON Expression 10000XL) at 1,200-1,600 dpi, with images saved as (uncompressed) TIFF files to assess the relative growth of the seedlings. The experiments described in this chapter had a randomized (blocked) one-way ANOVA design arranged on two parallel linear rows.

## 2.4.8 Root growth parameters

Root growth parameters were measured by using the rhizotron images obtained at 7, 14 and 21 days. The visible root system was traced manually using the “Segmented Line” tool of Fiji. The following definitions are used for the variables used to characterise root growth in images of the RS:

- Vertical Root Length (**VRL**): The Euclidean distance between the minimum and maximum vertical coordinates of the visible root system grown in the RS. The measured value is expressed in units of *mm*.
- Horizontal Root Length (**HRL**): The Euclidean distance between the minimum and maximum horizontal coordinates of the visible root system grown in the RS. The measured value is expressed in units of *mm*.
- Vertical Growth Rate (**VGR**): The difference between the **VRL** values at 2 different time points (*t*) divided by the time interval ( $\delta t$ ), i.e.,  $VGR_{ti} = [(VRL_{ti} - VRL_{t(i-1)}) / \delta t]$ . The calculated value is expressed in units of *mm day<sup>-1</sup>*.

- Horizontal Growth Rate (**HGR**): The difference between the **HRL** values at 2 different time points (t) divided by the time interval ( $\delta t$ ), i.e.,  $HGR_{ti} = [(HRL_{ti} - HRL_{t(i-1)}) / \delta t]$ . The calculated value is expressed in units of  $mm\ day^{-1}$ .
- Root Growth Rate (**RGR**): The weighted sum of the **VGR** and **HGR** values. The weights are defined by the corresponding RS dimensions of height (400 mm) and length (261 mm), i.e.,  $RGR_{ti} = (VGR_{ti} * 0.605144) + (HGR_{ti} * 0.394856)$ . The calculated value is expressed in units of  $mm\ day^{-1}$ .
- Average Root Growth Rate (**ARGR**): The average value of the **RGR** values from each time point (t), i.e.,  $ARGR = (\sum_{ti=1}^{ti=n} RGR_{ti})/n$ . The calculated value is expressed in units of  $mm\ day^{-1}$ .
- Average Vertical Growth Rate (**AVGR**): The average value of the **VGR** values from each time point (t), i.e.,  $AVGR = (\sum_{ti=1}^{ti=n} VGR_{ti})/n$ . The calculated value is expressed in units of  $mm\ day^{-1}$ .
- Average Horizontal Growth Rate (**AHGR**): The average value of the **HGR** values from each time point (t), i.e.,  $AHGR = (\sum_{ti=1}^{ti=n} HGR_{ti})/n$ . The calculated value is expressed in units of  $mm\ day^{-1}$ .

### 2.4.9 Substrate image RGB spectra

To assess the optical characteristics of each substrate, an RGB profile was obtained by scanning each the minirhizotrons ( $n = 4$ ) filled with the candidate RS substrates from experiment 1 (Section 2.5.1) at 1,600 dpi after reaching field capacity and prior to the seedlings being sown into them. The samples used in that experiment were of minirhizotron design A which had a 5 mm thick acrylic as the scanning surface. The average value of the percentage RGB histogram distributions was then computed by using the “Analyse/Color Histogram” command of Fiji (<http://www.fiji.sc>) after manually cropping the images to the rectangular section that included only the RS substrate. An additional black coloured sand (Flourite Black) was also tested later (experiment 2 - Section 2.5.2) for its optical properties by using the same method. This sand was chosen because it was clay-based and thus, hypothesized to give a more favourable root growth than the substrates already tested.

Finally, in order to extract the root foreground optical properties from the image and subsequently obtain their RGB profile for comparison with the rhizotron substrates, seedlings were grown for 2 weeks in the RS ( $n = 4$ ) and then subsequently scanned at 1,600 dpi prior to terminating the experiment. The visible root boundaries were then manually traced by using

the “Polygon selections” tool of Fiji to extract the root foreground from the image and subsequently obtain their RGB profile for comparison with the candidate RS substrates.

### **2.4.10 Image quality - Image Sharpness Index**

To assess the quality of the images obtained through different imaging surfaces an image sharpness index was used. The Image Sharpness Index (ISI) is a dimensionless measure of image sharpness which is computed by estimating the average value of the local greyscale variance at the scale of interest (Erasmus and Smith, 1982). The scale chosen here is a block radius of 1 pixel because root hairs are only 1 or 2 pixels thick at the image scale. Despite its simplicity, the method tends to be more robust to noise relative to most other candidates (Moreno and Calderero, 2013). A higher index value indicates a sharper image as the image intensity variation tends to be smaller when blurriness is stronger (Batten, 2000).

Image processing involved the following steps (Microsoft Visual C++ implementation):

- 1) The skeleton of the visible root system (centre line) was traced manually by using the “Segmented Line” tool of Fiji (<http://www.fiji.sc>).
- 2) Each of the (n) identified skeleton pixels were assigned a uniform probability ( $1 / n$ ) and then 4 pixels were randomly selected for each image to obtain unbiased estimates.
- 3) A rectangular section of 640 x 640 pixels was formed around each of the 4 randomly selected pixels. The size of this area was empirically determined to sufficiently cover the root hair zone adjacent to the root. If any of the 4 image regions overlapped, then the process was repeated until there was no region overlap.
- 4) The **ISI** measure described above was then computed for each of the 4 image sections.
- 5) Finally, the (4 x 3) values associated with each treatment were pooled together and analysed with Dunnett's T3 test for comparison of their mean values. This step was performed by using the R script provided by Wilcox, R. (2017), available for download at the url: <https://dornsifelive.usc.edu/labs/rwilcox/software/>.

### **2.4.11 Statistical Analysis**

The statistical analysis of the data was performed using the software R (version 3.5.0). The statistical significance test used for comparing the arithmetic averages of the experimental treatments was Dunnett's T3 test and was implemented with the “lincon” function of the freely available R script provided by Wilcox, (2017), which can be downloaded from the

following url: <https://dornsifelive.usc.edu/labs/rwilcox/software/>. The degree of statistical significance is represented by \*, \*\* and \*\*\* corresponding to a p value in the interval of (0.05, 0.01], (0.01, 0.001] and (0.001, 0] respectively. The 95% confidence interval of the difference between 2 treatments is represented by “95% CI”. The graphical outputs were also produced in R with the “ggplot2” and the “grid” packages. The convention adopted here is to annotate a graph only if a statistically significant difference was detected.

### **2.4.12 Rhizotron Substrate Selection**

To identify an RS substrate which could be used in future experiments, an assessment of root growth for each candidate substrate was required. The main aims could be summarised as:

- Aim 1: Test the construction of minirhizotron design A.
- Aim 2: Identification of an artificial sand which could be used in future experiments.
- Aim 3: Assess whether artificial substrate could produce similar root growth rates to soil.
- Aim 4: Identify potential minirhizotron improvements.

To test the initial minirhizotron design A, the minirhizotrons were filled with four growth substrates: “Bullion Soil”, “Pilmore Soil”, “Black Sand” and “Blue Sand” with four minirhizotrons per treatment. The physical properties of the soils used are described in Section 2.4.4 and all treatments were first sieved to 2 mm. The minirhizotrons were packed at a DBD of  $1.5 \text{ g cm}^{-3}$ , adjusted and kept at 15% gravimetric moisture content by weighting each of them every 2-3 days and adding the required amount of tap water to return them to 15%. 5 ml of the standard Hoagland's solution for nutrients were added every 3 days to all the samples. The experiment itself started in mid-May of 2017 and had a duration of 3 weeks.

### **2.4.13 Rhizotron Substrate Particle Size Distribution Comparison**

The initial assessment of potential growth substrate materials (Section 2.4.12) provided evidence that root growth in RS using the sand substrates tested was statistically significantly less than the soil treatments used, which was in violation of P1. A potential method to remedy this issue was to manipulate the Particle Size Range (PSR) of the substrate in order to change the distribution of pores in the RS to one that was more favourable for root growth. This was hypothesized because of the great importance that the pore network has in influencing the functions of the substrate (Pagliai and Vignozzi, 2002; Anderson and Croft, 2009) and how manipulating that volume can have an impact in root growth (Lipiec *et al.*, 2016; Poorter *et*

*al.*, 2012; Valentine *et al.*, 2012). By identifying a substrate which had a higher degree of similarity with the physical properties of the soil types tested in Experiment 1, it was hypothesized that this will translate to potential improvements in root growth which will in turn help the RS achieve P1.

In consideration of the results of the previous experiment a newly obtained aquarium sand was used to test the above-mentioned hypothesis. This substrate, i.e., “Flourite Black Sand” (Seachem), was reported to be clay-based and as such, it was thought that it might provide a better rooting environment for plants within the RS.

The experimental aims for this experiment are as follows:

- Aim 1: To determine if manipulation of the sand PSR could induce an improvement on root growth rates.
- Aim 2: To identify the PSR with the highest **ARGR** value.
- Aim 3: To characterise the physical properties of the sand in relation to the soil properties.

Minirhizotron design A was used to compare the **ARGR** of barley in different particle size distributions of “Flourite Black Sand” growth material. **Table 2.3** lists the distribution mixes of the 4 treatments used in this experiment expressed as a percentage of the total mass. The mixtures were created by combining the sieved fractions of two different sized versions of the same material: “Flourite Black” (4-2 mm) and “Flourite Black Sand” (2-0 mm).

**Table 2.3:** Particle size distribution treatments definition table (% of total mass).

<b>Treatment</b>	4 – 2.8 mm (Gravel)	2.8 – 2 mm (Gravel)	2.0 – 1.4 mm (Sand)	1.4 – 1 mm (Sand)	1 – 0.5 mm (Sand)	0.5 – 0 mm (Sand)
<b>4-0</b>	16.67	16.67	16.67	16.67	16.67	16.67
<b>Fraction</b>		20.0	20.0	20.0	20.0	20.0
<b>(mm)</b>			25.0	25.0	25.0	25.0
				33.33	33.33	33.33

The minirhizotrons were packed at a DBD of 1.5 g cm<sup>-3</sup>, adjusted and kept at 15% gravimetric moisture content by weighting each of them every 2-3 days and adding the required amount of tap water to return them to 15%. 5 ml of the standard Hoagland's solution

for nutrients were added every 3 days to all the samples. The experiment itself took place on early November of 2017 and had a duration of 3 weeks.

#### **2.4.14 Rhizotron Scanning Surface Selection**

To redefine the **LLWR** in terms of root traits it is essential to be able to measure those traits as accurately as possible. This includes both coarse features (roots) and features of finer scale, e.g., root hairs. Thus, it was critical to increase the quality of the images obtained in RS to increase the detection probability of the root system features. This experiment was designed to investigate the effect that different scanning surfaces have on image quality, more specifically the degree of image sharpness (**ISI**). The scanning surface with the highest **ISI** values could then be integrated in the existing RS design.

The experimental aims of this experiment could be summarised as:

- Aim 1: **ISI** assessment for different rhizotron scanning surfaces.
- Aim 2: Identification of the rhizotron scanning surface with the highest **ISI** value.

Three different scanning image surfaces were assessed for their **ISI** values. These were 4 mm thick low iron glass (Jaytec Glass Limited), 5 mm thick acrylic (PlasticSheets.com) and 2 mm thick acrylic (PlasticSheets.com). The minirhizotron design A was used with the test growth medium, “Flourite Black Sand”. This time lapse study took place in early February of 2018 and lasted for a period of 2 weeks with scanning taking place once a week. The entire rhizotron area was scanned at 1,600 dpi with a flatbed scanner (EPSON Expression 10000XL) and saved as a TIFF file. Three minirhizotron replicates were allocated per treatment.

#### **2.4.15 Assessment of plant responses to alternative growth substrate (“Flourite Black Sand”)**

The initial assessment of growth substrate in the minirhizotron design A, provided evidence that the initial selections of sands produced much reduced root growth rates compared with the two soil treatments (Section 2.4.12). To remedy that issue an alternative sand (Flourite Black) was introduced and its particle size distribution was modified to make its properties more comparable to soil (Section 2.4.13) but this required validation through comparison with soil. In addition, changing the scanning surface to improve image sharpness (Section 2.4.14) required modifications to the minirhizotron design A to be able to support the much thinner scanning surface. A further design change was added in the form of leaky pipes to

improve the control and allow automation of watering. In order to validate the final RS design the new system containing “Black Fluorite” growth substrate will have to be compared with the same design containing soil as the growth substrate.

The main aims may be summarised as follows:

- Aim 1: Test the new minirhizotron design B.
- Aim 2: Compare **ISI** values of the RS substrate to soil substrates.
- Aim 3: Compare root growth of RS substrate to soil substrates.

Minirhizotron design B was used to compare the **ISI** and **ARGR** values of four different RS substrates. The treatments compared were “Flourite Black”, “Pilmore Soil”, “Bullion Soil”, and “Flourite Black & Soil”. The “Flourite Black” substrate was the 4-0 mm treatment identified in the particle size distribution experiment (Section 2.4.13). The soil used in “Pilmore Soil” and the “Bullion Soil” was once again collected from their respective fields and sieved to 4 mm. An additional substrate “Flourite Black & Soil” was created by mixing the Flourite Black, Pilmore Soil and Bullion Soil on a mass basis of 50, 25 and 25 % respectively. This was done to assess if the soil component could increase root growth rates to be more similar to those of the pure soil treatment and to assess if soil addition leads to inferior imaging quality. The minirhizotron area section which contained visible root segments was manually selected, scanned at 1,600 dpi with a flatbed scanner (EPSON Expression 10000XL), and saved as a TIFF file. The experiment took place in mid-May of 2018 with scanning being performed on the 7<sup>th</sup>, 14<sup>th</sup> and 21<sup>st</sup> day of the experiment. Four minirhizotron replicates were allocated per treatment.

## 2.5 Results

**Figure 2.3** shows example representative images of each treatment used in the experiment designed for selecting a minirhizotron-based substrate described in Section 2.4.12.

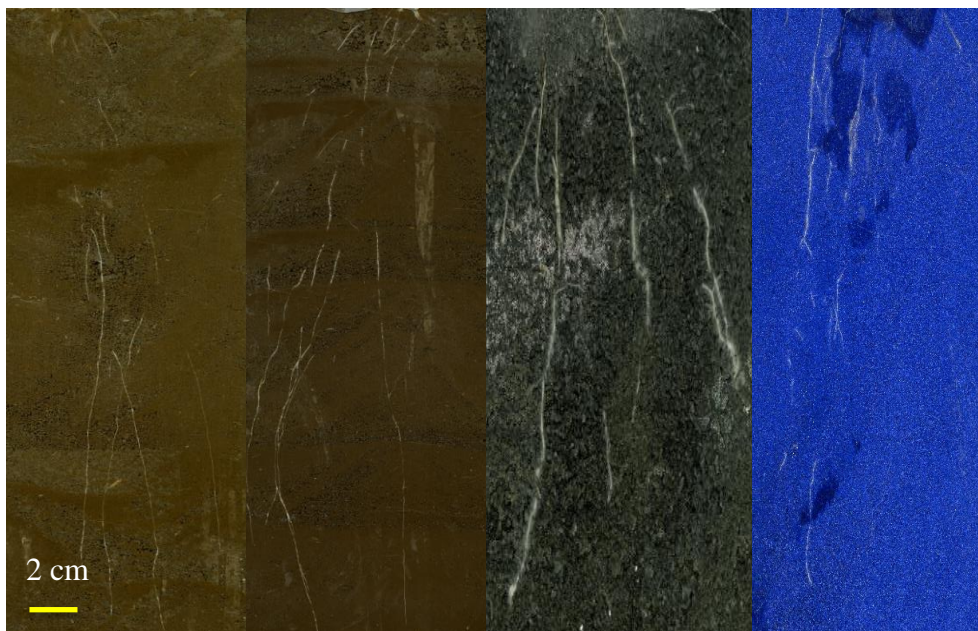


**Figure 2.3:** Spring barley root systems, growing in the four different substrates **A)** Bullion soil, **B)** Pilmore Soil, **C)** Black sand and **D)** Blue sand in minirhizotron design A. Images obtained using Epson scanner at 1600 dpi, on day 14 since transfer of seedling rhizotron.

**Figure 2.4 (A)**, is a summary graph for the **ARGR** of each substrate and it demonstrates that the **ARGR** within the “Black Sand” treatment was statistically significantly less at  $6.424 \pm 1.433 \text{ mm day}^{-1}$ , than both the “Bullion Soil” at  $15.544 \pm 0.298 \text{ mm day}^{-1}$  and the “Pilmore Soil” treatment at  $15.428 \pm 1.311 \text{ mm day}^{-1}$  with a 95% CI of (-12.427, -5.812) and (-12.304, -5.704) respectively. Likewise, the “Blue Sand” treatment at  $3.007 \pm 2.929 \text{ mm day}^{-1}$  was statistically significantly less than both the “Pilmore Soil” and the “Bullion Soil” treatments with a 95% CI of (-19.454, -5.619) and (-18.738, -6.104) respectively. Therefore, both sand treatments significantly inhibited **ARGR** in comparison with the soil treatments.

**Figure 2.4 (B)**, is a summary graph for the **AVGR** of each substrate and it demonstrates that the **AVGR** within the “Black Sand” treatment was statistically significantly less at  $6.737 \pm 1.901 \text{ mm day}^{-1}$  than both the “Bullion Soil” at  $18.432 \pm 0.499 \text{ mm day}^{-1}$  and the “Pilmore Soil” treatment at  $17.68 \pm 1.991 \text{ mm day}^{-1}$  with a **95% CI** of (-16.016, -7.373) and (-15.612, -6.274) respectively. Likewise, the “Blue Sand” treatment at  $3.086 \pm 3.581 \text{ mm day}^{-1}$  was statistically significantly less than both the “Pilmore Soil” and the “Bullion Soil” treatments with a 95% CI of (-23.749, -6.943) and (-22.219, -6.969) respectively. Therefore, both sand treatments significantly inhibited **AVGR** in comparison with the soil treatments.

**Figure 2.4 (C)**, is a summary graph for the **AHGR** of each substrate and it demonstrates that the **AHGR** within the “Black Sand” treatment was statistically significantly less at  $5.945 \pm 1.641 \text{ mm day}^{-1}$  than both the “Bullion Soil” at  $11.118 \pm 1.464 \text{ mm day}^{-1}$  and the “Pilmore

Soil” treatment at  $11.977 \pm 0.504 \text{ mm day}^{-1}$  with a 95% CI of (-8.918, -1.428) and (-9.714, -2.351) respectively. Likewise, the “Blue Sand” treatment at  $2.886 \pm 1.935 \text{ mm day}^{-1}$  was statistically significantly less than both the “Pilmore Soil” and the “Bullion Soil” treatments with a 95% CI of (-12.447, -4.016) and (-13.492, -4.69) respectively. Therefore, both sand treatments significantly inhibited **AHGR** in comparison with the soil treatments.

**Figure 2.4 (D)**, is a summary graph for the **VRL** of each substrate and it clearly demonstrates that the vertical root length was less for both sands when compared to the soils. It also demonstrates that most samples for the soil treatments had almost reached the 400 mm limit of the **RS** by the end of week 2. This will imply that the difference in **AVGR** between the soil and the sand treatments will be even higher if they were not restricted by the size of the **RS**. It can also be observed, that the **VRL** of the “Black Sand” was higher in comparison to the “Blue Sand”.

**Figure 2.4 (E)**, is a summary graph for the **HRL** of each substrate and it clearly demonstrates that the horizontal root length was less for both sands when compared to the soils. It also demonstrates that most samples for the soil treatments had almost reached the 261 mm limit of the **RS** by the end of week 3. The figure also suggests that the **HRL** of the “Black Sand” was higher in comparison to the “Blue Sand”.

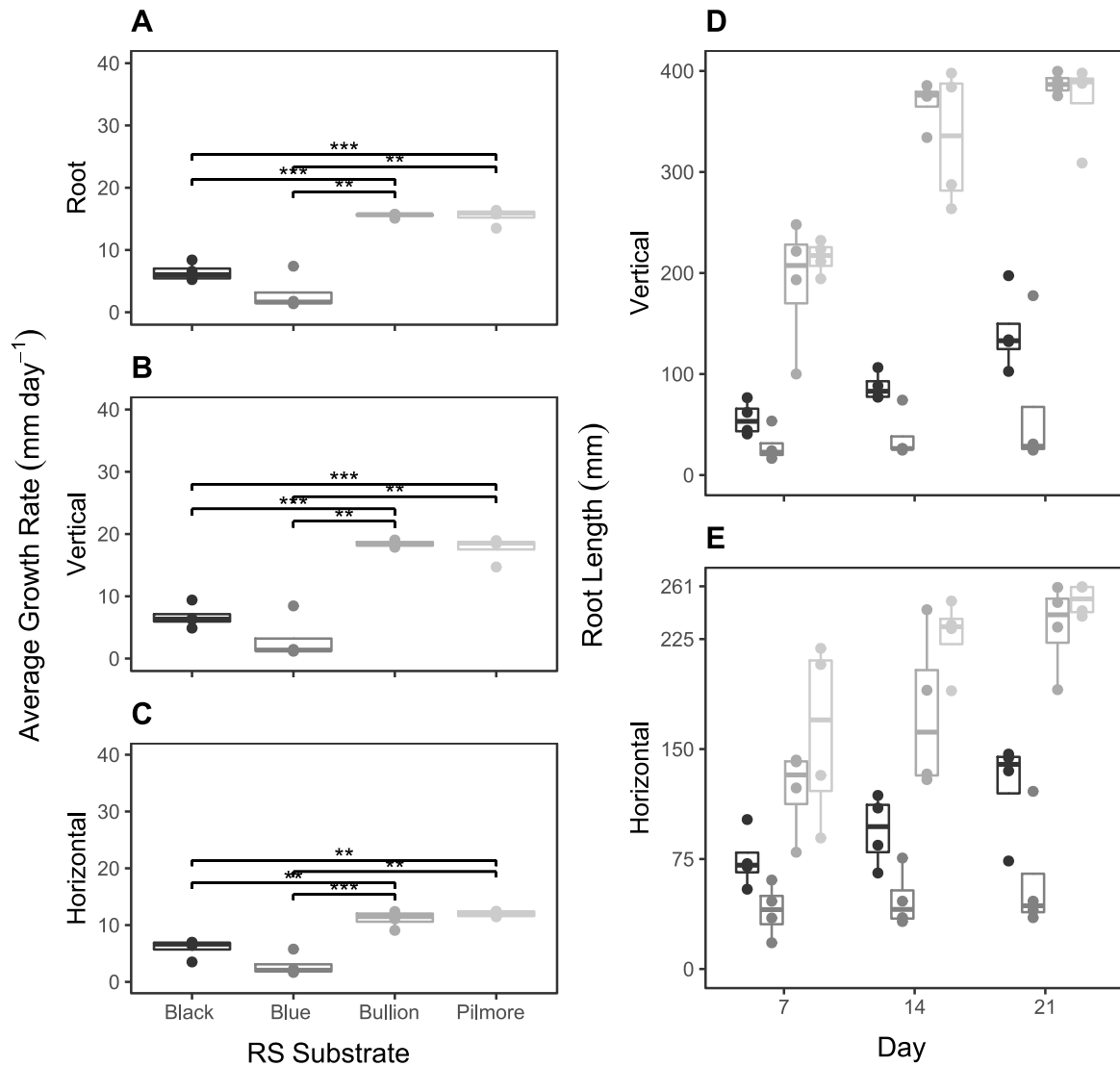


**Figure 2.4:** Summary graphs of spring barley root growth in growth substrates (Black sand, Blue sand, Bullion soil and Pilmore Soil) in rhizotrons for a period of 21 days, **A) ARGR vs. substrate, B) AVGR vs. substrate, C) AHGR vs. substrate, D) VRL vs. time and E) HRL vs. time.**

Both coloured sands tested had a statistically significantly lower **ARGR**, **AVGR** and **AHGR** when compared to the soil treatments which implied that the sands were unsuitable for future experiments. Comparisons of root lengths in both the vertical and the horizontal directions also supported this conclusion. This was a clear indication that the sands tested had properties which differed from soil. However, this could potentially be explained, at least partially, by the observation that a noticeable amount of substrate slumping occurred across the samples as the scanning surface was not robust enough to support the weight of the growth matrix across the entire RS surface. The reduction in substrate occupied volume led to changes in the dry

bulk density which depends on volume. This added an additional uncertainty component as to whether the differences in root growth were the result of differences in substrate properties or compaction caused by slumping. Ultimately, this error was affecting all of the samples which made it a random error, and in consideration of the rather strong root growth differences between both soil treatments to the sand treatments, it was decided that future experiments would explore the use of alternative natural sands to ensure P4 was satisfied.

In addition, this experiment revealed a number of issues with minirhizotron design A that could be potentially improved in future work:

- 1) The packing of the rhizotrons clearly demonstrated the issue of estimating the rhizotron volume accurately as the scanning surface was not thick enough to support the weight of the growth matrix across the A3 size, which allowed bowing and slumping of the substrates giving misleading volume estimates and imprecise calculated dry bulk densities.
- 2) The addition of nutrient solution was a laborious/time consuming task because it required making large volumes of Hoagland's solution prior to the experiment in addition to weighting and manually adding the appropriate amount for each rhizotron every time.

**Figure 2.5** shows summary root growth graphs of each treatment used in the experiment designed for selecting an optimum particle size range for the “Flourite Black” substrate described in Section 2.4.13.

**Figure 2.5 (A)**, is a summary graph for the **ARGR** of each PSR and it demonstrates that the **ARGR** within the “4-0” treatment was statistically significantly higher than the “1.4-0”, “2-0” and the “2.8-0” treatments with a 95% CI of (-0.067, 5.513), (0.031, 5.636) and (-0.099, 6.993) respectively. The mean values of the treatments were  $10.9 \pm 1.199$ ,  $8.177 \pm 0.607$ ,  $8.066 \pm 0.857$  and  $7.452 \pm 1.483$  mm day<sup>-1</sup> respectively.

**Figure 2.5 (B)**, is a summary graph for the **AVGR** of each PSR and it demonstrates that the **ARGR** within the “4-0 mm” treatment was statistically significantly higher than the “1.4-0”, “2-0” and the “2.8-0” treatments with a 95% CI of (0.133, 6.514), (1.047, 7.567) and (2.384, 8.732) respectively. A statistically significant difference was also observed for the comparison of “2.8-0” and “1.4-0” with a 95% CI of (-4.718, 0.249). The mean values of the treatments were  $12.815 \pm 1.365$ ,  $9.491 \pm 0.979$ ,  $8.508 \pm 1.098$  and  $7.257 \pm 0.938$  mm day<sup>-1</sup> respectively.

**Figure 2.5 (C)**, is a summary graph for the **AHGR** of each PSR and it demonstrates that the **AHGR** within the “4-0” treatment was statistically significantly higher than the “1.4-0” treatment with a 95% CI of (-0.642, 4.248). The mean values of the treatments were  $7.964 \pm 1.005$ ,  $6.162 \pm 0.33$ ,  $7.39 \pm 1.419$  and  $7.752 \pm 2.696$  mm day<sup>-1</sup> in the order given in the previous paragraph.

**Figure 2.5 (D)**, is a summary graph for the **VRL** of each PSR and it suggests that the vertical root length was highest for the “4-0” treatment across each time point.

**Figure 2.5 (E)**, is a summary graph for the **HRL** of each **PSR** and it appears to indicate that the horizontal root length was similar among treatments across each time point.

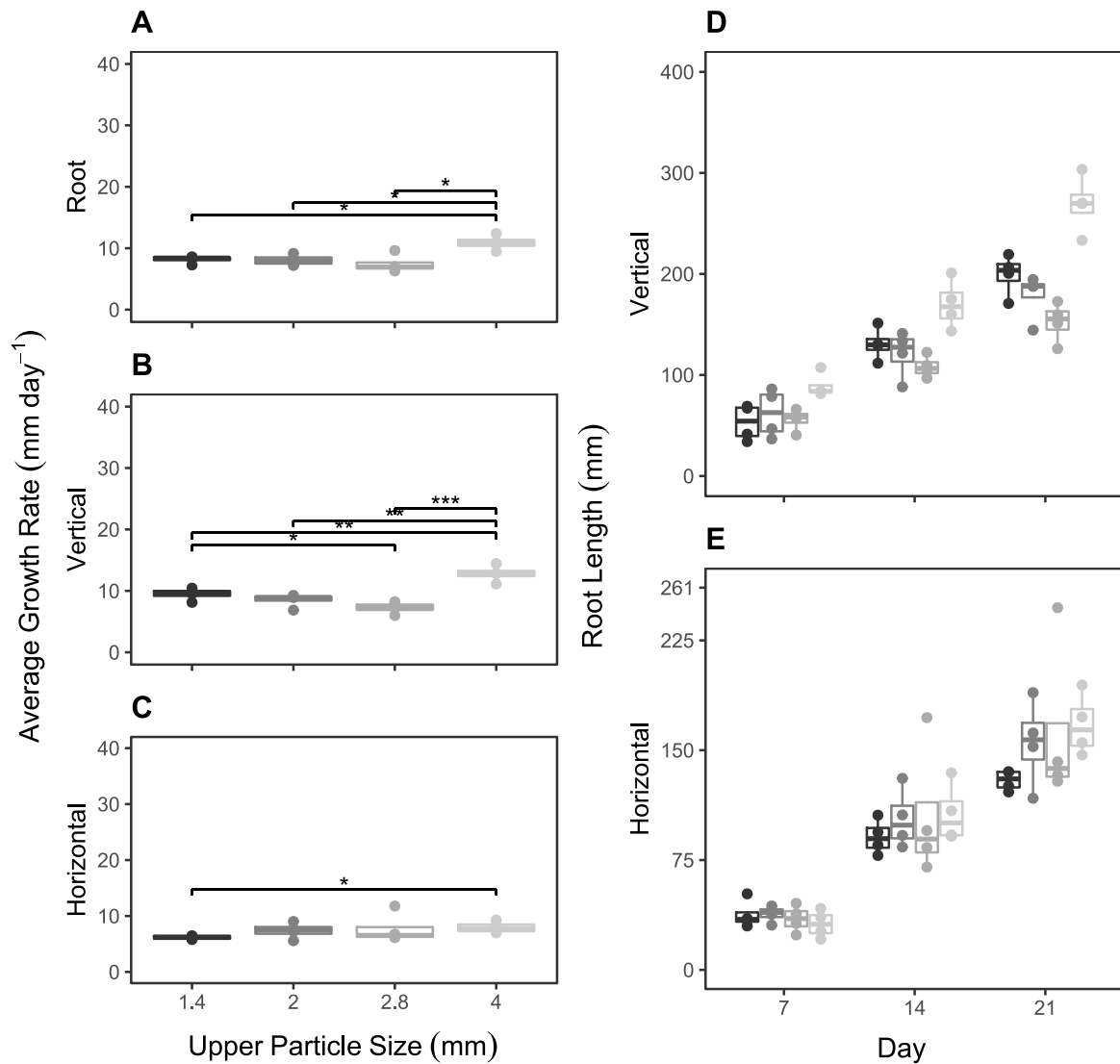


**Figure 2.5:** Summary graphs of spring barley root growth in growth substrates (1.4-0, 2.0-0, 2.8-0 and 4.0-0) in rhizotrons for a period of 21 days, **A) ARGR vs. substrate, B) AVGR vs. substrate, C) AHGR vs. substrate, D) VRL vs. time and E) HRL vs. time.**

Root growth appears to be improved for the “Flourite Black Sand” when it has an increased proportion of larger sized particles (4-0 mm) rather than a smaller particle size range. This is probably because this combination of particles generated physical properties that had a higher degree of similarity to the soil treatments in terms of both the water release and penetrometer resistance curves. However, the growth rates observed in this experiment, were comparable to the previously tested “Black Sand” and “Blue Sand” from experiment 1 (Section 2.4.12). This similarity in growth rates could be explained by the rather different environmental conditions when comparing the Scottish climate on mid-May and early November. Even though both experiments did take place in a glasshouse, differences in temperature and light do exist across seasons and at that time it was hypothesized that this was probably the reason for the comparable growth rates. As a consequence, this led to the decision to adopt the 4-0 mm mixture as the standard RS substrate in future experiments.

**Figure 2.6** shows examples of images obtained through the different imaging surfaces tested as described in Section 2.4.14. Root hairs can be seen much clearer in the image taken through the 2 mm acrylic surface (**Figure 2.6 (C)**). However, to produce an objective test for the image quality, **ISI** was (see Section 2.4.10) used to assess the images. **Figure 2.7** summarises the comparison between the different scanning surfaces, and it demonstrates that the 2 mm thick acrylic had a higher **ISI** relative to both the 4 mm glass and the 5 mm acrylic with a 95% CI of (25.033, 55.830) and (34.773, 65.668) respectively. The mean **ISI** values for each treatment were  $67.922 \pm 15.409$ ,  $27.491 \pm 5.17$  and  $17.702 \pm 5.641$  respectively.

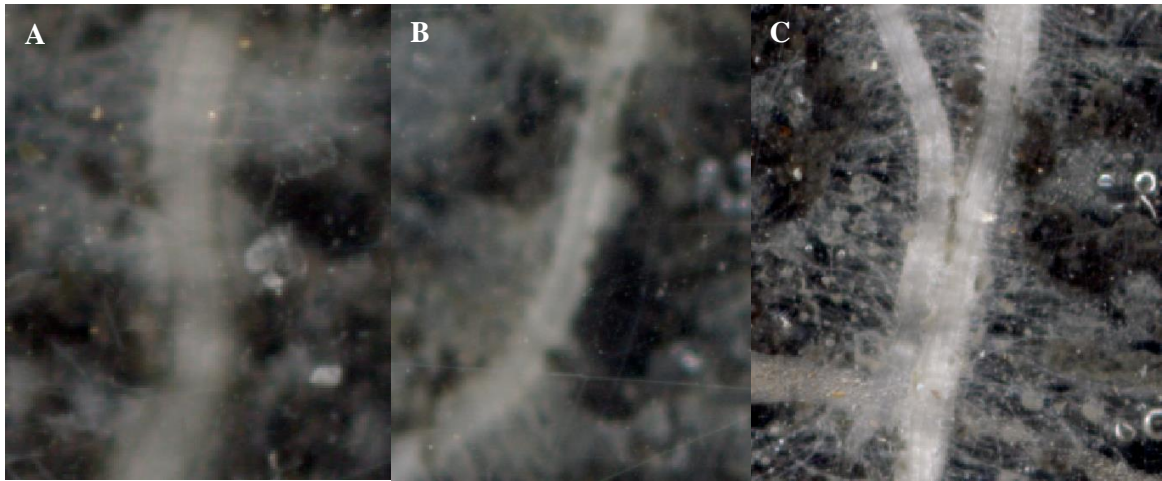


**Figure 2.6:** Rhizotron scanning surface experiment comparing imaging quality for **A)** 4 mm thick, low iron, reinforced glass, **B)** acrylic - 5 mm thick and **C)** acrylic - 2 mm thick, scanned at 1,600 dpi.

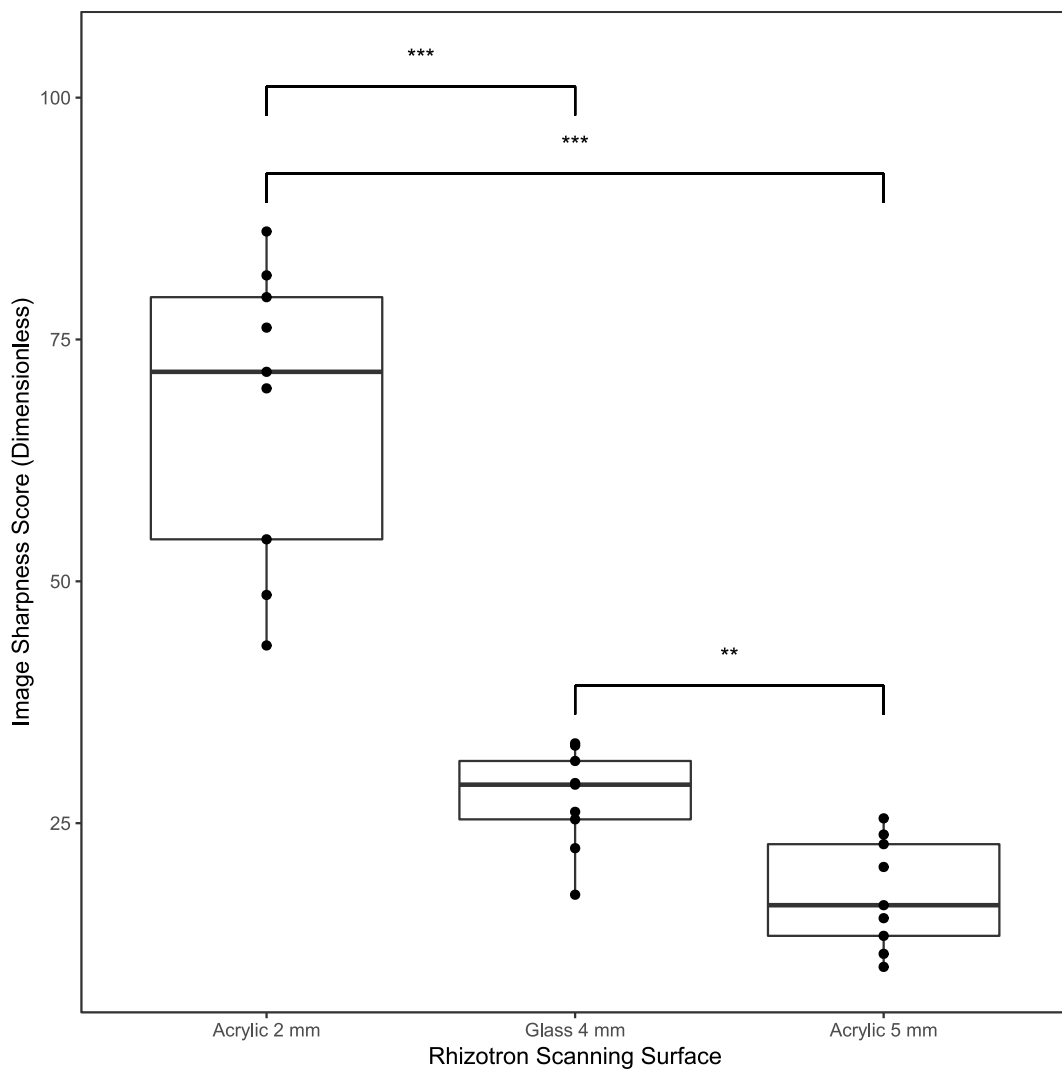


**Figure 2.7: ISI** boxplot comparison for three different RS scanning surfaces. Higher Image Sharpness (**ISI**) score indicates a higher quality image.

The 2 mm acrylic substrate had the highest **ISI** index value and as such, it was selected to be scanning surface to be integrated in future RS designs. However, issues with the strength resulting in bowing of the imaging surface meant that the minirhizotron design A would need be modified to ensure that the 2 mm acrylic can resist the combination of forces coming from the sand substrate, the water solution added to the rhizotron, and the growing root system.

**Figure 2.8** and **Figure 2.9** are summary graphs of the comparison between the different minirhizotron substrates described in Section 2.4.15.

**Figure 2.8** summarises the image quality comparison between the different rhizotron substrates, and it demonstrates that the **ISI** value of “Flourite Black” at  $58.662 \pm 27.825$  was statistically significantly higher relative to both “Pilmore Soil” at  $29.24 \pm 20.837$  and “Bullion Soil” at  $34.898 \pm 8.03$  with a respective 95% CI of (7.411, 51.432) and (4.743, 42.784). The same was true when comparing it with “Flourite Black & Soil” at  $34.707 \pm 14.547$  with a 95% CI of (3.789, 44.121), indicating that this uniform substrate gives a sharper image.

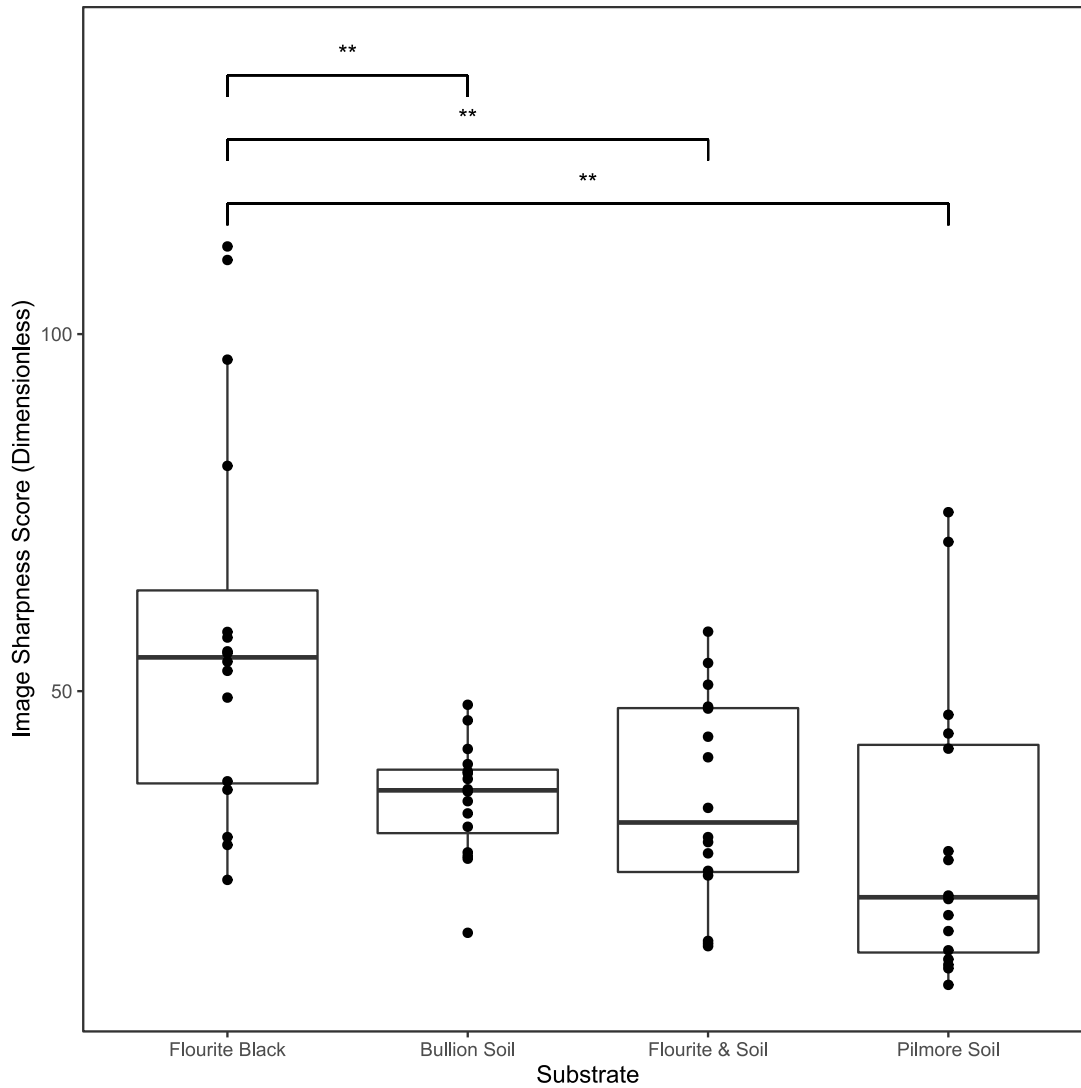


**Figure 2.8:** ISI boxplot comparison for four different RS substrates. Higher Image Sharpness (ISI) score indicates a higher quality image.

**Figure 2.9 (A)**, is a summary of the **ARGR** values obtained from this experiment and it demonstrates that no statistically significant effects could be detected across the different substrates. The 95% CI of “Flourite Black” relative to “Flourite Black & Soil”, “Bullion Soil” and “Pilmore Soil” was (-15.361, 6.951), (-14.19, 8.527) and (-17.905, 7.193) respectively. The mean values of the treatments were  $11.109 \pm 5.44$ ,  $18.924 \pm 5.677$ ,  $16.732 \pm 6.823$  and  $19.228 \pm 2.207 \text{ mm day}^{-1}$  respectively.

**Figure 2.9 (B)**, is a summary graph for the **AVGR** values obtained from this experiment and it demonstrates that no statistically significant effects could be detected across the different substrates. The 95% CI of “Flourite Black” relative to “Flourite Black & Soil”, “Bullion Soil” and “Pilmore Soil” was (-18.303, 9.309), (-18.29, 9.348) and (-21.792, 9.262) respectively.

The mean values of the treatments were  $12.865 \pm 6.368$ ,  $22.991 \pm 8.076$ ,  $21.564 \pm 8.047$  and  $23.194 \pm 3.818$  mm day<sup>-1</sup> respectively.

**Figure 2.9 (C)**, is a summary graph for the **AHGR** values obtained from this experiment and it demonstrates that no statistically significant effects could be detected across the different substrates. The 95% CI of “Flourite Black” relative to “Flourite Black & Soil”, “Bullion Soil” and “Pilmore Soil” was (-11.55, 4.035), (-9.569, 8.933) and (-12.03, 4.105) respectively. The mean values of the treatments were  $8.416 \pm 4.306$ ,  $12.691 \pm 2.449$ ,  $9.327 \pm 5.644$  and  $13.149 \pm 2.37$  mm day<sup>-1</sup> respectively.

**Figure 2.9 (D)**, is a summary graph for the **VRL** of each substrate and it suggests that the vertical root length was less for “Flourite Black” when compared to the rest of the treatments although, it does generally appear to overlap to varying degrees with the other treatments. It also demonstrates that some samples for the soil treatments had almost reached the 400 mm limit of the RS by the end of week 2, which was similar to experiment 1 (Section 2.5.1). This will imply that the difference in **AVGR** between the “Flourite Black” and the other treatments will be higher if they were not restricted by the size of the RS. The samples for the rest of the treatments had almost completely reached the 400 mm limit of the RS by the end of week 3.

**Figure 2.9 (E)**, is a summary graph for the **HRL** of each substrate and it generally indicates a similar trend with that observed for **VRL**. It also demonstrates that most samples for the soil treatments had almost reached the 261 mm limit of the RS by the end of week 3. The figure also suggests that the **HRL** of the “Flourite Black” was higher in comparison to the “Blue Sand”.

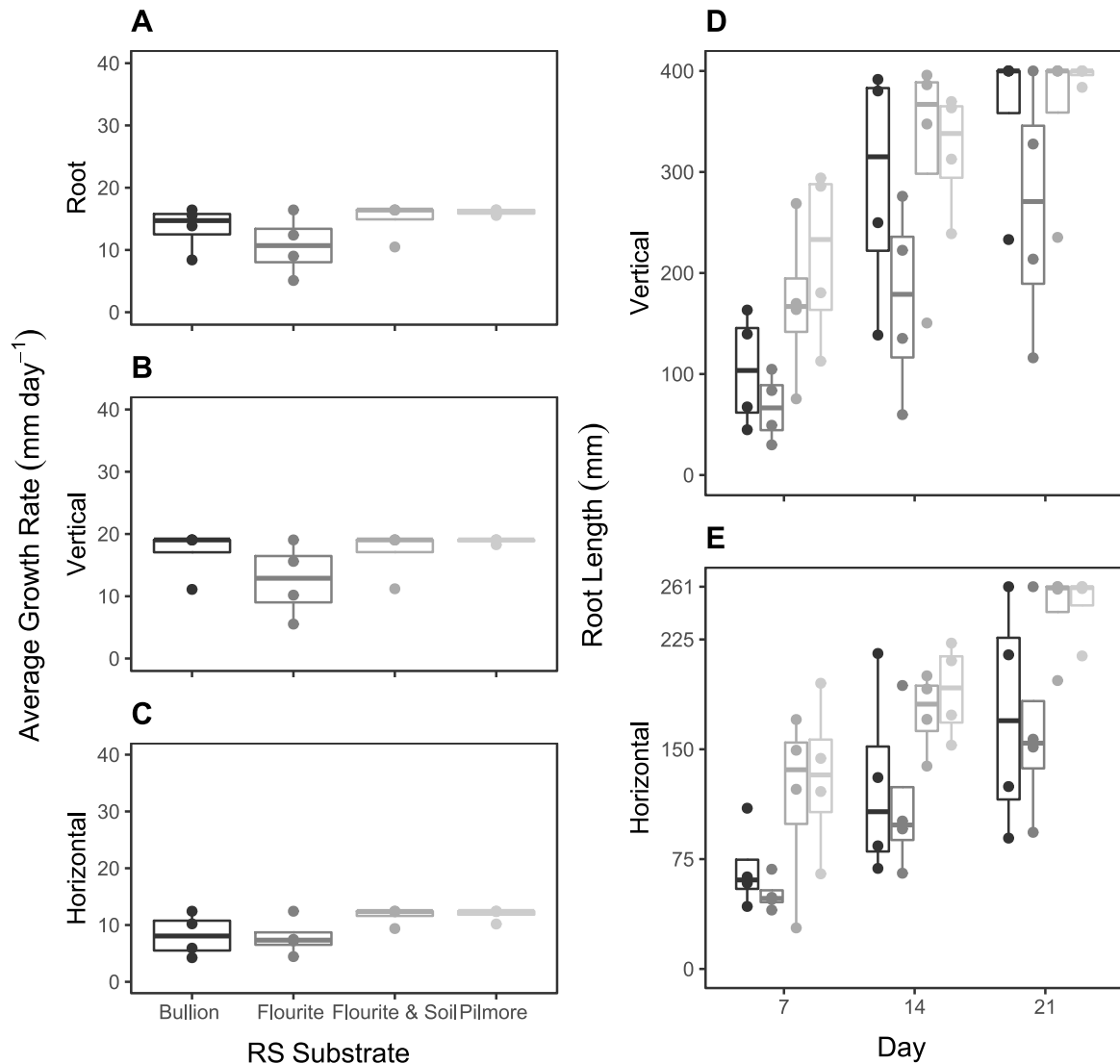


**Figure 2.9:** Summary graphs of spring barley root growth in growth substrates (Flourite Black, Flourite and soil, Bullion soil and Pilmore soil) in rhizotrons for a period of 21 days, **A) ARGR vs. substrate**, **B) AVGR vs. substrate**, **C) AHGR vs. substrate**, **D) VRL vs. time** and **E) HRL vs. time**.

Image sharpness was clearly superior for “Flourite Black”. This was also the case when comparing it to the mixed substrate as the soil component of this treatment reduced the image quality.

Root growth for “Flourite Black” was generally less than the treatments “Flourite and soil”, Pilmore soil and Bullion soil. However, the failure to detect a statistically significant effect seems to suggest that they were still comparable. This was a positive outcome because P4 was reasonably achieved with the introduced changes to the system. It should also be noted

that the root growth rates observed here are superior to those observed in experiment 2 which had comparable growth rates to experiment 1. The difference being that this experiment was performed around mid-May the same period as experiment 1 as opposed to early November for experiment 2, suggesting that seasonality does have an effect. Although, this could also be explained in part by the rather large reduction in substrate slumping achieved with minirhizotron design B.

In conclusion, based on the results of this validation experiment minirhizotron design B including the “Flourite Black” growth substrate will become the standard RS unit in future LLWR experiments.

In addition to the above, by using the methodology outlined in Section 2.4.4, the water release curve, and the penetrometer resistance curve were obtained for each of the various RS substrate candidates which enabled an assessment of the physical properties of each substrate.

**Figure 2.10 (A)** demonstrates the fitted loess models which estimate the conditional mean of penetrometer resistance to the matric suction of the soil. Although there was high variability for the fitted models on average the 4-0 mm substrate was somewhat closer to the soil treatments than the 2-0 mm substrate however, both sand treatments were noticeably different from the soil treatments. It should also be noted that at matric suction of just 20 kPa the PR values were  $\geq 2$  MPa, the LLWR threshold.

**Figure 2.10 (B)** demonstrates the fitted van Genuchten models describing the relationship between the volumetric water content and the matric suction of the soil. Although, there was high variability at low water potentials the model demonstrates that the water release curves of both of the “Flourite Black” followed a similar trend to that observed from the PR curve. It also appears that the water release curve of the 4-0 mm “Flourite Black” treatment is quite similar to a mixture of clay loam soil ( $< 2$  mm) and pebble (3 – 5 mm) mixed on a percentage mass basis of 35 and 65 % respectively (see Figure 1 in Wang *et al.*, 2013) which in hindsight is not surprising as the material is listed as a commercial aquarium sand.

**Figure 2.10 (C)** demonstrates the estimated effective pore diameter ( $d$ ) for each substrate which was obtained from the water release curve fitted van Genuchten model (Section 2.4.4). Given its relation to the water release curve the same conclusion follows as discussed above.

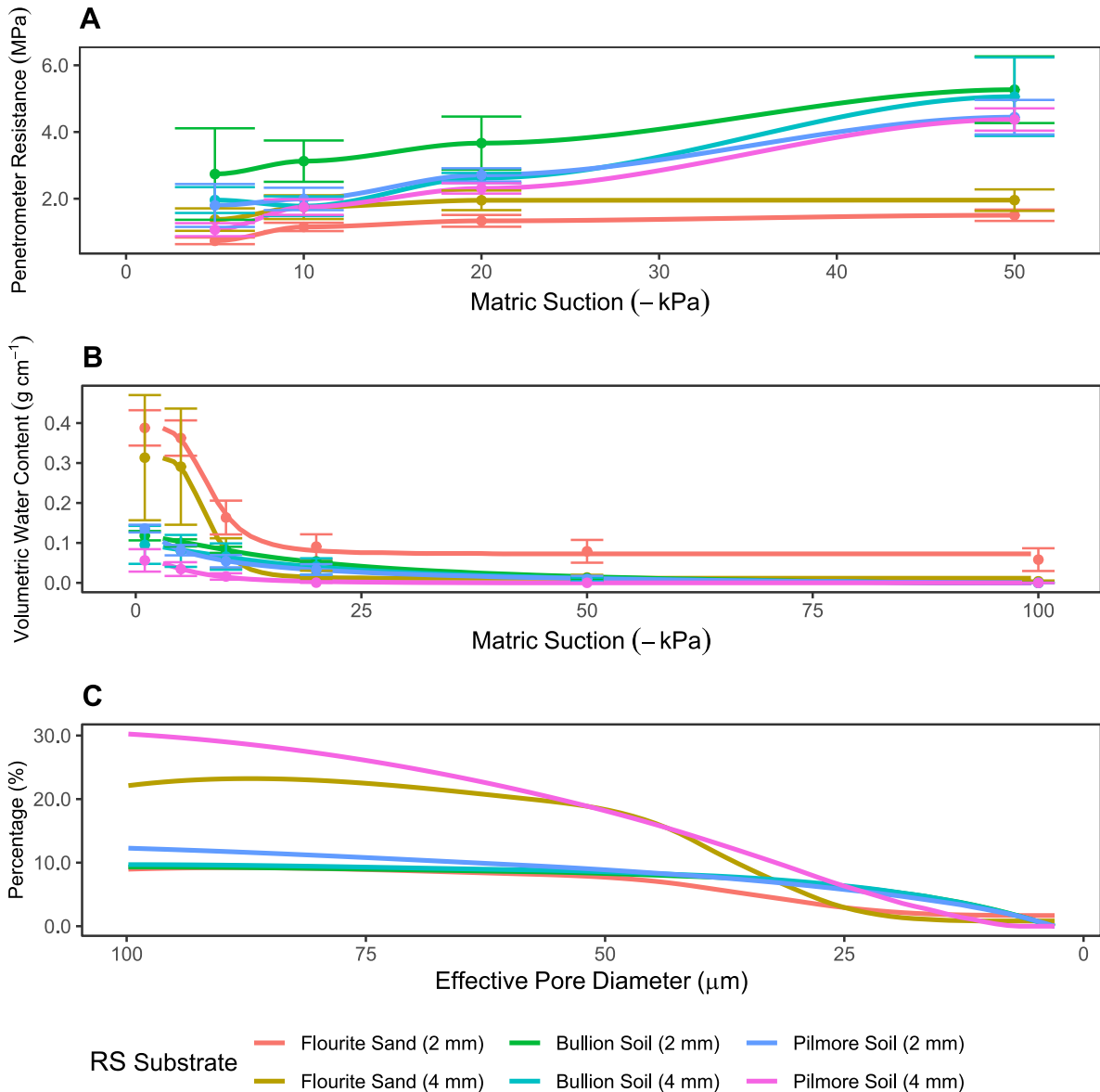


**Figure 2.10:** Physical properties of “Pilmore Soil”, “Bullion Soil” and “Flourite Black” packed at  $1.5 \text{ g cm}^{-3}$  for different PSD in terms of **A)** Water Release Curves (van Genuchten model), **B)** Penetrometer Resistance (loess regression) with mean and standard deviations shown and **C)** effective pore diameter profile.

Finally, by using the methodology outlined in Section 2.4.9, the RGB spectra were obtained for each of the various RS substrate candidates which enabled an assessment of the optical properties of each substrate. This is because differences in the distribution of the individual RGB spectra could potentially be exploited to obtain a better root segmentation from the background. **Figure 2.11** demonstrates the RGB spectra obtained from each material in addition to that from manually segmented root systems grown in RS. Two points of interest need to be pointed out concerning the spectra for roots (**A**) and “Flourite Black” (**F**):

1. The distributions of both the RGB and greyscale spectra are approximately identical suggesting, that a greyscale-based approach will provide almost identical results than methods exploiting differences in RGB spectra. This is significant because it implies that retaining only the greyscale spectrum does not lead to loss of image information. In practical terms, this translated to reduced scanning times during image acquisition, reductions in image file size and faster access speed during image processing.
2. The peaks of the RGB spectra of roots relative to those of “Flourite Black” are noticeably distinct which suggests that segmentation of roots might be possible with an automated image processing strategy.

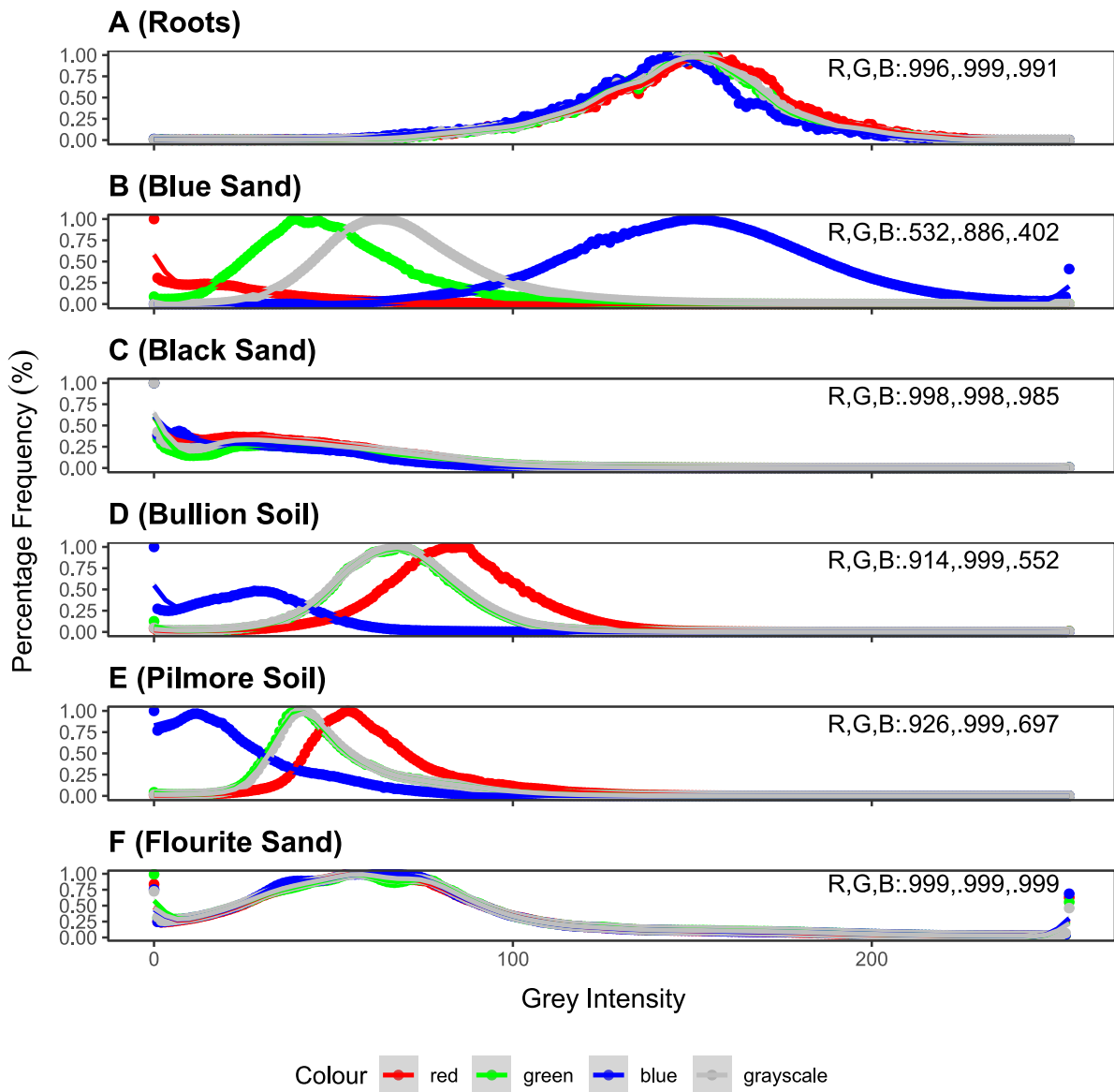


**Figure 2.11:** Histograms of RGB and greyscale spectra of tested rhizotron growth substrates with RGB mean values for **A)** Roots, **B)** Blue Sand, **C)** Black Sand, **D)** Bullion Soil, **E)** Pilmore Soil and **F)** Flourite Black.

## 2.6 Discussion

The process of developing the RS required consideration of a list of desirable properties that the system should have and as such, all the reported experiments were directly linked to the process of achieving those properties. As discussed in Section 2.2 existing systems did not completely satisfy all the requirements in imaging, size, growth substrate and costs which motivated the development of the RS system.

The first step was the development of a prototype, i.e., minirhizotron design A, which then had to be screened for its ability to satisfy the desired properties. The first experiment involved an assessment of different growth substrates to determine basic root growth parameters within this system. However, minirhizotron design A had a statistically significant lower root growth rate for artificial sands compared to soil. As a result, an alternative natural clay-based sand was sourced, i.e., “Flourite Black”, for future testing. The results of RGB histogram analysis also indicated that a black-coloured sand was more desirable to make the image processing step of separating roots from background easier as its RGB spectra were more distinct from roots than both soils and the other coloured sands. As such, “Flourite Black” was used in further minirhizotron optimisation experiments.

The second step was to try to remedy the issue of reduced root growth rates by testing the hypothesis that the physical properties of the sand could be made closer to the properties of the tested soils thus, achieving similar root growth rates. The results obtained supported the hypothesis as the 4-0 mm treatment of “Flourite Black” sand had a water release curve that was more similar to the soil treatments compared to the 2-0 mm treatment. This helped explain the statistically significantly higher root growth for the larger sized range of particles i.e., 4-0 mm. As a result, the 4-0 mm treatment of “Flourite Black” sand became the substrate which would be used in future experiments.

The third step involved testing of different rhizotron imaging surfaces to identify the one with superior image quality and as such, will increase the probability of detecting finer root traits such as root hairs. Among the different thicknesses of acrylic and glass tested the results indicated that image sharpness was statistically significantly higher for the 2 mm acrylic. However, integrating that into minirhizotron design A required modifications to the existing design. This in conjunction with the need to reduce the laborious and time-consuming task of manual watering of RS had motivated the development of minirhizotron design B. The

addition of screws and leaky pipes enabled the replacement of the imaging surface and removed the need for manual watering.

The final step in RS development was the validation of the latest design through comparison with soil. The results demonstrated that although a generally higher root growth rate was observed for the soil treatments, no statistically significant difference could be detected between Flourite sand and the soils with the same being true when comparing it to “Flourite Black” sand mixed with soil. However, the introduction of soil into the mixture led to a degradation in image sharpness with “Flourite Black” sand having a statistically significantly higher value than all other substrates. As such, the final design to be carried forward was based on minirhizotron design B with the 4-0 mm Flourite sand used as the growth substrate.

However, like all systems there are several limitations to the RS. In order to balance the requirements for root growth and image quality an artificial substrate was used. Although “Flourite Black” is an improvement compared to the other artificial sands it still lacks the complexity of soil. For example, it lacks organic matter which influences water retention properties (Kay *et al.*, 1997), and it doesn't have the biological complexity of organisms that characterize soil. Furthermore, even if soil was used as a substrate the RS substrate will still have a repacked structure which is not an accurate reflection of the spatial variability encountered in field soil. For example, penetrometer resistance is greater for field soils than packed cores (Perfect *et al.*, 1990) and even when comparing root growth in structured field soil containing clods to a homogeneously compacted soil, root morphological differences can be detected (Konôpka *et al.*, 2009). Another intrinsic disadvantage of minirhizotron systems is that root growth is effectively restricted to a thin layer which can potentially distort the naturally complex 3D root architecture and as such, the RS is technically classified as pseudo-3D. Furthermore, continuous root to glass contact could induce thigmotropic responses from the roots (Downie *et al.*, 2015) which can give misleading representations of the norm. In summary, whether the results obtained from the system are directly applicable to field soil is something to be established through field trials, but such a task will require a significant investment in time and resources and as such, it is outside the scope of this study. It should also be noted that although significant efforts were made to provide as much information as possible in terms of measured physical properties of the sand it will be interesting to also study its chemical properties. For example, cation-exchange capacity is of great importance for root nutrient availability (Hillel, 2003). However, such investigations are also outside the scope of this study.

## 2.7 Conclusions

This chapter was dedicated to describing both the motivation and the development of an experimental unit, i.e., RS, which will provide the basis for conducting future experiments. The proposed RS system was developed with the specific criteria of superior image quality and the root growth rate in the RS substrate being comparable to those from a soil substrate. This process involved the selection of (1) the imaging surface of the RS and (2) the root growth substrate used in the RS. In the case of (1) the imaging surface chosen was an acrylic surface of 2 mm thickness having outperformed the acrylic of 5 mm thickness and the low iron glass of 5 mm thickness in terms of the **ISI** index, a measure of image sharpness. For the case of the RS substrate a comparison of artificial sands and soil types led to the selection of a black coloured sand (Flourite Black) as it was judged to have a superior contrast. However, to ensure (2) the selected sand was sieved to a range of sized fractions and each was compared to the soil substrates. The 4-0 mm sized fraction of sand was determined to be the most similar relative to the soil treatments based on the comparison of root growth rates. The resulting RS unit was developed to be a sand-based, particle size adjusted substrate which enables the manipulation of the LLWR stressors while giving comparable root growth rates to soil and sufficiently detailed images for imaging fine root traits such as root hairs. As a consequence, the minirhizotron-based system was judged to sufficiently satisfy its design requirements and allow for the modification of the LLWR model through the integration of root traits.

## 3. Root trait imaging and image analysis

### 3.1 Introduction

Roots are responsible for numerous functions that determine the survival and growth of plants. Roots provide anchorage to the soil, acquire mineral nutrients and water, transport and store resources and synthesize a plethora of metabolites (Gregory, 2008; Schmidt, 2014). Furthermore, they have a central role in ecosystem functioning (Bardgett, *et al.*, 2014). For example, plant roots influence nutrient and carbon cycling in terrestrial ecosystems (de Kroon and Visser, 2003) and root turnover is estimated to account for approximately one third of the global primary productivity (Gill and Jackson, 2000). Root biomass itself accounts for a significant amount of the total plant biomass which can range from 16 % in tropical forests to 77 % in grasslands (Poorter *et al.*, 2012). Roots also have a myriad of dynamic interactions with soil microbial organisms which can have both positive and negative outcomes for plant health (Hinsinger *et al.*, 2009; Raaijmakers *et al.*, 2009). As such, strategies for enhancing the resource acquisition of crops are more frequently identified as of increasing importance for achieving sustainable food production (Tian and Doerner, 2013). A number of those strategies aim for more efficient utilization of soil resources through selection of root traits in order to facilitate the transition from high-input monoculture based agriculture to productive, sustainable agroecosystems with low inputs (Schmidt, 2014). In particular, root morphology is increasingly recognized to be of vital importance to a range of fields including plant nutrition, physiology, breeding, and ecology (Rogers and Benfey, 2015) with some characterising it as the most important of all (Lu, Wang and Wang, 2019). As such, the ability to image roots in real time in an accurate and precise way can be a catalyst for increasing crop yield and quality in agriculture (Chen *et al.*, 2018).

More traditional approaches to study roots are based on destructive root sampling such as soil auguring and ingrowth cores (do Rosário *et al.*, 2000) or excavation trenches (Van Noordwijk *et al.*, 2000). However, those methods are labour intensive, time-consuming and make the repeated measurement of roots impossible without the introduction of undesirable effects (Taylor *et al.*, 1991). Other proposed methods which are less direct such as “the core break technique” also have several limitations, e.g., soil core crumbling during its removal from the sampling tube (Bennie *et al.*, 1987). However, since the 1990s non-destructive imaging methods have become increasingly popular in plant sciences (Li *et al.*, 2014). In general,

imaging of plant root systems has evolved in two directions: (1) high-throughput phenotyping using high resolution 3D methods for small scale processes, and (2) high-throughput phenotyping using optical methods. The 1<sup>st</sup> category involves powerful set-ups such as X-ray Computed Tomography which is widely used to build and test root-soil interactions models (Dunbabin *et al.*, 2013). Unfortunately, these methods are not generally considered to be high throughput due to costs and other factors (Li, Zhang and Huang, 2014). The latter category includes “minirhizotrons”, which are usually transparent tubes in field applications (Vamerali *et al.*, 2012). A portion of the root system will then grow along the interface of the soil and the transparent container and the images can be captured by installing a coloured camera (and a light source) or some other custom-made imaging system, e.g., scanners (Rewald and Ephrath 2013). The advantages of this method are its high imaging speed and its non-destructive nature which avoids the introduction of undesirable effects from modifying the soil during measurements across different time points thus, enabling time-lapse studies (Johnson *et al.*, 2001). Unfortunately, one of the biggest limitations of minirhizotrons is the time consuming step of image processing as standard image processing methods can involve manually tracing the root system (Yu *et al.*, 2019). This limitation is further exacerbated due to the high replication which should ideally be chosen in experiments to account for the heterogeneous horizontal distribution of roots (Rewald and Ephrath, 2013). Alternatively, minirhizotron systems may be used as a flat/box closed system for monitoring of root growth along its transparent surface. A number of examples exist which utilize a wide range of substrates for root support and include gel (Bengough *et al.*, 2004), filter paper (Gioia *et al.*, 2017), glass beads (Courtois *et al.*, 2013), grids of toothpicks (Nguyen and Stangoulis, 2019), peat (Dresbøll *et al.*, 2013) and soil (Le Marie *et al.*, 2016).

In Chapter 2 the development of a flat/box type minirhizotron system (RS) was described satisfying a series of criteria one of which was the ability to image roots growing in the RS. As sufficiently high-quality imaging was achieved the next step in this process was the development of methods which enable the detection and quantification of the root traits of interest *before* and *after* destructive sampling of the root system. The standardization of the image environment and quality was hypothesized to offer the opportunity for automated analysis instead of manual analysis of the images. This chapter describes a set of 3 different algorithms which were custom developed, in order to help reduce the amount of time required for image processing and help optimise the procedure of quantifying root traits.

## 3.2 Minirhizotron System

### 3.2.1 Minirhizotron-based root imaging methods

Minirhizotrons enable inspection of their root/glass interfaces by using a miniature video camera to obtain continuous, non-destructive recordings of roots that can then be analysed (Upchurch and Ritchie, 1983). This process was further optimised by the development of methods designed to facilitate the analysis of minirhizotron recordings by manually tracing the roots (Cheng *et al.*, 1991). Further developments led to the introduction of software which enables the user to interactively identify and trace roots with a PC mouse (Hendrick and Pregitzer, 1993). This development also enables a higher precision in estimates of root count at different time points but generally requires more time than manual counting methods (Vamerali *et al.*, 1999).

Today, there are several imaging platforms which have completely automated algorithms for root detection, e.g., systems involving the growth of seedlings on filter paper (Dupuy *et al.*, 2017). However, the process of segmenting roots which are growing in soil is a complex one with most of the available software requiring the user to manually perform this segmentation (Möller *et al.*, 2019). Thus, the majority of tools currently available to researchers are designed to offer an efficient and user-friendly interaction by using a mouse point and click system (Möller *et al.*, 2019) for both commercial (e.g. WinRHIZO Tron (Regent Instruments)) and non-commercial (e.g. RootNav (Pound *et al.*, 2013)) software.

At the same time, there are also software designed to automatically segment roots from soil in 2D images. In general, most of the algorithms in use involve a contrast enhancement step prior to subsequent thresholding and binarization. Usually, geometric features of the root system (e.g. the ratio of root length to diameter) are used at the end of the algorithm to assign a pixel to either the background or foreground (Zeng *et al.*, 2008). However, automated root detection in rhizotron systems is a rather complicated process due to the low contrast of the image. The issue of the root background being complex will invariably mean that the images obtained will vary with soil conditions, lighting and root colour and as such, unsupervised machine learning methods will have mixed performance results (Yu *et al.*, 2019). As a result, the process of separating foreground from background is a complex one and proposed algorithms are invariably composed of multiple steps (Stockman *et al.*, 1990).

Root segmentation algorithms are usually “bottom-up” approaches which apply successively several filters until the only pixels remaining correspond to the root foreground (Pound *et al.*, 2013). Nater *et al.*, (1992), introduced the concept of artificial neural systems to increase the accuracy of automated root detection in rhizotron images. This method requires an initial training set calibration and as such, the accuracy of the results produced will be dependent on the degree of similarity between the sample and training images. Other authors recognising this complexity have used miSVM based methods to enhance the speed of re-training their model and achieve more optimum results when the background varies (Yu *et al.*, 2019). Vamerli *et al.*, (1999), identified the blue band of the spectrum as the starting point of their algorithm to better detect roots when their luminescence is similar to the background. In contrast, Zeng *et al.*, (2006), used the green band of the spectrum to extract the roots. Their method involved local entropy thresholding and machine learning (AdaBoost) as well as pre-processing steps such as linear stretching and matched filters. The algorithm was demonstrated to give good results for young bright roots however, the pre-processing step of matched filtering imposes restrictions on the shape of roots and as a result of that can miss small or jagged roots (Yu *et al.*, 2019). More recently, the same authors proposed another AdaBoost approach which effectively uses a Gibbs point process with a modified Candy model to detect roots (Zeng *et al.*, 2010). Although, the algorithm produced excellent results for their dataset the resolution of the images was rather low ( $640 \times 480$  dpi) making the computational cost of such an approach unfeasible for our images. Shojaedini and Heidari, (2013), defined level sets to achieve root segmentation from the background. This method was later modified by the addition of more pre-processing steps such as curvelet transformation to enhance weak root edges (Rahmanzadeh and Shojaedini, 2016). Lu *et al.*, (2019), used a hybrid of pre-processing methods and mathematical morphology to segment the roots from the soil background. Another option is the “RootFly” software which provides both manual annotation and automatic root detection functionality (Zeng *et al.*, 2008). The algorithm uses several pre-processing steps with subsequent matched filtering convolutions and classifiers to better detect roots. However, it does require an RGB image which has roughly a 3-fold memory size compared to a greyscale image. An additional overview of minirhizotron software can be found in the literature, e.g., Möller *et al.*, (2019).

Ultimately, if one was to consider the numerous possible combinations of experimental set-ups and treatments, the wide range of plants and varieties, and the extremely variable nature of the soil, it becomes clear that no single image processing method will be suitable to all

experimental conditions. The process of automated root detection will only be successful when the experimental conditions are standardized, and the image quality becomes reasonably consistent. As the RS unit was made to provide a consistent environment for imaging, it was hypothesized that the development of an automated algorithm may be feasible for this application. If successful, the algorithm would offer great speed in the image processing component of data collection. The process of root detection will inevitably require consideration of the root features, e.g., the length/width ratio of root segments (Stockman *et al.*, 1990). As such, the problem of root detection could be classified as a feature recognition problem, requiring knowledge of the geometrical architecture of root systems. However, even with clearly defined features detection issues arise, e.g., images of mature root systems have complex branched structures, composed of thousands of overlapping and crossing segments (Lobet *et al.*, 2017). Furthermore, the biological nature of root systems implies a dynamic environment which constantly changes, e.g., new roots have a light colour which becomes darker with age (Wells and Eis-senstat, 2001). In addition to the above, other aspects such as the resolution of the image can affect both the accuracy and precision of even basic parameters such as root length or diameter (Arnaud *et al.*, 2019).

### **3.2.2 Root hair imaging-based methods**

Conventional methods used to measure root hairs include root excavation from soil or hydroponics and subsequent imaging with light or electron microscopy (Gahoonia and Nielsen, 1997; Xie *et al.*, 2020). However, those methods have several disadvantages (Hammac *et al.*, 2011) including:

1. Root hairs have an estimated radius of only 3-8  $\mu\text{m}$  (Leitner *et al.*, 2010) and as such, the process of washing roots grown in soil makes it very difficult to estimate the degree of root hair loss prior to the washing process (Koebernick *et al.*, 2017).
2. Light and fluorescent microscopes are tedious to use because root hairs are 3D objects and as such cannot be constrained to a single focal plane.
3. The addition of stains, e.g., glutaraldehyde, in the fixation step of electron-microscopy damages the root hairs.

Imaging of root hairs in 3D soil volumes is also possible with synchrotron-based X-ray tomography although, the sample size at this resolution is at present extremely limited (Keyes *et al.*, 2013). Another option is to use high-resolution imaging to visualize the interaction of root hairs and particles in artificial media, e.g., transparent soil (Downie *et al.*, 2012). It

should also be noted, that root hairs may also be imaged using simpler setups such as high-resolution flatbed scanners but the measurements are normally done by manual tracing (Hammac *et al.*, 2011).

However, root hairs are much more difficult to measure relative to bulk roots and there are a few studies that have attempted to quantify them. Although camera-microscope tracing techniques can be used in simple transparent media such as petri dishes to quantify root hair area (Yazdanbakhsh and Fisahn, 2009) such methods again require simple substrates and become more difficult to use with increasing complexity in root architecture. Vincent *et al.*, (2017), commented on how root hair area estimation in minirhizotron studies was based on manual tracing and that to the best of their knowledge they could not find any minirhizotron based studies that quantified root hair area. The authors later presented a semi-automatic method based on multivariate logistic regression that uses both ImageJ and R to obtain estimates of root hair area for minirhizotron images. Although, this application is certainly time efficient it has being recently criticized by failing to provide measurements of root hair length and not having a clearly defined reference point where the measurement takes place along the root (Guichard *et al.*, 2019). Semi-automated methods for detecting root hairs have also been proposed (Inoue *et al.*, 1995; Narukawa *et al.*, 2009) although the user is required to manually select a number of binarization threshold and only 3.2 mm of root area was used for the analysis (Guichard *et al.*, 2019). Perhaps, the most common approach is manual tracing of roots hairs but, it has as disadvantage that it is prone to errors due to user bias. For example, in order to reduce errors from subjective user interpretation only clearly visible root hairs were segmented in the study of Koebernick *et al.*, (2017). In a similar manner, Chai *et al.*, (2019), assigned the task of manually counting root hairs to a researcher who was blind to the experimental condition due to concerns about researcher bias.

### 3.2.3 Algorithm 1 - Root length and root hair analysis

The main steps of the proposed algorithm may be summarised as follows:

1. Pre-processing (**Figure 3.1 (B)**): This step effectively isolates a sub-set of the image by negating the pixel values not satisfying a certain set of criteria. The main steps involve:
  - a. Circle removal filter
  - b. Variance and greyscale thresholding
  - c. Particle removal (pixel count < 1,500 and circularity > 0.6)

- d. Region growth
2. Vessel enhancement (**Figure 3.1 (C)**): This step enhances vascular structures to achieve a better segmentation from the background. This is achieved by applying the filter proposed by Frangi *et al.*, (1998) at a scale/sigma of 10 pixels.
3. Root segmentation (**Figure 3.1 (D)**): This step isolates the root areas from the background. The main steps involve:
  - a. (ImageJ) IsoData threshold (Ridler and Calvard, 1978)
  - b. Particle removal (pixel count < 5000 or circularity > 0.6)
  - c. Region expansion

The main outputs of the algorithm are root length, x and y dimensions of root length, total projected root area and mean root hair width to root width per unit segments. The root hair area is obtained by applying the (ImageJ) IsoData threshold (Ridler and Calvard, 1978) on the area adjacent to the detected roots after the end of step 3 (**Figure 3.2**). The mean value of the width of the root hair zone is then estimated, along with the mean width of the root in a unit segment of 10 pixels.

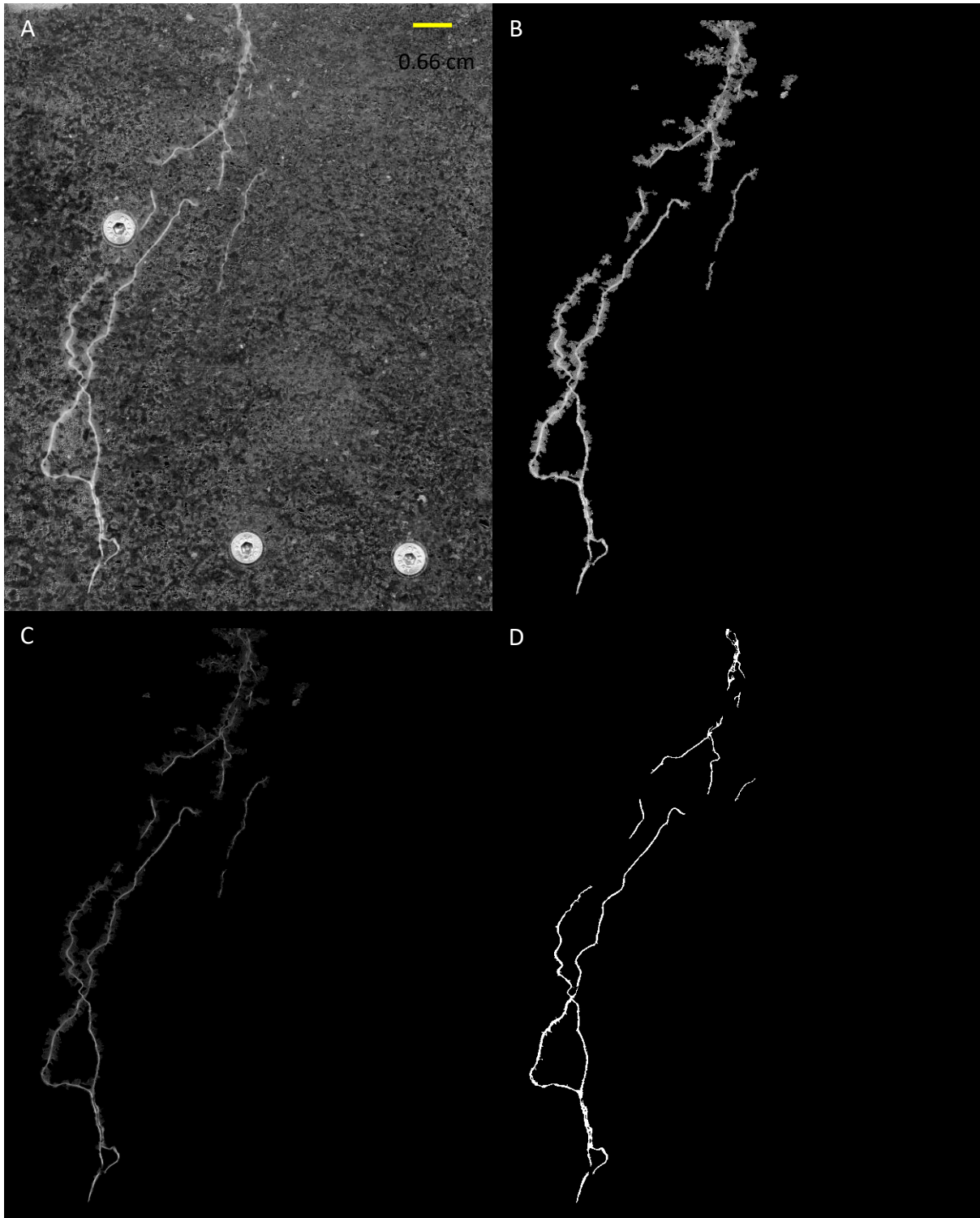


**Figure 3.1:** A) Minirhizotron image of a 14 day old spring barley seedling, B) Pre-processing for image subset selection, C) Vessel enhancement step for enhancing roots and D) Root segmentation step for extracting roots.

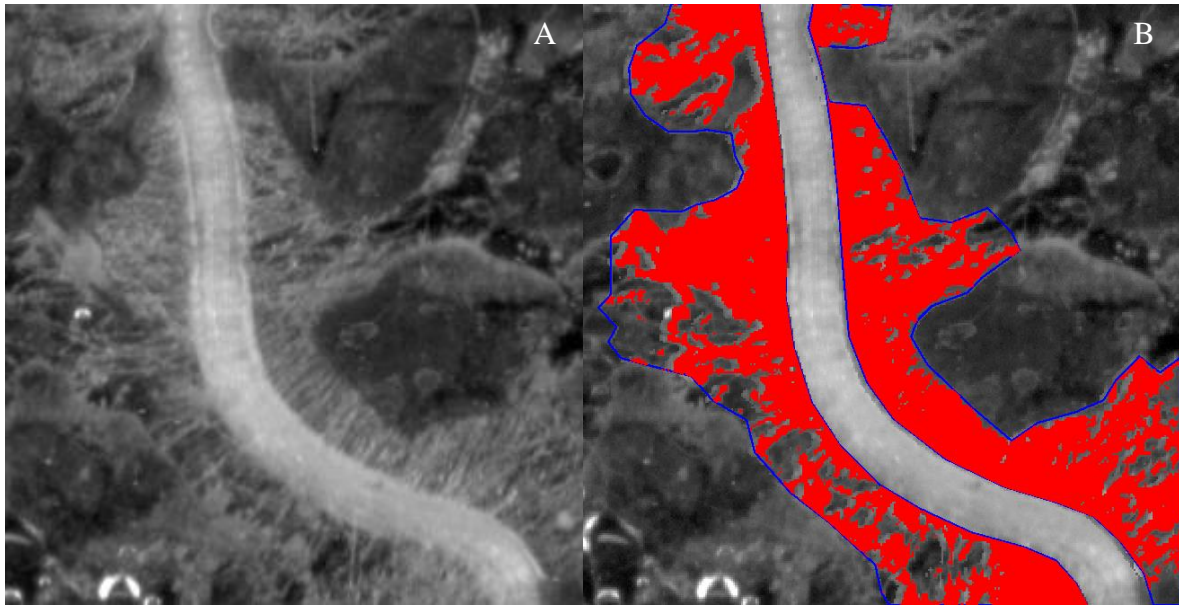


**Figure 3.2:** Magnified image of spring barley grown in the RS and scanned at 1,600 dpi. **A)** Raw image and **B)** Root hair boundary (blue) and detected root hair area (red) after thresholding the area adjacent to the root.

### 3.2.4 Root length and root hair area algorithms validation

The validation procedure for the root detection algorithm can be summarised as:

1. 10 minirhizotron images were randomly selected among a pooled dataset taken at 14 and 21 days of growth from previously performed experiments.
2. The skeleton of the visible root system (centre line) was traced manually by using the “Segmented Line” tool of Fiji (<http://www.fiji.sc>).
3. The algorithm predicted estimates of X and Y dimensional root lengths were compared to the manual ones.

The validation procedure for the root hair detection algorithm can be summarised as:

1. 5 minirhizotron images were randomly selected among a pooled dataset taken at 14 and 21 days of growth from previously performed experiments.
2. 4 image sections (300 x 300 pixels) containing root hairs were subjectively chosen by a user so that the sections spanned the length of the root system.
3. The root hair boundary was traced manually by using the “Polygon Selections” tool of Fiji.
4. The percentage of the root hair boundary area which was larger or equal to the (ImageJ) IsoData threshold value was estimated.

The execution speed of the algorithm was measured for a set of 8 images of 3-week-old seedlings grown in RS. This was achieved by using the R base function “system.time” and extracting the elapsed time from the outputs. The algorithm was estimated to have an average ( $\bar{x} \pm s$ ) execution time of  $151.02 \pm 34.20$  sec. The system properties of the PC were:

Processor: Intel® Core™ i5-6200U @ (Base) 2.30GHz (Max Turbo) 2.40GHz.

Installed memory (RAM): 16.0 GB (15.9 GB usable).

System type: 64-bit operating system, x64 based processor.

Windows Version: Windows 10.

## **3.3 Root cap and border cell measurements**

### **3.3.1 Root cap and border cell imaging methods**

The plant root cap is an important structure which offers protection to the root tip meristem from physical stresses exerted on it by the soil and determines the direction of root growth (Bengough and McKenzie, 1997). Specifically, 2 root cap associated traits are of interest here, (1) the geometry of the root tip and (2) the count of the root border cells (RBCs) produced by it. In terms of quantifying root tip geometry, there is currently only one published method for estimating root tip geometry in an automated way, the software known as ROSTA (Colombi *et al.*, 2017). This MatLab implementation enables the automated quantification of the root tip geometry for single root tips in images captured at a high resolution (2,400 dpi) flatbed scanner. The method essentially involves global thresholding to extract the root tip and subsequent ellipse fitting of the root tip perimeter to estimate eccentricity.

In contrast, there are a significant amount of reported methods for extracting, imaging and quantifying RBCs. Hawes *et al.*, (2000), immersed root tips in water for 30 seconds to extract RBCs and determined cell viability by using a vital stain, i.e., fluorescein diacetate (FDA). In a similar manner, Wuyts *et al.*, (2006), used a light microscope to count RBCs and assessed cell viability by also using FDA. Pan *et al.*, (2001), assessed average RBC count per root tip by counting them in five 20- $\mu$ l aliquots (100  $\mu$ l) under a light microscope. The authors also used a compound staining dye, i.e., fluorescein diacetate–propidium iodide (FDA–PI) to stain root tips and assess RBC viability under a fluorescent microscope. Furthermore, the authors also attempted to quantify RBCs in hydroponics but concluded that the estimates obtained

were not reliable due to RBCs dropping to the bottom of the water tanker. Vicré *et al.*, (2005), used bright field microscopy to assess RBC viability by immersing root tips in a drop of Calcein-AM about 10 to 15 min before acquisition of the images. Wang *et al.*, (2013), determined RBC viability in 8  $\mu$ l aliquots by staining them with 8  $\mu$ L of 0.4% “Trypan blue” for 3-5 min and subsequently counting white and blue cells (live / dead) under a Phenix100 optical microscope. Tran *et al.*, (2016), visualized RBCs under an Olympus BX60F5 fluorescence compound microscope by collecting them from root tips dipped into sterile water for 5 min, incubating them with  $1 \times 10^8$  CFU/ml. *R. solanacearum*-GFP for 30 min and then staining them with SYTOX Green or DAPI. It should also be stated that confocal laser scanning microscopy (CSLM) for 3D imaging is a relevant recent development in this context. For example, Kamiya *et al.*, (2016), used a Nikon C2 confocal microscope to image dead and live RBCs by soaking roots in staining solutions of 10  $\mu$ M of propidium iodide and 2  $\mu$ g/ml FDA respectively. In a similar manner, Bennett *et al.*, (2014), reported the use of a green fluorescent protein (GFP) or an alternative yellow fluorescent protein (YFP) for counting viable RBCs. Unfortunately, the above-mentioned methods all rely on manual counting of RBCs and do not offer automated image processing tools.

As a consequence, if the approach used here to quantify both root traits relied on existing methodologies, there will be 2 main limitations:

1. The time requirement for manually counting RBCs will be large, especially when multiple root tips are sampled from a single seedling.
2. After RBC counting, the same root tips will have to be cleared from the staining dyes and subsequently transferred and re-imaged in a high-resolution flatbed scanner.

If the RS was to become a high throughput system, then a more efficient methodology is required for quantifying the root micro traits after destructive sampling. As such, it was decided to use the method reported by Pan *et al.*, (2001), as a basis for quantifying RBC numbers. The method involves the use of a compound staining dye (FDA-PI) to directly assess RBC viability of root tips under a fluorescence microscope thus, avoiding the need for aliquots. The only major difference is the replacement of manual counting with an automated image processing algorithm after imaging of the root tips. This will reduce the amount of time required for image processing. A further optimisation was further made to the proposed methodology by developing a second automated image processing algorithm for determining root tip geometry from the images obtained from the microscope as the image quality was judged to be sufficient for quantifying root tip geometry.

### 3.3.2 Root tip staining and imaging procedure

After root destructive sampling, a cut was made with a scalpel ~10 mm above a selected root tip and gently placed on a microscope slide with tweezers. Any attached sand particles were then carefully picked off with the tweezers and the slide was immediately stained with a few drops of the FDA-PI compound (Pan *et al.*, 2001) and immediately covered with aluminium foil. After 5 minutes the slide was covered with a 1.7 mm thick cover slip and imaged by locating the appropriate focal plane and subsequently imaging using a Leica binocular microscope MFZ III under the GFP filter (FDA) and the Texas-Red filter (PI) with UV excitation.

### 3.3.3 Algorithm 2 – Root tip geometry and border cell analysis

#### 3.3.3.1 Root tip geometry

In order to quantify root tip geometry, the algorithm uses the following sequence of steps:

1. Greyscale (8-bit) conversion of PI stained root, imaged with Texas Red filter.
2. Morphological opening (Disk SE - radius = 20)
3. Otsu thresholding (Otsu, 1979)
4. Binary shape hole filling (if required)
5. Root contour extraction
6. Contour rotation
7. Skeletonization (Xia, 1986)
8. Savitzky-Golay polynomial filter (Savitzky and Golay, 1964) / convolution coefficients (Gory, 1990).
9. Conic model fitting / Braikenridge–Maclaurin theorem (Coxeter and Greitzer, 1967).

**Figure 3.3 (A)**, illustrates the original RGB image of the PI stained root tip obtained from the optical microscope. **Figure 3.3 (B)**, illustrates the greyscale display of the image by using only the values of the red channel which corresponds to the PI emission signal. **Figure 3.3 (C)**, shows the result of applying a morphological opening operator to enhance larger structures. **Figure 3.3 (D)**, is the result of binary transformation to isolate the root. **Figure 3.3**

(E), is the output of root contour extraction to isolate the boundary of the root. **Figure 3.3 (F)**, is the rotated version of the root outline to ensure that the root tip has a vertical orientation for technical reasons relating to the efficiency of the polynomial filter applied in the next step. **Figure 3.3 (H)**, is the result of fitting a conic section equation to the root tip extremum. This is achieved by first approximating the root contour with a 3<sup>rd</sup> order polynomial filter (Savitzky and Golay, 1964) and subsequently fitting a conic equation by using the Braikenridge-Maclaurin theorem (Coxeter and Greitzer, 1967). The conic with the minimum distance between the root contour and itself is selected by randomly sampling 5 points around the root tip extremum.

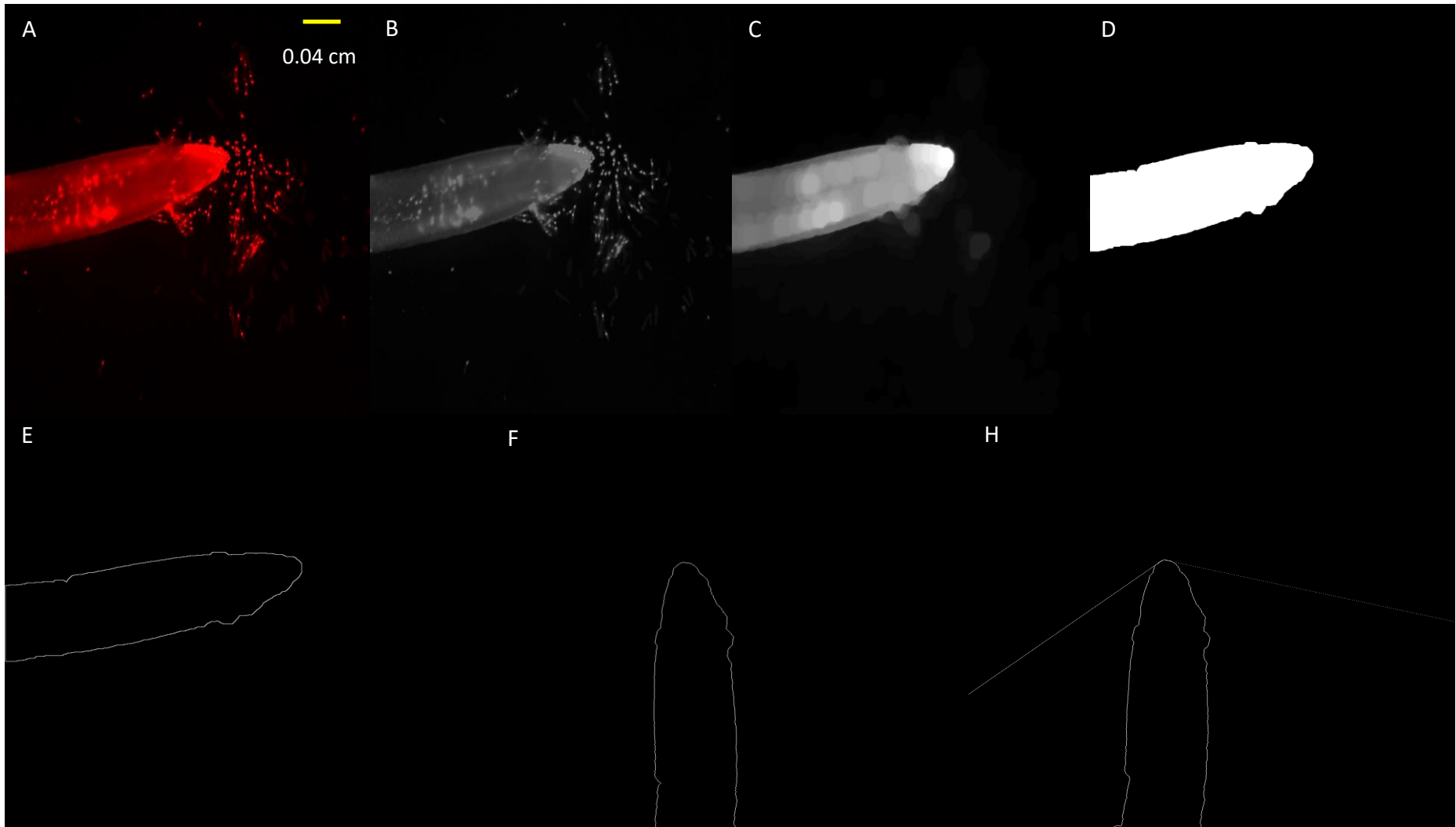


**Figure 3.3:** Root tip geometry algorithm, **A)** Raw image, **B)** Greyscale conversion, **C)** Morphological opening, **D)** Binarization, **E)** Root Contour extraction, **F)** Root contour rotation and **H)** Conic fitting.

### 3.3.3.2 Dead border cell segmentations

In order to quantify the count of non-viable RBCs, the algorithm uses the following sequence of steps:

1. Greyscale (8-bit) conversion of PI stained root, imaged with Texas Red filter.
2. (White) Top-hat filter (Disk SE,  $r = 15$ )
3. Blob enhancement filter (Li, Sone and Doi, 2003)
4. Cell nuclei binarization
5. Cell nuclei count

**Figure 3.4 (A)**, illustrates the original RGB image of the PI stained root tip obtained from the optical microscope. **Figure 3.4 (B)**, illustrates the greyscale display of the image by using only the values of the red channel which corresponds to the PI emission signal. **Figure 3.4 (C)**, shows the result of applying a morphological (white) top hat operator to remove larger structures. **Figure 3.4 (D)**, is the output of applying a blob enhancement filter (Li, Sone and Doi, 2003). **Figure 3.4 (E)**, is the result of binary transformation to segment the cell nuclei.

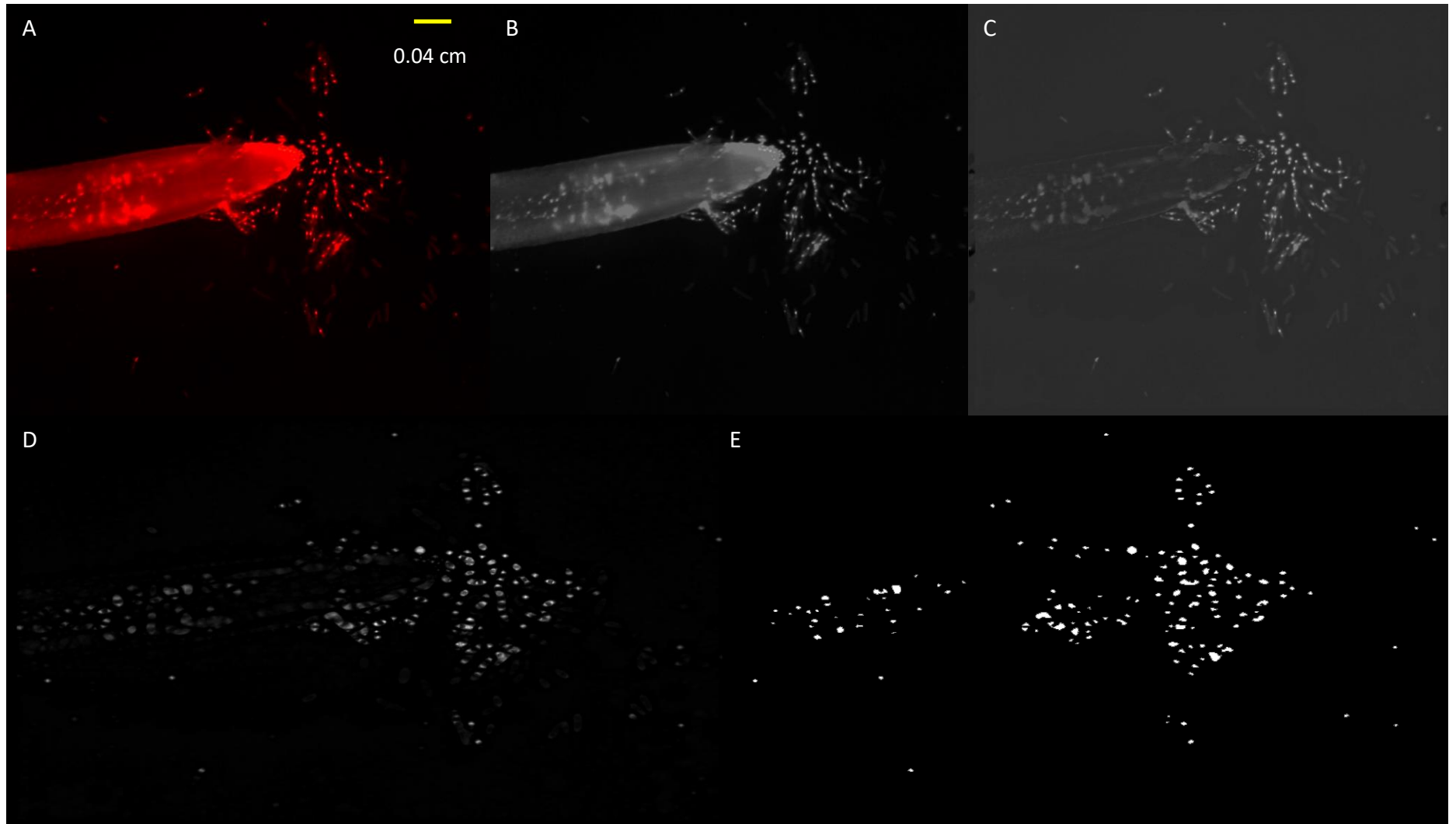


**Figure 3.4:** Non-viable RBCs algorithm, **A)** Raw image, **B)** Greyscale conversion, **C)** Top hat filter, **D)** Blob enhancement and **E)** Binarization.

### 3.3.3.3 Live border cell segmentations

In order to quantify the count of viable RBCs, the algorithm uses the following sequence of steps:

1. Greyscale (8-bit) conversion of FDA stained root
2. (White) Top-hat filter (Disk SE,  $r = 15$ )
3. Vessel enhancement filter (Frangi *et al.*, 1998)
4. Cell binarization
5. Cell count

**Figure 3.5 (A)**, illustrates the original RGB image of the FDA stained root tip obtained from the optical microscope. **Figure 3.5 (B)**, illustrates the greyscale display of the image by using only the values of the green channel which corresponds to the FDA emission signal. **Figure 3.5 (C)**, shows the result of applying a morphological (white) top hat operator to remove larger structures. **Figure 3.5 (D)**, is the output of applying a vessel enhancement filter (Frangi *et al.*, 1998). **Figure 3.5 (E)**, is the result of binary transformation to segment the cells.

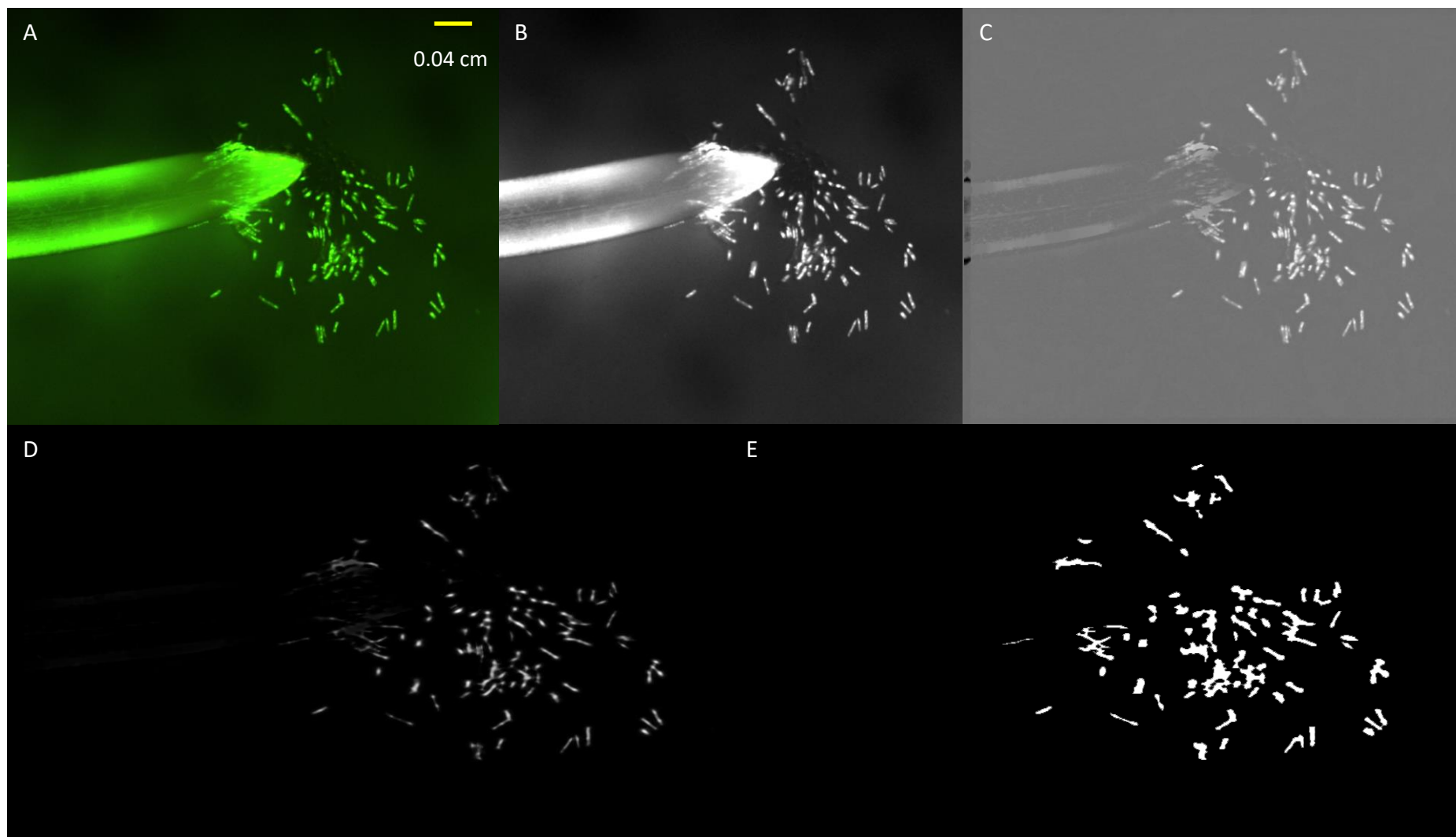


**Figure 3.5:** Viable RBCs algorithm, **A**) Raw image, **B**) Greyscale conversion, **C**) Top hat filter, **D**) Vessel enhancement and **E**) Binarization.

### **3.3.4 Root border cell algorithm validation**

In order to assess the accuracy of algorithms described in Section 2.3.2 the following procedure was performed:

1. 5 images were randomly selected from a pooled set of images and their corresponding FDA and PI stained images were extracted.
2. The area of RBCs nuclei and cells in the PI and FDA stained images respectively, were manually segmented by using the “Polygon selections” tool in Fiji.
3. The binary masks obtained were then overlaid to their respective algorithm output images to assess their prediction accuracy in the form of an error matrix.

### **3.3.5 Root border cell quantification**

In order to obtain **RBC** estimates from the output of the segmentation algorithms described above the following method was used:

1. The **RBC** segmented areas mentioned in the segmentation validation analysis above were examined and 20 clearly defined cell outlines were selected from each of the 5 images.
2. A total of 100 cell outlines were then pooled together and imported in the statistical software R.
3. The R package “fitdistrplus” was then used to assess the goodness of fit of various probability distributions to the training dataset.
4. The selected distribution parameters were then integrated into their respective algorithms to generate estimates of cell numbers by using the particle binary areas from the output images produced by the algorithms.

## **3.4 Washed root system assessment**

### **3.4.1 Root morphology methods based on destructive sampling**

One of the most common methods for obtaining root morphological information involves the destructive sampling, washing and subsequent measurement of the plant root system. The process of measuring “Washed Root Systems” (WRS) is both invariably time consuming and labour demanding but, it is usually the only available option for obtaining information about the root system as opposed to the much more accessible stem of the plant (Box, 1996). In

general, WRS quantification methods could be classified as being either manual or automatic. Manual methods are very common and are usually based on the line-intersect method (Newman, 1966) which estimates the “Total Root Length” (TRL) by visually counting the grid line-root intercepts and obtaining the product of the number of intersects with a conversion factor pertaining to the size of the grid system (Tennant, 1975). The main advantage of this method is its simplicity, but it is time-consuming and inaccurate, with the error being proportionally increased with the number of fine roots in the sample (Costa *et al.*, 2002).

Automated methods on the other hand, involve the imaging and digitization of the WRS which is subsequently analysed with either a semi-automated or fully automated image processing algorithm to obtain estimates of root traits, including the TRL. These methods are becoming more popular today due to the development and accessibility of both computer hardware and software and, the software’s ability to process simple RGB or greyscale images in a range of settings. For example, IJ-Rhizo (Pound *et al.*, 2013) is a plugin which was designed to perform semi-automated analysis of roots in the popular and freely available software “ImageJ”. Another example of a semi-automated and freely available software is RootNav (Pierret *et al.*, 2013) and does not require any previously installed software to use (i.e., stand-alone software). However, perhaps the most widely used software in root research today is WinRHIZO™ (Arsenault *et al.*, 1995), another stand-alone software but not freely available. Unfortunately, despite its popularity, this software requires a high contrast between the root and the background, which restricts its use to very clear images, e.g., washed root systems on uniform background (Svane *et al.*, 2019). In other words, the presence of image noise such as scratches, non-uniform illumination or background break-ups, could give erroneous estimates of TRL.

In the images obtained in this research it was found that the lack of resistance to noise was responsible for noticeable errors. In practise, that required the addition of a pre-processing step for noise removal to mitigate this issue prior to image analysis. Fortunately, most available software’s have utilities to filter out noise, e.g., dust filter which can mitigate the errors. However, even after testing with various software, errors persistent in most cases and adaptation of the algorithm parameters for each software was a time-consuming step. Furthermore, software such as WinRHIZO™ require a commercially available licence and can only be installed on a single PC per licence. As such, to increase the efficiency of the overall process of analysing WRS an algorithm (A3) was developed for the retrieval of basic

root architecture in a more robust and automated way. As previously, A3 was written in the Rcpp language to make it more accessible and user friendly. A description of the algorithm follows (Section 2.4.2) with a subsequent validation of the proposed algorithm (Section 2.4.3) and discussion (Section 2.4.4).

However, it should be noted from the onset that A3 was designed to obtain a robust and fast way to extract the basic root parameters of WRS. In theory, numerous root traits could be defined and quantified when studying WRS, specific root length (SRL) and root length density (RLD) are perhaps most commonly studied (Weemstra *et al.*, 2016). SRL (root length per unit root biomass) is a morphological trait that provides information about the amount of resources needed to increase the surface area between roots and soil (Kramer-Walter *et al.*, 2016). RLD (root length per unit volume of soil) is an architectural trait describing the capacity of a root network to explore a given volume of soil and acquire limited resources (Ravenek *et al.*, 2016). However, the estimation of both SRL and RLD, requires estimation of the total root length (TRL) of the WRS (Delory *et al.*, 2017). This was one of the primary reasons why the validation analysis in Section 2.4.3 used TRL as the parameter of the analysis.

### **3.4.2 Algorithm 3 – WRS total root length analysis**

In order to quantify TRL, the algorithm uses the following sequence of steps:

1. Greyscale (8-bit) conversion (if input image is in RGB format)
2. Median filter ( $r = 2$ )
3. Maximum entropy thresholding (Li and Lee, 1993)
4. Particle removal based on pixel size threshold (threshold = 10, 000)
5. Morphological closing (Disk SE, radius = 5)
6. Morphological opening (Line (135 and 45 degrees) SEs, radius = 2)
7. Particle removal based on pixel size threshold (threshold = 3, 000)
8. Morphological dilation (Disk SE, radius = 2)
9. Region growth with binary mask
10. Particle removal based on pixel size threshold (threshold = 30, 000)
11. Skeletonization (Xia, 1986)
12. Skeleton pruning (Solís Montero and Lang, 2012)
13. Root system analysis

**Figure 3.6 (A)**, illustrates the original greyscale image of washed root system. **Figure 3.6 (B)**, is the result of thresholding (maximum entropy) to obtain a binary image containing both root and noise. **Figure 3.6 (C)**, shows the output of the particle removal process to remove some of the noise. **Figure 3.6 (D)**, is the output of a series of morphological operators and area reconstruction to further reduce noise and reconstruct the original root binary area. **Figures 3.6 (D) and (E)** are the results of skeletonization and subsequent skeleton pruning respectively, to arrive at the final root skeleton image.

After the segmentation of the WRS from the background the following root parameters were estimated:

1. Total Root Length (TRL) was estimated by skeletonization of the foreground material and subsequent multiplication of the number of pixels by an image size conversion factor.
2. Total Root Area (TRA) (or Projected Area) was estimated by counting the foreground pixels and again multiplying it by a size conversion factor.
3. Root Average Diameter (RAD) was estimated by averaging the Euclidean distance map values of the root skeleton.

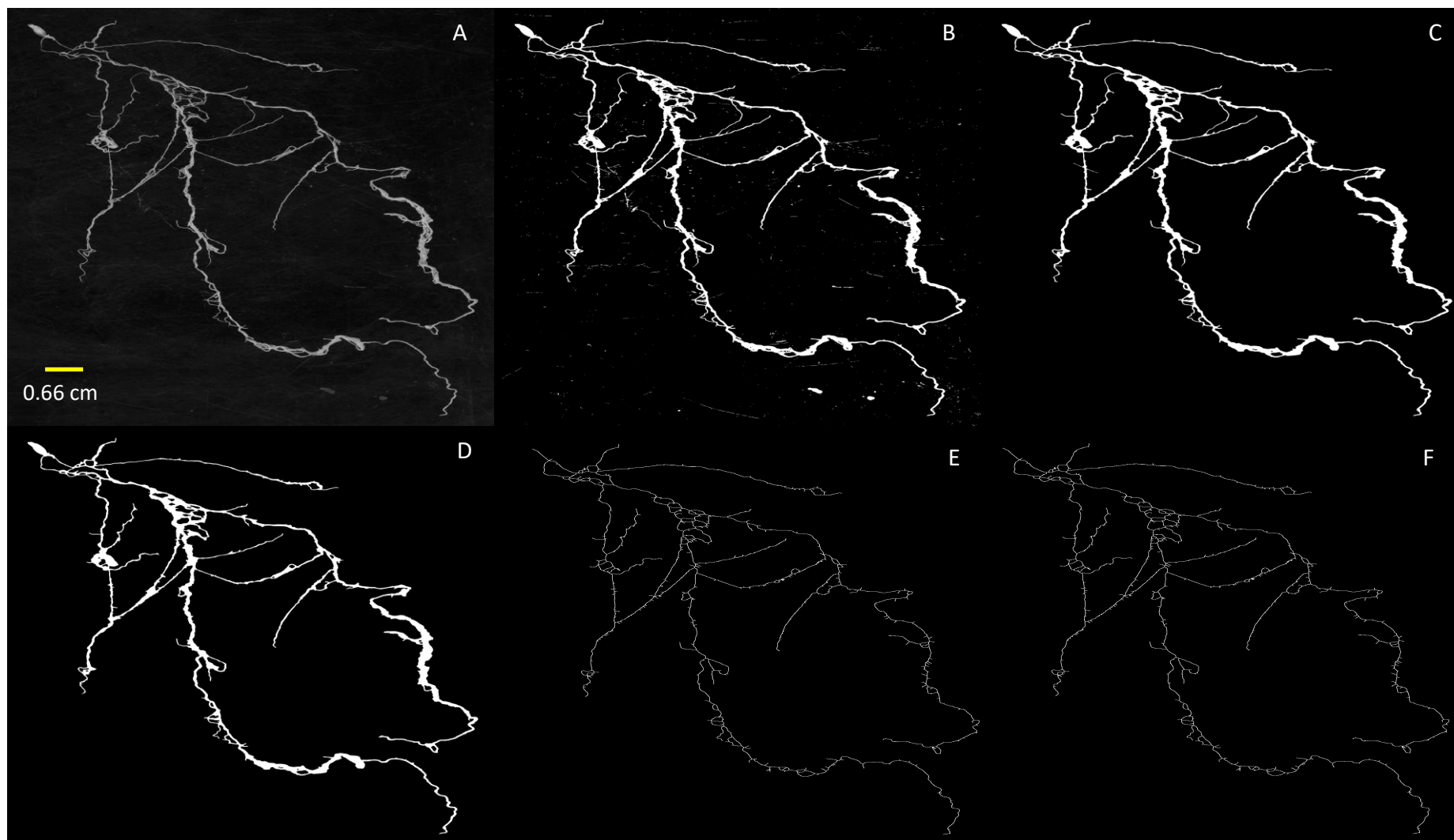


**Figure 3.6:** TRL quantification image processing main steps **A)** Median filtering (Step 2), **B)** Maximum entropy thresholding (Step 3), **C)** Particle removal (Step 4), **D)** Binarization (Step 10), **E)** Skeletonization (Step 11) and **F)** Skeleton pruning (Step 12).

### 3.4.3 WRS parameter extraction algorithm validation

In order to validate A3, seedlings ( $n = 14$ ) were grown in the RS for a period of three weeks. At the end of the growth period, the seedlings were extracted from the rhizotrons, their stems were cut, and their root systems were gently washed with tap water to remove attached RS sand particles. The seedlings were then placed on a moistened rectangularly shaped (420 x 297 x 2 mm) scanning acrylic and scanned at 800 dpi. The obtained images were then downsized to a 400 dpi resolution by using Fiji (to reduce their file size to a size which allowed for image analysis across all of the following image processing software:

1. ARIA, (Pace *et al.*, 2014)
2. EZ-Rhizo, (Armengaud *et al.*, 2009)
3. GiaRoots, (Galkovskyi *et al.*, 2012)
4. RootReader2D, (Clark *et al.*, 2013)
5. WinRHIZO™ (Regent Instruments, Québec, Canada)

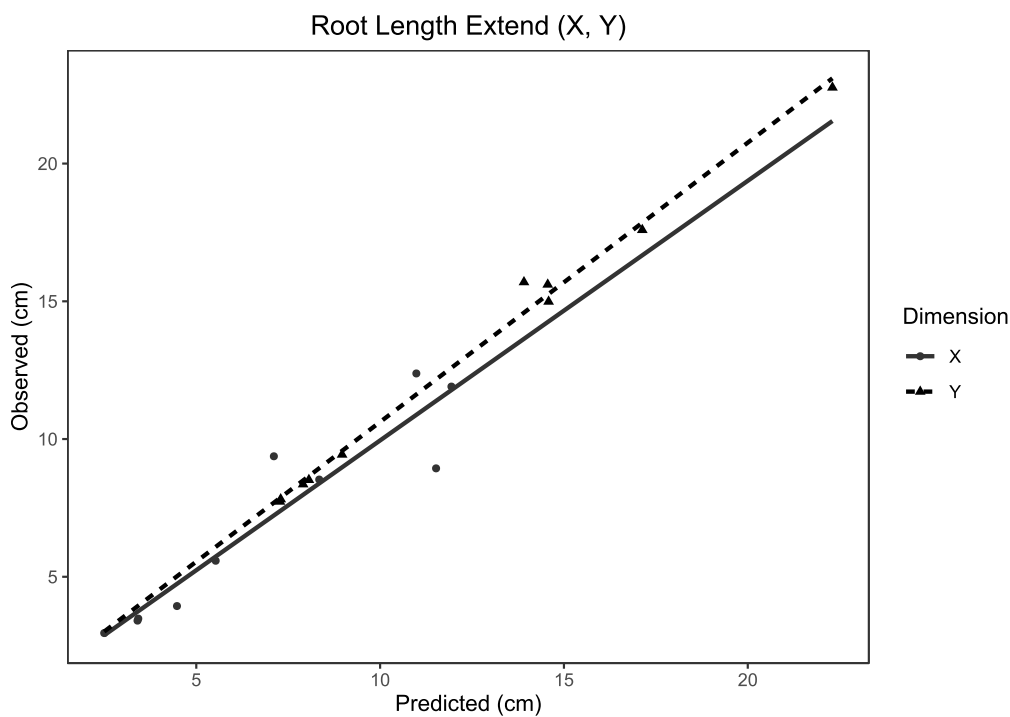
The reduced resolution images were then analysed in Fiji by manually tracing the skeleton of the visible root systems (centre line) with the “Segmented Line” tool. The traced skeletons were used to obtain observed TRL estimates which were then compared to the predicted TRL estimates of the automated image processing software tested. For each software used, a regression relationship was fitted between the observed and predicted estimates of TRL by using the R base function “lm”. The function “linearHypothesis” from the R package “car” was then used to test the hypothesis that the slope of each of the fitted linear regression models was equal to 1.

It should be stated that every effort was made to provide identical parameters for each of the above-mentioned software and ensure identical settings however, due to intrinsic differences such as different noise removal strategies/options, the parameters used may deviate in some cases. The mean ( $\bar{x} \pm s$ ) user execution time of the above described algorithm was  $\approx 18.27 \pm 8.50$  sec (see Section 3.2.4 for PC specifications). The reason user time is reported instead of elapsed time is because the algorithm uses parallel processing which means that the user time > elapsed time.

### 3.5 Results

**Figure 3.7** demonstrates the relationship between the manually measured estimates of X and Y dimensional root lengths and the algorithm predicted estimates (Section 3.2.4). The slope of the fitted linear regression models for X and Y root lengths were 0.94 and 1.01 respectively with a residual sum of squares value of 0.39 and 0.04 which indicates a good agreement between the algorithm and the measured data.

**Figure 3.8** is a summary of the root hair area overlap between the algorithm predicted root hair area and the manually traced total root hair area. The mean root hair overlap value for the analysed sections was  $78.083 \pm 15.945$  % which shows that most of the root hair area is correctly captured.



Software	Intercept	Slope	RSS	F	p
X	0.5248	0.9425	0.3875	0.2254	0.6477
Y	0.4802	1.0140	0.0459	0.2168	0.6539

**Figure 3.7:** Validation graph for A1 demonstrating the observed vs. predicted X and Y dimensional root lengths.

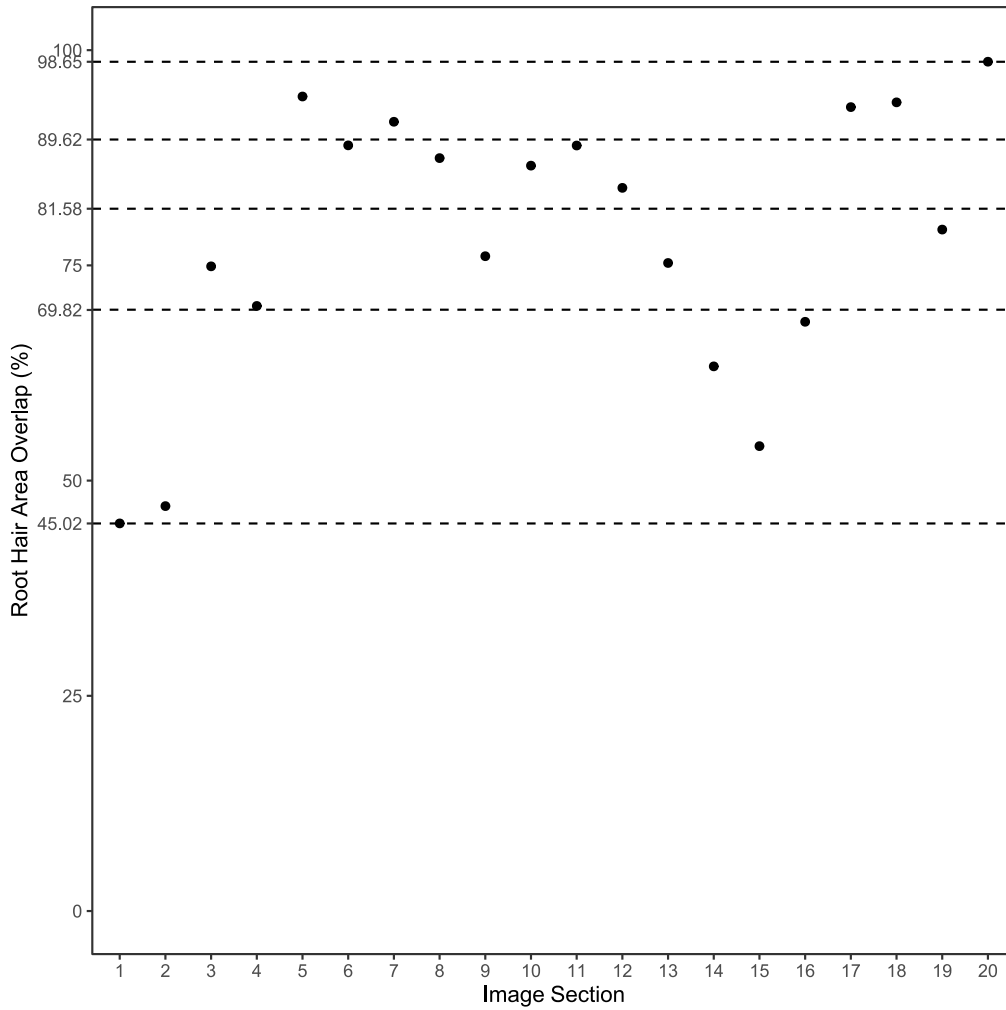


**Figure 3.8:** Root hair area overlap of the predicted root hair area relative to the manually traced total root hair area for 20 different (300 x 300 pixels) image sections. The dashed lines represent the 0 (min), 1<sup>st</sup>, 2<sup>nd</sup> (Median), 3<sup>rd</sup> and 4<sup>th</sup> (max) quartiles.

**Table 3.1** is an error matrix which summarises the binary prediction accuracy between the algorithm predicted area covered by border cells and the manually measured area for the FDA (viable cells) and the PI (non-viable cells) images (Section 3.3.4). The combined mean percentage of true positives and true negatives are 99 % for both the FDA and the PI images which indicates an excellent agreement between the predicted and observed border cell areas. The elapse execution time of the above described algorithm was  $\approx$  3 sec (see Section 3.2.4 for PC specifications).

**Table 3.1:** Error matrix showing the % pixel prediction errors of 5 images for the algorithms described in Section 3.3.2.

	Img 1	Img 2	Img 3	Img 4	Img 5	$\bar{x} \pm s$	
<b>FDA</b>							
True Positives (TP)	0.21	1.4	1.71	1.47	0.52	1.062	$\pm$
						0.656	
True Negatives (TN)	98.85	97.28	97.32	97.56	98.56	97.914	$\pm$
						0.737	
False Positives (FP)	0.15	0.11	0.31	0.24	0.06	0.174	$\pm$
						0.101	
False Negatives (FN)	0.78	1.21	0.66	0.73	0.86	0.848	$\pm$
						0.215	
<b>PI</b>							
True Positives (TP)	0.51	0.07	0.34	0.37	0.05	0.268	$\pm$
						0.201	
True Negatives (TN)	99.07	99.26	99.08	99.03	99.72	99.232	$\pm$
						0.362	
False Positives (FP)	0.27	0.66	0.41	0.49	0.21	0.408	$\pm$
						0.304	
False Negatives (FN)	0.15	0.01	0.17	0.11	0.02	0.092	$\pm$
						0.456	

**Figure 3.9** and **Table 3.2** summarise the goodness of fit of four probability distribution models relating the cell (FDA) and nuclei (PI) binary areas obtained from the algorithm to the number of border cells counted in the training dataset (Section 3.3.5). The log-normal

distribution was then selected for integration into the algorithm because of its good performance and ease of programming into the programming language RCPP.

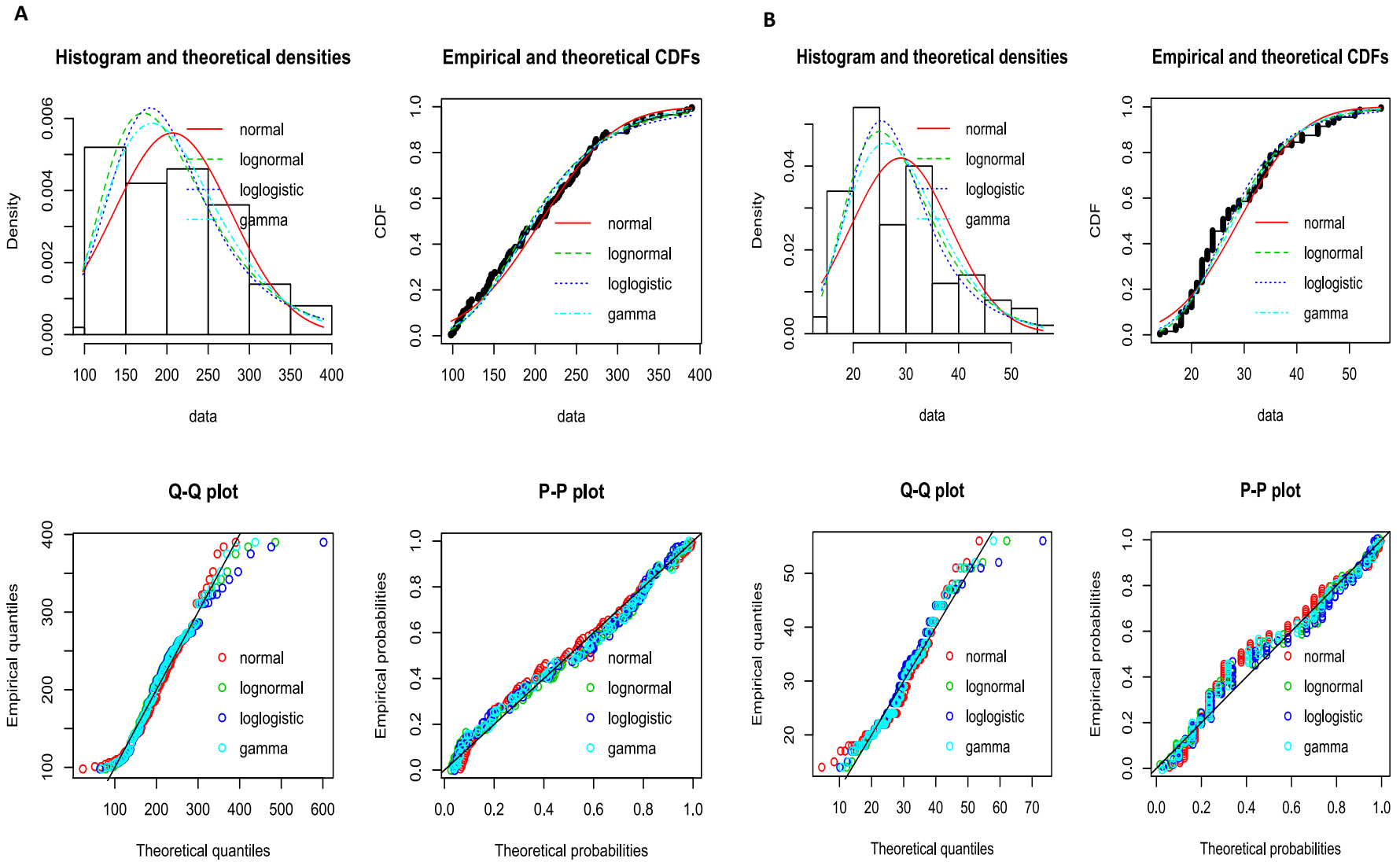


**Figure 3.9:** Probability distribution fitting diagnostic plots for **A**) live (FDA) and **B**) dead (PI) RBC populations.

**Table 3.2:** Summary goodness of fit statistics for live (FDA) and dead (PI) RBC populations.

<b>FDA</b>				
	Normal	Lognormal	Loglogistic	Gamma
Kolmogorov	0.0692	0.0758	0.0688	0.0618
Smirnov statistic				
Cramer von	0.0959	0.1249	0.1268	0.085
Mises statistic				
Anderson	0.7728	0.8073	0.9113	0.5923
Darling statistic				
Akaike's	1141.116	1134.894	1141.574	1133.992
Information				
Criterion				
Bayesian	1146.327	1140.104	1146.785	1139.203
Information				
Criterion				
<b>PI</b>				
	Normal	Lognormal	Loglogistic	Gamma
Kolmogorov	0.16	0.1293	0.1217	0.1416
Smirnov statistic				
Cramer von	0.4016	0.1918	0.1998	0.242
Mises statistic				
Anderson	2.4261	1.061	1.2013	1.3824
Darling statistic				
Akaike's	738.422	720.2671	726.5632	723.9357
Information				
Criterion				
Bayesian	743.6323	725.4774	731.7736	729.1461
Information				
Criterion				

**Figure 3.10** demonstrates the relationship between the observed and the algorithm predicted total root length for the proposed method and a range of other software (Section 3.4.3). **Table 3.3** is a summary of the goodness of fit statistics obtained for testing the hypothesis that the slope of the regression line for each software was equal to 1.

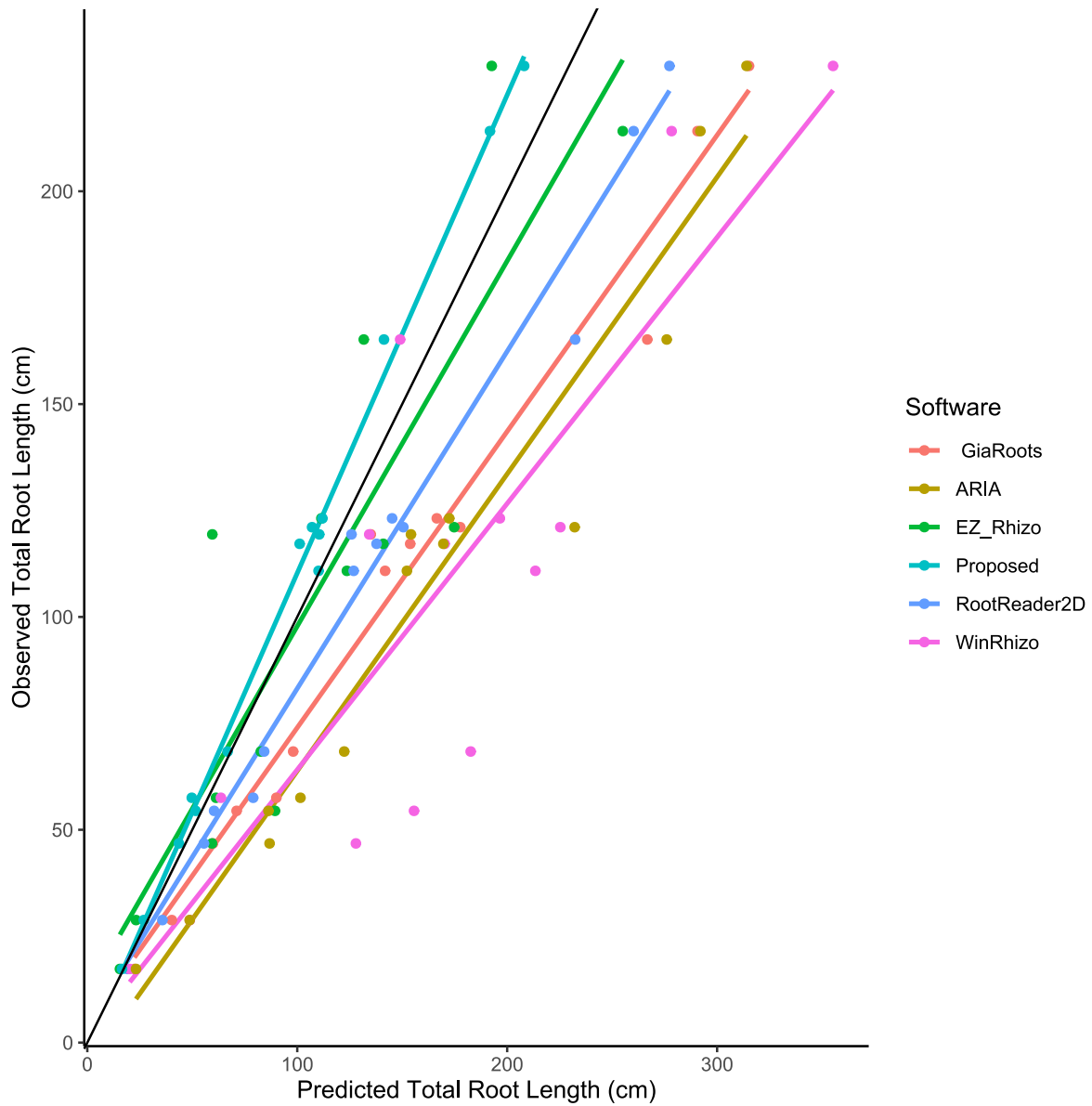


**Figure 3.10:** Observed *vs.* Predicted values of TRL for tested automated 2D software and the proposed algorithm. The solid black line represents the 1:1 identity line.

**Table 3.3:** Summary statistics for the linear regression model of the form  $y = x$ .

Software	RSS	Sum of Sq	F	Pr(>F)
Proposed	221.58	2048.4	55.467	8.65E-07***
RootReader2D	1,581.1	10,302	39.092	5.55E-06***
GiaRoots	2,869	30,821	64.45	3.82E-07***
ARIA	5,882	47,947	48.908	1.70E-06***
EZ_Rhizo	12,567	547.91	0.2616	0.7741
WinRHIZO™	27,260	53,070	11.681	0.001527**

### 3.6 Discussion

The algorithms described above enable the detection and quantification of roots and root hairs of spring barley seedlings grown in the RS (A1), root border cells and root tip geometry from microscope images (A2) and a more accurate estimate of TRL after washing of the root system (A3). The validation analysis in Section 3.2.4 enabled an estimation of the error associated with the proposed algorithm (A1) for detecting and quantifying roots grown in the RS. The percentage error ( $\bar{x} \pm s$ ) for the X (**HGR**) and Y (**VGR**) root system dimensions were respectively  $9.89 \pm 10.58 \%$  and  $5.37 \pm 2.7 \%$  so the approximate percentage error in **RGR** was estimated as  $15.26 \pm 13.28 \%$ . As discussed with numerous examples in Section 3.2.1 the majority of softwares used are for manual tracing of the root systems in minirhizotron studies. As such, if the tolerance for error is judged to be acceptable then the user can benefit from a significant reduction in the time required for analysing images. The estimated amount of time required for executing the algorithm was  $151.02 \pm 34.20$  sec for seedlings at 3 weeks of growth. The amount of time it takes for manual tracing of the root system even with commercial software such as WinRHIZO Tron will clearly be significantly longer even for an experienced user. Furthermore, the reported timing of the software is expected to have an inverse relationship with the seedling age as the visible part of the root system will only cover a fraction of the RS area depending of course on the cultivar and the

experimental treatment. The operator could simply scan only the section of the visible system and achieve reductions in both scanning times and image processing times. Finally, it should be noted that other automated algorithms exist such as the one proposed by Zeng *et al.*, (2010). Although, obtaining excellent results for the test images, the resolution was only 640 × 480 dpi. The effective RS root containing area is approximately 11,200 x 18,200 dpi at the 1,600 dpi scanning resolution used. In other words, the previous resolution contains only 0.15 % of the pixels in comparison to our application which was projected to lead to unacceptable image processing times, assuming that the software does support such an image size. An alternative option would be to then crop the images and analyse small sections but the process will be laborious and require significant amounts of time. Similarly, reducing the image resolution to lower than 1,600 dpi was found to make root hair structures indistinguishable in the obtained images.

The root hair area is quantified by creating a buffer zone of 0.5 cm around the root and applying a binary threshold. It should be emphasized here that the estimate of root hair area is simply an indication of the projected area covered by root hairs. The analysis is restricted to the focal plane of the image which means that there will always be root hairs that are not visible, either because they are out focus or are covered by other root material or sand particles. This is however, an intrinsic limitation of the RS, the analysis is only restricted to the thin interface of the scanning surface the substrate/root mixture. Furthermore, although a number of authors tend to consider only clearly visible root hairs (Koebernick *et al.*, 2017; Chai *et al.*, 2019) in their analysis this was avoided here because it was found to give a misleading underestimation of the total root hair area, especially at areas of high root hair density. In theory, a second order derivative based approach for edge detection could work for segmentating reasonably defined root hair segments but that was later rejected due to the above reasons.

The proposed RBC and root tip assesment using a microscope based method has the advantages of allowing both the determination of RBC viability and the assesment of root tip geometry from the same set of images. The algorithm itself requires approximately 3 seconds due to the small file size of the images. This enables rapid assesment of two of the root

microtraits of interest and helps in making the RS data analysis step more efficient. It must be noted that the procedure of generating random observations of cell area from the underlying lognormal distribution until the cell aggregate area is covered, is similar in principle to the approach used by Bengough *et al.*, (2001). The authors estimated cell numbers in root cross sections by effectively modelling the number of cells with the observed dimensions and fitting them into a circle of varying radius. This sequence of 2D sections form the basis for extrapolating to the 3D case of the root cap but the 3D case was not considered here. The proposed method effectively provides an overview of cell projected area which is then translated into an unbiased estimate of the number of border cells. However, cells are 3-D structures and as such a number of them are either overlapping with other cells or are out of focus although, the latter issue can be reduced by taking more than 1 image to capture the out of focus cells and subsequently summing them. In terms of the root tip shape, this geometrical parameter is usually reported to be modelled as an (approximate) elliptical half-spheroid (Mckenzie *et al.*, 2013; Colombi *et al.*, 2017). As such the choice of modelling the root tip cross section as a conic section should be a similar but more flexible approach as an ellipse is just one case of the conic with the parabola and hyperbola cases allowed for in cases when the root tip eccentricity exceeds that of the ellipse.

Although a range of methods were compared in Section 3.4.3, perhaps the most commonly reported method for quantifying WRS is the system known as WinRHIZO™ (Regent Instruments, Québec, Canada). WinRHIZO™ is a commercially available image analysis system composed of both image acquisition components such as flatbed scanners (although not required) and a computer program for image processing. It estimates a range of root morphology and architectural traits (e.g. projected root area), providing significantly more information for the root system than simply its TRL. Other properties that contributed to WinRHIZO™ becoming a standard image processing tool are its ability to detect and correct for root overlap and produce root diameter distributions for the total root system (Arsenault *et al.*, 1995). As such, WinRHIZO™ is often used as a reference to evaluate the accuracy of new image analyses tools (Himmelbauer *et al.*, 2004; Pierret *et al.*, 2013). However, examination of **Figure 3.10** and **Table 3.3** clearly suggest that it had the poorest performance with the largest model RSS by some margin. In contrast, the proposed algorithm had the

smallest model RSS when testing the hypothesis that its regression line was the 1:1 line (**Table 3.3**). The reason for the poor accuracy of WinRHIZO™ was probably root overlapping which results in a significant underestimation of TRL (Bauhus and Messier, 1999). Although, the software uses a root correction factor to correct for this it can be insufficient when root clusters occur such as the presence of root stumps in the root system (Wang and Zhang, 2009). More recently Delory *et al.*, (2017), suggested that procedures such as increasing the contrast between fine roots and background by staining the roots and to avoid overlapping roots by not exceeding a RLD of 1 cm cm<sup>-2</sup> can increase the accuracy of WinRHIZO™. However, the aim is always efficiency and the addition of extra steps will only make the process of obtaining TRL more complex and time demanding. Of course, results will always vary between software packages, image acquisition systems and resolution (Rose and Lobet, 2019) but the validation analysis did try to keep all parameters as similar as possible. In summary, the proposed method could be potentially useful as an alternative tool although, there other candidates such as RootReader2D that also performed well.

### 3.7 Conclusions

This chapter is dedicated to the introduction of three image processing algorithms which could be integrated into the RS overall measurement methodology and extract estimates of both macro and micro traits either *in situ* or *ex situ*. The first algorithm (A1) allows for automated root detection and quantification of the root system grown in the RS. This tool also allows for an estimation of the projected root hair area after the root detection part of the algorithm is complete, with root hair to root width estimation. The benefits of the algorithm are that it obtains *in situ* estimates of root traits in an automated way, offering significant reductions in image processing times relative to manual tracing methods provided that the user is willing to accept an error tolerance of around 15 % in their **RGR** estimate. The second algorithm (A2) was designed to retrieve estimates of the number of viable and non-viable root border cells after staining extracted root tips in a compound FDA/PI mixture and imaging under a fluorescence microscope. This method also quantifies the geometry of the extracted root tips from the same set of pair images. The very quick image processing times (3 seconds) offer a very convenient and efficient way to extract information about two of the

root micro-traits considered in this study. The third algorithm (A3) involves the detection and quantification of WRS, more specifically its TRL and diameter profile. The motivation behind the design of this application was to further complement the collection of methods with a fast (18.27 sec), user friendly, free of cost and of a higher accuracy method relative to most alternatives. In summary, these custom developed methods will be an essential component in developing the overall experimental procedure of manipulating the LLWR soil stressors in the RS and subsequently assessing the root trait response to those treatments for different cultivars in Chapters 4 and 5.

## 4. Constraints to the application of the LLWR

### 4.1 Introduction

Global food security is a major challenge for current and future generations (FAO, 2009). Major issues such as drought stress are negatively influencing plant growth, survival and reproduction (Barnabas *et al.*, 2008) and are responsible for large crop yield reductions (Khan *et al.*, 2015; Ryan *et al.*, 2016). Drought severity is also projected to increase due to increasing global temperatures (Asseng *et al.*, 2015). Similar concerns also exist for flooding frequency and severity (Trenberth, 2011), especially considering that approximately 10 % of cultivated land surface that suffers from poor drainage and waterlogging (Koevoets *et al.*, 2016). The above climatic effects are exacerbated when one considers the negative consequences of soil compaction brought upon by heavy agricultural machinery which increase the mechanical resistance of the soil and, reduces the oxygen availability to roots by modifying soil pore structure (Lipiec *et al.*, 2012). As such, it is important to understand how the soil physical conditions of water stress, oxygen stress and mechanical stress interact to impact root growth (Mohammadi *et al.*, 2010).

The least limiting water range (LLWR) is model which connects the important soil stressors of penetrometer resistance (a measure of mechanical resistance), lack of oxygen and water potential to the physiological limits of plant growth (da Silva *et al.*, 1994). The physiological limits of plant growth are practically interpreted to be limiting values for penetrometer resistance (PR - 2 MPa), air filled porosity at hypoxic conditions (AFP - 10%), matric suction at field capacity (FC - a measure of soil water-holding capacity) (0.01 MPa) and matric suction at the permanent wilting point (PWP - 1.5 MPa). PR, AFP, PWP values represent the point at which root growth effectively stops and by integrating them in the LLWR model it is possible to estimate in a computationally feasible way the range of soil volumetric water concentration for optimum plant growth. FC represents the maximum likely water level under field conditions, unless geographic condition mean water is held in the soil location. However, this model makes the (erroneous) implicit assumption that all plants have identical physiological responses, something which contradicts the fact that plant responses to soil physical stresses are known to be influenced by a range of root traits (Bengough *et al.*, 2011).

The variable spectrum of plant root responses to the soil stressors must be considered in order to reformulate the LLWR.

Root micro-traits are known to have a wide range of functions that are critical for plant root growth and survival. For example, root hairs are a common anatomical characteristic of most vascular plants and are known to dramatically increase the total surface area of the root system (Jones and Dolan, 2012) and, have a major role in the uptake of both nutrients and water (Gilroy and Jones, 2000). The presence and abundance of root hairs are known to significantly increase root water uptake (Carminati *et al.*, 2017) by enhancing root-soil contact (Carminati *et al.*, 2009). Furthermore, they can increase soil adhesion to roots (Moreno-Espindola *et al.*, 2007; Czarnes *et al.*, 1999), and offer greater mechanical anchorage to the plant (Bengough *et al.*, 2016; Haling *et al.*, 2014). Root hairs also increase the ability of roots to penetrate through soil (Haling *et al.*, 2013), which is of great importance in compact soils (Lynch *et al.*, 2014) and, influence soil structure development (Koebernick *et al.*, 2017). In a similar manner, the plant root cap offers advantages in root soil penetration. Experiments involving the removal of the root cap in roots clearly demonstrated that removal of the root cap reduces the ability of the root to penetrate compacted soil (Iijima *et al.*, 2003; Vollsnes *et al.*, 2010). There is also evidence that the geometry of the root tip can influence the ability of the root to successfully penetrate the soil (Colombi *et al.*, 2017). Another root cap associated trait are root border cells defined as “the cells that disperse into suspension within seconds when root tips are placed into water” (Hawes, *et al.*, 2000). The root tip excreted mucilage-border cell matrix acts as a lubricant which reduces the coefficient of root-soil friction (Mckenzie *et al.*, 2013). Roots grown in compacted soil conditions often respond by increasing the rate of production of the mucilage-border cell matrix (Iijima *et al.*, 2000). As a consequence, root micro-trait assessment is necessary as they determine the root growth response in a range of LLWR soil associated conditions.

The purpose of this chapter is to describe the design and implementation of an experimental protocol whose purpose was to effectively combine the experimental unit described in Chapter 2 with the methodologies developed in Chapter 3. This will enable the creation of an

experimental setup which allows for the monitoring of root growth while manipulating the LLWR soil stressors and ultimately, enable the quantification of a range of root micro-traits *via* destructive sampling. The examination of the responses can then be used to explain how root traits influence root elongation rates for the various LLWR stressors.

## 4.2 Aims

The main aims could be summarised as:

- Design and implement a multifactorial experiment with factors being the LLWR stressor variables.
- Assess whether root micro-traits can be measured with the methods described in Chapter 3.
- Determine the effect that the LLWR stressor variables have on root growth.
- Determine the effect that the LLWR stressor variables have on root micro-traits.

This experiment relied on the manipulation of the LLWR limits of substrate strength and water availability. As such, to facilitate the description of the experiment the following two definitions are introduced here for clarity:

Dry Bulk Density (DBD) – a measure of RS substrate density.

Irrigation Event (IRE) – a 3-minute slow dripping irrigation event.

## 4.3 Methods

### 4.3.1 Experimental Procedure

The seeds used in this experiment were the same as in Chapter 2, i.e., spring barley (*Hordeum vulgare var. Optic*). The germination procedure for the seeds was as described in Section 2.4.5. The experiment took place at the James Hutton Institute, Invergowrie, Dundee DD2 5DA, Scotland, between the start of March and end of April in 2019. The glasshouse growth conditions were as described in Section 2.4.6. RS scanning was performed every 7 days for a period of 3 weeks by using the procedure specified in Section 2.4.7.

The experiment had a 3 by 3 factorial design with the factors being DBD and IRE. In order to impose the LLWR soil constraints the experiment had a randomized (blocked) structure with the RS units arranged in two parallel linear rows with 4 treatment replicates. The treatments for DBD were 1.4, 1.5 and 1.6 g cm<sup>-3</sup> and the treatments of IRE were 2, 4 and 6 irrigation events per day (**Table 4.1**) with an event having a duration of 3 minutes. The original Hoagland’s nutrient delivery system was replaced with an alternative controlled release fertiliser, i.e., “Scotts Osmocote”, manufactured by “Everris”. This change was made to better mimic the slow release of nutrients in soil systems rather than delivering all the nutrients in single non-continuous water-carried events. This was achieved by individually grinding to dust 0.3 g of fertilizer with a mortar and pestle for each RS unit and subsequently mixing the fine powder with the required mass of RS substrate and mixing them thoroughly prior to RS packing.

At the end of the 3-week period the RS units were opened one at a time and a total of 6 actively growing root tips were selected from the actively growing region, to be stained and imaged as described in Section 3.3.2. After, the root systems were cut from the RS units and stored in 50% ethanol:dH<sub>2</sub>O in tubes. At a later date the roots were washed and imaged using an A2 flatbed scanner (Epson Expression 1600XL-PRO (300 dpi/82 µm – 1500 dpi/15 µm)).

**Table 4.1:** 3-minute irrigation event timings used in each of the three levels for the experimental factor IRE.

	<b>2 IRE</b>	<b>4 IRE</b>	<b>6 IRE</b>
07:00		✓	✓
09:00	✓		✓
11:00		✓	✓
13:00			✓
15:00	✓	✓	✓
17:00		✓	✓

## 4.3.2 Root growth parameters

Root growth parameters and root hair area estimation were measured from the RS images obtained at 7, 14 and 21 days *via* analysis using algorithm 1 (see Section 3.2.3). Root border cells and root tip eccentricity were measured from the optical microscope images obtained during destructive sampling and analysed by using algorithm 2. In addition to the root growth parameters defined in Section 2.4.7 additional definitions are introduced here:

**Root Hair to Root Ratio (RHtRR):** The ratio of the root hair zone width to the root zone width for unit segments of a length of 10 pixels ( $mm\ mm^{-1}$ ).

**Root Border Cell Count (RBCC):** The sum of viable and non-viable root border cells. For clarity, a root border cell is defined to be a cell that is detached from the root tip when in solution (n).

**Root Tip Eccentricity (RTE):** The geometrical eccentricity of the root tip modelled as a conic section (dimensionless). A higher value indicates a blunter root tip shape.

## 4.3.3 Statistical Analysis

The statistical analysis of the data was performed using the software R (version 3.5.0). The statistical significance test used for comparing the arithmetic averages of the experimental treatments was implemented with the “t2way” function from the R package “WRS2” Wilcox, (2017). This test is similar to ANOVA but performs better with small sample sizes by using an adjusted critical value and thus, does not report degrees of freedom. Post-hoc analysis was performed with the “mcp2atm” function from the same package. The degree of statistical significance is represented by \*, \*\* and \*\*\* corresponding to a p value in the interval of (0.05, 0.01], (0.01, 0.001] and (0.001, 0] respectively. Principal components analysis (PCA) was performed with the R basic function “prcomp” and the data was centered and scaled for the analysis. Visualization of the biplots and 3D PCA plots was achieved with the packages “ggfortify” and “pca3d” respectively. The graphical outputs were also produced in R with the “ggplot2” and the “grid” packages.

### 4.3.4 LLWR for RS Substrate

In order to put the results of this chapter into context of the LLWR concept the LLWR range had to be determined for the RS substrate. As such, the RS substrate used was packed into a series of cylindrically shaped rings (4.5 mm diameter x 5.0 mm height) to create repacked soil cores of different dry bulk densities (1.4, 1.5 and 1.6 g cm<sup>-3</sup>) with 4 replicates per treatment. The gravimetric moisture content of each soil core was first adjusted to 20 % to give it consistency and make packing of the core easier. Cores were saturated with degassed water, then subjected to a sequence of different matric suctions (5, 10, 20 and 50 kPa) *via* the use of sand and tension tables and their penetrometer resistance and mass were measured at each stage to estimate the soil strength and the water release curve respectively (Bengough and Mullins, 1990). The resulting data were then used to estimate the LLWR range by using the function “llwr” from the R package “soilphysics”. It should also be noted that the reason for the small upper limit of -50 kPa was because that by -50 kPa ~95% of the pores were air filled (see **Figure 2.10 (C)**).

## 4.4 Results

A statistically significant difference was detected for **ARGR** (psi = 42.6274, p = 0.0215\*) between the comparison of 1.4 *vs.* 1.6 g cm<sup>-3</sup> DBD treatments. This was also the case for **AHGR** (psi = 28.1657, p = 0.0438\*) and **AVGR** (psi = 52.0637, p = 0.0357\*). This suggests that the above three variables had significant reductions at a higher substrate density. In addition to the above, a statistically significant difference was also detected for **ARGR** (psi = 30.5872, p = 0.0444\*) between the comparison of 4 *vs.* 6 IRE treatments with the higher water concentration having reduced growth rates. However, for the cases of **AHGR** and **AVGR** there were no statistically significant differences. A statistically significant interaction effect was detected for **ARGR** (psi = 33.4462, p = 0.0467\*) between the comparison of 2 *vs.* 4 IRE treatments in both the 1.4 and 1.6 g cm<sup>-3</sup> DBD treatments. A higher **ARGR** was observed for the lowest water concentration treatments when compared to medium water concentration treatments at lower densities with the opposite effect being true for higher densities. A similar interaction effect was also detected for **AVGR** (psi = 56.5362,

$p = 0.0227^*$ ). Furthermore, a second interaction effect was detected for **ARGR** ( $\psi = 44.7760$ ,  $p = 0.0097^{**}$ ) between the comparison of 2 vs. 6 IRE treatments in both the 1.4 and 1.6 g cm<sup>-3</sup> DBD treatments. A higher **ARGR** was observed for the lowest water concentration treatments when compared to the largest water concentrations treatments at lower densities with the opposite effect being true for higher densities. A similar interaction effect was also detected for **AVGR** ( $\psi = 66.3187$ ,  $p = 0.0102^*$ ). In general, given the overlap of statistically significant differences for **ARGR** and **AVGR** the results suggest that the growth response was primarily dominated by vertical instead of horizontal growth.

**Table 4.2**, is a summary of the rank scores of **ARGR**, **AHGR** and **AVGR**, for each of the experimental treatments. The largest **ARGR** value corresponded to the 1.4 g cm<sup>-3</sup> DBD and 2 IRE treatment while the smallest corresponded to the 1.6 g cm<sup>-3</sup> DBD and 2 IRE treatment. In other words, for the driest treatments of two IRE the DBD value determined the **ARGR** with a higher density slowing down growth rates. A similar pattern appears to exist for the cases of **AHGR** and **AVGR** with the exception that the 2 IRE and 1.4 g cm<sup>-3</sup> DBD treatment was ranked 2<sup>nd</sup> instead of 1<sup>st</sup> for the case of **AHGR**. In summary, it will appear that both horizontal and vertical root growth rates responded similarly in each treatment as did the overall measure of root growth. **Figure 4.1**, summarises the root values for **ARGR**, **AHGR** and **AVGR** obtain by application of A1 and demonstrate the relationships between the various DBD and IRE experimental treatments. **Figure 4.2**, displays the actual root lengths as a function of time for the above described experimental treatments.

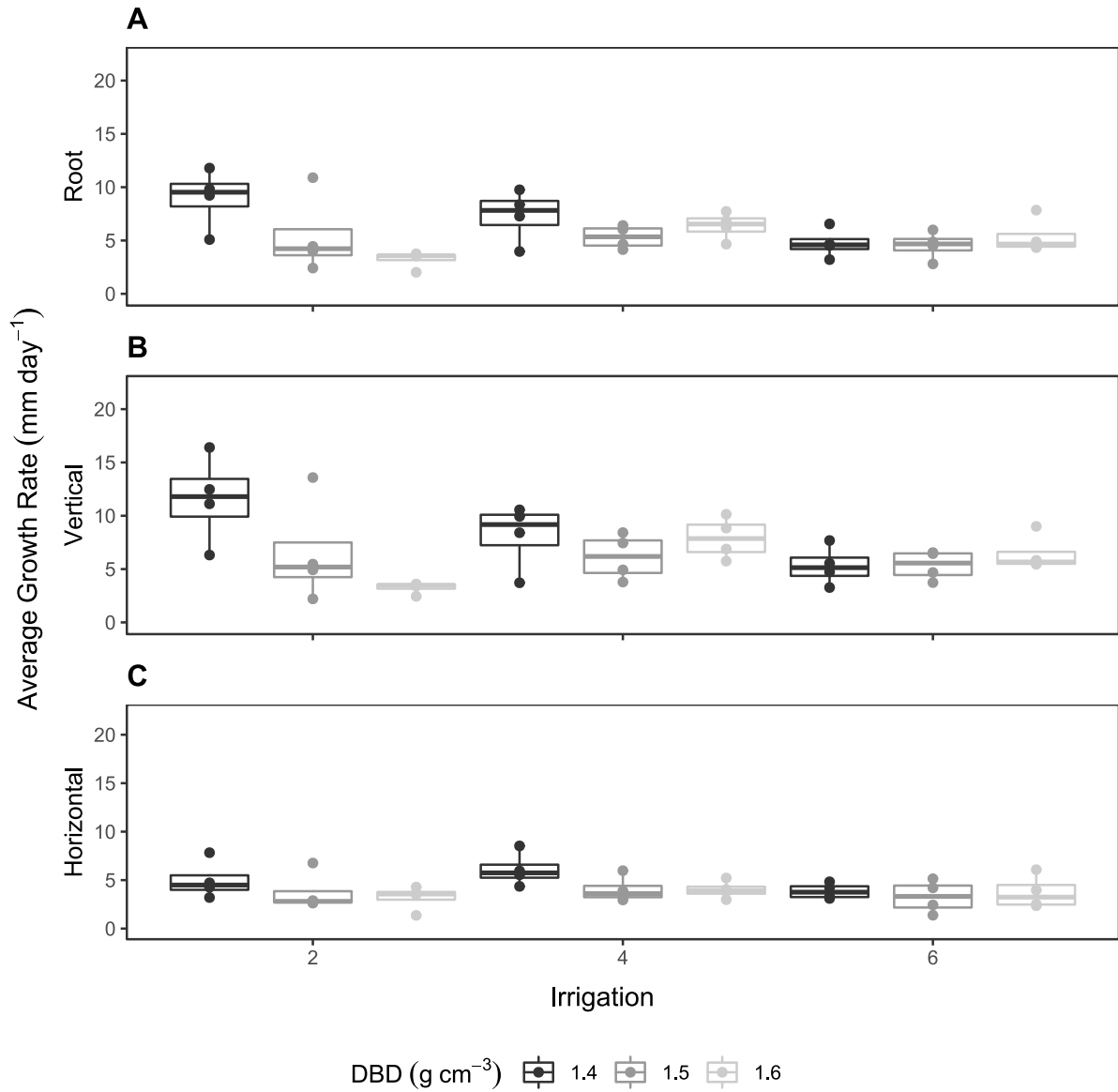


**Figure 4.1:** Average spring barley growth rates for a period of 21 days as a function of IRE and grouped by DBD for root (A) Vertical length (B) and Horizontal length (C).

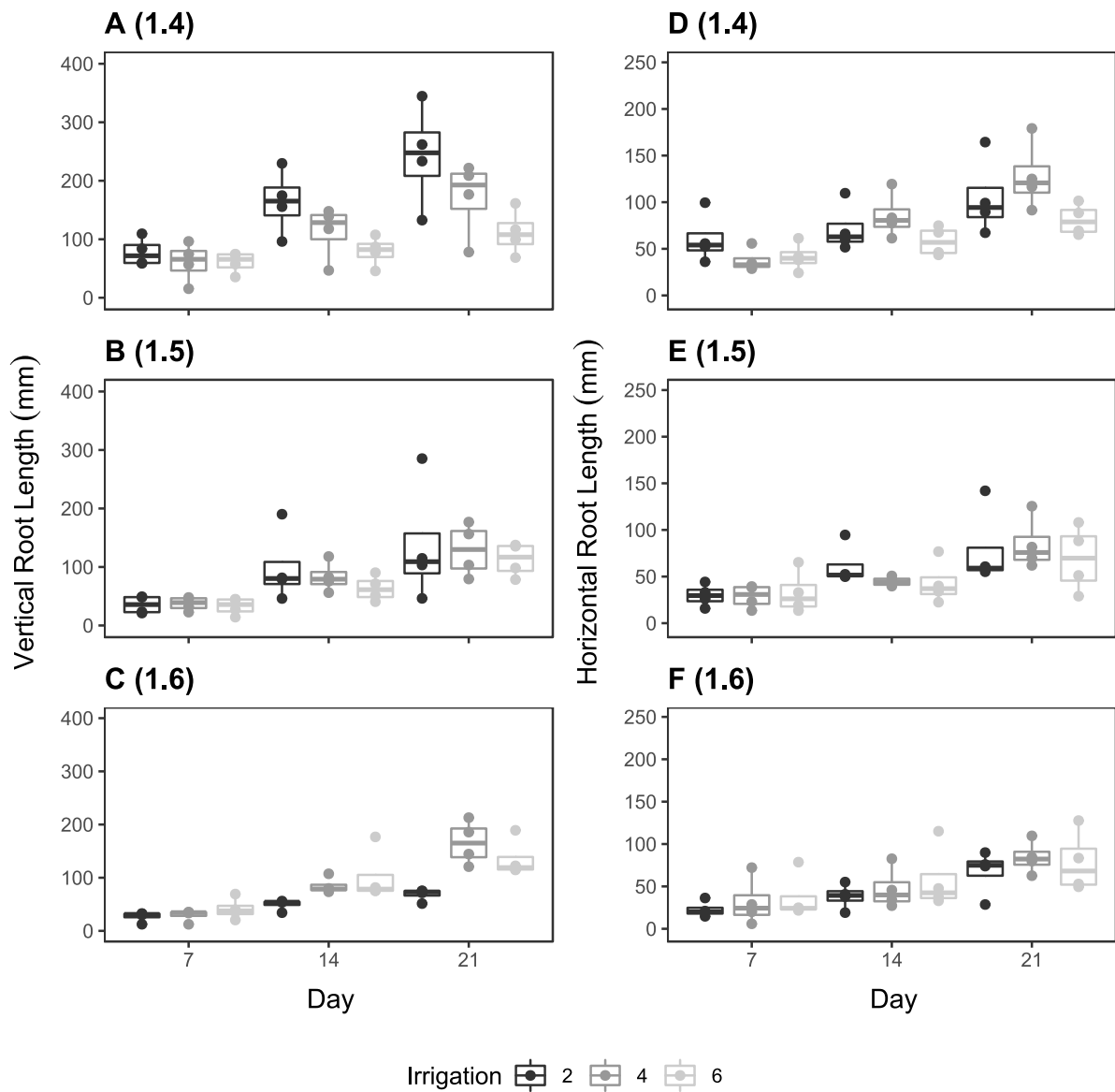


**Figure 4.2:** Horizontal and vertical root lengths of spring barley grown for a period of 21 days and grouped by IRE for 1.4 (A, D), 1.5 (B, E) and 1.6 (C, F) DBD ( $\text{g cm}^{-3}$ ) treatments.

**Table 4.2:** Root growth rankings for **ARGR**, **AHGR** and **AVGR** averages across DBD and IRE treatments.

DBD (g cm <sup>-3</sup> )	IRE	<b>ARGR</b> (mm day <sup>-1</sup> )	<b>AHGR</b> (mm day <sup>-1</sup> )	<b>AVGR</b> (mm day <sup>-1</sup> )
1.4	2	8.98 (1)	5 (2)	11.58 (1)
	4	7.34 (2)	6.1 (1)	8.16 (2)
	6	4.74 (7)	3.86 (5)	5.31 (8)
1.5	2	5.44 (4)	3.75 (6)	6.55 (4)
	4	5.31 (6)	4.04 (3)	6.14 (6)
	6	4.54 (8)	3.29 (8)	5.35 (7)
1.6	2	3.23 (9)	3.2 (9)	3.25 (9)
	4	6.37 (3)	4.01 (4)	7.9 (3)
	6	5.38 (5)	3.73 (7)	6.45 (5)

Similar to the root growth rates figures above, **Figure 4.3** summarises the average values for **RHtRR** and demonstrate its relationships between the various DBD and IRE experimental treatments. **Figure 4.4**, shows the observed **RHtRR** values as a function of time for all the treatments.

Global statistical comparisons for **RHtRR** across different treatments of DBD ( $F = 3.1590$ ,  $p = 0.257$ ) and IRE ( $F = 0.3193$ ,  $p = 0.861$ ) failed to detect any simple main effects. Furthermore, global testing failed to detect any statistically significant interaction effects ( $F = 1.4971$ ,  $p = 0.861$ ).

**Table 4.3**, is a summary of the rank scores of **RHtRR**, for each of the experimental treatments. The largest **RHtRR** value corresponded to the 1.6 g cm<sup>-3</sup> DBD and 6 IRE treatment while the smallest corresponded to the 1.5 g cm<sup>-3</sup> DBD and 6 IRE treatment. This suggests that for the wettest treatments of 6 IRE the DBD value determined the **RHtRR** with a lower density reducing the values. However no statistically significant effects were observed and the average difference among the treatments was 0.63.

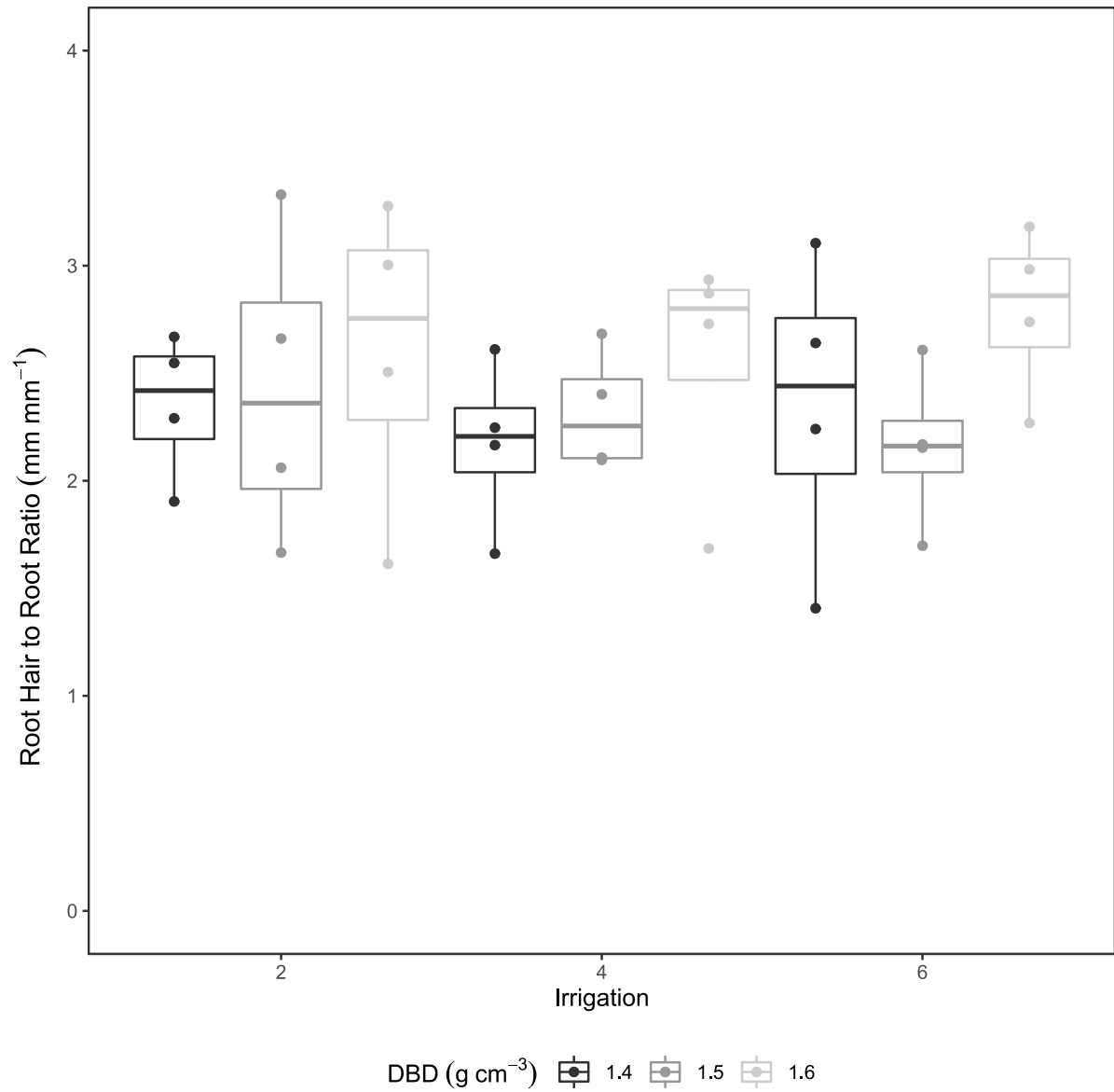


**Figure 4.3:** Average spring barley **RHtRR** grown for a period of 21 days as a function of IRE and grouped by DBD.

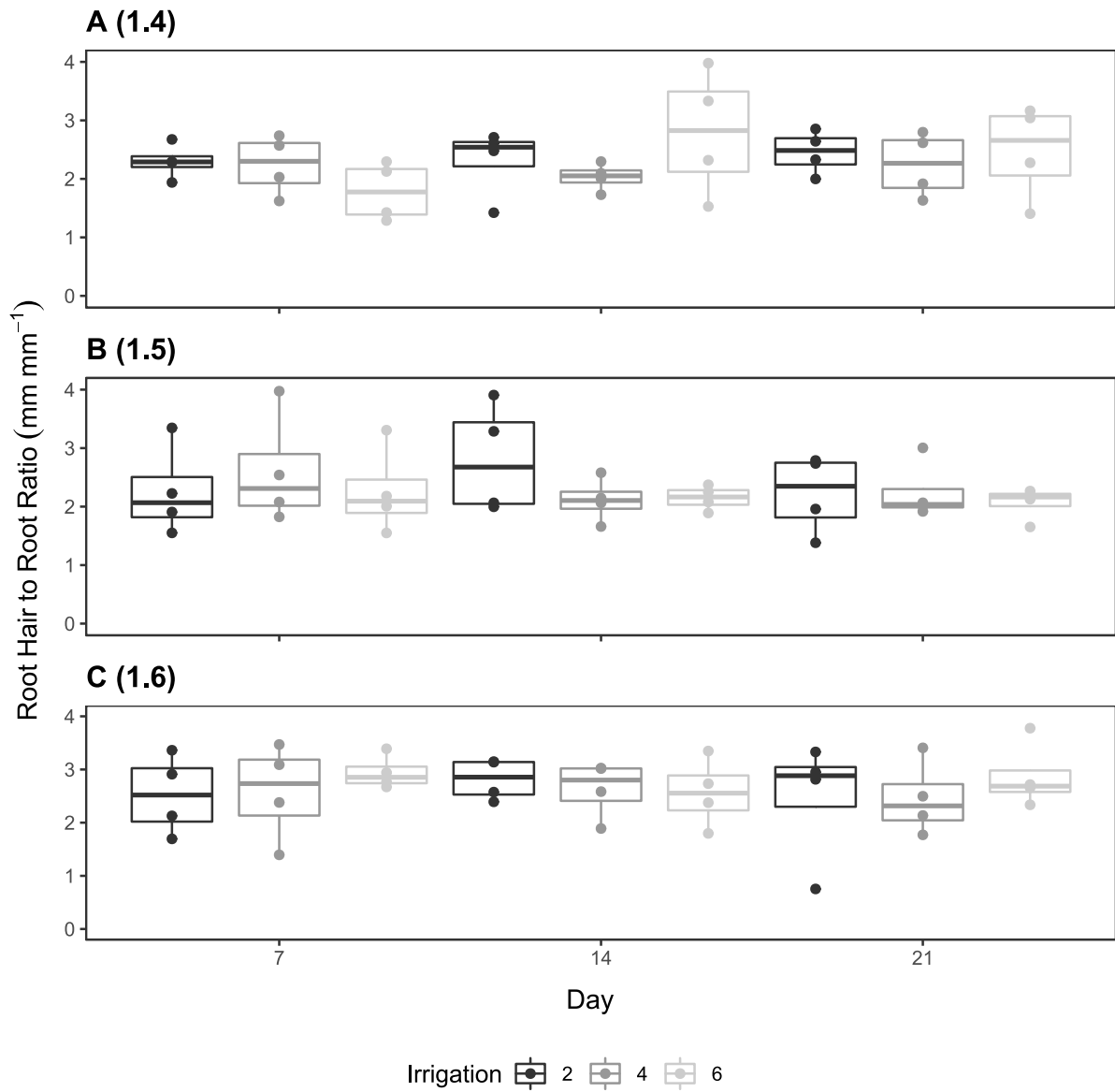


**Figure 4.4: RHtRR** of spring barley grown for a period of 21 days and grouped by IRE for 1.4 (A, D), 1.5 (B, E) and 1.6 (C, F) DBD (g cm<sup>-3</sup>) treatments.

**Table 4.3:** Rankings for **RHtRR** averages across DBD and IRE treatments.

DBD (g cm <sup>-3</sup> )	IRE	<b>RHtRR</b> (mm mm <sup>-1</sup> )
1.4	2	2.35 (5)
	4	2.17 (8)
	6	2.35 (6)
1.5	2	2.43 (4)
	4	2.32 (7)
	6	2.16 (9)
1.6	2	2.6 (2)
	4	2.56 (3)
	6	2.79 (1)

**Figure 4.5**, demonstrates the **RBCC** values across DBD (**A**) and IRE (**B**) treatments.

Global testing for **RBCC** indicated statistically significant differences across the DBD ( $F = 8.0872$ ,  $p = 0.047^*$ ) treatments but not for the IRE treatments ( $F = 0.8362$ ,  $p = 0.68$ ) and their interaction effects ( $F = 3.9328$ ,  $p = 0.528$ ). Post hoc testing indicated statistically significant differences for **RBCC** between the highest DBD treatment (1.6 g cm<sup>-3</sup>) and the lower DBD treatments of 1.4 g cm<sup>-3</sup> ( $\psi = -62$ ,  $p = 0.0246^*$ ) and 1.5 g cm<sup>-3</sup> ( $\psi = -56.75$ ,  $p = 0.0325^*$ ) with higher **RBCC** values being observed at higher substrate density treatments.

**Table 4.4**, is a summary of the rank scores of **RBCC**, for each of the experimental treatments. The largest **RBCC** value corresponded to the 1.6 g cm<sup>-3</sup> DBD and 6 IRE treatment while the smallest corresponded to the 1.4 g cm<sup>-3</sup> DBD and 6 IRE treatment. This suggests that for the wettest treatments of 6 IRE the DBD value determined the **RBCC** with a lower density reducing the number of RBCs.

The reason **RBCC** was defined as the sum of viable and non-viable cells was because for most cases the non-viable cells were almost entirely the entire population of cells present.

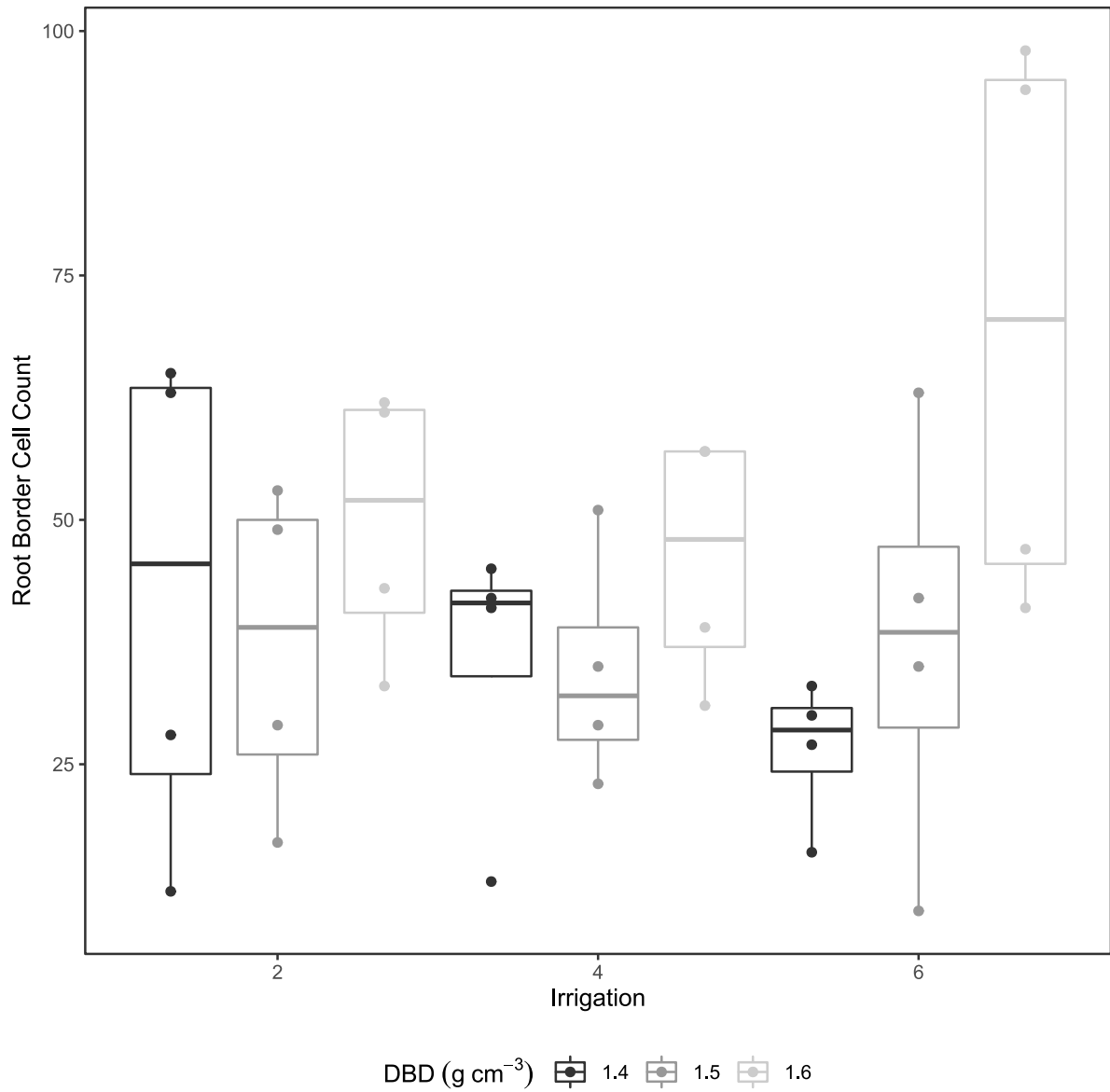


**Figure 4.5:** RBCC of spring barley at the end of a 21-day growth period as a function of IRE and grouped by DBD.

**Table 4.4:** Rankings for **RBCC** averages across DBD and IRE treatments.

DBD (g cm <sup>-3</sup> )	IRE	<b>RBCC</b>
1.4	2	42 (4)
	4	35 (7/8)
	6	27 (9)
1.5	2	37 (6)
	4	35 (7/8)
	6	38 (5)
1.6	2	50 (2)
	4	46 (3)
	6	70 (1)

**Figure 4.6**, demonstrates the **RTE** values across DBD (**A**) and IRE (**B**) treatments. Global testing indicated statistically significant differences across the DBD treatments ( $F = 11.9108$ ,  $p = 0.013^*$ ) but not for the IRE treatments ( $F = 0.0644$ ,  $p = 0.971$ ) and their interaction effects ( $F = 4.0423$ ,  $p = 0.518$ ). Post hoc testing indicated statistically significant differences for **RTE** between the highest DBD treatment (1.6 g cm<sup>-3</sup>) and the lower treatments of 1.4 ( $\text{psi} = -3.8039$ ,  $p = 0.0048^{**}$ ) and 1.5 ( $\text{psi} = -3.2055$ ,  $p = 0.0124^*$ ) with the higher substrate densities having more eccentric root tip geometries suggesting a less curved root tip shape.

**Table 4.5**, is a summary of the **RTE** associated results from the statistical comparisons across different treatments of DBD and IRE. The largest **RTE** value corresponded to the 1.6 g cm<sup>-3</sup> DBD and 2 IRE treatment while the smallest corresponded to the 1.4 g cm<sup>-3</sup> DBD and 2 IRE treatment. This suggests that for the driest treatments of 2 IRE the DBD value determined the **RTE** with a lower density reducing the **RTE**.

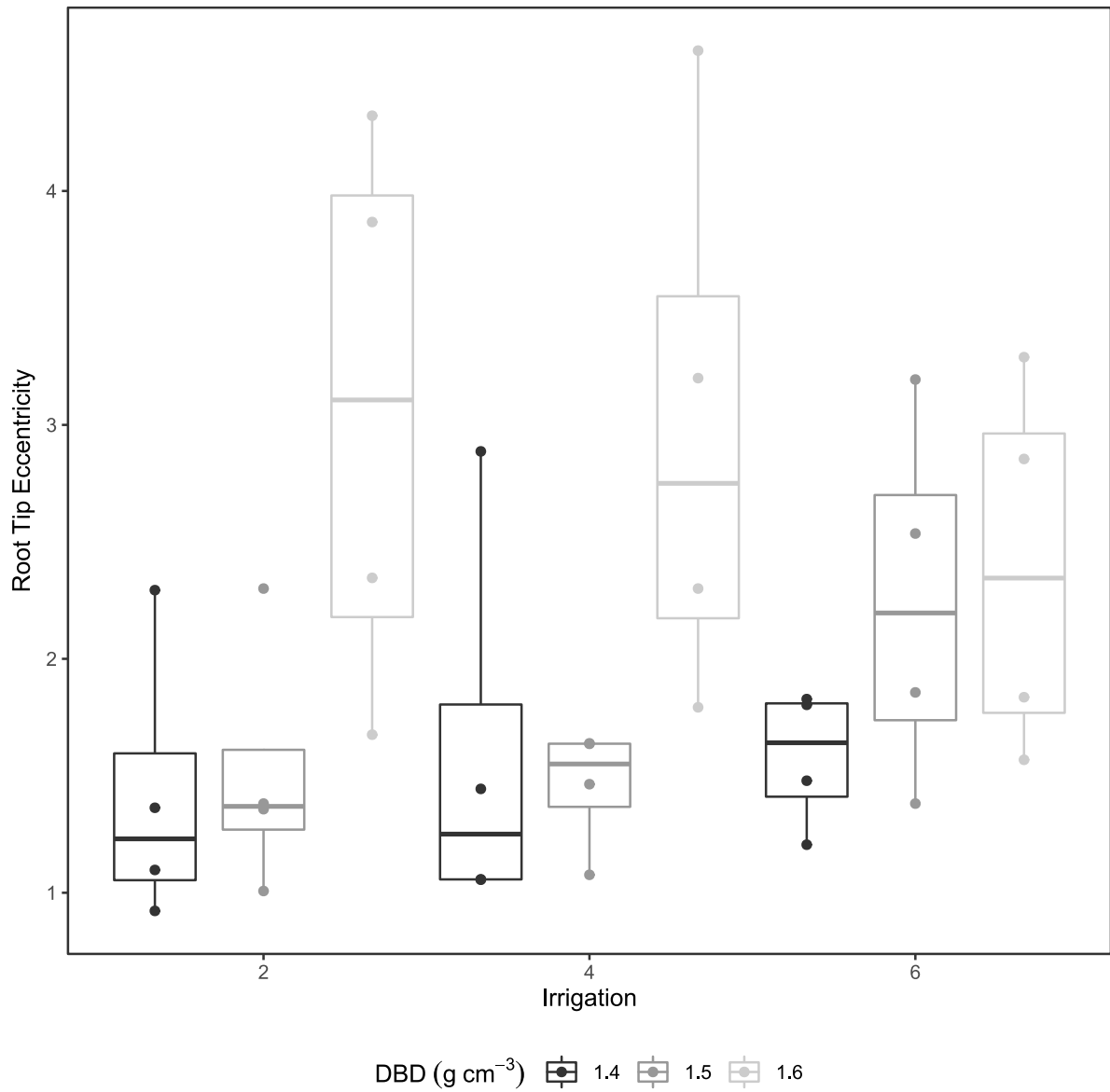


**Figure 4.6:** RTE of spring barley at the end of a 21-day growth period as a function of IRE and grouped by DBD.

**Table 4.5:** Rankings for **RTE** averages across DBD and IRE treatments.

DBD (g cm <sup>-3</sup> )	IRE	<b>RTE</b>
1.4	2	1.42 (9)
	4	1.61 (5)
	6	1.58 (6)
1.5	2	1.51 (7)
	4	1.45 (8)
	6	2.24 (4)
1.6	2	3.05 (1)
	4	2.97 (2)
	6	2.39 (3)

In summary, plant root **ARGR**, **AHGR** and **AVGR** were higher for the lowest bulk density treatments in comparison to the highest bulk density treatments. A medium amount of water gave higher **ARGR** when compared to the wettest treatments. Furthermore, at the highest bulk density treatments increasing amounts of water had a positive effect on **ARGR** and **AVGR**. In contrast, at the lowest bulk density treatments the driest treatments had a higher **ARGR** and **AVGR**. Root hair area did not appear to be responsive to either experimental factor of bulk density and water. **RBCC** increased at the highest bulk density treatments but did not vary significantly with water quantity. **RTE** also had similar effects with **RBCC** with the highest bulk density treatments having a higher **RTE** resulting in less curved root tips but, the amount of water did not have a significant influence on root tip shape.

To assess the level of correlation between the different root traits principal components analysis was applied, using the **ARGR**, **AVGR**, **AHGR**, **RHtRR**, **RBCC** and **RTE** variables. **Figure 4.7**, is a series of PCA biplots for all possible combinations of the first three principal components. **Table 4.6**, is a summary of the variance explained by each principal component and also of the correlations between the variables and the components. Inspection of the above-mentioned figure and table suggest the following conclusions based on the relationship of PC1 and PC2 capturing a total of 64.34 % of variation:

1. Root hair to root ratio was positively correlated with root border cell count.
2. Root hair to root ratio and root border cell count were not correlated with root tip geometry and average root growth rate.
3. Root tip geometry and average root growth rate were negatively correlated.
4. Average root growth rate was slightly more correlated with average vertical growth rate in comparison to average horizontal growth rate.
5. No evidence of clustering for each treatment category.

**Figure 4.8**, demonstrates a snapshot of a 3D PCA plot rotated at 90 °. This plot captures a larger amount of variation by integrating the 3<sup>rd</sup> PCA component accounting for 79.99 % of the total variation. Examination of this figure suggests:

1. Root hair to root ratio, root border cell count and root tip geometry were not correlated between them and with average root growth rate.
2. Average root growth rate was slightly more correlated with average vertical growth rate in comparison to average horizontal growth rate.
3. Some evidence of a separation of the 1.6 g cm<sup>-3</sup> DBD from the other DBD treatments.

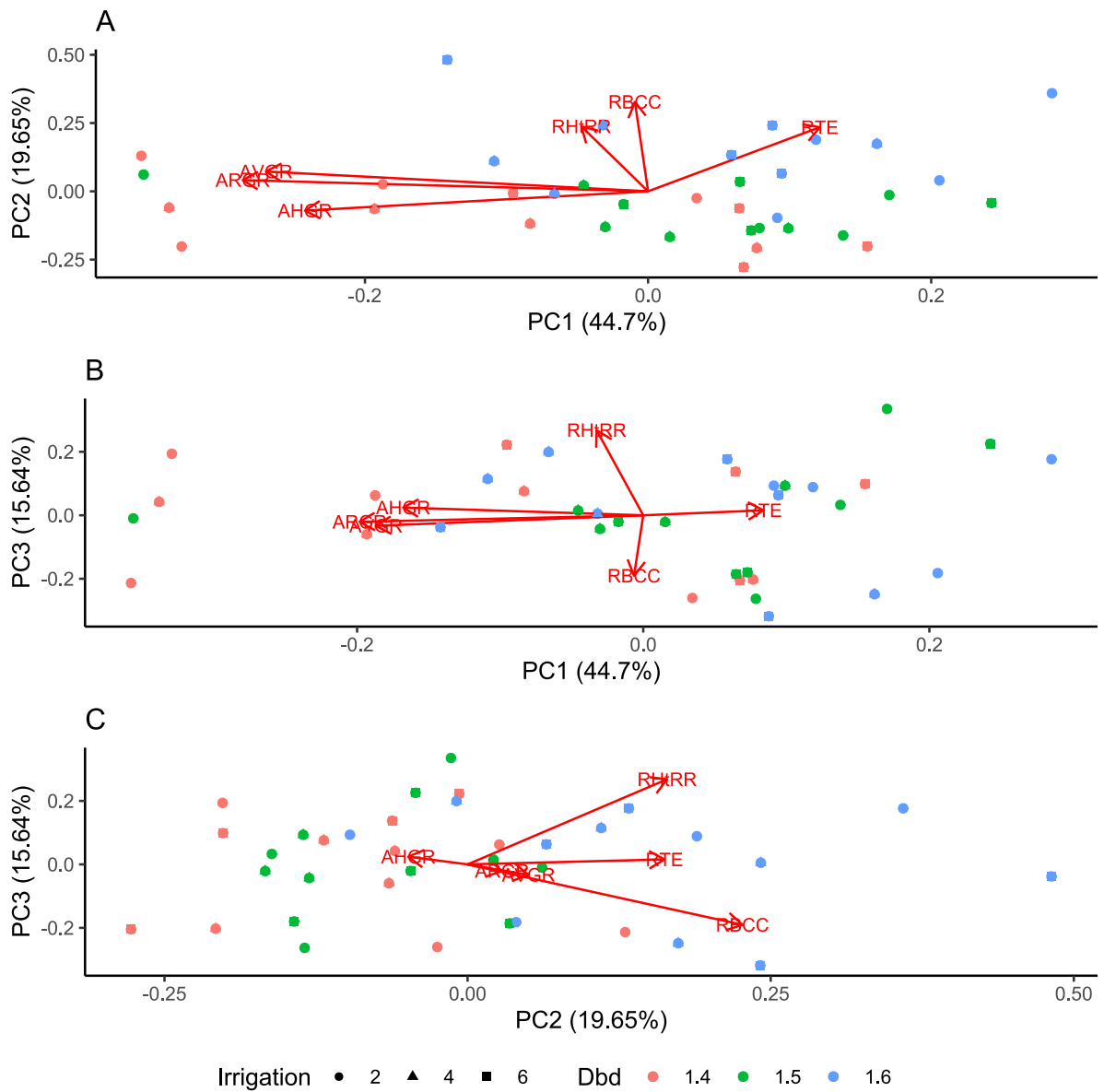


**Figure 4.7:** Principal Component Analysis biplots for **A) PC2 vs. PC1**, **B) PC3 vs. PC1** and **C) PC3 vs. PC2**.

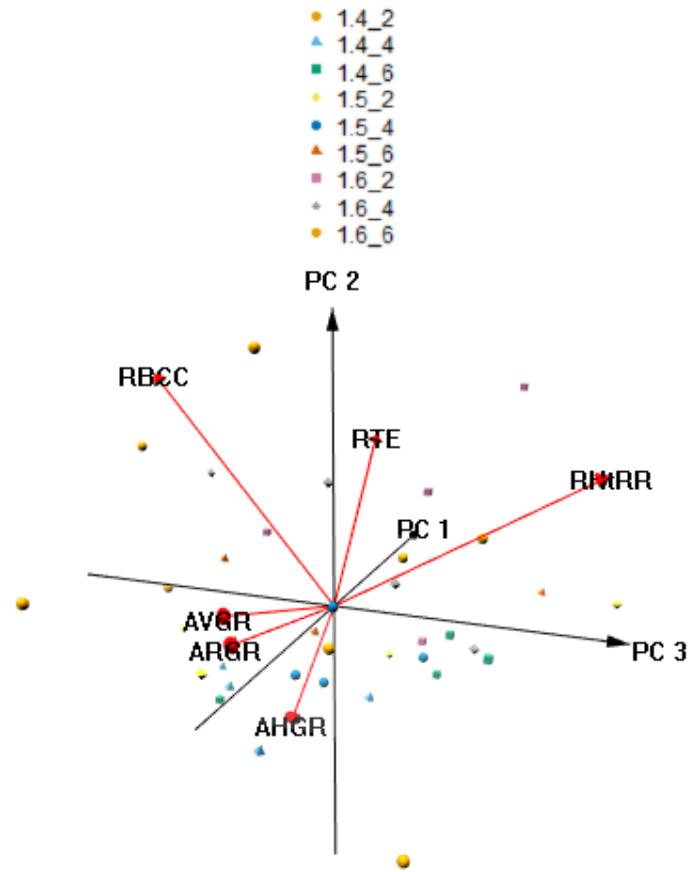


**Figure 4.8:** Principal Component Analysis 3D plot snapshot with loadings and coloured by experimental treatment.

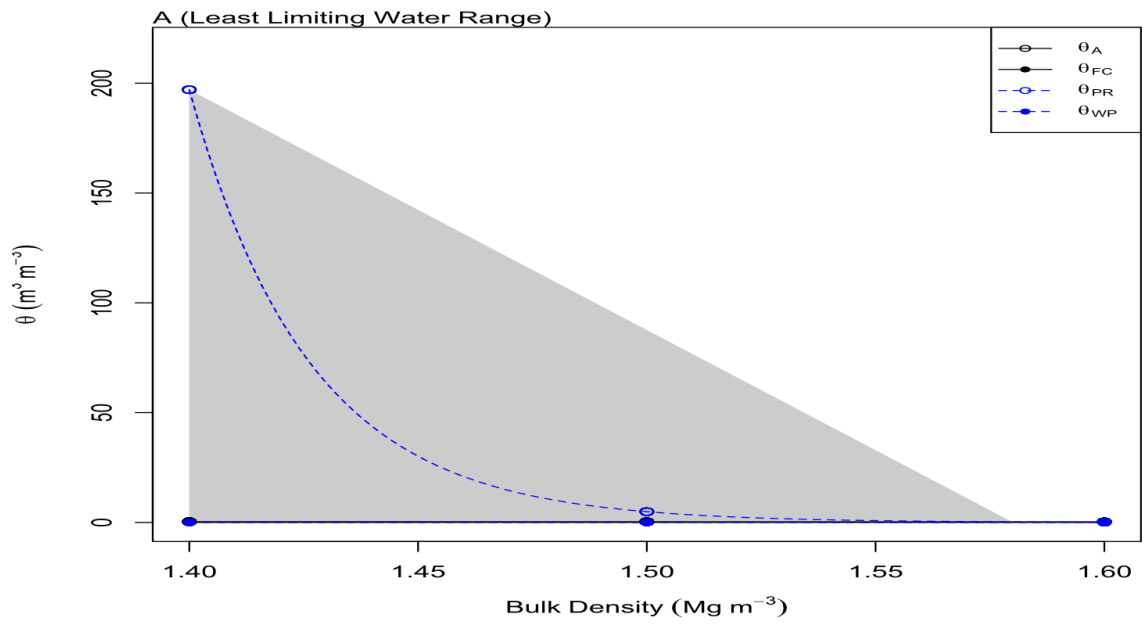
**Table 4.6:** Principal Components Analysis (PCA) of component importance, correlations and statistical significance.

Importance of components						
	PC1	PC2	PC3	PC4	PC5	PC6
Standard deviation	1.638	1.0858	0.9688	0.8887	0.6411	1.58E-10
Proportion of variance	0.447	0.1965	0.1564	0.1316	0.0685	0.00E+00
Cumulative Proportion	0.447	0.6434	0.7999	0.9315	1	1.00E+00
Data/Components Correlations						
	PC1	PC2	PC3	PC4	PC5	PC6
<b>ARGR</b>	-0.5962	0.0854	-0.0624	0.1572	-0.1904	-0.7565
<b>AHGR</b>	-0.5047	-0.1471	0.0731	0.1417	0.8112	0.2004
<b>AVGR</b>	-0.5621	0.1511	-0.0994	0.1454	-0.4926	0.6225
<b>RHtRR</b>	-0.0981	0.4947	0.8064	-0.3085	0.0099	1.67E-11
<b>RBCC</b>	-0.0194	0.6819	-0.573	-0.3908	0.2315	-4.31E-11
<b>RTE</b>	0.2525	0.4884	0.0468	0.8284	0.0968	-3.40E-11
3-way statistical significance tests (F, p)						
	PC1	PC2	PC3	PC4	PC5	PC6
DBD	8.9205, 0.036*	21.1522, 0.001*	0.0706, 0.967	0.8475, 0.674	2.0326, 0.409	0.821, 0.681
IRE	4.384, 0.16	1.2625, 0.562	0.0098, 0.996	1.2832, 0.554	0.9038, 0.663	4.9008, 0.125
DBD:IRE	11.4852, 0.094	2.3567, 0.734	1.5237, 0.856	5.1051, 0.398	10.1474, 0.136	1.5257, 0.854

**Figure 4.9 (A)**, illustrates the predicted LLWR range for the RS substrate. The figure demonstrates that the LLWR area can't be defined as the regression lines corresponding to the limiting values of aeration, field capacity and permanent wilting point are identical and correspond to 0. Further investigation revealed that the reason for this was mainly the poor fit in Busscher's PR model (**Figure 4.9 (B)**) with an  $r^2$  value of almost 0 which was estimated with the function "fitbusscher" from the same "soilphysics" package. The fit for de Silva's model (**Figure 4.9 (C)**), was much better with an  $r^2$  value of almost 1. Nevertheless, as the LLWR model uses both sub-models then the LLWR is clearly erroneous for our data and no predictions can be made.

The soil strength (**Figure 4.10 (A)**) and water release (**Figure 4.10 (B)**) curves of cores filled with RS sand, packed at 1.4, 1.5 and 1.6 g cm<sup>-3</sup> DBD are shown below. **Table 4.7** summarises the established relationship (see **Figure 2.10**) between volumetric water content, degree of saturation and air-filled porosity at a matric potential range of -1 - -100 kPa for the 4 mm treatment of "Flourite Black" packed at 1.5 g cm<sup>-3</sup>. The degree of saturation was estimated to be 36, 27 and 16 % for the 6, 4 and 2 IRE treatments respectively, with the values being almost identical across DBD treatments. This was achieved by weighting a subsample (n = 2) of the RS units at random times between 07:00 – 17:00 throughout the 3-week growth period and subsequently averaging the values obtained for each sample. Based on the established water release curve of the RS substrate (**Table 4.7**) the above-mentioned values will respectively correspond to a matric potential ( $\Psi$ ) of -5, -7 and -10 kPa and an air-filled porosity of 26.47, 28.81 and 32.34 %. The PR mean values corresponding to -5, -7 and -10 kPa matric potential were respectively 0.9377, 1.4743 and 2.2792 MPa.

Finally, **Table 4.8** is a summary of whether a statistically significant effect was detected for each of the measured variables and the PC components for the experimental factors used and their interaction.



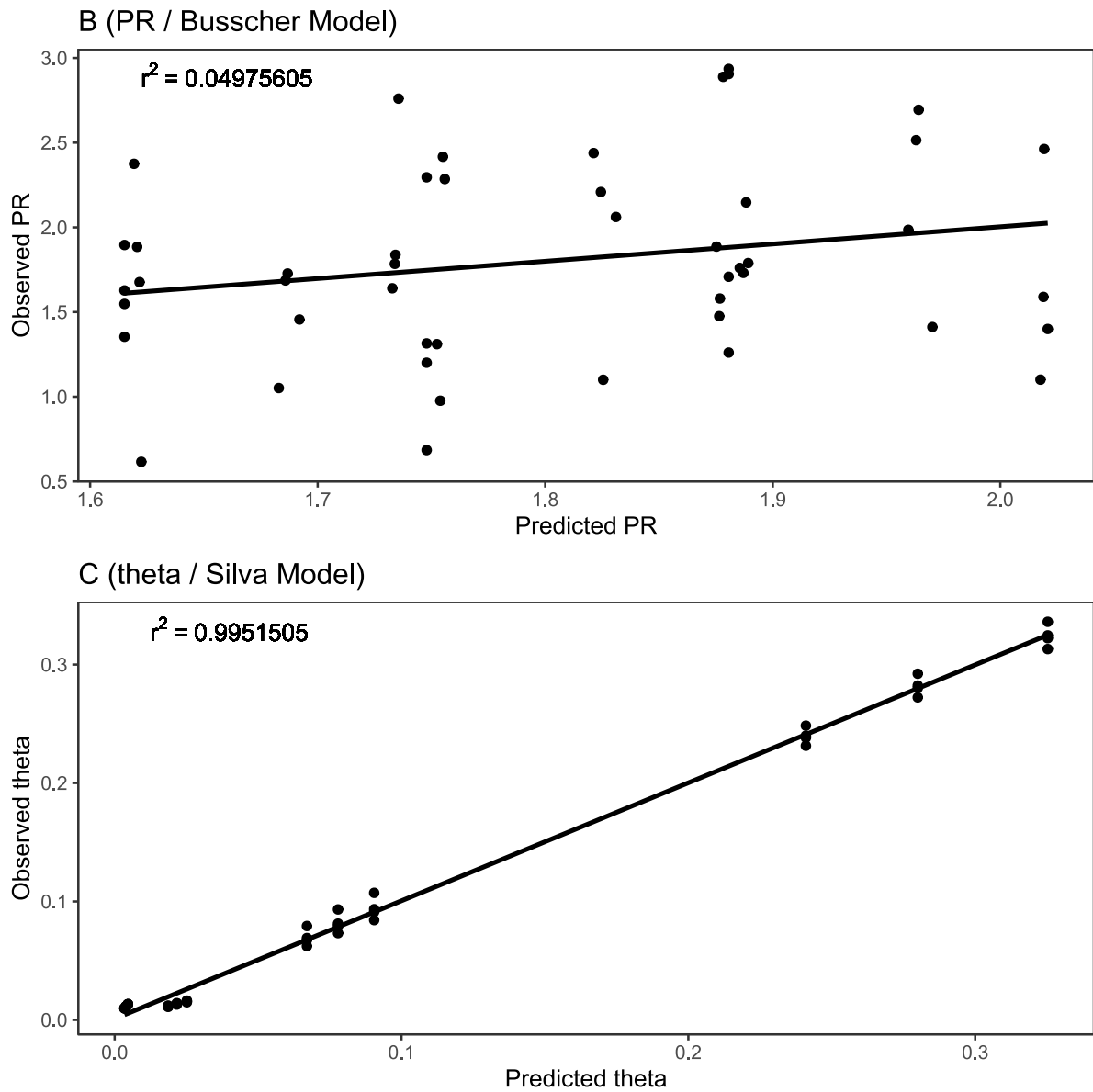


**Figure 4.9:** Least Limiting Water Range for RS substrate (A), with sub models fitted for Buescher's PR model (B) and Silva's volumetric water content model (C).

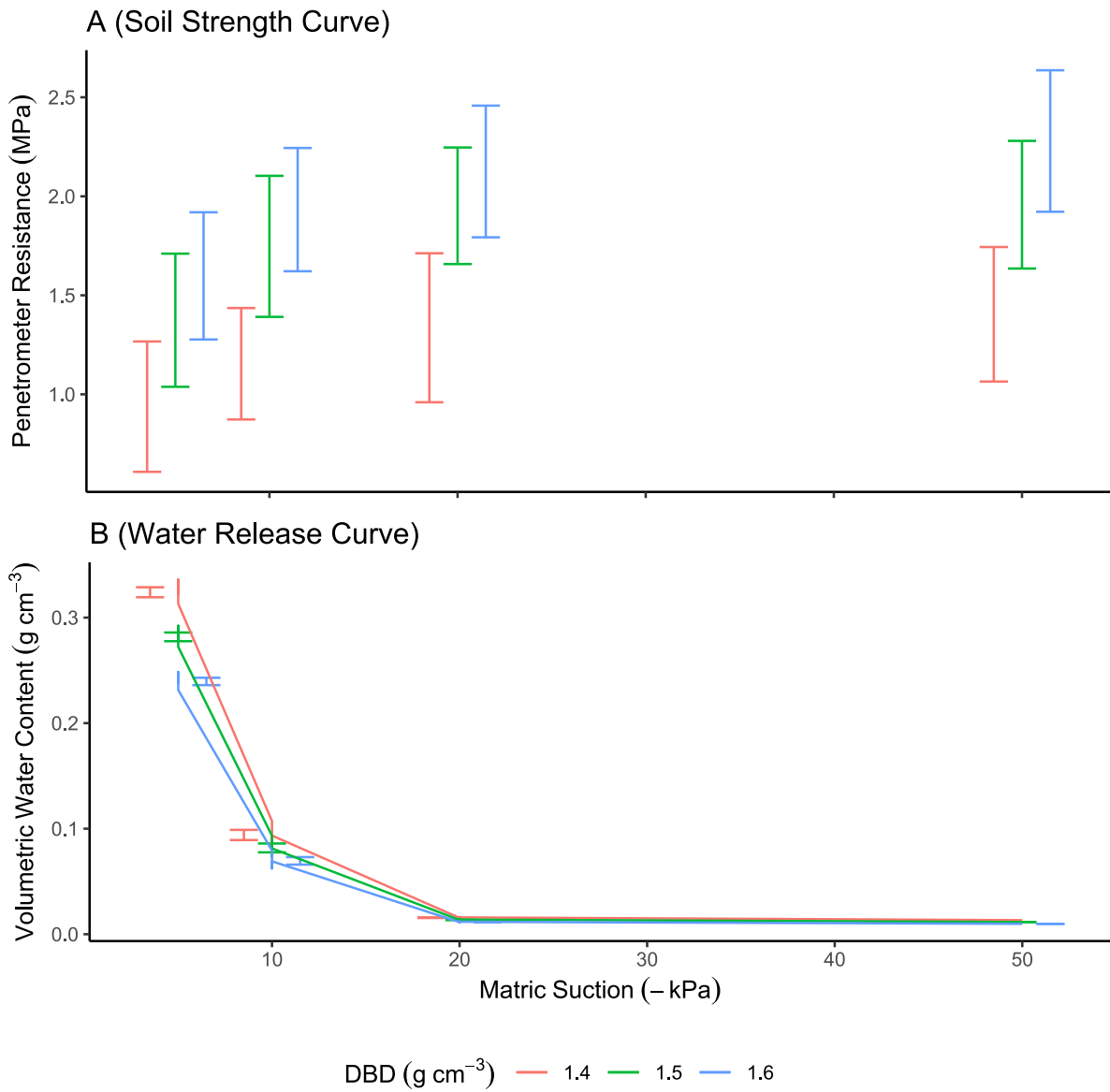


**Figure 4.10:**  $\bar{x} \pm s$  of RS substrate strength curves (A) and water release curves (B) for dry bulk density values of 1.4, 1.5 and 1.6 g cm<sup>-3</sup> with connecting lines for the mean values.

**Table 4.7:** RS sand volumetric water content ( $\theta$ ), degree of saturation ( $s$ ) and air-filled porosity ( $f_a$ ) corresponding to different matric potential ( $\Psi$ ) for cores packed at a density of  $1.5 \text{ g cm}^{-3}$ .

$\Psi$ (kPa)	$\theta$ (%)	$s$ (%)	$f_a$ (%)
-1	$32.91 \pm 3.33$	$81.22 \pm 8.66$	$7.39 \pm 3.67$
-5	$13.02 \pm 3.23$	$36.42 \pm 12.51$	$26.47 \pm 4.03$
-10	$5.68 \pm 1.32$	$15.92 \pm 4.49$	$32.34 \pm 3.31$
-20	$4.62 \pm 1.08$	$12.48 \pm 3$	$34.66 \pm 2.07$
-50	$2.45 \pm 0.98$	$6.41 \pm 2.57$	$37.29 \pm 2.38$
-100	$1.56 \pm 0.16$	$4.14 \pm 0.6$	$38 \pm 1.41$

**Table 4.8:** Statistically significant effects summary for variables and PC components.

	<b>DBD</b>	<b>IRE</b>	<b>Interactions</b>
<b>ARGR</b>	✓	✓	✓
<b>AVGR</b>	✓	✗	✓
<b>AHGR</b>	✓	✗	✗
<b>RHtRR</b>	✗	✗	✗
<b>RBCC</b>	✓	✗	✗
<b>RTE</b>	✓	✗	✗
PC1	✓	✗	✗
PC2	✓	✗	✗
PC3	✗	✗	✗
PC4	✗	✗	✗
PC5	✗	✗	✗
PC6	✗	✗	✗

## 4.5 Discussion

Bengough *et al.*, (2011), suggested maize root elongation rate is halved at a matric potential of -500 kPa and a PR value of 2 MPa. In terms of matric potential only a fraction of that magnitude was achieved in this study compared to the reported value in maize. The reason for this narrow range in  $\Psi$  and large range in  $\theta$  was clearly due to the dominance of the large pores in the RS substrate (see Section 2.5.5). Nevertheless, the gradual decrease in  $\theta$  offered a spectrum of decreasing water availability and enabled for the manipulation of water stress although it was restricted on the macro-pore scale, with a 23% reduction in **ARGR** between the 2 and 6 IRE treatments. As for the estimated PR range a spectrum was also ranging from 0.9377 to 2.2792 MPa. This time the reduction in **ARGR** was 29 % between the 1.4 and 1.6 g cm<sup>-3</sup> DBD treatments. Again, this reduction in root growth indicates that an increase in the DBD translates to an increase in mechanical impedance by reducing root elongation rates. The findings obtained were thus, in agreement with the general trend of an inverse relationship between DBD and root elongation rates (Jin *et al.*, 2013). As for the 50 % reduction in growth LLWR associated threshold, i.e., **ARGR** = 4.49 mm day<sup>-1</sup>, this was achieved for the treatments of 1.5 g cm<sup>-3</sup> DBD at 6 IRE (4.54 mm day<sup>-1</sup>, rank = 8) and for 1.6 g cm<sup>-3</sup> DBD at 2 IRE (3.23 mm day<sup>-1</sup>, rank = 9). It is interesting that at medium density the slowest growth rate was observed for the most wet treatments but for high density the slowest growth rate corresponded to the driest treatments, implying an interaction effect (**Table 4.8**).

Bengough *et al.*, (2016), concluded root hairs enhanced root penetration ability in low density (1.0 – 1.2 g cm<sup>-3</sup>) soils but not in higher bulk density (1.5 g cm<sup>-3</sup>). In a similar manner, no significant differences could be detected for the **RHtRR** root trait across the 1.4 – 1.6 g cm<sup>-3</sup> bulk density range tested ( $p = 0.257$ ). A potential explanation of this effect stems from the fact that the PR values for the treatments were not sufficiently distinct at -5 kPa although they were somewhat more distinct at -10 kPa. Nevertheless, no clear conclusion could be made as to the true magnitude of the difference among the treatments due to the inherent variability, at least for a matric potential range of 0 – 50 kPa. Although, the difference was large enough to induce a statistically significant difference in terms of **ARGR** this effect was perhaps not enough to induce a change in root hair area. Root hairs are also critical for solute absorption

(Carminati *et al.*, 2017) and as such, intuitively at least, one might expect a reduced **RHtRR** for the higher IRE treatments. However, there was no evidence of a statistically significant difference between the IRE treatments ( $p = 0.861$ ). Results from Haling *et al.*, (2014), also suggest a differential response in root hair length among different strength and water treatments. Although, root hair length is not reported here a differential response between treatments will have affected the estimates of root hair area which will in turn affect **RHtRR** but, no such variation was detected here. However, it must be considered that the minimum and maximum PR values of the treatments used by Haling *et al.*, (2014), were 0.03 and 4.45 MPa respectively so the range used was wider than the range used here, i.e., 0.9377 to 2.2792 MPa. In a similar manner, the high and low water concentration treatments had a matric potential of around -7.5 and -40 kPa respectively with a significantly lower matric potential limit in comparison to the one used in this study, i.e., -10 kPa. This could help explain why the corresponding **RHtRR** responses were not detected in the results reported here.

Iijima *et al.*, (2003), reported that the effect of compaction on the rate of cell division in the cap meristem was a positive one for compacted roots. The authors estimated the sum of viable and non-viable cells to be 4960 and 3540 in compacted (PR = 3.8 MPa) and loose (PR = 0.2 MPa) sand respectively. Although the lower and upper values of PR used in this study were larger and smaller respectively, the range of PR values used was sufficient to induce a similar response. Results from Somasundaram *et al.*, (2009), further support the conclusion that a more compact soil increases RBC production. This effect was also detected here with the 1.6 g cm<sup>-3</sup> DBD treatment having a statistically significant higher **RBCC** relative to the 1.4 ( $p = 0.02464^*$ ) and 1.5 ( $p = 0.03254^*$ ) treatments. The same authors also examined the interaction between soil density and water and found a higher RBC production for wet soil relative to dry soil. However, our results are not in agreement with this conclusion ( $F = 0.8362$ ,  $p = 0.68$ ). They also detected an interaction effect between soil mechanical impedance and soil water status which suggested that the number of RBCs increased with soil moisture content in compact soil treatment. However, there was no evidence of such an interaction effect in this study ( $F = 3.9328$ ,  $p = 0.528$ ). It should also be noted, that the **RBCC** values reported are in truth an underestimation of the true values. This is because a portion of the cells will have adhered to the adjacent sand particles and the acrylic surface.

Furthermore, some detached RBCs will also inevitably leach towards the lower parts of the RS unit. This could potentially be assessed at some point in the future by collecting the solutes at the bottom and the adjacent sand particles for analysis.

In terms of **RTE**, a statistically significant difference was detected among DBD treatments ( $F = 11.9108$ ,  $p = 0.013^*$ ). More precisely, the  $1.6 \text{ g cm}^{-3}$  DBD treatment differed with both the  $1.4$  ( $p = 0.00482^{**}$ ) and the  $1.5$  ( $p = 0.013^*$ ) treatments. The findings reported here are in agreement with those reported by Iijima *et al.*, (2003), who found maize root caps were reduced in size under a higher mechanical impedance. Colombi *et al.*, (2017), reported that a smaller tip radius-to-length ratio accounted for an increased root elongation rate under high ( $1.45 - 1.6 \text{ g cm}^{-3}$ ) and moderate ( $1.2 \text{ g cm}^{-3}$ ) soil DBD across 14 Swiss winter wheat (*Triticum aestivum*) cultivars. Iijima *et al.*, (2003), also found that the removal of the root cap in maize resulted in blunter shape for the decapped root tip which had a higher penetration resistance ( $0.52 \text{ MPa}$ ) relative to the intact root cap ( $0.31 \text{ MPa}$ ). This is because a blunter root tip is known to have a more spherical deformation pattern as opposed to a cylindrical one thus, enhancing the penetration force (Greacen *et al.*, 1968).

This study had limitations, some of which could be overcome but others could not. For example, an intrinsic limitation was the inability to measure the RS substrate matric potential and instead relying on the water release curve and weighting of the RS units. It must be considered that although this method was valid at the start of the experiment it will probably underestimate matric potential at later stages of root growth when the mass and the water requirements of the root system increase and these factors cannot be separated from the overall RS unit. Unfortunately, preliminary tests indicated that assessing the matric potential of the sand was not possible due to the poor connectivity between the sand and the minitensiometer's probe as the RS substrate layer thickness was only 4 mm and raised uncertainties as to whether the estimates provided were true. An alternative option would have been to simply flood the rhizotron to varying degrees. However, this option was avoided due to difficulties in achieving and maintaining viable root growth rates in the thin sand layer. Furthermore, similar setups examining the effect of waterlogging on plants indicated that the effect of waterlogging on root growth was to simply halt its development beyond the

waterlogged layer (Dresbøll *et al.*, 2013). This effect in conjunction with the study having a duration of 3 weeks was the reason behind the use of irrigation events.

One limitation that could be overcome in future studies is the issue of the sample size. Practical limitations allowed for a maximum sample size of 4 minirhizotrons per treatment. This will inevitably limit the accuracy of statistical estimation as factorial experiments normally require a minimum sample size of 10 (Everitt, 1975). Other authors also further suggest that in addition to the previous recommendation, that the subjects-to-variables ratio should be no lower than 5 (Bryant and Yarnold, 1995). However, this limitation, could be addressed in other experiments where time and resource availability is not as limited.

Finally, there was a fundamental problem in designing this study as no reports of this type existed at the start of this work. To the author's knowledge only partial comparisons could be made, mostly in relation to root elongation rate with PR and matric suction but not accounting for the variation in root-micro traits when both factors are being manipulated except, for the case of RBC examined by Somasundaram *et al.*, (2009) but for maize plants not barley. At the same time, it is this lack of empirical data which motivated the design and implementation of this novel experiment always considering the limitations discussed above.

## 4.6 Conclusions

Minirhizotron units have been used widely in the past to assess root growth (Johnson *et al.*, 2001) and in some cases even succeeded in measuring fine root traits such as root hairs *in situ* (Koebernick *et al.*, 2017). However, to the author's knowledge, this is the first-time that automated imaging-based methods were integrated into an experimental protocol which enabled both the manipulation of the LLWR soil stressors and the measurement of fine root traits. The minirhizotron unit was successfully used to induce a spectrum of root growth responses across the DBD and IRE treatments required to assess the LLWR responses. Furthermore, *in situ* estimates of root hair area and *ex situ* estimates of root border cells and root tip geometry were successfully captured.

**ARGR** values were statistically significantly higher for the lower DBD treatment of 1.4 g cm<sup>-3</sup> when compared to the highest DBD treatment of 1.6 g cm<sup>-3</sup>. In a similar manner, ARGGR

was higher for the medium IRE treatment of 4 when compared to the wettest IRE treatment of 6. The **RHtRR** values were unresponsive to both the experimental treatments of DBD and IRE. A higher DBD treatment ( $1.6 \text{ g cm}^{-3}$ ) also increased the values of both **RBCC** and **RTE** in comparison to the lower DBD treatments ( $1.4$  and  $1.5 \text{ g cm}^{-3}$ ). The same effect was not observed in relation to IRE treatments. There was also no strong evidence of a correlation between the root micro-traits and root growth rates and between the root micro-traits themselves across the experimental treatments.

In conclusion, this chapter demonstrated by using the barley cultivar “Optic” that the suggested experimental protocol can be successfully used to measure root micro-traits in barley under various LLWR soil stressor treatments. This in turn will enable the design of a larger scale experiment which will attempt to assess if any differences in root micro-traits exist across different genotypes of barley. The measured responses will in turn, allow for an assessment of how the root micro-traits influence the LLWR boundaries.

## 5. Variation in root traits associated with LLWR

### 5.1 Introduction

The majority of modern crop plants have high-water requirements and lack drought tolerance (FAO and ITPS, 2015). However, the costs associated with the supply of irrigation water are increasing (White *et al.*, 2013). In addition, the issue of water availability will be exacerbated by climate change which will have a wide spectrum of effects on crop plants (Srivastava and Misra, 2018). Combating the above-mentioned issues while trying to increase food production for an ever-increasing global population is a major challenge (FAO, 2009). Furthermore, other issues such as soil compaction due to heavy machinery use in modern agricultural practices increase the mechanical resistance of the soil and reduce its porosity with corresponding reductions in the amount of oxygen available to plant roots (Lipiec *et al.*, 2012). As such, several models have attempted to model the complex and dynamic relationship between the three soil stressors of soil mechanical impedance, water availability and oxygen consumption in relation to root growth (Keller *et al.*, 2015; Bartholomeus *et al.*, 2008).

One example of a model that attempts to describe the above mentioned relationship is the least limiting water range (LLWR) model (da Silva *et al.*, 1994). This aims at integrating the three soil stressors mentioned above in a single index-like variable within the context of plant growth. It is a mathematically quantitative model, computationally feasible and clearly integrates important soil variables such as dry bulk density, porosity, matric suction and soil strength (usually measured as penetrometer resistance). The plant component of the model is considered in the form of a set of 4 limiting values representing the point where root growth effectively stops. Those values are penetration resistance (PR - 2 MPa), air filled porosity at hypoxic conditions (AFP - 10%), matric potential at field capacity (FC - a measure of soil water-holding capacity) (0.01 MPa) and matric suction at the permanent wilting point (PWP - 1.5 MPa). The resulting output is a range of soil volumetric water concentration within which plant growth is believed to be optimum. Unfortunately, the model is limited by not considering that the plant responses to soil physical stressors are strongly influenced by the

range of root traits that the plant has (Bengough *et al.*, 2011). For the model to become more accurate, it must take account of the effect of the root traits.

Chapter 4 introduced an experimental protocol which effectively integrated the minirhiztron system (RS) developed in Chapter 2 and the imaging techniques of Chapter 3. It was demonstrated that the experimental procedure allowed the manipulation of LLWR soil stressors and successfully induced a spectrum of responses on the barley variant Optic, in terms of root growth as an increase in substrate bulk density and water availability caused a corresponding increase in root growth rates similar to what was reported in the literature, e.g., Jin *et al.*, (2013). The root micro-traits were then successfully imaged and quantified by using a mixture of *in situ* and *ex situ* techniques and the differences between the treatments were assessed.

As a consequence of the above, the aim of this chapter was to finally demonstrate that the procedure could be used to capture the genotypic variability in root traits of spring barley. This was achieved by applying the previously mentioned protocol to a total of 4 spring barley genotypes grown in the RS system. The spring barley (*Hordeum vulgare*) varieties chosen for this experiment were Optic (1), KWS Sassy (2), Derkado (3) and Golden Promise (4). These varieties were chosen based on results from Newton *et al.*, (2020), from two field-grown plant trials involving all four of the above mentioned varieties. In the 2013-2015 trial Optic had a 15.17 % reduction in yield when switching from inversion to non-inversion tillage practices while Golden Promise experienced only a much smaller 4.17 % reduction in yield, suggesting that it's much more adapted to compacted soil conditions. Derkado also had a smaller reduction in yield (10.76 %) suggesting it's also better adapted to non-inversion tillage relative to Optic but, Optic had a higher yield (10 %) under inversion tillage suggesting that Optic performed better under less compacted conditions. In the 2016 trial Optic experienced a 20.14 % reduction in yield but KWS Sassy performed marginally better (17.16 %). However, KWS Sassy also had a higher yield (10 %) relative to Optic under inversion tillage suggesting it also performs better under less compacted conditions.

The responses obtained in terms of root growth rates and root micro-traits were then measured with the established methodologies and the extent to which root growth could be

explained as a function of the root micro-traits was investigated. This was done in order to try to answer the primary research question of this thesis, i.e., if root trait variation due to genotypic differences could explain the relative performance of plants in different soil conditions.

## 5.2 Aims

The main aims could be summarised as:

- Demonstrate the validity of the experimental protocol as a plant phenotyping platform by applying the protocol to 4 different barley cultivars.
- Determine the effect that the LLWR stressor variables have on root growth for each cultivar.
- Determine if root trait variation can explain potential differences between cultivars in terms of root elongation rates
- Assess if a root micro-trait based function model is an appropriate descriptor of the root growth responses.

## 5.3 Methods

The germination procedure for the seeds was as described in Section 2.4.5. The experiment took place at the James Hutton Institute, Invergowrie, Dundee DD2 5DA, Scotland, starting in August 2019 and completing in mid-March 2020. The glasshouse growth conditions were as described in Section 2.4.6. RS scanning was performed every 7 days for a period of 3 weeks by using the procedure specified in Section 2.4.7. The experiment was a three-way, 4 x 2 x 3, ANOVA with the factors being Variety, DBD and IRE. **Table 5.1**, is a summary of the year of introduction, pedigree and breeder of the varieties used. The experiment itself had once again a randomized (blocked) structure with the RS units arranged in two parallel linear rows with 4 treatment replicates. The treatments for DBD were 1.4, and 1.6 g cm<sup>-3</sup> and the treatments of IRE were 2, 4 and 6 irrigation events per day with an event having a duration of 3 minutes. As described previously in Section 4.3.1 this experiment also made use of a controlled release fertiliser (Scots Osmocote) for nutrient delivery by grinding it and

subsequently mixing it with the RS substrate prior to RS packing. RS scanning and destructive sampling methods used in this experiment were as described in Section 4.3.1.

**Table 5.1:** Year of introduction, pedigree and breeder information for the varieties used in this experiment.

Variety	Year	Pedigree (Newton <i>et al.</i> , 2020)	Breeder
Optic	1992	(Corniche*Force)*Chad	New Farm Crops Ltd. (Syngenta)
KWS Sassy	NA	Publican*Concerto	KWS
Derkado	1988	Lada*Salome	VEB Berlin
Golden Promise	1968	Maythorpe Ray Mutant	Gamma-Zenica

In summary, the experiment described here had an identical methodology to the one described in the previous chapter except for two points:

- 1) The 1.5 g cm<sup>-3</sup> DBD treatment was removed to make the number of treatments manageable.
- 2) The experiment was split in 4 batches with each batch consisting of a single replicate from all the treatments, i.e., 4 x 2 x 3 = 24 RS units. Each successive batch was setup 2 weeks apart from each other so that everything could become manageable due to its scale.

The statistical analysis performed was identical to the one described in Section 4.3.3. In addition, the three-way ANOVA test function “t3way” was used from the same R package. The correlation coefficient reported here is “percentage bend variance” implemented with the function “pbcorp” using default parameters, from the same R package. Principal components analysis (PCA) was performed with the R basic function “prcomp” and the data was centered and scaled for the analysis.

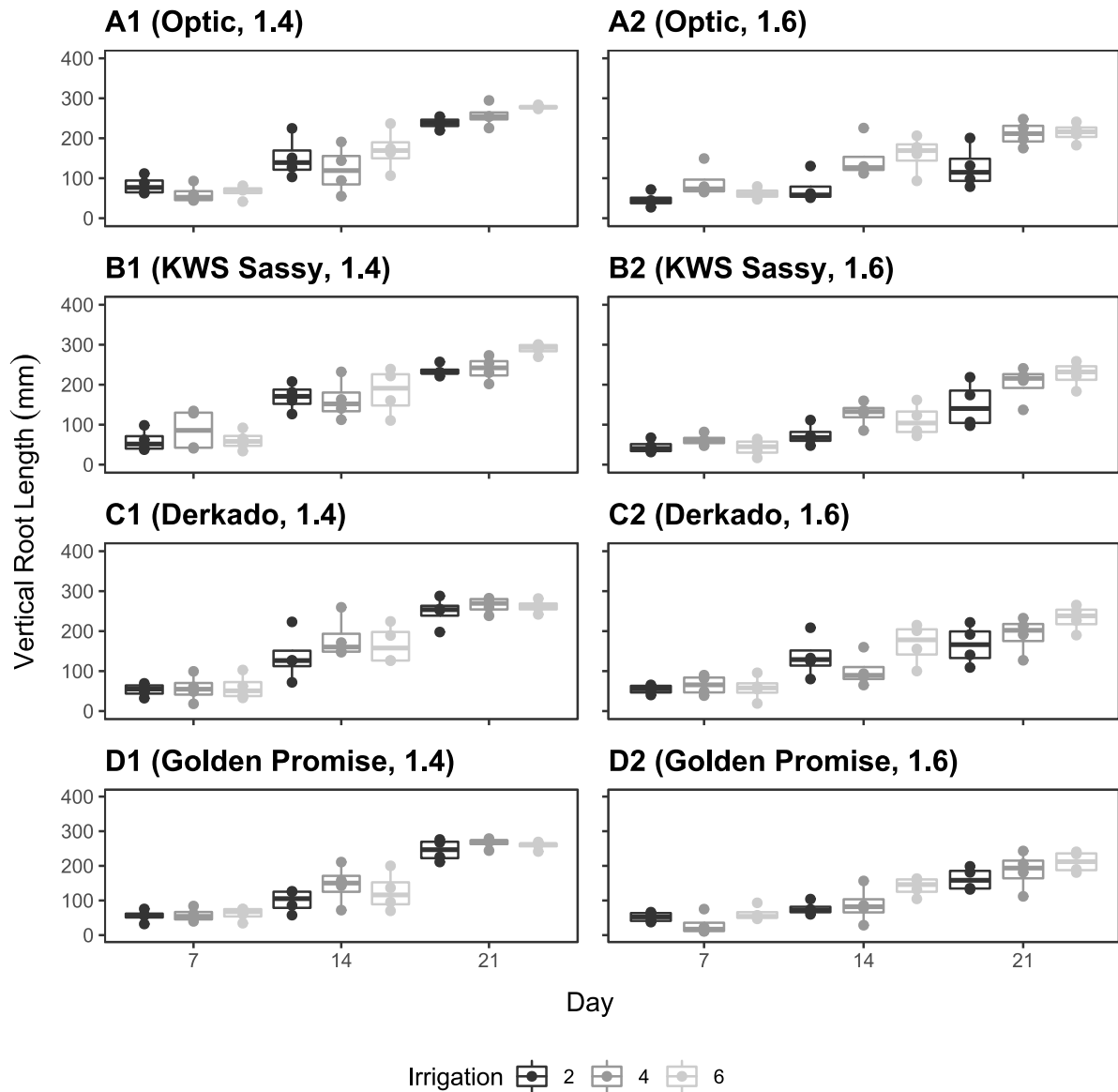
## 5.4 Results

In order to determine the treatment effects on the varieties chosen the RS units were scanned every 7 days for 21 days. **Figure 5.1**, displays the observed vertical root lengths as a function of time across a 3 week period. The graphs are grouped by the IRE factor, column arranged by the DBD factor and row arranged by the Variety factor. **Figure 5.2**, shows the observed horizontal root length in a format similar to **Figure 5.1**. **Figure 5.3**, is a series of graphs which summarise the **AHGR (A)**, **AVGR (B)** and **ARGR (C)** values against the IRE treatments and grouped by the DBD factor with the 1<sup>st</sup>, 2<sup>nd</sup>, 3<sup>rd</sup> and 4<sup>th</sup> row graphs corresponding to the Optic, KWS Sassy, Derkado and Golden Promise varieties respectively.

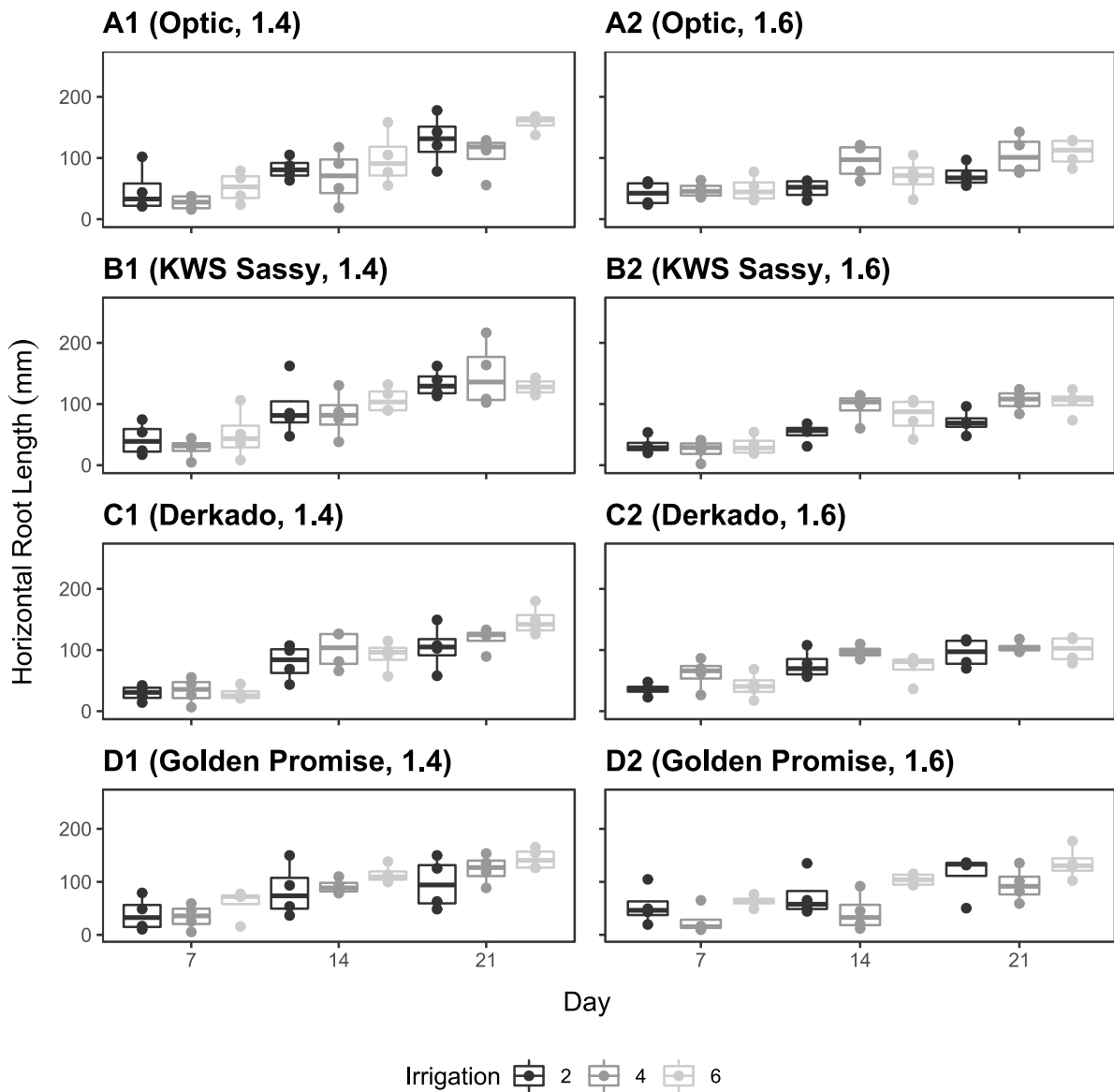
No statistically significant 3-way interaction effects were detected among the factors of Variety, DBD and IRE ( $F = 9.4748$ ,  $p = 0.2990$ ). Furthermore, no statistically significant 2-way interactions were detected between DBD and IRE ( $F = 5.8456$ ,  $p = 0.077$ ), Variety and IRE ( $F = 2.6050$ ,  $p = 0.895$ ) and Variety and DBD ( $F = 1.859$ ,  $p = 0.638$ ). In terms of main effects, no statistically significant effect was detected for the factor of Variety ( $F = 0.3680$ ,  $p = 0.96$ ). However, statistically significant main effects were detected for the factors of DBD ( $F = 165.2779$ ,  $p = 0.0001^{**}$ ) and IRE ( $F = 78.6173$ ,  $p = 0.001^{*}$ ). Subsequent pair-wise comparisons for the IRE treatments found that all pairwise comparisons differed in a statistically significant way with an increase in IRE corresponding to an increase in root growth rates. A similar relationship was also found for both **AVGR** and **AHGR**. The only statistically significant effects were the main effects of DBD for **AVGR** ( $F = 93.5490$ ,  $p = 0.0001^{**}$ ) and **AHGR** ( $F = 38.9383$ ,  $p = 0.001^{*}$ ) and also, of IRE for **AVGR** ( $F = 20.8185$ ,  $p = 0.0001^{**}$ ) and **AHGR** ( $F = 15.1172$ ,  $p = 0.003^{*}$ ). A lower DBD had a positive effect on the root growth rates of all three variables. As such, the best performing treatment was for the lowest DBD treatment and the highest IRE treatment.

**Table 5.2**, is a summary of the average values of **ARGR**, **AVGR** and **AHGR** for each experimental treatment and also their rank among the varieties (rows). However, no discernible patterns to the growth rates are identified as the ranks are randomly distributed and more importantly, the differences among the values are very small with a mean **ARGR**

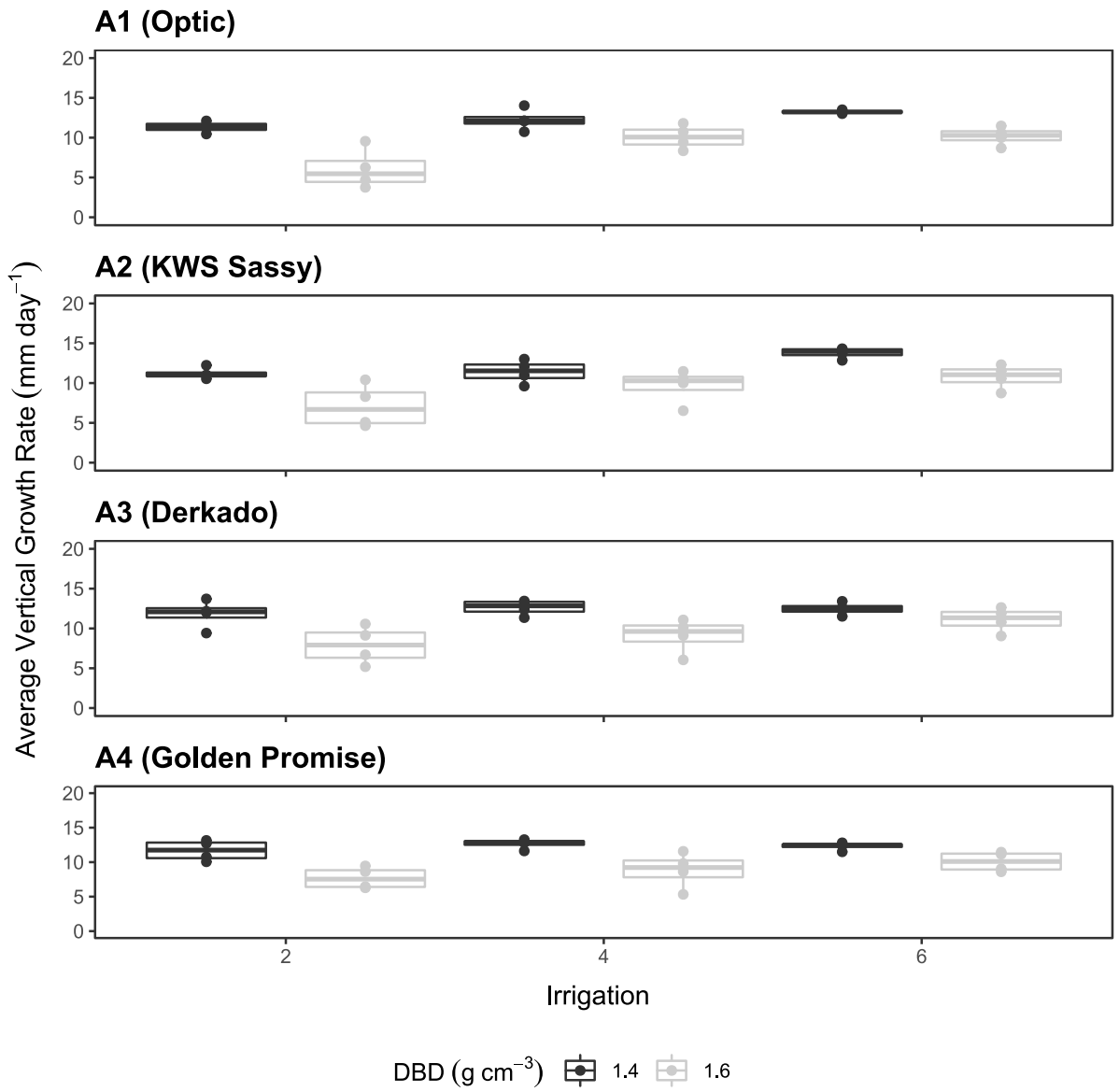
treatment difference of 0.831 mm day<sup>-1</sup> suggesting no practical difference when comparing the varieties.

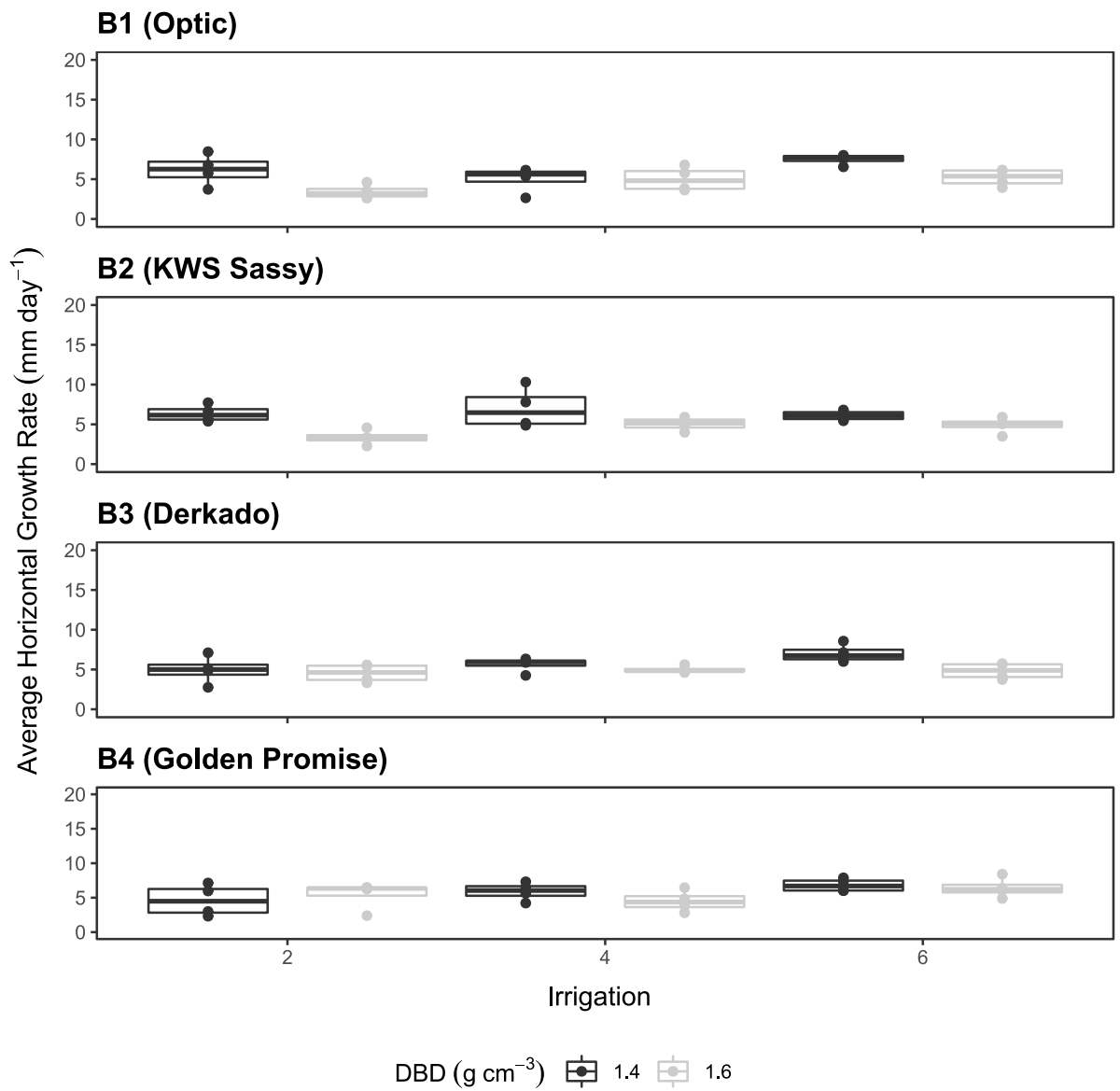


**Figure 5.1:** Vertical root length summary graphs for 21 days grouped by IRE treatment for 1.4 (X1) and 1.6 (X2) DBD (g cm<sup>-3</sup>) treatments. The varieties used were Optic (A), KWS Sassy (B), Derkado (C) and Golden Promise (D).



**Figure 5.2:** Horizontal root length summary graphs for 21 days grouped by IRE treatment for 1.4 (X1) and 1.6 (X2) DBD ( $\text{g cm}^{-3}$ ) treatments. The varieties used were Optic (A), KWS Sassy (B), Derkado (C) and Golden Promise (D).





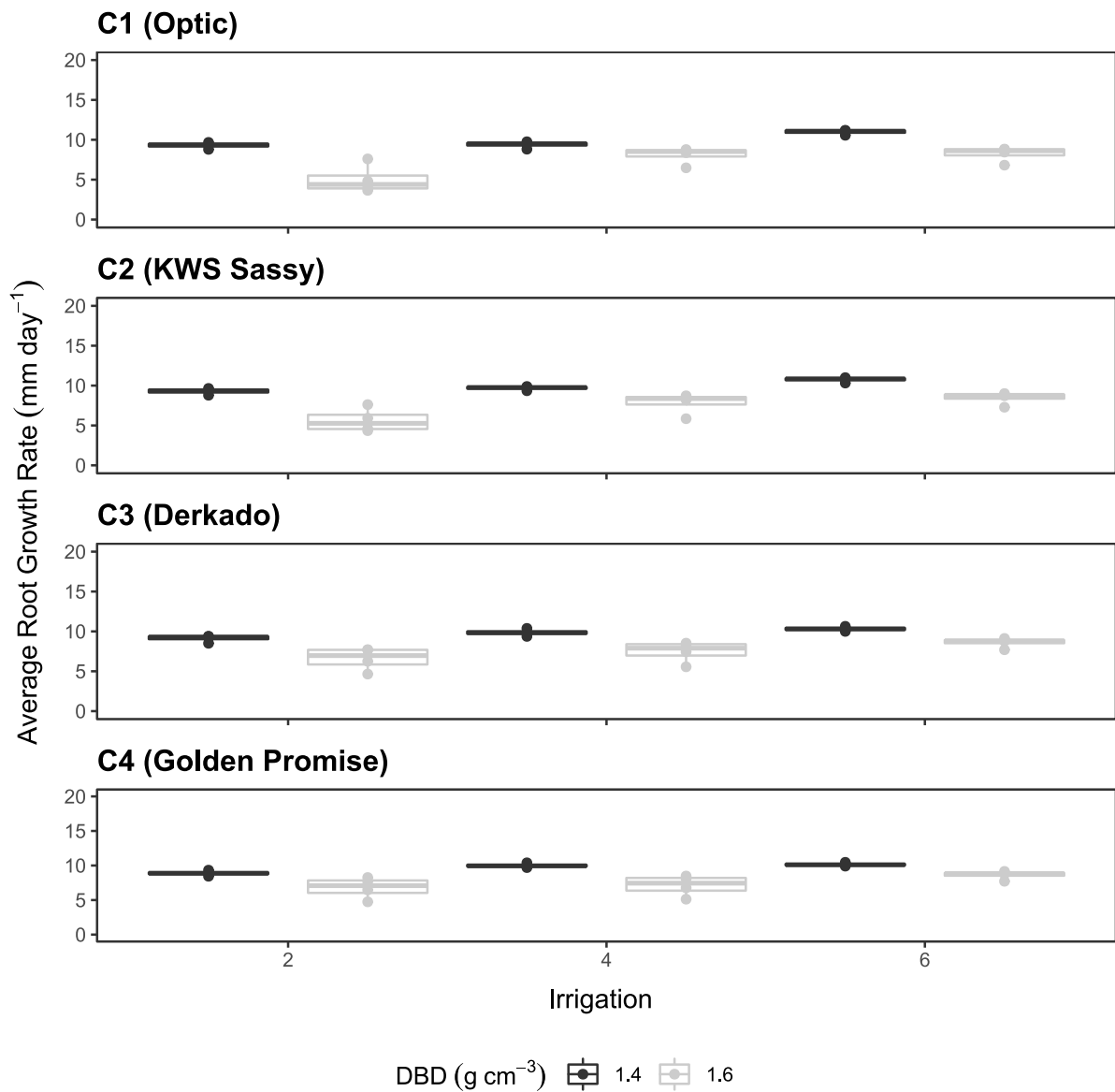


**Figure 5.3:** Average horizontal (A), vertical (B) and root (C) growth rates vs. IRE treatment grouped by DBD treatments. The varieties used were Optic (X1), KWS Sassy (X2), Derkado (X3) and Golden Promise (X4).

**Table 5.2:** Root growth rankings for **ARGR**, **AHGR** and **AVGR** averages across DBD and IRE treatments for the varieties Optic, KWS Sassy, Derkado and Golden Promise. Values in parenthesis are the rank order in any row.

<b>DBD</b> (g cm <sup>-3</sup> )	<b>IRE</b>	Optic	KWS Sassy	Derkado	Golden Promise
<b>ARGR (mm day<sup>-1</sup>)</b>					
<b>1.4</b>	<b>2</b>	9.3 (1)	9.28 (2)	9.12 (3)	8.88 (4)
	<b>4</b>	9.39 (4)	9.69 (3)	9.86 (2)	10 (1)
	<b>6</b>	10.97 (1)	10.75 (2)	10.31 (3)	10.15 (4)
<b>1.6</b>	<b>2</b>	5.02 (4)	5.63 (3)	6.57 (2)	6.79 (1)
	<b>4</b>	8.08 (1)	7.83 (2)	7.47 (3)	7.12 (4)
	<b>6</b>	8.22 (4)	8.46 (3)	8.61 (2)	8.63 (1)
<b>AVGR (mm day<sup>-1</sup>)</b>					
<b>1.4</b>	<b>2</b>	11.33 (3)	11.19 (4)	11.83 (1)	11.67 (2)
	<b>4</b>	12.25 (3)	11.42 (4)	12.62 (2)	12.67 (1)
	<b>6</b>	13.24 (2)	13.78 (1)	12.46 (3)	12.31 (4)
<b>1.6</b>	<b>2</b>	6.06 (4)	7.11 (3)	7.9 (1)	7.7 (2)
	<b>4</b>	10.07 (1)	9.64 (2)	9.09 (3)	8.83 (4)
	<b>6</b>	10.19 (3)	10.79 (2)	11.09 (1)	10.06 (4)
<b>AHGR (mm day<sup>-1</sup>)</b>					
<b>1.4</b>	<b>2</b>	6.18 (2)	6.35 (1)	4.96 (3)	4.6 (4)
	<b>4</b>	5.01 (4)	7.03 (1)	5.63 (3)	5.91 (2)
	<b>6</b>	7.5 (1)	6.11 (4)	7.02 (2)	6.82 (3)
<b>1.6</b>	<b>2</b>	3.41 (3)	3.35 (4)	4.54 (2)	5.4 (1)
	<b>4</b>	5.01 (2)	5.05 (1)	4.98 (3)	4.5 (4)
	<b>6</b>	5.21 (2)	4.9 (3)	4.81 (4)	6.43 (1)

**Figure 5.4**, displays the **RHtRR** values across 21 days. The graphs are grouped by the IRE factor, column arranged by the DBD factor and row arranged by the Variety factor. **Figure 5.5**, is a series of graphs which summarise the average **RHtRR** values against the IRE treatments and grouped by the DBD factor with the 1<sup>st</sup>, 2<sup>nd</sup>, 3<sup>rd</sup> and 4<sup>th</sup> row graphs corresponding to the Optic, KWS Sassy, Derkado and Golden Promise variety respectively.

No statistically significant 3-way interaction effects were detected among the factors of Variety, DBD and IRE ( $F = 10.9797$ ,  $p = 0.168$ ). Furthermore, no statistically significant 2-way interaction effect was detected between Variety and IRE ( $F = 6.5353$ ,  $p = 0.458$ ), Variety and DBD ( $F = 1.7942$ ,  $p = 0.635$ ) and DBD and IRE ( $F = 3.0362$ ,  $p = 0.237$ ). In addition to the above, no statistically significant main effects were detected for the factors of Variety ( $F = 3.8307$ ,  $p = 0.320$ ), DBD ( $F = 0.0178$ ,  $p = 0.900$ ) and IRE ( $F = 0.7037$ ,  $p = 0.710$ ). In general, the **RHtRR** parameter was unresponsive to all experimental factors.

**Table 5.3**, is a summary of the average **RHtRR** values for each experimental treatment and also their rank among the varieties (rows). No pattern is apparent in the rankings and the mean differences are small for each treatment, suggesting that the across Variety comparison effects were not significant.

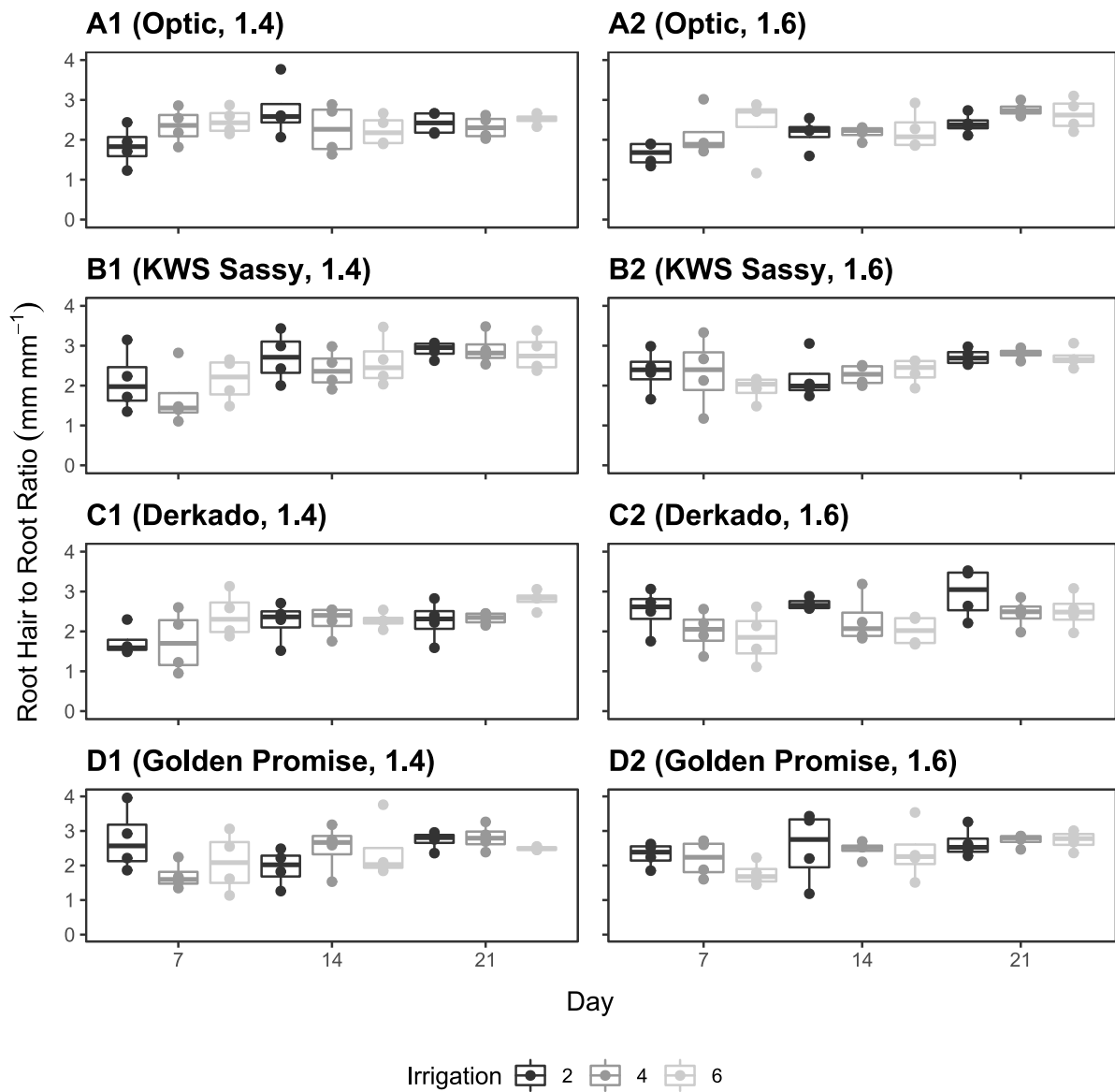


**Figure 5.4:** RHtRR summary graphs for 21 days grouped by IRE treatment for 1.4 (X1) and 1.6 (X2) DBD ( $\text{g cm}^{-3}$ ) treatments. The varieties used were Optic (A), KWS Sassy (B), Derkado (C) and Golden Promise (D).

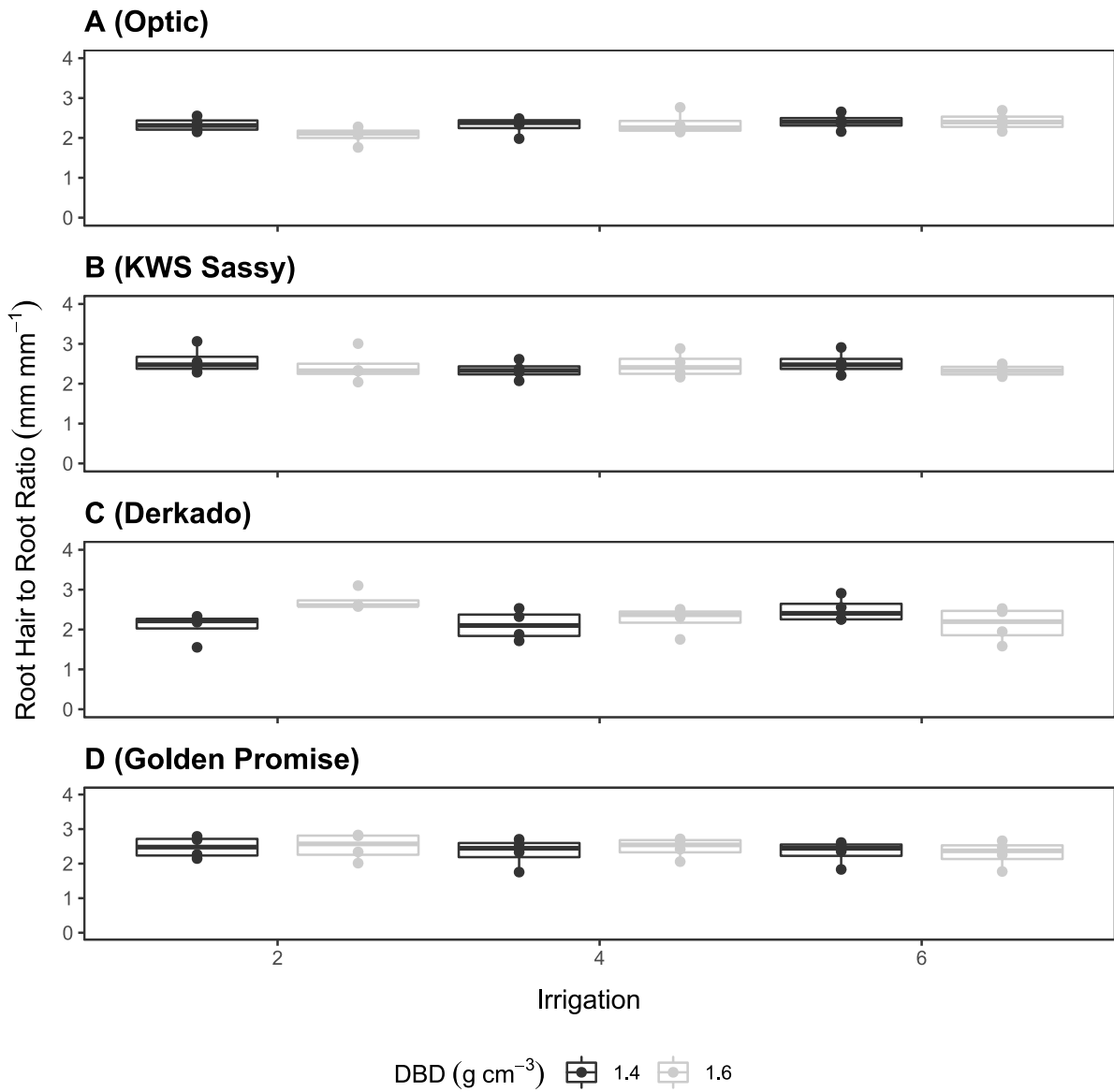


**Figure 5.5:** Average **RHtRR** of spring barley grown for 21-days as a function of IRE and grouped by DBD treatment. The varieties used were Optic (**A**), KWS Sassy (**B**), Derkado (**C**) and Golden Promise (**D**).

**Table 5.3:** Rankings for **RHtRR** (mm mm<sup>-1</sup>) averages across DBD and IRE treatments for the varieties Optic, KWS Sassy, Derkado and Golden Promise. Values in parenthesis are the rank order in any row.

<b>DBD</b> (g cm <sup>-3</sup> )	<b>IRE</b>	Optic	KWS Sassy	Derkado	Golden Promise
<b>1.4</b>	<b>2</b>	2.33 (3)	2.57 (1)	2.08 (4)	2.47 (2)
	<b>4</b>	2.31 (3)	2.34 (1/2)	2.11 (4)	2.34 (1/2)
	<b>6</b>	2.4 (3)	2.52 (1)	2.49 (2)	2.33 (4)
<b>1.6</b>	<b>2</b>	2.07 (4)	2.42 (3)	2.72 (1)	2.5 (2)
	<b>4</b>	2.35 (3)	2.47 (1/2)	2.25 (4)	2.47 (1/2)
	<b>6</b>	2.41 (1)	2.33 (2)	2.13 (4)	2.29 (3)

**Figure 5.6**, is a series of graphs that summarise the **RBCC** values against the IRE treatments and grouped by the DBD factor with the 1<sup>st</sup>, 2<sup>nd</sup>, 3<sup>rd</sup> and 4<sup>th</sup> row graphs corresponding to the Optic, KWS Sassy, Derkado and Golden Promise variety respectively.

No statistically significant 3-way interaction effects were detected among the factors of Variety, DBD and IRE ( $F = 2.2045$ ,  $p = 0.919$ ). There was also a no statistically significant 2-way interaction effect between Variety and IRE ( $F = 9.1212$ ,  $p = 0.273$ ). However, a statistically significant 2-way interaction effect was detected between DBD and IRE ( $F = 7.9347$ ,  $p = 0.03^*$ ). Further examination revealed a statistically significant difference in **RBCC** values for the 4 vs. 6 IRE comparison in the 1.4 and 1.6 DBD treatments ( $\psi = -30$ ,  $p = 0.007^*$ ). For the highest bulk density treatments the 4 IRE treatment had a higher **RBCC** compared to the 6 IRE treatment with the opposite effect being true for the lowest bulk density treatment. In addition to the above, a statistically significant 2-way interaction effect was detected between Variety and DBD ( $F = 9.1384$ ,  $p = 0.05^*$ ). Further examination revealed a statistically significant difference in **RBCC** values for the 1.4 vs. 1.6 DBD comparison in the Derkado and Optic varieties ( $\psi = 30.7500$ ,  $p = 0.0157^*$ ). Furthermore, a statistically significant difference was detected for the 1.4 vs. 1.6 DBD comparison in the Derkado and KWS Sassy varieties ( $\psi = 31$ ,  $p = 0.0255^*$ ). Derkado had a higher **RBCC** for

the 1.4 DBD treatments whereas KWS Sassy and Optic had a higher **RBCC** for the 1.6 DBD treatments. No statistically significant main effects were detected for the factors of Variety ( $F = 0.9186$ ,  $p = 0.84$ ) and IRE ( $F = 3.1775$ ,  $p = 0.225$ ). However, a statistically significant main effect was detected for the factor of DBD ( $F = 6.7426$ ,  $p = 0.013^*$ ) with the higher DBD treatments having higher **RBCC** compared to the lower DBD treatments.

**Table 5.4**, is a summary of the average **RBCC** values for each experimental treatment and also their rank among the varieties (rows). It is of note, that for the 1.4 DBD treatments the Optic variety had the lowest **RBCC** averages across the water treatments.

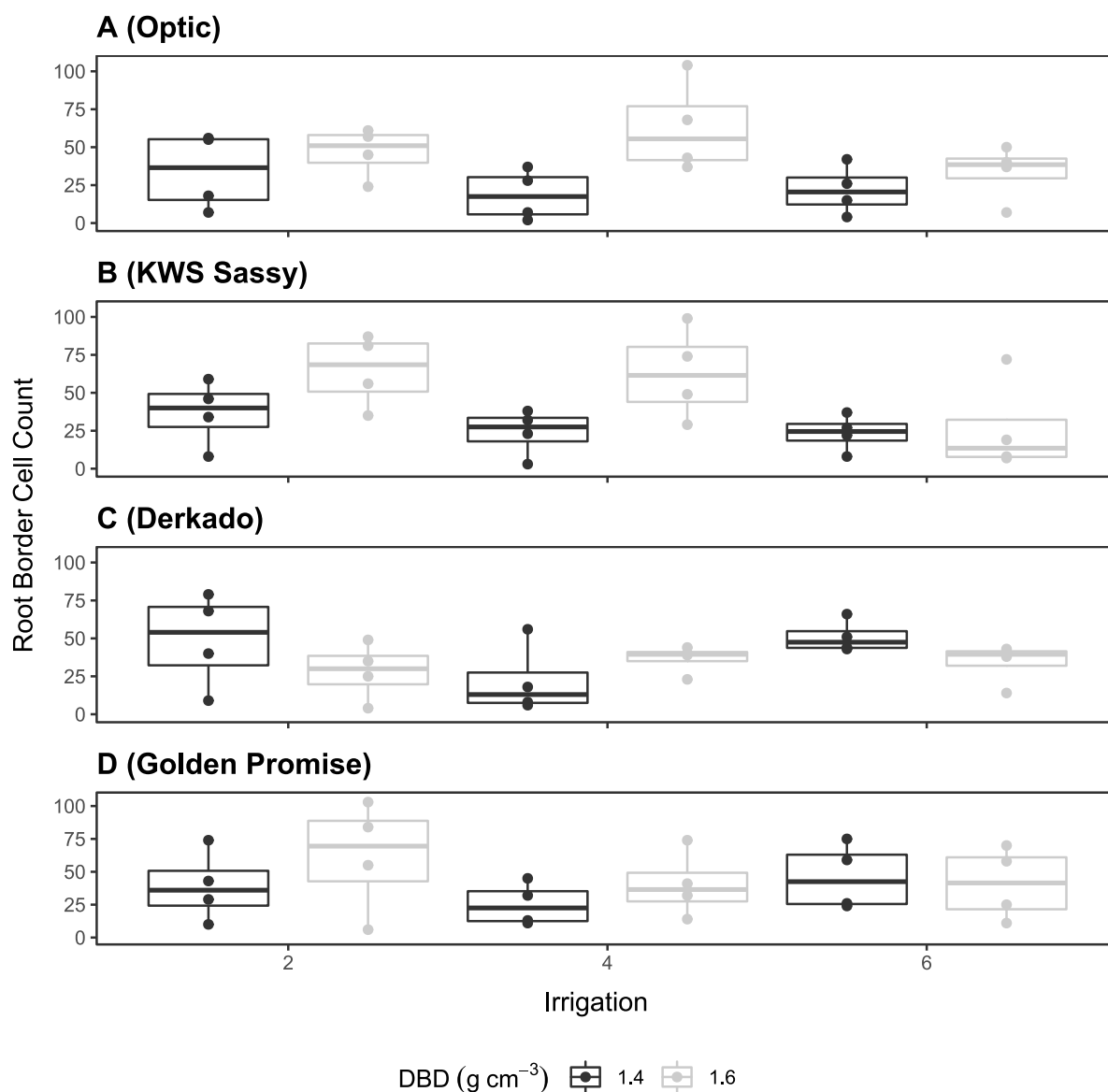


**Figure 5.6:** RBCC spring barley at the end of a 21-day growth period as a function of IRE and grouped by DBD treatment. The varieties used were Optic (A), KWS Sassy (B), Derkado (C) and Golden Promise (D).

**Table 5.4:** Rankings for RBCC averages across DBD and IRE treatments for the varieties Optic, KWS Sassy, Derkado and Golden Promise. Values in parenthesis are the rank order in any row.

<b>DBD</b> (g cm <sup>-3</sup> )	<b>IRE</b>	Optic	KWS Sassy	Derkado	Golden Promise
<b>1.4</b>	<b>2</b>	34 (4)	36.75 (3)	49 (1)	39 (2)
	<b>4</b>	18.5 (4)	24 (2)	22 (3)	25.25 (1)
	<b>6</b>	21.75 (4)	23.5 (3)	51 (1)	46 (2)
<b>1.6</b>	<b>2</b>	46.75 (3)	64.75 (1)	28.25 (4)	62 (2)
	<b>4</b>	63 (1)	62.75 (2)	36.5 (4)	40.25 (3)
	<b>6</b>	33.5 (3)	26.5 (4)	34 (2)	41 (1)

**Figure 5.7**, is a series of graphs which summarise the **RTE** values against the IRE treatments and grouped by the DBD factor with the 1<sup>st</sup>, 2<sup>nd</sup>, 3<sup>rd</sup> and 4<sup>th</sup> row graphs corresponding to the Optic, KWS Sassy, Derkado and Golden Promise variety respectively. A higher **RTE** signifies a deviation from circular geometry and a less curved root tip.

No statistically significant 3-way interaction effects were detected among the factors of Variety, DBD and IRE ( $F = 8.5947$ ,  $p = 0.33$ ). Furthermore, no statistically significant 2-way interactions were detected between DBD and IRE ( $F = 3.6449$ ,  $p = 0.192$ ), Variety and IRE ( $F = 12.1444$ ,  $p = 0.158$ ) and Variety and DBD ( $F = 8.0003$ ,  $p = 0.083$ ). In addition to the above, a statistically significant main effect was detected for the factor of DBD ( $F = 49.0434$ ,  $p = 0.0001^{**}$ ) with a higher bulk density increasing the **RTE**. Also, a statistically significant main effect was detected for the factor of Variety ( $F = 10.5093$ ,  $p = 0.037^{*}$ ). Subsequent pair-wise comparisons for the Variety treatments found that the differences were between the Optic vs. Golden Promise ( $\psi = 1.4547$ ,  $p = 0.0164^{*}$ ) and the Optic vs. KWS Sassy ( $\psi = -1.0424$ ,  $p = 0.0235^{*}$ ) comparisons. Golden Promise and KWS Sassy had generally higher values for **RTE** and therefore more elliptical root tips when compared to Optic across treatments. In addition, a statistically significant main effect was detected for the factor of IRE ( $F = 7.2187$ ,  $p = 0.0460^{*}$ ). Subsequent pair-wise comparisons for the IRE treatments found that the difference was between the 4 vs. 6 ( $\psi = 1.1870$ ,  $p = 0.0214^{*}$ ) comparison with the 4 IRE treatments generally having larger **RTE** values.

**Table 5.5**, is a summary of the average **RTE** values for each experimental treatment and also their rank among the varieties (rows). It should be noted that the variety KWS Sassy had the highest ranks for the 1.4 g cm<sup>-3</sup> DBD treatments while Golden Promise had the largest values for the 1.6 g cm<sup>-3</sup> DBD with the exception of the small difference for the 6 IRE treatment.

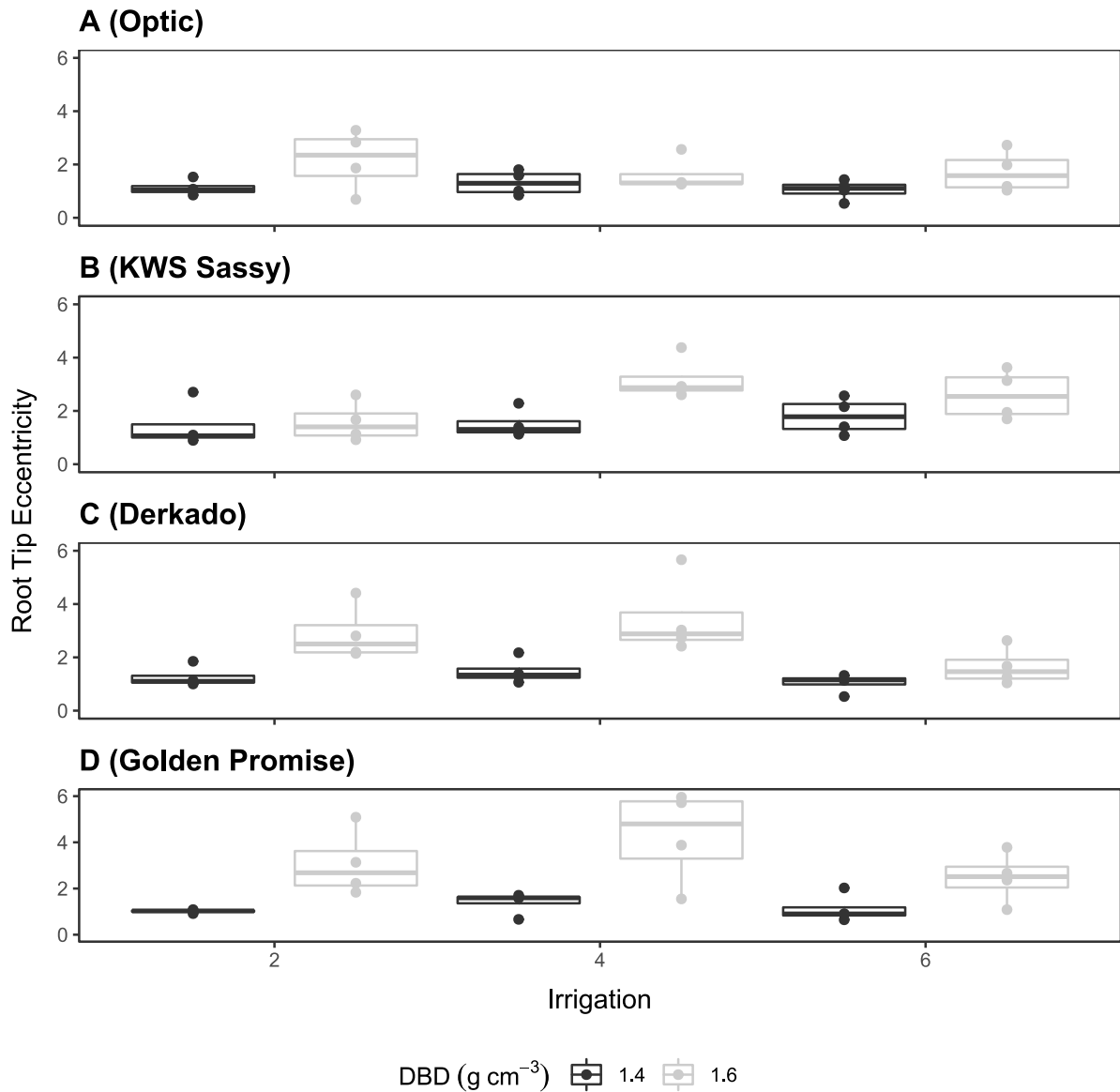


**Figure 5.7:** RTE spring barley at the end of a 21-day growth period as a function of IRE and grouped by DBD treatment. The varieties used were Optic (A), KWS Sassy (B), Derkado (C) and Golden Promise (D).

**Table 5.5:** Rankings for **RTE** averages across DBD and IRE treatments for the varieties Optic, KWS Sassy, Derkado and Golden Promise. Values in parenthesis are the rank order in any row.

<b>DBD</b> (g cm <sup>-3</sup> )	<b>IRE</b>	Optic	KWS Sassy	Derkado	Golden Promise
<b>1.4</b>	<b>2</b>	1.12 (3)	1.43 (1)	1.26 (2)	1.01 (4)
	<b>4</b>	1.31 (4)	1.51 (1)	1.48 (2)	1.39 (3)
	<b>6</b>	1.04 (2/3)	1.8 (1)	1.04 (2/3)	1.12 (2)
<b>1.6</b>	<b>2</b>	2.17 (3)	1.58 (4)	2.89 (2)	3.07 (1)
	<b>4</b>	1.61 (4)	3.18 (3)	3.46 (2)	4.27 (1)
	<b>6</b>	1.73 (3)	2.6 (1)	1.65(4)	2.47 (2)

**Figure 5.8**, is a series of PCA biplots for all possible combinations of the first three principal components. **Table 5.6**, is a summary of the variance explained by each principal component, the correlations between the variables and the components and their statistical significance. **Figure 5.9**, demonstrates a snapshot of a 3D PCA plot and it captures a larger amount of variation by integrating the 3<sup>rd</sup> PCA component.

Based on the relationship of PC1 and PC2 capturing a total of 59.67 % of variation the following conclusions can be made:

1. **ARGR** and **RHtRR** were not correlated.
2. **ARGR** was strongly negatively correlated with **RTE** and moderately negatively correlated with **RBCC**.
3. **RBCC** and **RTE** were correlated.
4. No evidence of clustering for each treatment category.

In addition, based on the relationship of PC1, PC2 and PC3 accounting for 74.88% of the total variation we can further conclude:

1. **RBCC** and **RTE** were moderately correlated.

2. **RHtRR** and **RTE** were slightly negatively correlated.
3. **RHtRR** and **RBCC** were negative correlated.
4. **ARGR** was slightly more correlated with **AVGR** in comparison to **AHGR**.
5. No evidence of clustering across different treatments.

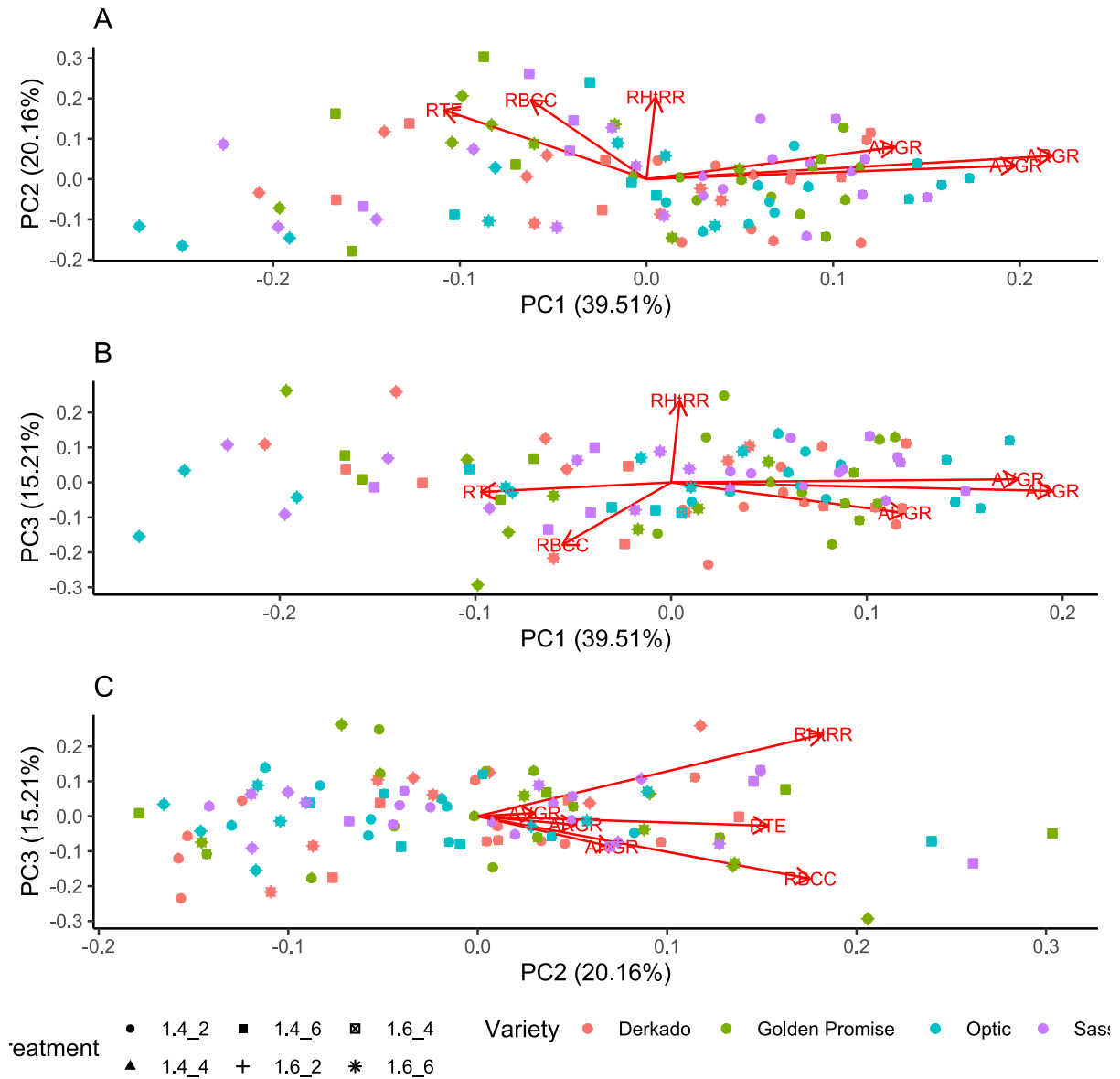


**Figure 5.8:** Principal Component Analysis biplots for **A) PC2 vs. PC1**, **B) PC3 vs. PC1** and **C) PC3 vs. PC2**.

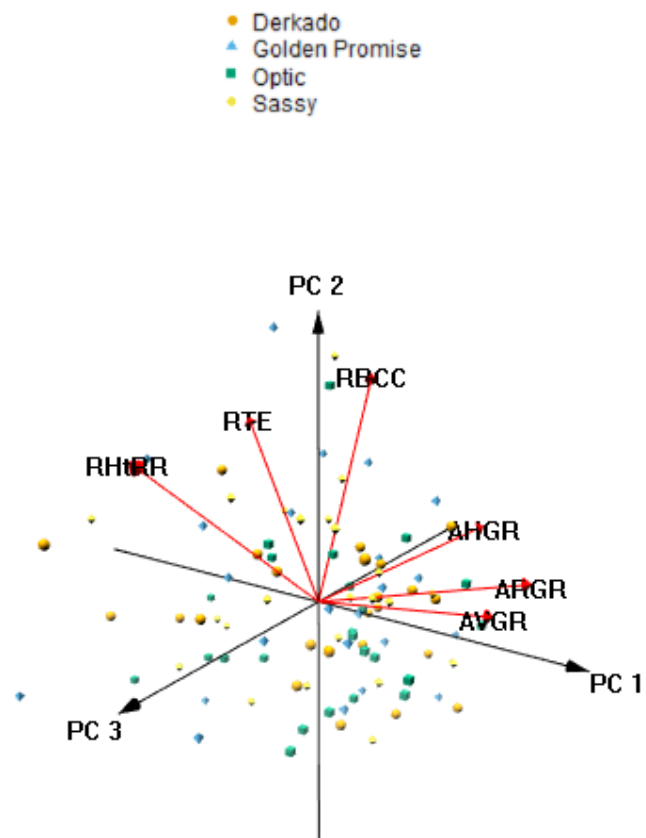


**Figure 5.9:** Principal Component Analysis 3D plot snapshot with loadings and coloured by spring barley cultivar.

**Table 5.6:** Principal Components Analysis (PCA) of component importance, correlations and statistical significance.

Importance of components						
	PC1	PC2	PC3	PC4	PC5	PC6
Standard deviation	1.5396	1.1	0.9553	0.8901	0.8455	2.32E-10
Proportion of variance	0.3951	0.2016	0.1521	0.132	0.1192	0.00E+00
Cumulative Proportion	0.3951	0.5967	0.7488	0.8808	1	1.00E+00
Data/Components Correlations						
	PC1	PC2	PC3	PC4	PC5	PC6
<b>ARGR</b>	0.628189	0.166386	-0.07876	0.120571	0.139415	7.33E-01
<b>AHGR</b>	0.571595	0.097005	0.029188	0.486893	0.189072	-6.25E-01
<b>AVGR</b>	0.385004	0.228352	-0.28259	-0.8025	-0.05912	-2.69E-01
<b>RHtRR</b>	0.014148	0.588197	0.756565	-0.07191	-0.27616	-1.44E-11
<b>RBCC</b>	-0.17902	0.566189	-0.57702	0.312701	-0.46546	-1.32E-11
<b>RTE</b>	-0.31334	0.494182	-0.08804	-0.03802	0.805237	1.23E-12
3-way statistical significance tests (F, p)						
	PC1	PC2	PC3	PC4	PC5	PC6
Variety	0.8906, 0.84	2.7748, 0.47	0.5607, 0.92	0.4086, 0.95	3.8793, 0.32	6.7546, 0.13
DBD	<b>325.7024</b> , <b>0.0001***</b>	1.0169, 0.32	0.6926, 0.42	0.0001, 0.99	2.3716, 0.13	0.1233, 0.73
IRE	<b>105.0729</b> , <b>0.001**</b>	0.5439, 0.77	2.7954, 0.278	0.6089, 0.745	10.3642, 0.011*	1.9027, 0.413
Variety:DBD	2.2847, 0.548	2.5564, 0.497	0.7674, 0.87	2.9599, 0.435	<b>17.2253</b> , <b>0.004**</b>	3.3362, 0.397
Variety:IRE	3.0754, 0.843	1.3953, 0.973	0.9471, 0.991	4.478, 0.685	<b>24.8699</b> , <b>0.007**</b>	<b>23.5292</b> , <b>0.013*</b>

DBD:IRE	3.9309,	6.4162,	<b>10.0345,</b>	0.2213,	1.5908,	4.0402,
	0.164	0.06	<b>0.017*</b>	0.898	0.466	0.165
Variety:DBD:IRE	17.1978,	1.8778,	0.5426,	5.2521,	6.4271,	7.071,
	0.05	0.944	0.998	0.601	0.478	0.44

---

Based on the analysis of the correlation between **ARGR** and the micro-traits of **RHtRR** (cor = 0.0803, p = 0.4368), **RBCC** (cor = -0.1501, p = 0.14425) and **RTE** (cor = -0.4192, p = 2e-05\*\*) the traits of **RBCC** and **RTE** were selected for modelling. This was because they both had the same-sign, negative correlation with **ARGR**, even though the only statistically significant correlation was with **RTE**. A 2-variate linear interaction model was then constructed with the function “lm” in R and then the subsequently predicted vs. observed **ARGR** values were plotted (**Figure 10**). The plot clearly demonstrates the lack of fitness between the predicted and observed values which suggests a poor prediction ability for the interaction model. To further understand the pattern of the data a running interval smoother (Wilcox, 2017) estimating the conditional mean value was added to **Figure 5.10** (non-linear curve). The pattern suggests that the root-trait based model could be used to predict not the individual points but the average for **ARGR** values  $\geq 8$  mm day<sup>-1</sup>. Furthermore, the model itself becomes approximately linear beyond the 8 mm day<sup>-1</sup> threshold value and this is demonstrated by estimating the Theil-Sen (Wilcox, 2017) regression line (linear segment) shown on **Figure 5.10**. In other words, the average **ARGR** can be predicted with a linear model for values  $\geq 8$  mm day<sup>-1</sup> with a fair amount of accuracy but with low precision.

Finally, **Table 5.7** is a summary of whether a statistically significant effect was detected for each of the measured variables and the PC components for the experimental factors used and their interaction.

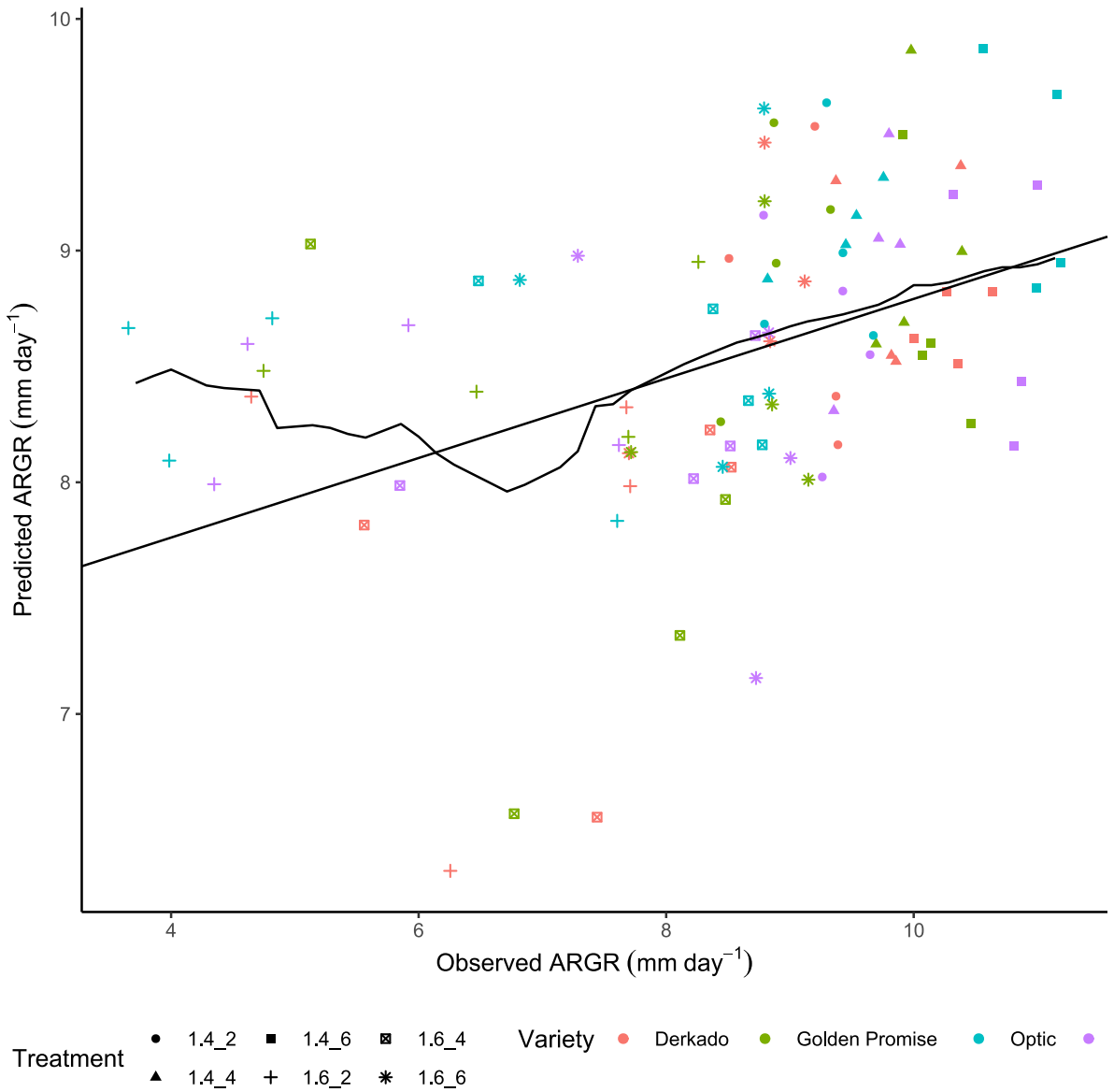


**Figure 5.10:** Predicted **ARGR** vs. Observed **ARGR** plot. The non-linear curve estimates the conditional mean value and the linear segment represent the Theil-Sen regression line.

**Table 5.7:** Statistically significant effects summary for variables and PC components.

	<b>DBD</b>	<b>IRE</b>	<b>Variety</b>	<b>Interactions</b>
<b>ARGR</b>	✓	✓	✗	✗
<b>AVGR</b>	✓	✓	✗	✗
<b>AHGR</b>	✓	✓	✗	✗
<b>RHtRR</b>	✗	✗	✗	✗
<b>RBCC</b>	✓	✗	✗	✓
<b>RTE</b>	✓	✓	✓	✗
PC1	✓	✓	✗	✗
PC2	✗	✗	✗	✗
PC3	✗	✗	✗	✓
PC4	✗	✗	✗	✗
PC5	✗	✓	✗	✓
PC6	✗	✗	✗	✓

## 5.5 Discussion

**ARGR**, **AVGR** and **AHGR** all displayed a similar pattern across varieties. Root growth rates were influenced not by the type of variety but by the substrate bulk density and water status with increased water content and decreased substrate bulk density giving higher growth rates. Water concentration had a contrasting effect from that reported in Chapter 4 for the Optic variety, but this was probably because of the higher water demand for roots due to the hot months of August and September. Perhaps the most significant point is the fact that differences across contrasting varieties were very small with the average maximum difference across varieties for each treatment being only 1.21 mm day<sup>-1</sup>. This clearly supports the lack of statistically significant differences reported above and suggests that no variety truly performed best or worst. The results obtained are not similar to those reported by other authors (Bengough and Mullins, 1991; Colombi *et al.*, 2017; Wang *et al.*, 2021), who detected statistically significant differences between genotypic root elongation rates for various density treatments of wheat (*Triticum aestivum*) grown in soil columns. A potential

explanation for the lack of statistical significance could be that the above-mentioned studies all used different varieties of wheat instead of barley. Furthermore, the plants were grown in soil filled plastic tubes with diameter and height ranging from 4.9-15 cm and 4-45 cm respectively. In contrast, the RS unit was a rectangular solid with a width of just 0.8 cm and as such root growth was significantly more restricted in the horizontal direction. The differences in species and growth conditions could all be factors influencing whether statistical significance is found. Nevertheless, the results are in agreement with the general observed pattern of an inverse relationship between DBD and root elongation rates reported in the literature (Jin *et al.*, 2013).

**RHtRR** lacked any statistically significant interaction effects or any main effects with the experimental factors considered here. Root hairs are known to vary significantly across different cereals species and varieties at the seedling stage (Haling *et al.*, 2010), so the findings are not in agreement with this for the tested conditions. Furthermore, root hairs were demonstrated to be highly responsive to abiotic stresses such as high soil strength (Haling *et al.*, 2011) which increases root-soil contact and as such, causes reductions in root hair length (Haling *et al.*, 2013). Haling *et al.*, (2014) reported root hair length differed for a range of different strength and water treatments which had a range of PR between 0.04 - 4.45 MPa and matric potential between -7.5 to -40 kPa. The lack of any statistically significant effects could be potentially explained by the range of PR and matric potential values used here was narrower, being respectively 0.9377 - 2.2792 MPa and -5 to -10 kPa with other studies which detected significant differences, e.g., Haling *et al.*, (2014).

For **RBCC**, there were no 3-way interaction effects but there was a statistically significant 2-way interaction effect between Variety and DBD. However, the effect of that interaction was not clear based on the inspection of their interaction plot. Interestingly the p value obtain was exactly 0.05 and as such it is debatable whether to technically accept it as a statistically significant difference, especially when no clearly discernible differences exist. In addition, there was a second significant interaction between DBD and IRE which demonstrated that the 4 vs. 6 IRE comparison was influenced by the DBD with Optic and KWS Sassy differing for the 1.6 DBD treatments and Derkado and Golden Promise differing for the 1.4 DBD

treatments. In other words, for the higher density treatments Optic and KWS Sassy produced more RBCs under medium water availability (4 IRE) but for the lower bulk density treatments Derkado and Golden Promise produced more RBCs under high water availability (6 IRE). Somasundaram *et al.*, (2009), examined the interaction between soil bulk density and water content in maize and concluded that the number of RBCs increased with soil water content in compact soil treatment. As such, the results reported here are not in agreement as for the case of Optic and KWS Sassy the higher bulk density treatments produced the most RBCs under medium water availability and for the case of Derkado and Golden Promise the highest **RBCC** was observed for the low bulk density treatments. Finally, **RBCC** was increased in a more compact soil environment which is in agreement with the literature (Iijima *et al.*, 2003; Somasundaram *et al.*, 2009) but once again, there were no significant differences across varieties.

**RTE**, lacked any statistically significant interaction effects but, statistically significant main effects were detected for all factors. An increase in DBD increased **RTE** (more elliptical root tips) which is in agreement with what was reported by other authors when the soil density increases (Iijima *et al.*, 2003; Colombi *et al.*, 2017). For IRE, the statistically significant difference was between the 4 vs. 6 comparison with a percentage difference of 35.26 % on favour of the 4 IRE treatment. **RTE** was also the only trait showing differences with Variety as the variety Optic also differed in comparison to both KWS Sassy and Golden Promise with the latter varieties having a higher **RTE** with a percentage increase of 34.82 and 48.60 % respectively relative to KWS Sassy.

Since the primary objective of this study was to determine if root trait variability could help explain the variation in root growth rates of varieties and it is unfortunate that all the measured variables had no statistically significant differences among varieties with the exception for **RTE**. In fact, one of the key findings was the measured root growth rates and root traits all responded to the manipulation of DBD and IRE which proved to be significant factors, something which generally was not the case for the factor Variety. This was further supported by the fact that the only significant correlation with **ARGR** was that of **RTE**. The interaction model of **RBCC** and **RTE** was clearly of a poor fit yet, it must be noted that the

model does predict with high accuracy the average response for **ARGR** values  $\geq 8 \text{ mm day}^{-1}$  and can be approximated very well with a linear form which is convenient. Interestingly, the samples corresponding to an **ARGR**  $< 8 \text{ mm day}^{-1}$  all shared one feature, they were all packed at  $1.6 \text{ g cm}^{-3}$  DBD and collectively made up 26 % of the total population. A possible interpretation could be that for cases where growth is “sufficient” ( $\geq 8 \text{ mm day}^{-1}$ ) the average response could be predicted accurately but with poor precision by having knowledge of **RBCC** and **RTE**. A statement about the average response is simply the extent to which we can make predictions in this context.

It should also be noted that a recent study from Newton *et al.*, (2020), indicated that KWS Sassy demonstrated an adaptation when switching from inversion to non-inversion tillage by having a relative small reduction in yield in comparison to the other varieties tested which included Optic and Golden Promise. As suggested by the authors, the higher soil density of the non-inversion tillage treatment may indicate the presence of contrasting root traits that offer an advantage to the other cultivars in the higher strength soil. However, all the root traits measured here showed no statistically significant differences for variety except for the case of **RTE** when comparing Optic to Derkado and Golden Promise. This raises the question if the differential response was due to either (1) root micro-traits and or other traits (e.g., stem or leaves) not considered here or (2) the possibility of a differential response in root micro-traits among different varieties when exposed to the more complex substrate of soil and the variable field conditions and (3) the likelihood that the varieties tested simply did not differ to any significant extent but other varieties may differ. All the above must be considered in future experiments to find an explanation to the obtained results.

## 5.6 Conclusions

The results demonstrated that the RS unit combined with the image analysis is a valid approach in plant root phenotyping. A spectrum of root responses was achieved after manipulation of the RS substrate conditions and a range of macro and micro root traits were successfully imaged and quantified using a mixture of time-lapse scanning and optical microscopy. **ARGR**, **AVGR** and **AHGR** all demonstrated similar behaviour, increasing with higher water availability and decreasing with a higher substrate density. However, there was

no evidence of any significant variation between varieties used, with the average maximum difference across varieties for each treatment being small ( $1.21 \text{ mm day}^{-1}$ ). **RHtRR** also lacked any variation among varieties but, this could have been due to the treatment range not being extreme enough in terms of PR and matric potential. **RBCC** was higher with increased substrate bulk density but different varieties produced more RBCs under different conditions of bulk density and water. **RTE** showed a similar increase with a higher substrate bulk density but performed best for medium water availability. Furthermore, **RTE** was the only trait which showed a strong correlation with **AVGR** suggesting that perhaps root geometry could be a more distinguishable micro-trait among varieties, at least for spring barley. Finally, the root trait-based interaction model developed with the data demonstrated that not all micro-traits are relevant when trying to predict root growth and even then, sometimes the best outcome to be expected is a reasonably good prediction of the average response and always subject to conditions.

## 6. General discussion and conclusions

### 6.1 Introduction

Barley (*Hordeum vulgare* L.) is the fourth largest cereal crop produced worldwide (Stanca *et al.*, 2016). It is largely used as an animal feed (80-90 %), with approximately 10 % of it used in beer production. It is also used as a staple crop for human consumption (Stanca *et al.*, 2016) as well as a high valued product in whisky. However, drought stress is a major limiting factor in many places around the world such as West Asia and North Africa where yield is limited due to factors such as low (< 300 mm) rainfall (Solh and van Ginkel, 2014). Drought effects are predicted to become more severe with increasing global temperatures (IPCC, 2014) which constitutes a major challenge for achieving sustainability in agriculture (Fleming and Vanclay, 2010). In order to address those issues it is vital to understand the complex relationship between the various root traits and the way they influence root elongation rates under different soil conditions. In order, to study this complex interaction however, an appropriate experimental system had to be selected which will enable for the quantification of the above mentioned variables while limiting the variation originating from the complex field soil conditions.

Minirhizotrons systems have been used ever since they were originally proposed by Bates in 1937 (Upchurch, 1987). They have the advantages of allowing repeated, non-destructive, *in situ* measurement of roots growing against its transparent surface (Johnson *et al.*, 2001). The first objective of this study was to develop a minirhizotron system (RS) which enabled the manipulation of the LLWR soil stressors of mechanical impedance, water and oxygen availability while also allowing for the quantification of root micro-traits in barley seedlings of at least 3 weeks old (Chapter 2). To achieve that, a list of 4 properties was created which clearly specified the requirements that the proposed RS unit should have. This in turn, led to a series of experiments to determine (1) the RS substrate type and particle size range which allowed for sufficient root elongation rates and (2) the imaging surface material type and thickness for imaging the finer root trait of root hairs. An acrylic based design was chosen for the RS unit because of its higher hardness, transparency and reduced effects on root growth

(Cai, 2006) which also kept the cost of the RS unit low (£10) and allowed for the imaging of roots and root hairs.

The second objective was to make the RS platform as efficient as possible by reducing the time required for analysing data. This was achieved through the development of image-processing algorithms which enable the automatic detection and quantification of both coarse and fine root traits (Chapter 3). Algorithm 1 (A1) allowed for the detection and measurement of (visible) roots and root hairs growing in the RS units which enabled an assessment of root growth rates and root hair area. Algorithm 2 (A2) enabled the detection and quantification of root tip border cells and eccentricity after destructive sampling of the root system and imaging under a fluorescence microscope. Algorithm 3 (A3) enabled the detection and quantification of root length parameters at the final stage of destructive sampling, the scanning of the washed root system. Each of the presented algorithms was custom developed and implemented in the Rcpp language, a hybrid of C++ and R which may be run from the R console for user accessibility and ease of usage. Collectively, these algorithms allowed for an assessment of the root traits of interest for this study in an efficient way which in turn, allowed for an upgrade in the number of RS units used in future experiments.

The third objective was to effectively integrate the above described methods into a single experimental protocol which will allow for the systematic manipulation of the LLWR soil stressors and the measurement of coarse and fine root traits (Chapter 4). Chapter 4 investigated the validity of this protocol by successfully inducing a spectrum of root growth responses for a range of experimental treatments by manipulating sand dry bulk density and the degree of saturation and, subsequently measuring the root traits of interest either *in situ* or *ex situ*. It was found that root growth rates in the form of **ARGR**, **AHGR** and **AVGR** were largest for the driest and lowest density treatment with a higher density causing reductions in growth something which is consistent with other studies reported in the literature, e.g., (Jin *et al.*, 2013). **RHtRR** was demonstrated to be unresponsive to the LLWR soil stressors as neither increasing density nor water availability caused a significant response in contrast to results from Haling *et al.*, (2014). **RBCC** increased with both substrate density and water availability which was in agreement with the literature, e.g., Somasundaram *et al.*, (2009). **RTE**

also increased in higher density treatments similar to what was reported by, e.g., Colombi *et al.*, (2017), however, this effect was only observed for the drier instead of wetter treatments suggesting that the amount of water influences that relationship.

The fourth objective was to investigate how root traits potentially shift the LLWR upper and lower limits. Chapter 5 examined this by applying the experimental protocol from Chapter 4 to the spring barley cultivars of Optic, KWS Sassy, Derkado and Golden Promise. The application of LLWR soil stressors induced a spectrum of responses similar to those found for the variety Optic in the previous chapter. A decrease in substrate density and an increase in water availability had the effect of generally increasing root growth rates for all varieties. However, the effect of water appears to contradict the results obtained in Chapter 4 for the Optic variety. A possible explanation for this might be that the experiment in Chapter 4 started in March and finished in April of 2019 in a 2-month period. In contrast, the experiment in Chapter 5 started in August 2019 and finished in March 2020. It is possible that the warm months of August and September created a higher water demand for the plant roots and as such growth was enhanced under a higher water concentration as almost 2 of the replicates were both finished by mid October 2019. Nevertheless, there were no significant differences across varieties for both root growth rates and root micro-traits except for some cases in **RTE**. This was unfortunate, as it effectively meant that there were no genotypic differences to develop the root trait-based model. Nevertheless, a simple linear interaction model was tested by using the root micro traits of **RBCC** and **RTE**. This interaction model could be used to obtain an accurate, but imprecise, linear approximation of **AVGR** for the spring barley cultivars tested subject to the condition that **ARGR** was “sufficient”, i.e., **ARGR**  $\geq 8 \text{ mm day}^{-1}$ .

## 6.2 Genotypic variation of root traits

In Chapter 5 the genotypic variation of root micro-traits was investigated by studying 4 cultivars of spring barley. **Table 6.1** summarises the overall grand average responses of root micro-traits to the experimental treatments and demonstrates that there were no statistically significant differences between the cultivars in terms of both root growth rates and micro-traits. One way to interpret this result is the lack of significant differences in root micro-traits was responsible for the lack of significant differences in root growth rates between the cultivars. If we assume root growth rates are a function of the micro-traits, then that will mean that either (1) the root cultivars did not differ to any significant extent or (2) the range of conditions tested were not extreme enough to induce a differential response or (3) the variability between sample replicates exceeded the variability between root traits.

For (1), it is unfortunately difficult to assess to what extent differences exist due to the difficulty in locating studies which compare their relative performance. However, a recent study from Newton *et al.*, (2020), described a field-based trial which included the cultivars KWS Sassy, Optic and Golden Promise. The authors found evidence that KWS Sassy and Derkado was better adapted when switching tillage practices from inversion to non-inversion tillage. The varieties Optic and Golden Promise could also be identified as potentially tillage treatment-adapted however, these older varieties had a lower yield. The non-inversion tillage treatment had a higher soil bulk density and as a result it was theorised that the presence of contrasting root traits could explain the above observation. However, based on the results presented in Chapter 5 there were no significant genotypic differences for any of the measured root traits. One explanation could be that the plants used in the seasonal trials were grown for significantly longer and as such, any significant genotypic differences did not manifest at such an early growth stage. At more mature plant stages other root traits not considered here such as increased branching at depth could be significant factors explaining the difference among cultivars. However, such traits are highly dependent on soil and seasonal climatic differences as well as plant phenological stage (Wasson *et al.*, 2012). All of those need to be considered when trying to extrapolate from seedling to mature stages.

For (2), the range of PR and matric potential achieved were respectively 0.9377 - 2.2792 MPa and -5 to -10 kPa. In the LLWR model the PR critical value corresponds to 2.0 MPa and as such the required PR range was achieved in this study. The LLWR 50 % root growth reduction threshold criterion was achieved for the condition of 1.6 DBD at 2 IRE. As for the matric potential range the values corresponding to the field capacity and the permanent wilting point were respectively -10 kPa and -1,500 kPa. As a consequence, it must be recognized that the lower limit of the range used corresponded to the upper limit of the LLWR model, i.e., -10 kPa. However, as was demonstrated in Chapter 2 this was the result of the particle size manipulation which resulted in the water release curve deviating from that of more developed soils. In particular, the reason for the very high “dry end” was because almost all the pores (~ 95%) were restricted to only up to -50 kPa. This effectively means that the substrate lacked a significant fraction of meso-pores and any micro-pores. As a consequence, the sand dried fast and seedling mortality was found to be very high for sand treatments less than 2 IRE.

Another thing to be recognized are the intrinsic limitation of the RS system used as minirhizotron-based systems are pseudo-3D and effectively limit growth to an approximately 2D scale. This limitation will of course have an impact on root growth since the size restriction will in turn impose physical limitations on roots and influence future root elongation rates (Poorter *et al.*, 2012). In addition, continuous root to glass contact could induce thigmotropic responses from the roots (Downie *et al.*, 2015) which can give misleading representations of the norm. Ultimately, the validity of any method should be its approximation to field soil conditions, but soil is a much more complex material compared to the RS substrate. The RS sand based substrate lacks organic matter which influences water retention properties (Kay *et al.*, 1997), and it does not have the biological complexity of organisms that characterize soil. The repacked structure of the sand is also very different from that of soil and does not accurately reflect the spatial variability of structure encountered in field conditions. PR values in field soil are known to be higher and more variable in comparison to repacked soil systems (Perfect *et al.*, 1990) and it is not unusual to detect root morphological differences even when comparing field soil to a homogeneously compacted soil (Konôpka *et al.*, 2009).

As such, it is very much an active debate whether root phenotyping on seedlings yields valid predictions about future root growth as root architecture at later stages can deviate from that during its early stages (Atkinson *et al.*, 2014). The same may be said about root properties aside from architecture which can influence root survival and growth under soil stress. For example, biomechanical properties such as root tensile strength and Young's modulus are known to increase with age, probably due to the accumulation of compounds such as cellulose (Loades *et al.*, 2015). This will naturally influence the root ability to grow under conditions of higher soil strength. Nevertheless, the study of seedling root morphology could yield useful information about the root morphology at later stages of growth (Tuberosa *et al.*, 2002). For barley there are studies which used root traits at the seedling stage as an indicator of enhanced yield at later stages and detected significant correlations under different drought conditions (Chloupek *et al.*, 2010; Svacina *et al.*, 2014).

Another limiting factor in this study was the large variability due to the inherent restrictions in the sample size used. Ideally it is best to have an estimate of the sample size needed when designing an experiment. However, this was not possible here due to the lack of comparable studies found in the literature. At best only partial comparisons were possible as most of the articles identified examined the relationship between root elongation rates and the soil stressor factors of PR and matric suction. However, no measurements were performed on the range of root micro-traits considered here except for the study of Somasundaram *et al.*, (2009) but even then, the study was restricted only to **RBCC** and the plant species used was maize and not barley which was used in this study. On the other hand, the experiment reported in Chapter 4 enabled an indication of the sample size required by performing power analysis on **AVGR** and the theoretical sample size required was practically unfeasible ( $n > 54$ ) based on the resource availability. An alternative option would have been to use basic guidance in factorial experiment designing with authors recommending a minimum sample size of 10 (Everitt, 1975) and that the subjects-to-variables ratio should be no lower than 5 (Bryant and Yarnold, 1995). The latter option will require a sample size of 25 minirhizotrons and even if one was to adopt only the previous suggestion of using just 10 minirhizotrons then the study will still have been unfeasible. In summary, resource availability was a major limitation in this study, but the highest practically possible sample size was used, and this

was mitigated by the reduction in image analysis by the development of the analysis algorithms.

Something that must be considered is the difficulty in scaling from root micro-traits to the coarse scale of the root system. For example, root hairs aid the penetration of roots into soil and this was demonstrated when comparing hairless to wildtype varieties for both barley (Haling *et al.*, 2014) and maize (Bengough *et al.*, 2016). However, although this effect was demonstrated for individual roots it is not clear how to translate this effect when considering the coarser scale of the root system. For instance, Bailey *et al.*, (2002), compared the pull-out resistance of hairless *Arabidopsis* mutants with wild types and failed to detect any statistically significant differences. Similar argument could also be constructed about the other micro-traits considered in this study. Although there is evidence of the importance of root border cell production and root tip geometry in aiding root penetration (Mckenzie *et al.*, 2013; Colombi *et al.*, 2017), it is difficult to express in a mechanistic way the advantages in root penetration ability originating from those traits.

Another issue to consider is the extent to which more complex long-term effects may influence root growth but are difficult to quantify and to consider when trying to make predictions about root growth rates. An example of that could be the formation of “rhizosheath”, a layer of strongly bound and more aggregated soil that adheres firmly to the root surface (Koebernick *et al.*, 2017). This structure is rather variable both in terms of dimensional extent and chemical composition between species (Brown *et al.*, 2017) and between genotypes of the same species (George *et al.*, 2014). The influence of this rhizosheath on changing the adjacent soil structure can be significant as it is believed to influence the overall stability of the rhizosphere (Hallett *et al.*, 2009). Yet, the formation and development of this complex mixture of microbes and root exudates requires time and due to its nature, it will be extremely difficult to assess to what extent such effects could be integrated in a mechanistic model.

**Table 6.1:** The overall responses (grand average among varieties  $\pm$  grand standard deviation) of root micro-traits to the experimental treatments used in the experiment described in Chapter 5.

<b>DBD</b> (g cm <sup>-3</sup> )	<b>IRE</b>	<b>ARGR</b> (mm day <sup>-1</sup> )	<b>AVGR</b> (mm day <sup>-1</sup> )	<b>AHGR</b> (mm day <sup>-1</sup> )	<b>RHtRR</b> (mm mm <sup>-1</sup> )	<b>RBCC</b>	<b>RTE</b>
	2	9.15 $\pm$ 0.19	11.51 $\pm$ 0.3	5.52 $\pm$ 0.87	2.36 $\pm$ 0.21	39.69 $\pm$ 6.54	1.21 $\pm$ 0.18
1.4	4	9.74 $\pm$ 0.26	12.24 $\pm$ 0.58	5.9 $\pm$ 0.84	2.28 $\pm$ 0.11	22.44 $\pm$ 2.95	1.42 $\pm$ 0.09
	6	10.55 $\pm$ 0.38	12.95 $\pm$ 0.69	6.86 $\pm$ 0.58	2.44 $\pm$ 0.09	35.56 $\pm$ 15.09	1.25 $\pm$ 0.37
	2	6 $\pm$ 0.83	7.19 $\pm$ 0.83	4.18 $\pm$ 0.98	2.43 $\pm$ 0.27	50.44 $\pm$ 16.78	2.43 $\pm$ 0.69
1.6	4	7.63 $\pm$ 0.42	9.41 $\pm$ 0.56	4.89 $\pm$ 0.26	2.39 $\pm$ 0.11	50.63 $\pm$ 14.23	3.13 $\pm$ 1.11
	6	8.48 $\pm$ 0.19	10.53 $\pm$ 0.49	5.34 $\pm$ 0.75	2.29 $\pm$ 0.12	33.75 $\pm$ 5.92	2.11 $\pm$ 0.49

**ARGR:** Average root growth rate

**AVGR:** Average vertical growth rate

**AHGR:** Average horizontal growth rate

**RHtRR:** Root hair to root ratio

**RBCC:** Root border cell count

**RTE:** Root tip eccentricity

## 6.3 LLWR modification

In order to improve upon the LLWR it is necessary to understand its current limitations. An intrinsic limitation is the models' interpretation of the plant root growth limiting conditions being determined solely by volumetric water content and dry bulk density. Consideration of the critical value of the soil field capacity from a process-based approach will require assessment of a number of soil properties which include (Mohammadi *et al.*, 2010): (1) Saturated hydraulic conductivity of the soil (2) Pore size distribution index used in the Campbell soil moisture characteristics model (3) Saturated volumetric water content and (4) Air filled porosity at  $-10$  kPa matric potential. Furthermore, the state of field capacity will also be dependent on plant associated variables: (1) Soil oxygen consumption rate and (2) Root zone depth. For the case of the permanent wilting point, the critical value of the average water content at the onset of plant stress will depend on the properties (De Jong *et al.*, 2006): (1) potential transpiration rate and (2) soil hydraulic properties, e.g., conductivity. Furthermore, plant associated variables such as root density will also have a strong influence on the limiting value of stress onset while evidence supports that other traits such as a narrower angular spread of roots are also significant (Jin *et al.*, 2015). In a similar manner, determining the minimum air porosity of the soil will require an assessment of variables which are known to significantly influence the process and include (Bartholomeus *et al.*, 2008): (1) Soil type, (2) Soil temperature and (3) Soil depth. As for the limiting value for soil penetration resistance, i.e., 2 MPa, it is known that stress onset occurs in the form of a linear decrease in root elongation rates until they reach a high penetrometer pressure (Whalley *et al.*, 2006). This limiting value was demonstrated to vary among species, e.g., 0.8 MPa for cotton roots (Bengough *et al.*, 2011). Root traits that are known to influence this include: (1) an increase in the steepness of root angular spread (Jin *et al.*, 2015) and (2) the (poorly understood) ability of roots to exploit networks of continuous channels in soil (Bengough *et al.*, 2006).

At this point it should be emphasized that when the LLWR was first formulated in the work of da Silva *et al.*, (1994), the authors explicitly demonstrated that factors such as soil texture can have a strong influence on the LLWR limits. In fact, the subsequent development of soil

pedo-transfer functions (da Silva and Kay, 1997; Silva *et al.*, 2008) clearly demonstrated the dependency of the LLWR on soil properties such as clay content and organic carbon content. This demonstrates that the existing model does indeed take into account existing soil conditions and temporal changes in soil texture. However, it will be instructive to consider how the LLWR could be generalized to better reflect temporal soil changes. For example, Keller *et al.*, (2015), integrated the LLWR model into a previously published soil compaction model known as SoilFlex (Keller *et al.*, 2007). This enabled an assessment of dry bulk density changes around the wheel-soil interface created during the movement of heavy agricultural machinery. The corresponding variation in LLWR caused by the variation in dry bulk density could then allow for an understanding of the effect that agricultural machinery has on root growth conditions in the context of water availability. Future integration of models with good prediction abilities in the LLWR model could increase its importance as a soil quality index.

Another issue with the LLWR is that there is a certain degree of ambiguity when it comes to the dimensional extent of the soil system considered in the LLWR. Originally, the LLWR model only considered the top 20 cm of the soil system. However, if one was to consider the soil system beyond the top 20 cm limit then an agricultural soil for example would be expected to be directly affected by the nature of the agricultural practises used (Bengough *et al.*, 2006) which will subsequently influence the LLWR across different time points. In a similar manner, if one was to assess the LLWR at different time points then it should vary with factors such as changing soil structure, climatic variability, soil diversity, etc. Furthermore, the soil water release curve sub-model used by the LLWR will be expected to vary across the season rather erratically at times due to hysteresis effects. In other words, the location, time, anthropogenic and non-anthropogenic factors will not be constant effects in the LLWR model.

Finally, the limitations in the sub-models used by the LLWR needs to be considered. In section 4.4 it was demonstrated that the Busscher model for PR values was a poor descriptor for the dataset associated with the RS substrate. As such, the LLWR itself could not be defined for this application and preventing a direct comparison of the LLWR model

predictions about optimum growth with the observed growth rates. The fit of both sub-models used by the LLWR should always be checked and if alternative models exist which are applicable and have a better fit then they need to be considered as alternatives. For instance, it might be of use to consider alternative PR models such as the one proposed by Jakobsen and Dexter, (1987) and compare the fitness of the models. It will be interesting if this model could be integrated in the “llwr” function of the R package “soilphysics” so that users may compare the results.

## 6.4 Summary of key conclusions

1. Custom-developed minirhizotron-based root phenotyping platforms allow for high resolution imaging, but their development must be guided by specific criteria which define the properties that the system should have.
2. A variety of root micro-traits can be imaged by using only basic lab equipment.
3. The proposed RS based experimental protocol successfully induced a spectrum of root growth responses when manipulating the LLWR related soil stressors of DBD and IRE.
4. Significant differences in **ARGR**, **AVGR**, **AHGR**, **RBCC** and **RTE** were detected among different treatments of the soil stressor factors of DBD and IRE.
5. Genotypic variability was not a factor causing significant differences for the four spring barley varieties tested except **RTE**.
6. Root micro-traits could not explain the differences in root growth rates among the different substrate treatments on the variety level however, they were successful in predicting the average response on the individual plant level.
7. Future experiments should try to extend the system to A2 dimensions and assess if any genotypic differences can be detected at later development stages. The integration of sensors to measure water potential will also be ideal.
8. It is strongly recommended to select genotypes with known root trait differences e.g., root hair density, or varieties which are known to have contrasting growth rates in different soil conditions based on several published field-based experiments.

Furthermore, the sample size should increase from 4 to 8 to increase subject to variable ratio and reduce the errors in the descriptive and inferential statistics.

## 6.5 Future research

Oxygen sensors (150 x 6 mm) have been used in the past to assess the oxygen status of minirhizotrons (Dresbøll *et al.*, 2013). Perhaps a slight extension to the RS width could still have a good enough focusing plane of the root/scanning surface for good quality images and allow for an *in situ* estimate of the oxygen concentration. In a similar manner it is possible to use mini-tensiometers that also have a shaft with a diameter of 6 mm. However, as mentioned in Chapter 4 there is the issue of poor connectivity between the probe and the substrate. Increasing the width of the rhizotron by 2 mm should provide better contact between the probe and the sand (**Figure 6.1 (A)**) but perhaps, the addition of finer sand particles could still be required to achieve adequate readings. If successfully integrated into the existing RS design, these probes will offer a much more accurate and repeated assessment of the oxygen and water status of the RS substrate.

Based on the root growth conditions used in this study seedlings can be grown at least three weeks for the four spring barley cultivars tested. It will be interesting to extend beyond this time period in a more long-term study but that will require an increase in the dimensions of the RS and its associated flatbed scanner. Although, the RS system and the flatbed scanner were both A3 sized (297 x 420 mm) the system could be modified to work on an A2 scale (420 x 594 mm). This will require an enlargement of the standard RS unit which should be easy enough to do and subsequently scanning the RS unit twice, one for each half of the RS unit (**Figure 6.1 (B)**). That will of course require a larger manual input, scanning times and time required for image analysis but it is theoretically possible to achieve that. However, if the proposed design is successfully implemented, the list of benefits will probably shadow those disadvantages as the RS will allow for root growth for a period of up to 5 weeks potentially and *in situ* estimates of oxygen concentration and matric potential. Furthermore, if the design is strictly implemented with mechanical precision such as the accurate drilling of the holes in the RS scanning surface there could be further benefits in the image processing

component. For example, a fixed RS could reduce the computation times of several steps in the algorithms used since the effective root growth area will always be in a set of specific coordinates, excluding the outer area of the RS and the screw areas and implementing the algorithm only for the RS substrate covered zone.

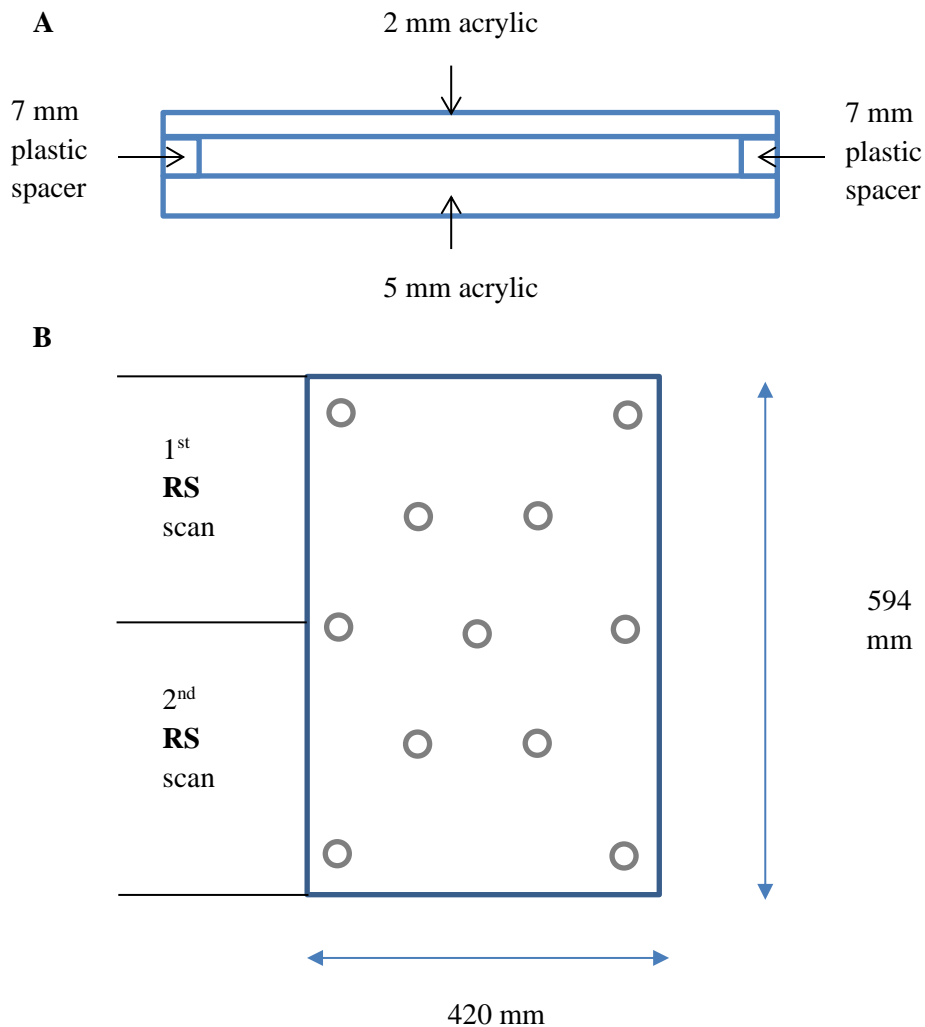


**Figure 6.1:** Schematic diagram of the proposed A2 sized **RS** unit **A)** Top view and **B)** Front view.

It should also be noted that although this study focused on the root traits of **ARGR**, **AVGR**, **AHGR**, **RHtRR**, **RBCC** and **RTE**, the list of traits doesn't have to be restricted to only those. For example, examination of root cortical regions could yield useful information between DBD treatments and can be integrated to the existing experimental protocol by using

laser ablation tomography (Chimungu *et al.*, 2015). In a similar manner it will not be difficult or time consuming to obtain information about other parts of the plant which are easily accessible e.g. stem diameter. If the above proposed method allows for seedlings to reach more mature stages, then with additional time investment a significant amount of information could be obtained in comparison to the current list of traits.

## References

- Agbicodo E.M., Fatokun C.A., Muranaka S., Visser R.G.F. and van der Linden C.G., (2009). Breeding drought tolerant cowpea: Constraints, accomplishments, and future prospects. *Euphytica*, 167, 353–370.
- Akmal M. and Hirasawa T., (2004). Growth responses of seminal roots of wheat seedlings to a reduction in the water potential of vermiculite. *Plant Soil*, 267, 319–328.
- Anderson K. and Croft H., (2009). Remote sensing of soil surface properties. *Prog. Phys. Geogr.* 33, 457–473.
- Anjum F., Yaseen M., Rasul E., Wahid A. and Anjum S., (2003). Water stress in barley (*Hordeum vulgare* L.). Effect on chemical composition and chlorophyll contents. *Pakistan J. Agr. Sci.* 40, 45–49.
- Armengaud P., Zambaux K., Hills A., Sulpice R., Pattison R.J., Blatt M.R. and Amtmann A., (2009). EZ-Rhizo: integrated software for the fast and accurate measurement of root system architecture. *Plant J.*, 57, 945–956.
- Armstrong W. and Gaynard T.J., (1976). The critical oxygen pressures for respiration in intact plants. *Physiol Plant*, 37, 200–206.
- Arnaud M., *et al.* (2019). EnRoot: A narrow-diameter, inexpensive and partially 3D-printable minirhizotron for imaging fine root production. *Plant Methods*. BioMed Central, 15(1), p. 1–9. doi: 10.1186/s13007-019-0489-6.
- Arsenault J.L., Pouleur S., Messier C. and Guay R., (1995). WinRHIZO, a root-measuring system with a unique overlap correction method. *HortScience* 30, 906.
- Asseng S., Ewert F., Martre P., Rötter R.P., Lobell D.B., Cammarano D., *et al.*, (2015). Rising temperatures reduce global wheat production. *Nat. Clim. Chang*, 5, 143–147. doi: 10.1038/nclimate2470.
- Atkinson J.A., *et al.*, (2014). Branching out in roots: Uncovering form, function, and regulation. *Plant Physiology*, 166(2), 538–550. doi: 10.1104/pp.114.245423.

- Atwell B.J., (1988). Physiological responses of lupin roots to soil compaction. *Plant and Soil*, 111, 277–281.
- Aust W.M., Burger J.A., Carter E.A., Preston D.P. and Patterson S.C., (1998). Visually determined soil disturbance classes used as indices of forest harvesting disturbance. *South J Appl For*, 22, 245–250.
- Badri D.V. and Vivanco J.M., (2009). Regulation and function of root exudates. *Plant Cell Environ.*, 32, 666–681. doi: 10.1111/j.1365-3040.2009.01926.x.
- Bailey P.H.J., Currey J.D. and Fitter A.H., (2002). The role of root system architecture and root hairs in promoting anchorage against uprooting forces in *Allium cepa* and root mutants of *Arabidopsis thaliana*. *Journal of Experimental Botany*, 53, 333–340.
- Bao Y., Aggarwal P., Robbins N.E., Sturrock C.J., Thompson M.C., Tan H.Q., *et al.*, (2014). Plant roots use a patterning mechanism to position lateral root branches toward available water. *Proc. Natl. Acad. Sci.*, 111, 9319–9324. doi: 10.1073/pnas.1400966111.
- Barber S.A., (1995). Soil Nutrient Bioavailability: A Mechanistic Approach, 2nd Edn. New York, NY: Wiley.
- Bardgett R.D., Mommer L. and de Vries F.T., (2014). Going underground: root traits as drivers of ecosystem processes. *Trends in Ecology and Evolution*, 29, 692–699.
- Barnabas B., Jäger K. and Fehér A., (2008). The effect of drought and heat stress on reproductive processes in cereals. *Plant Cell Environ*, 31, 11–38.
- Bartholomeu, R.P., *et al.* (2008). Critical soil conditions for oxygen stress to plant roots: Substituting the Feddes-function by a process-based model. *Journal of Hydrology*, 360(1–4), 147–165. doi: 10.1016/j.jhydrol.2008.07.029.
- Bates T.R. and Lynch J.P., (1996). Stimulation of root hair elongation in *Arabidopsis thaliana* by low phosphorus availability. *Plant. Cell Environ.*, 19, 529–538. doi: 10.1111/j.1365-3040.1996.tb00386.x.

Bates T.R. and Lynch J.P., (2000). The efficiency of *Arabidopsis thaliana* (*Brassicaceae*) root hairs in phosphorus acquisition. *Am. J. Bot.*, 87, 964–970. doi: 10.2307/2656995.

Batten C., (2000). Autofocusing and astigmatism correction in the scanning electron microscope. PhD thesis, University of Cambridge.

Bauhus J. and Messier C., (1999). Evaluation of fine root length and diameter measurements obtained using RHIZO image analysis. *Agron. J.*, 91, 142–147.

Bayuelo-Jiménez J.S., Gallardo-Valdéz M., Perez-Decelis V.A., MagdalenoArmas L., Ochoa I. and Lynch J.P., (2011). Genotypic variation for root traits of maize (*Zea mays* L.) from the Purhepecha Plateau under contrasting phosphorus availability. *Field Crops Res*, 121, 350–362. doi:10.1016/j.fcr.2011.01.001.

Bengough A.G. and McKenzie B.M., (1997). Sloughing of root cap cells decreases the frictional resistance to maize (*Zea mays* L.) root growth. *Journal of Experimental Botany*, 48: 885–893.

Bengough A.G. and Mullins C.E., (1990). The resistance experienced by roots growing in a pressurised cell by roots growing in a pressurized cell. A reappraisal. *Plant and Soil*, 123, 73–82.

Bengough A.G. and Mullins C.E., (1991). Penetrometer resistance, root penetration resistance and root elongation rate in two sandy loam soils. *Plant and Soil*, 131(1), 59–66. doi: 10.1007/BF00010420.

Bengough A.G., Bransby M.F., Hans J., McKenna S.J., Roberts T.J. and Valentine T.A., (2006). Root responses to soil physical conditions; growth dynamics from field to cell. *Journal of Experimental Botany*, 57, 437–447.

Bengough A.G., *et al.*, (2011). Root elongation, water stress, and mechanical impedance: A review of limiting stresses and beneficial root tip traits. *Journal of Experimental Botany*, 62(1), 59–68. doi: 10.1093/jxb/erq350.

- Bengough A.G., Gordon D.C., Al-Menaie H., Ellis R.P., Allan D., Keith R., *et al.*, (2004). Gel observation chamber for rapid screening of root traits in cereal seedlings. *Plant Soil*, 262, 63–70. doi:10.1023/B:PLSO.0000037029.82618.27.
- Bengough A.G., Iijima M. and Barlow P.W., (2001). Image analysis of maize root caps - Estimating cell numbers from 2-D longitudinal sections. *Annals of Botany*, 87(5), 693–698. doi: 10.1006/anbo.2001.1392.
- Bengough G., Loades K. and McKenzie B.M., (2016). Root hairs aid soil penetration by anchoring the root surface to pore walls. *Journal of Experimental Botany*, 67(4), 1071–1078. doi: 10.1093/jxb/erv560.
- Bennett T., *et al.*, (2014). Precise control of plant stem cell activity through parallel regulatory inputs. *Development (Cambridge)*, 141(21), 4055–4064. doi: 10.1242/dev.110148.
- Bennie A.T.P., Taylor H.M. and Georgan P.G., (1987). An assessment of the core-break method for estimating rooting density of different crops in the field. *Soil and Tillage Research*, 9, 347–353.
- Bernick N., *et al.*, (2017). High-resolution synchrotron imaging shows that root hairs influence rhizosphere soil structure formation. *New Phytologist*, 216(1), 124-135. doi: 10.1111/nph.14705.
- Betz C.L., Allmaras R.R., Copeland S.M., Randall G.W., (1998). Least limiting water range: traffic and long-term tillage influences in a Webster soil. *Soil Science Society of America Journal*, 62, 1384–1393.
- Bingham I.J., Bengough A.G. and Rees R.M., (2010). Soil compaction–N interactions in barley: Root growth and tissue composition. *Soil and Tillage Research*, 106, 241–246.
- Bonser A.M., Lynch J. and Snapp S., (1996). Effect of phosphorus deficiency on growth angle of basal roots in *Phaseolus vulgaris*. *New Phytologist*, 132, 281–288. doi:10.1111/j.1469-8137.1996.tb01847.x.

Box J.E., (1996). Modern methods for root investigation. In: *Plant Roots: The Hidden Half*, Marcel Dekker, New York, p. 193–237.

Boyer J.S., (1996). Advances in drought tolerance in plants. *Adv. Agron.*, 56, 187–218.

Braam J., Davis R.W., (1990). Rain, wind, and touch-induced expression of calmodulin and calmodulin-related genes in Arabidopsis. *Cell*, 60, 357–364.

Brown G.G., Edwards C.A., Brussaard L., (2004). How earthworms affect plant growth: burrowing into the mechanisms. In: Edwards CA, editor. *Earthworm ecology*. Boca Raton: CRC Press, p. 13–49.

Brown L.K., George T.S., Dupuy L.X. and White P.J., (2013). A conceptual model of root hair ideotypes for future agricultural environments: what combination of traits should be targeted to cope with limited P availability?. *Annals of Botany*, 112, 317–330.

Brown L.K., George T.S., Neugebauer K. and White P.J., (2017). The rhizosheath – a potential trait for future agricultural sustainability occurs in orders throughout the Angiosperms. *Plant and Soil*, 445, 565–575. doi: 10.1007/s11104-017-3220-2.

Bryant F.B. and Yarnold P.R., (1995). Principal-components analysis and exploratory and confirmatory factor analysis. In L. G. Grimm & P. R. Yarnold (Eds.), *Reading and understanding multivariate statistics* (p. 99–136). American Psychological Association.

Busscher W.J. and Sojka R.E., (1987). Enhancement of subsoiling effect on soil strength by conservation tillage. *Trans. ASAE*, 30, 888-892.

Cai G., Vanderborght J., Klotzsche A., van der Kruk J., Neumann J., Hermes N. and Vereecken H., (2016). Construction of Minirhizotron Facilities for Investigating Root Zone Processes. *Vadose Zone Journal*, 15(9), 1-13. doi: <https://doi.org/10.2136/vzj2016.05.0043>.

Camejo D., Jimenez A., Alarcon J.J., Torres W., Gomez J.M. and Sevilla F., (2006). Changes in photosynthetic parameters and antioxidant activities following heat-shock treatment in tomato plants. *Funct. Plant Biol.*, 33, 177–187. doi: 10.1071/FP05067.

Camejo D., Rodriguez P., Morales M.A., Dell'amico J.M., Torrecillas A. and Alarcon J.J., (2005). High temperature effects on photosynthetic activity of two tomato cultivars with different heat susceptibility. *J. Plant Physiol.*, 162, 281–289. doi: 10.1016/j.jplph.2004.07.014.

Carminati A., *et al.*, (2017). Root hairs enable high transpiration rates in drying soils. *New Phytologist*, 216(3), 771–781. doi: 10.1111/nph.14715.

Carminati A., Vetterlein D., Weller U., Vogel H.J. and Oswald S.E., (2009). When Roots Lose Contact. *Vadose Zone Journal*, 8(3), 805-809.

Chai H.H., Chen F., Zhang S.J., Li Y.D., Lu Z.S., Kang Y.J. and Yu L., (2019). Multi-chamber petaloid root-growth chip for the non-destructive study of the development and physiology of the fibrous root system of *Oryza sativa*. *Lab Chip*, 19, 2383.

Chamen T., Alakukku L., Pires S., Sommer C., Spoor G., Tijink F. and Weisskopf P., (2003) Prevention strategies for field traffic-induced subsoil compaction: a review, Part 2. Equipment and field practices. *Soil & Tillage Research* 73, 161–174. doi:10.1016/S0167-1987(03)00108-9.

Chen X., Li Y., He R., *et al.*, (2018). Phenotyping field-state wheat root system architecture for root foraging traits in response to environment × management interactions. *Sci Rep.*, 8(1), 2642.

Cheng W., Coleman D.C. and Box Jr.J.E., (1991). Measuring root turnover using the minirhizotron technique. *Agric. Ecosyst. Environ.* 34, 261–267.

Chimungu J.G., Brown K.M. and Lynch J.P., (2014). Large root cortical cell size improves drought tolerance in maize. *Plant physiology*, 166(4), 2166–2178. doi: <https://doi.org/10.1104/pp.114.250449>.

Chimungu J.G., Loades K.W. and Lynch J.P. (2015). Root anatomical phenes predict root penetration ability and biomechanical properties in maize (*Zea Mays*). *Journal of Experimental Botany*, 66(11), 3151–3162. doi: <https://doi.org/10.1093/jxb/erv121>.

- Chloupek O., Dostál V., Středa T., Psota V. and Dvořáčková O., (2010). Drought tolerance of barley varieties in relation to their root system size. *Plant Breed.*, 129, 630–6.
- Clark L.J., Whalley W.R., Leigh R.A., Dexter A.R. and Barraclough P.B., (1999). Evaluation of agar and agarose gels for studying mechanical impedance in rice roots. *Plant and Soil*, 207, 37–43.
- Clark R.T., Famoso A.N., Zhao K., Shaff J.E., Craft E.J., Bustamante C.D., McCouch S.R., Aneshansley D.J. and Kochian L.V., (2013). High-throughput two-dimensional root system phenotyping platform facilitates genetic analysis of root growth and development. *Plant Cell Environ*, 36, 454–466.
- Colombi T., Kirchgessner N., Walter A. and Keller T., (2017). Root tip shape governs root elongation rate under increased soil strength. *Plant Physiology*, 174, 2289–2301.
- Comas L.H., Mueller K.E., Taylor L.L., Midford P.E., Callahan H.S. and Beerling D.J., (2012). Evolutionary patterns and biogeochemical significance of angiosperm root traits. *Int. J. Plant Sci.*, 173, 584–595.
- Costa C., Dwyer L.M., Zhou X., Dutilleul P., Hamel C., Reid L.M., *et al.*, (2002). Root morphology of contrasting maize genotypes. *Agron. J.*, 94, 96–101.
- Courtois B., Audebert A., Dardou A., Roques S., Ghneim-Herrera T., Droc G., Frouin J., Rouan L., Gozé E., Kilian A., Ahmadi N. and Dingkuhn M., (2013). Genome-wide association mapping of root traits in a Japonica Rice panel. *PLoS One*, 8, e78037.
- Courtois B., McLaren G., Sinha P.K., Prasad K., Yadav R. and Shen L., (2000). Mapping QTLs associated with drought avoidance in upland rice. *Mol. Breed.*, 6, 55–66.
- Coxeter H.S.M. and Greitzer S.L., (1967). *Geometry Revisited*, Washington, DC: Mathematical Association of America, p. 76.
- Cussler E.L., (1997). *Diffusion: Mass Transfer in Fluid Systems* (2nd ed.). New York: Cambridge University Press. ISBN 0-521-45078-0.

- Czarnes S., Hiller S., Dexter A.R., Hallett P.D. and Bartoli F., (1999). Root:soil adhesion in the maize rhizosphere: the rheological approach. *Plant and Soil*, 211, 69–86.
- Da Silva A.P. and Kay B.D., (1997). Estimating the least limiting water range of soils from properties and management. *Soil Science Society of America*, 61, 877–883.
- Da Silva A.P., Kay B.D. and Perfect E., (1994). Characterization of the Least Limiting Water Range of Soils. *Soil Science Society of America*, 58(6), 1775-1781. doi: <https://doi.org/10.2136/sssaj1994.03615995005800060028x>.
- Daryanto S., Wang L. and Jacinthe P.A., (2016). Global synthesis of drought effects on maize and wheat production. *PLoS ONE* 11(5): e0156362. doi:<https://doi.org/10.1371/journal.pone.0156362>.
- De Jong Q.L., Metselaar K. and Van Dam J.C., (2006). Root water extraction and limiting soil hydraulic conditions estimated by numerical simulation. *Vadose Zone J.*, 5, 1264-1277.
- De Jong van Lier Q. and Gubiani P.I., (2015). ‘Além do “intervalo hídrico ótimo”’: Repensando a pesquisa em física do solo no Brasil’. *Revista Brasileira de Ciencia do Solo*, 39(4), 925–939. doi: 10.1590/01000683rbcs20140596.
- De Kroon H. and Visser E., (2003) *Root ecology, Ecological Studies*, 168. Springer Berlin Heidelberg.
- Degenhardt B. and Gimmler H., (2000). Cell wall adaptations to multiple environmental stresses in maize roots. *Journal of Experimental Botany*, 51, 595–603.
- Delory B.M., *et al.*, (2017). Accuracy and bias of methods used for root length measurements in functional root research. *Methods in Ecology and Evolution*, 8(11), 1594–1606. doi: 10.1111/2041-210X.12771.
- Dexter A.R. and Hewitt J.S., (1978). Deflection of plant roots. *J Agric Eng Res*, 23, 17–22. doi:10.1016/0021-8634(78)90075-6.
- Dexter A.R., (1987). Mechanics of root growth. *Plant and Soil*, 98, 303–312.

Dietrich D., (2018). Hydrotropism: How roots search for water. *Journal of Experimental Botany*, 69(11), 2759–2771. doi: 10.1093/jxb/ery034.

Dietrich D., Pang L., Kobayashi A., Fozard J.A., Boudolf V., Bhosale R., Antoni R., *et al.*, (2017). Root hydrotropism is controlled via a cortex-specific growth mechanism. *Nature Plants*, 68(13), 3441–3456. doi: <https://doi.org/10.1093/jxb/erx193>.

Do Rosário G., Oliveira M., van Noordwijk M., Gaze S.R., *et al.*, (2000). Auger sampling, ingrowth cores and pinboard methods. In: *Root methods*. Springer Berlin Heidelberg, Berlin, 175–210.

Donald R.G., Kay B.D. and Miller M.H., (1987). The effect of soil aggregate size on early shoot and root growth of maize (*Zea mays* L.). *Plant and Soil*, 103, 251–259.

Downie H., Holden N., Otten W., Spiers A.J., Valentine T.A. and Dupuy L.X., (2012). Transparent soil for imaging the rhizosphere. *PLoS ONE*, 7, e44276.

Downie H.F., Adu M.O., Schmidt S., Otten W., Dupuy L.X., White P.J. and Valentine, T.A., (2015). Challenges and opportunities for quantifying roots and rhizosphere interactions through imaging and image analysis. *Plant, Cell and Environment*, 38(7), 1213–1232. <https://doi.org/10.1111/pce.12448>

Dresbøll D.B., *et al.*, (2013). Timelapse scanning reveals spatial variation in tomato (*Solanum lycopersicum* L.) root elongation rates during partial waterlogging. *Plant and Soil*, 369(1–2), 467–477. doi: 10.1007/s11104-013-1592-5.

Dunbabin V.M., *et al.*, (2013). Modelling root-soil interactions using three-dimensional models of root growth, architecture and function. *Plant and Soil*, 372(1–2), 93–124. doi: 10.1007/s11104-013-1769-y.

Dupuy L., *et al.* (2010). The dynamics of root meristem distribution in the soil, p. 358–369. doi: 10.1111/j.1365-3040.2009.02081.x.

Dupuy L., Gregory P. J. and Bengough A. G., (2010). Root growth models: Towards a new generation of continuous approaches. *Journal of Experimental Botany*, 61(8), 2131–2143.

doi: 10.1093/jxb/erp389.

Dupuy L.X., *et al.*, (2017). Accelerating root system phenotyping of seedlings through a computer-assisted processing pipeline. *Plant Methods*. BioMed Central, 13(1), 1–14. doi: 10.1186/s13007-017-0207-1.

Eberbach P.L., Hoffmann J., Moroni S.J., Wade L.J. and Weston L.A., (2013). Rhizolysimetry: Facilities for the simultaneous study of root behaviour and resource use by agricultural crop and pasture systems. *Plant Methods*, 9, 3. doi:10.1186/1746-4811-9-3.

Erasmus S. and Smith K., (1982). An automatic focusing and astigmatism correction system for the SEM and CTEM. *J. Microscopy*, 127, 185-199.

Eshel A. and Beeckman T., (2012). *Plant roots: the hidden half*. New York, NY: CRC Press.

Everitt B.S., (1975). Multivariate analysis: the need for data and other problems. *British Journal of Psychiatry*, 126, 237-240.

Faget M., Liedgens M., Stamp P., Fluetsch P. and Herrera J.M., (2010). A minirhizotron imaging system to identify roots expressing the green fluorescent protein, *Computers and Electronics in Agriculture*, 74, 163-167.

Faget M., *et al.*, (2013). Root-root interactions: Extending our perspective to be more inclusive of the range of theories in ecology and agriculture using in-vivo analyses, *Annals of Botany*, 112(2), 253–266. doi: 10.1093/aob/mcs296.

Fang S., Yan X. and Liao H., (2009). 3D reconstruction and dynamic modelling of root architecture in situ and its application to crop phosphorus research. *Plant J*, 60(6), 1096–1108.

FAO and ITPS, (2015). Status of the World's Soil Resources (SWSR) – Main Report. Rome: Food and Agriculture Organization of the United Nations. [http://www.fao.org/documents/card/en/c/c6814873-efc3-41db-b7d3-2081a10ede50/#:~:text=The%20SWSR%20is%20a%20reference,regional%20assessments%](http://www.fao.org/documents/card/en/c/c6814873-efc3-41db-b7d3-2081a10ede50/#:~:text=The%20SWSR%20is%20a%20reference,regional%20assessments%20)

[20of%20soil%20change.&text=It%20provides%20a%20description%20and.and%20in%20e ach%20region%20separately](#) accessed 13/09/17.

Feldman L.J., (1984). Development and dynamics of the root apical meristem. *Am. J. Bot.*, 7, 1308–1314.

Fitter A., (2002). Characteristics and functions of root systems. In *Plant Roots: The Hidden Half*, 3rd ed., p. 15–32.

Fleming A. and Vanclay F., (2010). Farmer responses to climate change and sustainable agriculture. A review. *Agron Sustain Dev*, 30, 11–19. doi:10.1051/agro/2009028.

Food and Agriculture Organisation of the United Nations, (2009). *How to Feed the World in 2050*.

[http://www.fao.org/fileadmin/templates/wsfs/docs/expert\\_paper/How\\_to\\_Feed\\_the\\_World\\_i\\_2050.pdf](http://www.fao.org/fileadmin/templates/wsfs/docs/expert_paper/How_to_Feed_the_World_i_2050.pdf) accessed 13/09/17.

Foyer C.H., Descourvieres P. and Kunert K.J., (1994). Photo oxidative stress in plants. *Plant Physiology*, 92, 696–717.

Frangi A.F., *et al.*, (1998). Multiscale vessel enhancement filtering. *Lecture Notes in Computer Science (including subseries Lecture Notes in Artificial Intelligence and Lecture Notes in Bioinformatics)*, 1496(February), p. 130–137. doi: 10.1007/bfb0056195.

French A., Ubeda-Tomas S., Holman T.J., Bennett M.J. and Pridmore T., (2009). High-throughput quantification of root growth using a novel image-analysis tool. *Plant Physiol*, 150, 1784–1795.

Fujii N., *et al.*, (2018). Root-tip-mediated inhibition of hydrotropism is accompanied with the suppression of asymmetric expression of auxin-inducible genes in response to moisture gradients in cucumber roots. *PLoS ONE*, 13(1), 1–25. doi: 10.1371/journal.pone.0189827.

Furbank R.T., (2009). Plant phenomics: from gene to form and function. *Functional Plant Biology*, 36(11), v – vi.

Gahoonia T.S. and Nielsen N.E., (1997). Variation in root hairs of barley cultivars doubled soil phosphorus uptake. *Euphytica*, 98(3), 177–182. doi: 10.1023/A:1003113131989.

Gahoonia T.S. and Nielsen N.E., (2004). Barley genotypes with long root hairs sustain high grain yields in low-P field. *Plant Soil*, 262, 55–62. doi:10.1023/B:PLSO.0000037020.58002.ac.

Gahoonia T.S., Nielsen N.E., Joshi P.A. and Jahoor A., (2001). A root hairless barley mutant for elucidating genetic of root hairs and phosphorus uptake. *Plant Soil*, 235, 211–219. doi: 10.1023/A:1011993322286

Galkovskyi T., *et al.*, (2012). GiA Roots: Software for the high throughput analysis of plant root system architecture. *BMC Plant Biology*, 12. doi: 10.1186/1471-2229-12-116.

Galvan-Ampudia C.S., Julkowska M.M., Darwish E., Gandullo J., Korver R.A., Brunoud G., Haring M.A., Munnik T., Vernoux T. and Testerink C., (2013). Halotropism is a response of plant roots to avoid a saline environment. *Current Biology*, 23, 2044–2050.

Garbout A., Munkholm L.J., Hansen S.B., Petersen B.M., Munk O.L. and Pajor R., (2012). The use of PET/CT scanning technique for 3D visualization and quantification of real-time soil/plant interactions. *Plant Soil*, 352, 113-127.

Garg B.K., (2003). Nutrient uptake and management under drought: nutrient-moisture interaction. *Curr. Agric.*, 27, 1–8.

George T.S., Brown L.K., Ramsay L., White P.J., Newton A.C., Bengough A.G., Russell J. and Thomas W.T.B., (2014). Understanding the genetic control and physiological traits associated with rhizosheath production by barley (*Hordeum vulgare*). *New Phytologist*, 203, 195–205.

Gerendás J. and Ratcliffe R.G., (2002). Root pH regulation. *Plant Roots: The Hidden Half*, Ed 3. Marcel Dekker, New York, 553–570.

Gibbs J., Turner D.W., Armstrong W., Sivasithamparam K. and Greenway H., (1998). Response to oxygen deficiency in primary maize roots. II. Development of oxygen deficiency

in the stele has limited short-term impact on radial hydraulic conductivity. *Aust. J. Plant Physiol.*, 25, 759–763. doi: 10.1071/PP98087.

Gill R.A. and Jackson R.B., (2000). Global patterns of root turnover for terrestrial ecosystems. *The New Phytologist*, 147(1), 13–31.

Gilroy S. and Jones D.L., (2000). Through form to function: root hair development and nutrient uptake. *Trends Plant Sci*, 5, 56–60.

Gioia T., Galinski A., Lenz H., Müller C., Lentz J., Heinz K., Briese C., Putz A., Fiorani F., Watt M., *et al.*, (2017). GrowScreen-PaGe, a non-invasive, high-throughput phenotyping system based on germination paper to quantify crop phenotypic diversity and plasticity of root traits under varying nutrient supply. *Funct Plant Biol*, 44, 76-93.

Goss M.J., (1977). Effects of mechanical impedance on root-growth in barley (*Hordeum vulgare* L.). Effects on elongation and branching of seminal root axes. *Journal of Experimental Botany*, 28, 96–111.

Greacen E.L., Farrell D.A. and Cockroft B., (1968). Soil resistance to metal probes and plant roots. *Trans 9th Congr Int Soc Soil Sci*, 1, 769–779.

Gregory A.S., Watts C.W., Whalley W.R., Kuan H.L., Griffiths B.S., Hallett P.D. and Whitmore A.P., (2007). Physical resilience of soil to field compaction and the interactions with plant growth and microbial community structure. *European Journal of Soil Science*, 58, 1221–1232.

Gregory P.J., (2008). Plant roots: growth, activity and interactions with the soil. John Wiley & Sons.

Grierson C. and Schiefelbein J., (2002). Root hairs. In: *The Arabidopsis book*. American Society of Plant Biologists, Rockville.

Grossman A. and Takahashi H., (2001). Macronutrient utilization by photosynthetic eukaryotes and the fabric of interactions. *Annu. Rev. Plant Phys.*, 52, 163–210.

Grzesiak M.T., (2009). Impact of soil compaction on root architecture, leaf water status, gas exchange and growth of maize and triticale seedlings. *Plant Root*, 3, 10–16.

Guichard M., *et al.*, (2019). Root Hair Sizer: An algorithm for high throughput recovery of different root hair and root developmental parameters. *Plant Methods*, 15(1), 1–14. doi: 10.1186/s13007-019-0483-z.

Charles H., Godfray J., *et al.*, (2010). Food Security: The Challenge of Feeding 9 Billion. *Science*, 327, 812-817.

Haling R.E., Brown L.K., Bengough A.G., Valentine T.A., White P.J., Young I.M. and George T.S., (2014). Root hair length and rhizosheath mass depend on soil porosity, strength and water content in barley genotypes. *Planta*, 239, 643–651.

Haling R.E., Brown L.K., Bengough A.G., Young I.M., Hallett P.D., White P.J. and George T.S., (2013). Root hairs improve root penetration, root–soil contact, and phosphorus acquisition in soils of different strength. *Journal of Experimental Botany*, 64, 3711–3721.

Haling R.E., *et al.*, (2014). Root hair length and rhizosheath mass depend on soil porosity, strength and water content in barley genotypes. *Planta*, 239(3), 643–651. doi: 10.1007/s00425-013-2002-1.

Haling R.E., Simpson R.J., Culvenor R.A., Lambers H. and Richardson A.E., (2011). Effect of soil acidity, soil strength and macropores on root growth and morphology of perennial grass species differing in acid-soil resistance. *Plant Cell Environ*, 34, 444–456.

Haling R.E., Simpson R.J., Delhaize E., Hocking P.J. and Richardson A.E., (2010). Effect of lime on root growth, morphology and the rhizosheath of cereal seedlings growing in an acid soil. *Plant Soil*, 327, 199–212.

Hallett P.D., Feeney D.S., Bengough A.G., Rillig M.C., Scrimgeour C.M. and Young I.M., (2009). Disentangling the impact of AM fungi versus roots on soil structure and water transport. *Plant and Soil*, 314, 183–196.

Hammac W.A., *et al.*, (2011). High resolution imaging to assess oilseed species root hair responses to soil water stress. *Plant and Soil*, 339(1), 125–135. doi: 10.1007/s11104-010-0335-0.

Hammer G.L., Dong Z., McLean G., Doherty A., Messina C., Schussler J., Zinselmeier C., Paszkiewicz S. and Cooper M., (2009). Can changes in canopy and/or root system architecture explain historical maize yield trends in the us corn belt?. *Crop Science*, 49(1), 99–312.

Hawes M.C., *et al.*, (2000). The role of root border cells in plant defense. *Trends in Plant Science*, 5(3), 128–133. doi: 10.1016/S1360-1385(00)01556-9.

Heeraman D.A. and Juma N.G., (1997). A comparison of minirhizotron, core and monolith methods for quantifying barley (*Hordeum vulgare* L.) and fababean (*Vicia faba* L.) root distribution. *Plant and Soil volume*, 148, 29–4.

Heeraman D.A., Hopmans J.W. and Clausnitzer V., (1997). Three dimensional imaging of plant roots in situ with X-ray computed tomography. *Plant Soil*, 189, 167–179. doi:10.1023/B:PLSO.0000009694.64377.6f

Hendrick R.L. and Pregitzer K.S., (1993). Patterns of fine root mortality in two sugar maple forests. *Nature*, 361, 59–61.

Hendricks J.J., Hendrick R.L., Wilson C.A., Mitchell R.J., Pecot S.D. and Guo D., (2006). Assessing the patterns and controls of fine root dynamics: an empirical test and methodological review. *J Ecol.*, 94, 40–57. doi:10.1111/j.1365-2745.2005.01067.x.

Henry A., Cal A.J., Batoto T.C., Torres R.O. and Serraj R., (2012). Root attributes affecting water uptake of rice (*Oryza sativa* L.) under drought. *J. Exp. Bot.*, 63, 4751–4763.

Henry A., Gowda V.R.P., Torres R.O., McNally K.L. and Serraj R., (2011). Variation in root system architecture and drought response in rice (*Oryza sativa* L.): Phenotyping of the Oryza SNP panel in rainfed low land fields. *Field Crops Res*, 120, 205–214.

Hetz W., Hochholdinger F., Schwall M. and Feix G., (1996). Isolation and characterization of *rctcs*, a maize mutant deficient in the formation of nodal roots. *Plant J.*, 10, 845–857.

Hillel D., (2003). Introduction to Environmental Soil Physics. Academic Press, ISBN: 9780123486554.

Himmelbauer M.L., Loiskandl W. and Kastanek F., (2004). Estimating length, average diameter and surface area of roots using two different Image analyses systems. *Plant and Soil*, 260, 111–120. <https://doi.org/10.1023/B:PLSO.0000030171.28821.55>.

Hinsinger P., Bengough A.G., Vetterlein D. and Young I.M., (2009). Rhizosphere: biophysics, biogeochemistry and ecological relevance. *Plant and Soil*, 321, 117–152.

Hochholdinger F., Woll K., Sauer M. and Dembinsky D., (2004). Genetic dissection of root formation in maize (*Zea mays* L.) reveals root-type specific developmental programs. *Annals of Botany*, 93, 359–368.

Hoekstra F.A., Golovina E.A. and Buitink J., (2001). Mechanisms of plant desiccation tolerance. *Trends Plant Sci.* 6, 431–438.

Humphris S.N., Bengough A.G., Griffiths B.S., Kilham K., Rodger S., Stubbs V. and Young I.M., (2005). Root cap influences root colonisation by *Pseudomonas fluorescens* SBW25 on maize. *FEMS Microbiology Ecology*, 54, 123–130.

Hund A., Trachsel S. and Stamp P., (2009). Growth of axile and lateral roots of maize. I: Development of a phenotyping platform. *Plant and Soil*, 325, 335–349. doi:10.1007/s11104-009-9984-2.

Iijima M. and Kono Y., (1991). Interspecific differences of the root system structures of four cereal species as affected by soil compaction. *Japanese Journal of Crop Science*, 60, 130–138.

Iijima M., Barlow P.W. and Bengough A.G., (2003). Root cap structure and cell production rates of maize (*Zea mays*) roots in compacted sand. *New Phytologist*, 160(1), 127–134. doi: 10.1046/j.1469-8137.2003.00860.x.

- Iijima M., *et al.*, (2003). Root cap removal increases root penetration resistance in maize (*Zea mays* L.). *Journal of Experimental Botany*, 54(390), 2105–2109. doi: 10.1093/jxb/erg226.
- Iijima M., Griffiths B. and Bengough A.G., (2000). Sloughing of cap cells and carbon exudation from maize seedling roots in compacted sand. *New Phytologist*, 145, 477–482.
- Inoue Y., Yamaoka K., Kimura K. and Sawai K., (1995). Image processing-aided simple analysis method for root hair formation in plants. *Bioimages*, 3, 31–6.
- IPCC, (2014). Climate Change 2014: Synthesis Report. In: Proceedings of the Contribution of Working Groups I, II and III to the Fifth Assessment Report of the Intergovernmental Panel on Climate Change, eds Core Writing Team, R. K. Pachauri, and L. A. Meyer (Geneva: IPCC), 151.
- Itoh S., (1985). In situ measurement of rooting density by micro-rhizotron. *Soil Sci Plant Nutr.*, 31(4), 653–6.
- Iyer-Pascuzzi A.S., Symonova O., Mileyko Y., *et al.*, (2010). Imaging and analysis platform for automatic phenotyping and trait ranking of plant root systems. *Plant Physiology*, 152, 1148–1157.
- Jahnke S., Menzel M.I., van Dusschoten D., Roeb G.W., Bühler J., Minwyelet S., Blümmer P., Temperton V.M., Hombach T., Streun M., *et al.*, (2009). Combined MRI-PET dissects dynamic changes in plant structures and functions. *Plant J Cell Mol Biol*, 59, 634-644.
- Jakobsen B.F. and Dexter A.R., (1987). Effect of soil structure on wheat root growth, water uptake and grain yield. A computer simulation model. *Soil and Tillage Research*, 10, 331-345. doi: [https://doi.org/10.1016/0167-1987\(87\)90022-5](https://doi.org/10.1016/0167-1987(87)90022-5)
- Jeady C., *et al.*. (2016). RhizoTubes as a new tool for high throughput imaging of plant root development and architecture: Test, comparison with pot grown plants and validation. *Plant Methods BioMed Central*, 12(1), 1–18. doi: 10.1186/s13007-016-0131-9.
- Jin K., *et al.*, (2013). How do roots elongate in a structured soil?. *Journal of Experimental Botany*, 64(15), 4761–4777. doi: 10.1093/jxb/ert286.

- Jin K., *et al.*, (2015). The effect of impedance to root growth on plant architecture in wheat. *Plant and Soil*, 392(1–2), 323–332. doi: 10.1007/s11104-015-2462-0.
- Johnson D., Leake J.R. and Read D.J., (2001). Novel in-growth core system enables functional studies of grassland mycorrhizal mycelial networks. *New Phytol*, 152, 555–562.
- Johnson M., Tingey D., Phillips D. and Storm M., (2001). Advancing fine root research with minirhizotrons. *Environmental and Experimental Botany*, 45(3), 263–289.
- Jones V.A.S. and Dolan L., (2012). The evolution of root hairs and rhizoids. *Ann Bot*, 110, 205–212.
- Joslin J.D. and Wolfe M.H., (1999). Disturbances during minirhizotron installation can affect root observation data. *Soil Sci Soc Am J.*, 63(1), 218–21.
- Kamiya M., *et al.*, (2016). Control of root cap maturation and cell detachment by BEARSKIN transcription factors in Arabidopsis. *The Company of Biologists*, 143, 4063–4072. doi: 10.1242/dev.142331.
- Karley A.J., Valentine T.A. and Squire G.R., (2011). Dwarf alleles differentially affect barley root traits influencing nitrogen acquisition under low nutrient supply. *J. Exp. Bot.*, 62(11), 3917–27. doi: 10.1093/jxb/err089.
- Kay B.D., da Silva A.P. and Baldock J.A., (1997). Sensitivity of soil structure to changes in organic carbon content: Predictions using pedotransfer functions. *Canadian Journal of Soil Science*, 77(4), 655–667. doi: 10.4141/S96-094.
- Kaya M.D., Okçub G., Ataka M., Çıkılıç Y. and Kolsarıcıa Ö., (2006). Seed treatments to overcome salt and drought stress during germination in sunflower (*Helianthus annuus* L.). *Eur. J. Agron.*, 24, 291–295.
- Keller T., *et al.*, (2015). SoilFlex-LLWR: Linking a soil compaction model with the least limiting water range concept. *Soil Use and Management*, 31(2), 321–329. doi: 10.1111/sum.12175.

- Keller T., Defossez P., Weisskopf P., Arvidsson J. and Richard G., (2007). SoilFlex: a model for prediction of soil stresses and soil compaction due to agricultural field traffic including a synthesis of analytical approaches. *Soil & Tillage Research*, 93, 391–411.
- Keyes S.D., Daly K.R., Gostling N.J., Jones D.L., Talboys P., Pinzer B.R., Boardman R., Sinclair I., Marchant A. and Roose T., (2013). High resolution synchrotron imaging of wheat root hairs growing in soil and image-based modelling of phosphate uptake. *New Phytologist*, 198, 1023–1029.
- Khan M.I.R., Fatma M., Per T.S., Anjum N.A. and Khan N.A., (2015). Salicylic acid induced abiotic stress tolerance and underlying mechanisms in plants. *Front Plant Sci.*, 6, 1–17.
- Kirby J.M. and Bengough A.G., (2002). Influence of soil strength on root growth: experiments and analysis using a critical-state model. *European Journal of Soil Science*, 53, 119–127.
- Klepper B. and Kaspar T.C., (1994). Symposium on Rhizosphere Research in Honour of Howard M. Taylor [A Collection of 7 papers]. *Agronomy Journal*, 86(5), 745–795. doi: 10.2134/agronj1994.00021962008600050002x.
- Kobaissi A.N., Kanso A.A., Kanbar H.J. and Kazpard V.A., (2013). Morphophysiological changes caused by soil compaction and irrigation on *Zea mays*. *Eurasian Journal of Soil Science*, 2, 114–121.
- Koebnick N., *et al.*, (2017). High-resolution synchrotron imaging shows that root hairs influence rhizosphere soil structure formation. *New Phytologist*. doi: 10.1111/nph.14705.
- Koevoets I.T., *et al.*, (2016). Roots withstanding their environment: Exploiting root system architecture responses to abiotic stress to improve crop tolerance. *Frontiers in Plant Science*, 7, 1–19. doi: 10.3389/fpls.2016.01335.
- Konôpka B., Pagès L. and Doussan C., (2009). Soil compaction modifies morphological characteristics of seminal maize roots. *Plant, Soil and Environment*, 55(1), 1–10.

Kramer-Walter K.R., Bellingham P.J., Millar T.R., Smissen R.D., Richardson S.J. and Laughlin D.C., (2016). Root traits are multidimensional: specific root length is independent from root tissue density and the plant economic spectrum. *Journal of Ecology*, 104, 1299–1310.

Kurz W.A., Beukema S.J. and Apps M.J., (1996). Estimation of root biomass and dynamics for the carbon budget model of the Canadian forest sector. *Can J For Res.*, 26, 1973–9. doi:10.1139/x26-223.

Landi P., Giuliani S., Salvi S., Ferri M., Tuberosa R. and Sanguineti, M.C., (2010). Characterization of root–yield–1.06, a major constitutive QTL for root and agronomic traits in maize across water regimes. *J. Exp. Bot.*, 61, 3553–3562.

Lang I., *et al.*, (2014). Plasmolysis: Loss of turgor and beyond. *Plants*, 3(4), 583–593. doi: 10.3390/plants3040583.

Lawlor D.W. and Cornic G., (2002). Photosynthetic carbon assimilation and associated metabolism in relation to water deficits in higher plants. *Plant Cell and Environment*, 25, 275-294. doi:10.1046/j.0016-8025.2001.00814.x.

Lazorenic B., Sturrock C.J., Poljak M., Mooney S.J., (2016). Quantification of Aluminium-induced changes in wheat root architecture by x-ray micro-computed tomography. *Communications in Soil Science and plant Analysis*, 47, 263–274.

Le Marié C., *et al.*, (2014). Rhizoslides: Paper-based growth system for non-destructive, high throughput phenotyping of root development by means of image analysis. *Plant Methods*, 10(1), 1–16. doi: 10.1186/1746-4811-10-13.

Le Marie C., Kirchgessner N., Flußsch P., Pfeifer J., Walter A. and Hund A., (2016). RADIX: rhizoslide platform allowing high throughput digital image analysis of root system expansion. *Plant Methods*, 12, 40.

Le Marie C., Kirchgessner N., Marschall D., Walter A. and Hund A., (2014). Rhizoslides: Paper-based growth system for non-destructive, high throughput phenotyping of root

development by means of image analysis. *Plant Methods*, 10, 13. doi:10.1186/1746-4811-10-13.

Leitner D., Felderer B., Vontobel P. and Schnepf A., (2014). Recovering root system traits using image analysis exemplified by two-dimensional neutron radiography images of lupine. *Plant Physiol.*, 164, 24–35.

Leitner D., Klepsch S., Ptashnyk M., Marchant A., Kirk G.J.D., Schnepf A, Roose T., (2010). A dynamic model of nutrient uptake by root hairs. *New Phytologist*, 185, 792–802.

Letey J., (1985). Relationship between soil physical properties and crop production. *Adv Soil Sci*, 1, 277–294.

Li C.H. and Lee C.K., (1993). Minimum cross entropy thresholding. *Pattern Recognition*, 26(4), 617–625. doi: 10.1016/0031-3203(93)90115-D.

Li L., Zhang Q. and Huang D., (2014). A Review of Imaging Techniques for Plant Phenotyping. 20078–20111. doi: 10.3390/s141120078.

Li Q., Sone S. and Doi K., (2003). Selective enhancement filters for nodules, vessels, and airway walls in two- and three-dimensional CT scans. *Med Phys.*, 30(8), 2040-51. doi: 10.1118/1.1581411.

Li S., *et al.*, (2015). A dynamic root simulation model in response to soil moisture heterogeneity. *Mathematics and Computers in Simulation*, 113, 40–50. doi: 10.1016/j.matcom.2014.11.030.

Liao R.W., Liu J.M., An S.Q., Niu J.L., Liang H., Ren R.X., Le Z.Y., Cao Y.J. and Li W.J., (2010). Monitor of corn root growth in soil based on minirhizotron technique. *Trans CSAE*, 26, 156–161.

Lipiec J., *et al.*, (2012). Effects of soil compaction on root elongation and anatomy of different cereal plant species. *Soil and Tillage Research*, 121, 74–81. doi: 10.1016/j.still.2012.01.013.

- Lipiec J., *et al.*, (2016). Effect of sand grain shape on root and shoot growth of wheat seedlings. *Geoderma*, 265, 1–5. doi: 10.1016/j.geoderma.2015.10.022.
- Loades K.W., *et al.*, (2015). Effect of root age on the biomechanics of seminal and nodal roots of barley (*Hordeum vulgare* L.) in contrasting soil environments. *Plant and Soil*, 395(1–2), 253–261. doi: 10.1007/s11104-015-2560-z.
- Lobet G., *et al.*, (2014). Plant water uptake in drying soils. *Plant Physiology*, 164(4), 1619–1627. doi: 10.1104/pp.113.233486.
- Lobet G., *et al.*, (2017). Using a structural root system model to evaluate and improve the accuracy of root image analysis pipelines. *Frontiers in Plant Science*, 8, 1–11. doi: 10.3389/fpls.2017.00447.
- Lu W., Wang X. and Wang F., (2019). Adaptive minirhizotron for pepper roots observation and its installation based on root system architecture traits. *Plant Methods*. BioMed Central, 15(1), 1–14. doi: 10.1186/s13007-019-0414-z.
- Lynch J. P. and Brown K. M., (2001). Topsoil foraging - An architectural adaptation of plants to low phosphorus availability. *Plant Soil*, 237, 225–237. doi: 10.1023/A:1013324727040.
- Lynch J., (1995). Root architecture and plant productivity. *Plant Physiol.*, 109, 7–13.
- Lynch J.P., (2019). Root phenotypes for improved nutrient capture: an underexploited opportunity for global agriculture. *New Phytologist*, 223(2), 548–564. doi: 10.1111/nph.15738.
- Lynch J.P., Chimungu J.G. and Brown K.M., (2014). Root anatomical phenes associated with water acquisition from drying soil: targets for crop improvement. *Journal of Experimental Botany*, 65, 6155–6166.
- Ma L., *et al.*, (2019). Hydrogel-based transparent soils for root phenotyping in vivo. *Proceedings of the National Academy of Sciences of the United States of America*, 166(22), 11063–11068. doi: 10.1073/pnas.1820334116.

- Mancuso S. and Marras, A.M., (2006). Adaptive response of *Vitis* root to anoxia. *Plant Cell Physiol.*, 47(3), 401-9. doi: 10.1093/pcp/pcj007.
- Materechera S.A., Dexter A.R. and Alston A.M., (1991). Penetration of very strong soils by seedling roots of different plant species. *Plant Soil.* 135, 31–41.
- Mathieu L., Lobet G., Tocquin P. and Périlleux C., (2015). “Rhizoponics”: a novel hydroponic rhizotron for root system analyses on mature *Arabidopsis thaliana* plants. *Plant Methods*, 11, 3. doi: 10.1186/s13007-015-0046-x
- McDougall W.B., (1916). The growth of forest tree roots. *Amer. J. Bot.*, 3384392.
- McKenzie B., Bengough A., Hallett P., Thomas W., Forster B. and McNicol J., (2009). Deep rooting and drought screening of cereal crops: a novel field-based method and its application. *Field Crops Research*, 112(2), 165-171. doi: 10.1016/j.fcr.2009.02.012.
- Mckenzie B.M., *et al.*, (2013). Root-soil friction: Quantification provides evidence for measurable benefits for manipulation of root-tip traits. *Plant, Cell and Environment*, 36(6), 1085–1092. doi: 10.1111/pce.12037.
- McPhee K., (2005). Variation for seedling root architecture in the core collection of pea germplasm. *Crop Sci.*, 45, 1758–63.
- McWilliams D., (2003). Drought Strategies for Cotton, Cooperative Extension Service Circular 582, College of Agriculture and Home Economics, New Mexico State University, USA.
- Meister R, Rajani M.S., Ruzicka D., Schachtman D.P., (2014). Challenges of modifying root traits in crops for agriculture. *Trends Plant Sci*, 19, 779–788.
- Metzner R., *et al.*, (2015). Direct comparison of MRI and X-ray CT technologies for 3D imaging of root systems in soil: Potential and challenges for root trait quantification. *Plant Methods*, 11, 17.

Mohammadi M.H., Asadzadeh F. and Vanclooster M., (2010). Refining and unifying the upper limits of the least limiting water range using soil and plant properties. *Plant and Soil*, 334(1), 221–234. doi: 10.1007/s11104-010-0377-3.

Möller B., Chen H., Schmidt T., Zieschank A., Patzak R., Türke M., Weigelt A. and Posch S., (2019). rhizoTrak: a flexible open source Fiji plugin for user-friendly manual annotation of time-series images from minirhizotrons. *Plant and Soil volume*, 444, 519–534.

Moreno P. and Calderero F., (2013). Evaluation of Sharpness Measures and Proposal of a Stop Criterion for Reverse Diffusion in the Context of Image Deblurring. In Proceedings of the International Conference on Computer Vision Theory and Applications - Volume 1: VISAPP, 69-77, 2013 , Barcelona, Spain.

Moreno-Espindola I.P., Rivera-Becerril F., de Jesus Ferrara-Guerrero M. and DeLeon-Gonzalez F., (2007). Role of root-hairs and hyphae in adhesion of sand particles. *Soil Biology and Biochemistry*, 39, 2520–2526.

Nagel K.A., Kastenholz B., Jahnke S., van Dusschoten D., Aach T., Mühlich M., Truhn D., Scharr H., Terjung S., Walter A. and Schurr U., (2009). Temperature responses of roots: impact on growth, root system architecture and implications for phenotyping. *Functional Plant Biology*, 36, 947-959. doi: <https://doi.org/10.1071/FP09184>.

Nagel K.A., Putz A., Gilmer F., Heinz K., Fischbach A., Pfeifer J., *et al.*, (2012). GROWSCREEN-Rhizo is a novel phenotyping robot enabling simultaneous measurements of root and shoot growth for plants grown in soil-filled rhizotrons. *Funct Plant Biol.*, 39, 891–904.

Nakajima Y., Nara Y., Kobayashi A., Sugita T., Miyazawa Y., Fujii N., *et al.*, (2017). Auxin transport and response requirements for root hydrotropism differ between plant species. *J Exp Bot.*, 68(13), 3441-3456. doi: 10.1093/jxb/erx193.

Narayanan S., Mohan A., Gill K.S., Prasad P.V.V., (2014). Variability of root traits in spring wheat germplasm. *PLoS ONE*, 9, 0100317.

- Narukawa M., Kanbara K., Tominaga Y., Aitani Y., Fukuda K., Kodama T., *et al.*, (2009). Chlorogenic acid facilitates root hair formation in lettuce seedlings. *Plant Cell Physiol.*, 50, 504–14.
- Nassar N. and Ortiz R., (2007). Cassava improvement: challenges and impacts. *The Journal of Agricultural Science*, 145(2), 163 – 171.
- Nater E.A., Nater K.D. and Baker J.M. (1992). Application of artificial neural system algorithms to image analysis of roots in soil. *Geoderma*, 53, 237–253.
- Newman E.I., (1966). A method for estimating the total length of root in a sample. *J. Appl. Ecol.*, 3, 139–145.
- Newton A.C., *et al.*, (2020). Identifying spring barley cultivars with differential response to tillage. *Agronomy*, 10(5), 1–18. doi: 10.3390/agronomy10050686.
- Nguyen V.L. and Stangoulis J., (2019). Variation in root system architecture and morphology of two wheat genotypes is a predictor of their tolerance to phosphorus deficiency. *Acta Physiologiae Plantarum*. Springer Berlin Heidelberg, 41(7), p. 1–13. doi: 10.1007/s11738-019-2891-0.
- Nielsen, K.L., Lynch J.P. and Weiss H.N., (1997). Fractal geometry of bean root systems: Correlations between spatial and fractal dimension. *Am. J. Bot.*, 84, 26–33.
- Niklas K.J., (1992). Plant biomechanics: an engineering approach to plant form and function. Chicago: The University of Chicago Press.
- O’Callaghan F.E., Braga R.A., Neilson R., *et al.*, (2018). New live screening of plant-nematode interactions in the rhizosphere. *Sci Rep*, 8(1440). doi: <https://doi.org/10.1038/s41598-017-18797-7>.
- Olibone D., Encide-Olibone A.P. and Rosolem C.A., (2010). Least limiting water range and crop yields as affected by crop rotations and tillage. *Soil Use and Management*, 26(4), 485–493. <https://doi.org/10.1111/j.1475-2743.2010.00301.x>.

Pace J., Lee N., Naik H.S., Ganapathysubramanian B. and Lübberstedt T., (2014). Analysis of maize (*Zea mays* L.) seedling roots with the high-throughput image analysis tool ARIA (Automatic Root Image Analysis). *PLoS ONE*, 9, e108255.

Paez-Garcia A., *et al.*, (2015). Root traits and phenotyping strategies for plant improvement. *Plants*, 4(2), 334–355. doi: 10.3390/plants4020334.

Pagliai M. and Vignozzi N., (2002). Image Analysis and Microscopic Techniques to Characterize Soil Pore System. In: Blahovec J., Kutílek M. (eds) *Physical Methods in Agriculture*. Springer, Boston, MA.

Pan J.W., Zhu M.Y. and Chen H., (2001). Aluminum-induced cell death in root tips of barley. *Environ. Exp. Bot*, 46, 71–79.

Paya A.M., *et al.*, (2015). X-ray computed tomography uncovers root–root interactions: Quantifying spatial relationships between interacting root systems in three dimensions. *Frontiers in Plant Science*, 6, 1–12. doi: 10.3389/fpls.2015.00274.

Péret B., Clément M., Nussaume L. and Desnos T., (2011). Root developmental adaptation to phosphate starvation: better safe than sorry. *Trends Plant Sci.*, 16, 442–450. doi: 10.1016/j.tplants.2011.05.006.

Perfect E, Groenevelt P.H., Kay B.D. and Grant C.D., (1990). Spatial variability of soil penetrometer measurements at the mesoscopic scale. *Soil & Tillage Research*, 16 257–271.

Peterson R.L. and Farquhar M.L., (1996). Root hairs: specialized tubular cells extending root surfaces. *Bot Rev*, 62, 1–40.

Peuke A.D., Hartung W., Schraml C. and Rennenberg H., (2002). Identification of drought sensitive beech ecotypes by physiological parameters. *New Phytol.* 154, 373–388.

Pierret A., Gonkhamdee S., Jourdan C. and Maeght J.L., (2013). II\_Rhizo: an open-source software to measure scanned images of root samples. *Plant Soil*, 373, 531–539. doi: <https://doi.org/10.1007/s11104-013-1795-9>

Pineros M.A., Larson B.G., Shaff J.E., Schneider D.J., Falcao A.X., Yuan L., Clark R.T., Craft E.J., Davis T.W., Pradier P.L., *et al.*, (2015). Evolving technologies for growing, imaging and analyzing 3D root system architecture of crop plants. *J Integr Plant Biol*, 58, 230-241.

Pitman M.G., (1969). Adaptation of barley roots to low oxygen supply and its relation to potassium and sodium uptake. *Plant Physiology*, 44, 1233–1240.

Poorter H., *et al.*, (2012). Pot size matters: A meta-analysis of the effects of rooting volume on plant growth. *Functional Plant Biology*, 39(11), pp. 839–850. doi: 10.1071/FP12049.

Poorter H., Niklas K.J., Reich P.B., Oleksyn J., *et al.*, (2012). Biomass allocation to leaves, stems and roots: meta-analyses of interspecific variation and environmental control. *New Phytologist*, 193(1), 30–50.

Portas C.A.M. and Taylor H.M., (1976). Growth and survival of young plant roots in dry soil. *Soil Science*, 121, 170–175.

Pound M.P., French A.P., Atkinson J.A., *et al.*, (2013). RootNav: navigating images of complex root architectures. *Plant Physiol*, 162, 1802–1814. doi: <https://doi.org/10.1104/pp.113.221531>.

Raaijmakers J.M., Paulitz, T.C., Steinberg C., Alabouvette C. and Moenne-Loccoz Y., (2009). The rhizosphere: a playground and battlefield for soilborne pathogens and beneficial microorganisms. *Plant and Soil*, 321, 341–361.

Rafalski J.A., (2010). Association genetics in crop improvement. *Curr Opin Plant Biol*, 13, 174–180.

Raghothama K. and Karthikeyan A., (2005). Phosphate acquisition in Root physiology: From gene to function. New York: Springer, 37–49.

Rahmanzadeh B.H. and Shojaedini S. (2016). Novel automated method for minirhizotron image analysis: Root detection using curvelet transform. *International Journal of Engineering*, 29(3), 337-346.

- Ravenek J.M., Mommer L., Visser E.J.W., van Ruijven J., van der Paauw J.W., Smit-Tiekstra A., de Caluwe H. and de Kroon H., (2016). Linking root traits and competitive success in grassland species. *Plant and Soil*, 407, 39–53.
- Redjala T., Zelko I., Sterckeman T., Legue V. and Lux A., (2011). Relationship between root structure and root cadmium uptake in maize. *Environmental and Experimental Botany*, 71, 241–248.
- Rewald B. and Ephrath J.E., (2013). Minirhizotron techniques. *Plant roots: The hidden half* 42, 1–15.
- Richard C.A.I., *et al.*, (2015). High-throughput phenotyping of seminal root traits in wheat. *Plant Methods*, 11(1), 1–11. doi: 10.1186/s13007-015-0055-9.
- Richards R.A., Condon A.G. and Rebetzke G.J., (2001). Traits to improve yield in dry environments. In *Application of Physiology in Wheat Breeding*, p. 88–100.
- Robbins, N.E. and Dinneny J.R., (2015). The divining root: Moisture-driven responses of roots at the micro-and macro-scale. *J. Exp. Bot.*, 10, 1–10.
- Roberts J.A., Hussain A., Taylor I.B. and Black C.R., (2002). Use of mutants to study long-distance signalling in response to compacted soil. *Journal of Experimental Botany*, 53 45–50.
- Rogers E.D. and Benfey P.N., (2015). Regulation of plant root system architecture: implications for crop advancement. *Curr Opin Biotechnol*, 32(32C), 93–8.
- Rogers H.H. and Bottomley P.A., (1987). In situ nuclear magnetic resonance imaging of roots: influence of soil type, ferromagnetic particle content, and soil water. *Agron J.* 1987, 79(6), 957.
- Roose T. and Schnepf A., (2008). Mathematical models of plant–soil interaction. *Phil. Trans. R. Soc. A.*, 366, 4597–4611. doi: <http://doi.org/10.1098/rsta.2008.0198>.
- Rose L. and Lobet G., (2019). Accuracy of image analysis tools for functional root traits: A comment on Delory *et al.* (2017). *Methods in Ecology and Evolution*, 10(5), 702–711. doi: 10.1111/2041-210X.13156.

- Ross P.J., Williams J. and Bristow K.L., (1991). Equations for extending water-retention curves to dryness. *Soil Science Society of America Journal*, 55, 923–927.
- Rucker K.S., Kvien C.K., Holbrook C.C. and Hook J.E., (1995). Identification of peanut genotypes with improved drought avoidance traits. *Peanut Sci.*, 24, 14–18. doi: 10.3146/pnut.22.1.0003.
- Ryan P.R., *et al.*, (2016). Plant roots: Understanding structure and function in an ocean of complexity. *Annals of Botany*, 118(4), 555–559. doi: 10.1093/aob/mcw192.
- Sadras V.O. and Lawson C., (2013). Nitrogen and water-use efficiency of Australian wheat varieties released between 1958 and 2007. *European Journal of Agronomy*, 46, 34–41.
- Sadras V.O. and Richards R.A., (2014). Improvement of crop yield in dry environments: Benchmarks, levels of organisation and the role of nitrogen. *Journal of Experimental Botany*, 65(8), 1981–1995. doi: 10.1093/jxb/eru061.
- Samson B.K. and Sinclair T.R., (1994). Soil core and minirhizotron comparison for the determination of root length density. *Plant Soil.*, 161(2), 225–32.
- Savitzky A. and Golay M.J.E., (1964). Smoothing and Differentiation of Data by Simplified Least Squares Procedures. *Analytical Chemistry*, 36 (8), 1627–39. doi:10.1021/ac60214a047.
- Schimel J., Balsler T.C. and Wallenstein M., (2007). Microbial stress response physiology and its implications for ecosystem function. *Ecology*, 88, 1386–1394. doi: 10.1890/06-0219.
- Schmidt W., (2014). Root systems biology, *Frontiers in Plant Science*, 5, 1–2. doi: 10.3389/fpls.2014.00215.
- Schoppach R.M., Wauthélet D., Jeanguenin L. and Sadok W., (2013). Conservative water use under high evaporative demand associated with smaller root metaxylem and limited transmembrane water transport in wheat. *Funct Plant Biol*, 41, 257–269.
- Segal E., Kushnir T., Mualem Y. and Shani U., (2008). Microsensing of water dynamics and root distributions in sandy soils. *Vadose Zone J.*, 7, 1018–1026.

Segal E., Kushnir T., Mualem Y. and Shani U., (2008). Water uptake and hydraulics of the root hair rhizosphere. *Vadose Zone J*, 7, 1027–1034.

Sharp R.E., Silk W.K. and Hsiao T.C., (1988). Growth of maize primary root at low water potentials. I. Spatial distribution of expansive growth. *Plant Physiol.*, 87, 50-57.

Shearman V.J., Sylvester-Bradley R., Scott R.K., Foulkes M.J., (2005). Physiological processes associated with wheat yield progress in the UK. *Crop Science*, 45, 175–185

Shojaedini S. and Heidari M. (2013). A new method for root detection in minirhizotron images: Hypothesis testing based on entropy-based geometric level set decision. *International Journal of Engineering-Transactions A: Basics*, 27(1), 91.

Siegel-Issem C.M., Burger J.A., Powers R.F., Ponder F. and Patterson S.C., (2005). Seedling root growth as a function of soil density and water content. *Soil Sci Soc Am J*, 69, 215–226.

Silva A.P., Tormena C.A., Jonez F. and Imhoff S., (2008). Funcoes de pedotransferencia para as curvas de retencao de agua e de resistencia do solo a penetracao [Pedotransfer functions for the soil water retention and soil resistance to penetration curves]. *Revista Brasileira de Ciencia do Solo*, 32, 1–10.

Silva-Navas J., Moreno-Risueno M.A., Manzano C., Pallero-Baena M., NavarroNeila S., Téllez-Robledo B., *et al.*, (2015). D-Root: a system for cultivating plants with the roots in darkness or under different light conditions. *Plant J.*, 84, 244–255. doi: 10.1111/tpj.1299.

Singh V., van Oosterom E.J., Jordan D.R., Messina C.D., Cooper M. and Hammer G.L., (2010). Morphological and architectural development of root systems in sorghum and maize. *Plant Soil*, 333, 287–299.

Smit A.L., Bengough A.G., Engels C., van Noordwijk M., *et al.*, (2000). Root methods: a handbook. Springer Berlin Heidelberg.

Smith S. and De Smet I., (2012). Root system architecture: insights from Arabidopsis and cereal crops. *Phil Trans R. Soc B.*, 367, 1441–1452.

Smith P., *et al.*, (1979). Otsu\_1979\_otstu\_method. *IEEE Transactions on Systems, Man, and*  
228

*Cybernetics*, C(1), p. 62–66. doi: 10.1109/TSMC.1979.4310076.

Soileau J.M., Mays D.A., Khasawne F.E. and Kilmer V.J., (1974). Rhizotron-lysimeter research facility at TVA, Muscle-Shoals, Alabama. *Agron. J.*, 66828832.

Solh M. and van Ginkel M., (2014). Drought preparedness and drought mitigation in the developing World's drylands. *Weather Clim Extrem*, 3, 62–6.

Solís M.A. and Lang J., (2012). Skeleton pruning by contour approximation and the integer medial axis transform. *Computers and Graphics* (Pergamon), 36(5), 477–487. doi: 10.1016/j.cag.2012.03.029.

Somasundaram S., *et al.*, (2009). Rhizodeposition of mucilage, root border cells, carbon and water under combined soil physical stresses in *Zea mays* L. *Plant Production Science*, 12(4), 443–448. doi: 10.1626/pps.12.443.

Srivastava M. and Misra P., (2018). Climate Change: Impact on Plants. p. 165. Available at: <https://www.researchgate.net/publication/334696846>.

Stanca A.M., Gianinetti A., Rizza F. and Terzi V., (2016). Barley: an overview of a versatile cereal grain with many food and feed uses. In: Wrigly C (ed) *Encyclopedia of food grains*, 2nd edn. Academic Press, Oxford, p. 147–152.

Stein M. and Nothnagel Th., (1995). Some remarks on carrot breeding (*Daucus carota sativus* Hoffm.). *Plant Breeding*, 114(1), 1-11.

Stockman G., Smucker A.J.M. and Halgren R., (1990). Processing images of complex root systems. In *Abstr., Conf. Analytical Methods for Quantifying Root and Soil Dynamics*, 13–14, 18.

Subramanian R., Spalding E.P. and Ferrier N.J., (2013). A high throughput robot system for machine vision based plant phenotype studies. *Mach Vis Appl*, 24, 619-636.

Svačina P., Středa T. and Chloupek O., (2014). Uncommon selection by root system size increases barley yield. *Agron Sustain Dev.*, 34, 545–51.

- Svane S. F., *et al.*, (2019). A multispectral camera system for automated minirhizotron image analysis. *Plant and Soil*, 441(1–2), 657–672. doi: 10.1007/s11104-019-04132-8.
- Svistoonoff S., Creff A., Reymond M., Sigoillot-Claude C., Ricaud L., Blanchet A., *et al.*, (2007). Root tip contact with low-phosphate media reprograms plant root architecture. *Nat. Genet.*, 39, 792–796. doi: 10.1038/ng2041.
- Taiz L. and Zeiger E., (2006). *Plant physiology*. Sinauer Associates, Sunderland.
- Taylor B.N., Beidler K.V., Strand A.E., *et al.*, (2014). Improved scaling of minirhizotron data using an empirically-derived depth of field and correcting for the underestimation of root diameters. *Plant Soil*, 374(1–2), 941–8.
- Taylor H., Upchurch D., Brown J. and Rogers H., (1991). Some methods of root investigations. In: *Developments in Agricultural and Managed Forest Ecology*. Elsevier, 24, 553–564.
- Taylor H.M. and Ratliff L.F., (1969). Root elongation rates of cotton and peanuts as a function of soil strength and soil water content. *Soil Science*, 108, 113–119.
- Teixeira A., *et al.*, (2020). Myxospermous seed-mucilage quantity correlates with environmental gradients indicative of water-deficit stress: Plantago species as a model. *Plant and Soil*, 446(1–2), p. 343–356. doi: 10.1007/s11104-019-04335-z.
- Tennant D., (1975). A test of a modified line-intersect method of estimating root length. *J. Ecol.*, 63, 995–1101.
- Tester M. and Langridge P., (2010). Breeding technologies to increase crop production in a changing world. *Science*, 327(5967), 818-822.
- Tian X. and Doerner P., (2013). Root resource foraging: does it matter? *Front. Plant Sci.* 4, 303. doi: 10.3389/fpls.2013.00303.
- Tilman D., Balzer C., Hill J. and Befort B.L., (2011). Global food demand and the sustainable intensification of agriculture. *PNAS*, 108(50), 20260-20264;

Tormena C.A., Silva A.P. and Libardi P.L., (1999). Soil physical quality of a Brazilian Oxisol under two tillage systems using the least limiting water range. *Soil & Tillage Research*, 52, 223–232.

Tötzke C., *et al.*, (2017). Capturing 3D Water Flow in Rooted Soil by Ultra-fast Neutron Tomography. *Scientific Reports*, 7(1), 1–9. doi: 10.1038/s41598-017-06046-w.

Trachsel S., Kaeppler S.M., Brown K.M. and Lynch J.P., (2011). Shovelomics: high throughput phenotyping of maize (*Zea mays* L.) root architecture in the field. *Plant Soil*, 341, 75–87.

Trachsel S., Kaeppler S.M., Brown K.M. and Lynch J.P., (2013). Maize root growth angles become steeper under low N conditions. *Fields Crop Res*, 140, 18–31.

Tracy S.R., Black C.R., Roberts J.A., Sturrock C., Mairhofer S., Craigan J., *et al.*, (2012). Quantifying the impact of soil compaction on root system architecture in tomato (*Solanum lycopersicum*) by X-ray micro-computed tomography. *Annals of Botany Plant and Soil*, 353, 195–208.

Tracy S.R., Roberts J.A., Black C.R., McNeill A., Davidson R. and Mooney S.J., (2010). The X-factor: visualizing undisturbed root architecture in soils using X-ray computed tomography. *Journal of Experimental Botany*, 61, 311–313.

Tran T.M, MacIntyre A., Hawes M. and Allen C., (2016). Escaping Underground Nets: Extracellular DNases Degrade Plant Extracellular Traps and Contribute to Virulence of the Plant Pathogenic Bacterium *Ralstonia solanacearum*. *PLoS Pathog*, 12(6): e1005686. doi:10.1371/journal.ppat.1005686

Trenberth K.E., (2011). Changes in precipitation with climate change. *Clim. Res.*, 47, 123–138. doi: <https://doi.org/10.3354/cr00953>.

Tuberosa R., Sanguineti M.C., Landi P., Giuliani M.M., Salvi S. and Conti S., (2002). Identification of QTLs for root characteristics in maize grown in hydroponics and analysis of

their overlap with QTLs for grain yield in the field at two water regimes. *Plant Mol. Biol.*, 48, 697–712.

Uga Y., Sugimoto K., Ogawa S., Rane J., Ishitani M., Hara N., Kitomi Y., Inukai Y., Ono K., Kanno N., Inoue H., Takehisa H., Motoyama R., Nagamura Y., Wu J., Matsumoto T., Takai T., Okuno K. and Yano M., (2013). Control of root system architecture by DEEPER ROOTING 1 increases rice yield under drought conditions. *Nature Genetics*, 45, 1097–1102. doi: 10.1038/ng.2725.

United Nations Department of Economic and Social Affairs, Population Division, (2015). World Population Prospects, the 2015 Revision. <http://esa.un.org/unpd/wpp> accessed 13/09/17.

United Nations, (2015). Sustainable Development Goals. <http://www.un.org/sustainabledevelopment/hunger> accessed 13/09/17

Upchurch D.R. and Ritchie J.T., (1983). Root observations using a video recording system in mini-rhizotrons. *Agron J.*, 75(6), 1009–15.

Upchurch D.R., (1987). Conversion of minirhizotron-root intersections to root length density. In: Minirhizotron observation tubes: methods and applications for measuring rhizosphere dynamics.

Valentine T.A., *et al.*, (2012). Soil strength and macropore volume limit root elongation rates in many UK agricultural soils. *Annals of botany*, 110(2), 259–270. doi: 10.1093/aob/mcs118.

Vamerali T., Bandiera M., Mosca G., (2012). Minirhizotrons in modern root studies. In: Measuring roots: an updated approach. *Springer Berlin Heidelberg*, Berlin, 341–361.

Vamerali T., *et al.*, (1999). An approach to minirhizotron root image analysis. *Plant and Soil*, 217(1–2), 183–193. doi: 10.1007/978-94-017-3469-1\_31.

Van der Weerd L., Claessens M.M.A.E, Ruttink T., Vergeldt F.J., Schaafsma T.J. and Van As H. (2001): Quantitative NMR microscopy of osmotic stress responses in maize and pearl millet. *J Exp Bot*, 52(365), 2333–2343.

Van Dusschoten D., Metzner R., Kochs J., Postma J.A., Pflugfelder D., Bühler J., Schurr U. and Jahnke S. (2016). Quantitative 3D analysis of plant roots growing in soil using magnetic resonance imaging. *Plant Physiol*, 170, 1176-1188.

Van Genuchten M.T., 1980. A closed-form equation for predicting the hydraulic conductivity of unsaturated soils. *Soil Science Society of America Journal*, 44, 892–898.

Van Noordwijk M., Brouwer G., Meijboom F., *et al.*, (2000). Trench profile techniques and core break methods. *Root methods a Handb.*, 211–233.

Vicré M., *et al.*, (2005). Root Border-Like Cells of Arabidopsis. Root Border-Like Cells of Arabidopsis. Microscopical Characterization and Role in the Interaction with Rhizobacteria. *Plant Physiology*, 138, 998–1008. doi: 10.1104/pp.104.051813.As.

Vincent C., Rowland D., Na C. and Schaffer B., (2017). A high-throughput method to quantify root hair area in digital images taken in situ. *Plant and Soil*, 412, 61–80.

Violle C., Violle M.L., Navas D., Vile E., Kazakou C., Fortunel I. and Hummel G., (2007). Garnier Let the concept of trait be fonctionnal! *Oikos*, 116, p. 882-892 <https://doi.org/10.1111/j.2007.0030-1299.15559.x>

Vitousek P.M., Naylor R., Crews T., David M.B., Drinkwater L.E., Holland E., *et al.*, (2009). Nutrient imbalances in agricultural development. *Science*, 324, 1519–1520 <https://doi.org/10.1126/science.1170261>.

Voesenek L.A.C.J. and Sasidharan R., (2013). Ethylene—and oxygen signalling—drive plant survival during flooding. *Plant Biol.*, 15, 426–435. doi: <https://doi.org/10.1111/plb.12014>.

Vollsnes A.V., Futsaether C.M. and Bengough A.G., (2010). Quantifying rhizosphere particle movement around mutant roots using time-lapse imaging and particle image velocimetry. *European Journal of Soil Science*, 61, 926–939.

Walker J.M., (2009). *High-Throughput phenotyping in plants*, *Life Sciences*. doi: 10.1007/978-1-62703-239-1\_1.

- Walter A., Liebisch F. and Hund A., (2015). Plant phenotyping: from bean weighing to image analysis. *Plant Methods*, 11, 14. doi: <https://doi.org/10.1186/s13007-015-0056-8>.
- Wang H., *et al.*, (2013). Modeling the Soil Water Retention Curves of Soil-Gravel Mixtures with Regression Method on the Loess Plateau of China. *PLoS ONE*, 8(3), pp. 1–11. doi: 10.1371/journal.pone.0059475.
- Wang M., Ben and Zhang Q., (2009). Issues in using the WinRHIZO system to determine physical characteristics of plant fine roots. *Ecological Society of China.*, 29(2), 136–138. doi: 10.1016/j.chnaes.2009.05.007.
- Wang X., *et al.*, (2021). Wheat growth responses to soil mechanical impedance are dependent on phosphorus supply. *Soil and Tillage Research*, p. 104754. doi: 10.1016/j.still.2020.104754.
- Wang Y.N., Jiang H., Wang Y., Mang D.W., Li X.X. and Wang L.S., (2013). Response of mung bean root border cells to cadmium in relation to their status. *Acta Pedologica Sinica*, 50, 165-170.
- Wang Y.S, Jensen L.S and Magid J., (2016). Differential responses of root and root hair traits of spring wheat genotypes to phosphorus deficiency in solution culture. *Plant Soil Environ*, 62, 540–546.
- Wasaya A., *et al.*, (2018). Root Phenotyping for Drought Tolerance : A Review, p. 1–19. doi: 10.3390/agronomy8110241.
- Wasson A., Bischof L., Zwart A. and Watt M. (2016). A portable fluorescence spectroscopy imaging system for automated root phenotyping in soil cores in the field. *J Exp Bot*, 67, 1033-1043.37.
- Wasson A., Rebetzke G., Kirkegaard J., Christopher J., Richards R. and Watt M., (2014). Soil coring at multiple field environments can directly quantify variation in deep root traits to select wheat genotypes for breeding. *J. Exp. Bot.*, 65, 6231–6249.

Wasson A.P., *et al.*, (2012). Traits and selection strategies to improve root systems and water uptake in water-limited wheat crops. *Journal of Experimental Botany*, 63(9), 3485–3498. doi: 10.1093/jxb/ers111.

Weemstra M., Mommer L., Visser E.J.W., Ruijven J., Kuyper T.W., Mohren G.M.J. and Sterck F.J., (2016). Towards a multidimensional root trait framework: a tree root review. *New Phytologist*, 211, 1159–1169.

Wells C.E. and Eissenstat D.M., (2001). Marked differences in survivorship among apple roots of different diameter. *Ecology*, 82, 882–892.

Wen W.L, Guo X.Y, Zhao C.J, *et al.*, (2015). Crop roots configuration and visualization: a review. *Sci Agric Sin.*, 48, 436–48.

Whalley W.R, Leeds-Harrison P.B, Clark L.J. and Gowing D.J.G., (2005). Use of effective stress to predict the penetrometer resistance of unsaturated agricultural soils. *Soil and Tillage Research*, 84, 18–27.

Whalley W.R., Bengough A.G. and Dexter A.R., (1998). Water stress induced by PEG decreases the maximum growth pressure of the roots of pea seedlings. *Journal of Experimental Botany*, 49, 1689–1694.

Whalley W.R., Clark L.J., Gowing D.J.G., *et al.*, (2006). Does Soil Strength Play a Role in Wheat Yield Losses Caused by Soil Drying?. *Plant Soil*, 280, 279–290. doi: <https://doi.org/10.1007/s11104-005-3485-8>.

Whalley W.R., Clark L.J., Take W.A., Bird N.R.A., Leech P.K., Cope R.E. and Watts C.W., (2007). A porous-matrix sensor to measure the matric potential of soil water in the field. *European Journal of Soil Science*, 58, 18–25.

Whalley W.R., Watts C.W., Gregory A.S., Mooney S.J., Clark L.J. and Whitmore A.P., (2008). The effect of soil strength on the yield of wheat. *Plant and Soil*, 306, 237–247.

White P.J., George T.S., Gregory P.J., Bengough A.G., Hallett P.D. and McKenzie B.M., (2013). Matching roots to their environment. *Ann Bot*, 112, 207–22.

Whiteley G.M. and Dexter A.R., (1982). Root development and growth of oilseed, wheat and pea crops on tilled and non-tilled soil. *Soil & Tillage Research*, 2, 379–393.

Whitmore A.P. and Whalley W.R., (2009). Physical effects of soil drying on roots and crop growth, 60(10), 2845–2857. doi: 10.1093/jxb/erp200.

Wilcox R.R., (2017). *Modern Statistics for the Social and Behavioral Sciences: A Practical Introduction*, 2nd Ed., CRC press, ISBN: 978-1-4987-9678-1.

Wise R.R., Olson A.J., Schrader S.M. and Sharkey T.D., (2004). Electron transport is the functional limitation of photosynthesis in field-grown Pima cotton plants at high temperature. *Plant Cell & Environment*, 27, 717-724.

World Hunger Organisation, (2016). World Hunger and Poverty Statistics. <http://www.worldhunger.org/2015-world-hunger-and-poverty-facts-and-statistics> accessed 13/09/17.

Wuyts N., *et al.*, (2006). Banana rhizodeposition: characterization of root border cell production and effects on chemotaxis and motility of the parasitic nematode *Radopholus similis*. *Plant and Soil*, 283, 217–228. doi: 10.1007/s11104-006-0013-4.

Xia Y., (1986). New Thinning Algorithm for Binary Images. *Proceedings - International Conference on Pattern Recognition*, p. 995–997.

Xie Y., *et al.*, (2020). Phosphorus uptake and growth of wild-type barley and its root-hairless mutant cultured in buffered and non-buffered-p solutions. *Agronomy*, 10, 1556. doi: 10.3390/agronomy10101556.

Xu P., Cai X.T., Wang Y., Xing L., Chen Q. and Xiang C.B., (2014). HDG11 upregulates cell-wall-loosening protein genes to promote root elongation in Arabidopsis. *J. Exp. Bot.* 65, 4285–4295. doi: 10.1093/jxb/eru202.

Yamauchi A., (1993). Significance of root system structure in relation to stress tolerance in cereal crop. In: Low-input sustainable crop production system in Asia. *Korean Soc. Crop Sci.*, Korea, 347-360.

Yazdanbakhsh N. and Fisahn J., (2009). High throughput phenotyping of root growth dynamics, lateral root formation, root architecture and root hair development enabled by PlaRoM. *Functional Plant Biology*, 36, 938-946. doi: <https://doi.org/10.1071/FP09167>

Yu G., *et al.*, (2019). Root Identification in Minirhizotron Imagery with Multiple Instance Learning, 1–11. Available at: <http://arxiv.org/abs/1903.03207>.

Yu H., Chen X., Hong Y.Y., Wang Y., Xu P., Ke S.D., *et al.*, (2008). Activated expression of an Arabidopsis HD-START protein confers drought tolerance with improved root system and reduced stomatal density. *Plant Cell*, 20, 1134–1151. doi: 10.1105/tpc.108.058263.

Zaman-Allah M., Jenkinson D.M. and Vadez V., (2011). A conservative pattern of water use, rather than deep or profuse rooting, is critical for the terminal drought tolerance of chickpea. *J. Exp Bot*, 62, 4239–4252.

Zappala S., *et al.* (2013). Effects of X-Ray Dose On Rhizosphere Studies Using X-Ray Computed Tomography, *PLoS ONE*, 8(6). doi: 10.1371/journal.pone.0067250.

Zappala S., *et al.*, (2013). Quantifying the effect of soil moisture content on segmenting root system architecture in X-ray computed tomography images. *Plant Soil*, 370, 35–45.

Zarebanadkouki M., Meunier F., Couvreur V., Cesar J., Javaux M. and Carminati A., (2016). Estimation of the hydraulic conductivities of lupine roots by inverse modelling of high-resolution measurements of root water uptake. *Annals of Botany*, 118, 853–864.

Zeng G., Birchfield S.T. and Wells C. E., (2010). Rapid automated detection of roots in minirhizotron images. *Machine Vision and Applications*, 21(3), 309–317. doi: 10.1007/s00138-008-0179-2.

Zeng G., Birchfield S.T. and Wells C.E., (2006). Detecting and measuring fine roots in minirhizotron images using matched filtering and local entropy thresholding. *Machine Vision and Applications*, 17(4), 265–278.

Zeng G., *et al.*, (2008). Automatic discrimination of fine roots in minirhizotron images. *New Phytologist*, 177, 549–557.

Zhao J., Fu J., Liao H., He Y., Nian H., Hu Y., Qiu L., Dong Y. and Yan X., (2004). Characterization of root architecture in an applied core collection for phosphorus efficiency of soybean germplasm. *Chin. Sci. Bull.*, 49, 1611–1620.

Zhao X.C. and Schaller G.E., (2004). Effect of salt and osmotic stress upon expression of the ethylene receptor ETR1 in *Arabidopsis thaliana*. *FEBS Letters*, 562(1–3), 189–192. doi: 10.1016/S0014-5793(04)00238-8.

Zhu J. and Lynch J.P., (2004). The contribution of lateral rooting to phosphorus acquisition efficiency in maize (*Zea mays*) seedlings. *Funct. Plant Biol.*, 31, 949–958. doi: 10.1071/FP04046.

Zhu J.M., Kaeppler S.M. and Lynch J.P., (2005). Topsoil foraging and phosphorus acquisition efficiency in maize (*Zea mays*). *Funct Plant Biol*, 32, 749–762.

Zobel R.W., Del Tredici P. and Torrey J.G., (1976). Method for growing plants aeroponically. *Plant Physiol.* 57, 344–346. doi: 10.1104/pp.57.3.344.